Genetic, Cellular and Molecular Defects in Mouse Mutants with Severe Neural Tube Defects

Thesis

Genetic, Cellular and Molecular Defects in Mouse Mutants with Severe Neural Tube Defects

By

Anju Paudyal (BSc Genetics)

This thesis is presented for the degree of

Doctor of Philosophy

The Open University

MRC Mammalian Genetics Unit, Harwell

September 2010

DATE OF SUBMISSION : 15 SEPT 2010

DATE OF AWARD : 11 JAN 2011

For my family

Genetic, Cellular and Molecular Defects in Mouse Mutants with Severe Neural Tube Defects

Anju Paudyal

PhD

The Open University, 2010

Abstract

Neural tube defects are one of the most common birth defects. This thesis includes genetic, molecular and cellular analysis of three mouse mutants with neural tube defects. *chuzhoi* was identified from an ENU G3 screen and exhibits craniorachischisis through failure to initiate neural tube closure. In this thesis, I show that *chuzhoi* carries a point mutation affecting a splice-site in the *Ptk7* gene, leading to addition of three extra amino acids in the protein. Through phenotypic analysis I show that *chuzhoi* has a wider midline and a smaller length to width ratio, suggesting a defect in convergent extension. Previous work has shown that the Planar Cell Polarity (PCP) signalling pathway is required for the initiation of neural tube closure. Through genetic crosses between *chuzhoi* and mutants of PCP signalling, I show that *Ptk7* can influence the PCP pathway without being a direct component of the pathway. Carrying a mutation in *Scribble*, *Circletail* is another mutant displaying craniorachischisis. *Scribble* in *Drosophila* is required for the establishment of apical-basal polarity and to control the rate of cell proliferation. I show that mouse *Scribble* is not required for the establishment of apical-basal polarity nor to control proliferation, during neural tube closure. Previous work in zebrafish has shown that the axis elongation of an embryo requires PCP-dependent orientation of cell division. Here, I show that the orientation of cell division is random in mice during the shaping of the neural plate prior to the initiation of the neural tube closure. Mouse

mutants of *Tulp3* exhibit spina bifida and exencephaly. The molecular role of Tulp3 is largely unknown; however, domains present in the Tulp3 protein suggest that it may act as a transcription factor and/or be involved in protein-protein interactions. I provide evidence to suggest that Tulp3 is not likely to function as a transcription factor but may participate in many protein-protein interactions to deliver its role during mouse embryogenesis.

Acknowledgements

I would like to express my deepest gratitude to my supervisor, Jenny Murdoch, for her invaluable help, support and advice throughout my PhD, without which this thesis would not have been possible. Thanks to my second supervisor Andy Greenfield for his advice and discussion on my project. A huge thank you to Vicki Patterson for critically reading the first draft of this thesis and correcting my English. I would also like to thank the past and present members of the Neural Tube Development group at Harwell; Vicki Patterson, Christine Damrau, Dan Grimes, Ben Reeve, Rachel Poole and Katie Gaynor for general discussion and making the lab an enjoyable place to work. I am also indebted to many members of the core facilities at Harwell, especially Sara Wells and Michelle Stewart for looking after our mice, Stuart Townsend for his help with the confocal microscopy, the Histology group for providing an excellent service, Debbie Williams for her help with the Microarray screen and Real time assays, the GEMS core for help with designing pyrosequencing assays, SNP genotyping and sequencing, and Rosario Romero for her expert advice on the protein side of my project. Thank you to Dominic Norris and Alexander Ermakov for carrying out the G3 screen in which *chuzhoi* was identified, and to Andy Greenfield and Pam Siggers for carrying out the G3 screen in which *hitchhiker* was identified.

A special thank you also goes to all my fellow students at office 153 for keeping me happy and being there to listen to my rants. Thank you to Dan Grimes, Sneha Gole, Christine Damarau, Stuti Mehta, Sally Eaton and Vicki Patterson for proofreading the final draft of my theis.

A huge thank you to my dad for sharing his experiences as a past PhD student and supervisor of numerous PhD candidates and providing lots and lots of emotional support throughout. A special thank you also goes to my husband, Sudhir Kafle, for understanding and

supporting me for the past four years. I would also like to thank the rest of my family for their continuous support, encouragement and being there to entertain me in times of great need.

Finally, I thank the Medical Research Council for funding this research.

Word Count: 63578

Contents

Index of Figures

Index of Tables

Abbreviations

3-AT	3-aminotrazole
AD	Activation domain
ANP	Anterior neuropore
AP	alkaline phosphatase
BMP	Bone morphogenetic protein
bp	Base pair
BSA	bovine serum albumin
cDNA	Complementary DNA
CE	Convergent extension
Celsr1	*Cadherin, EGF LAG seven-pass G-type receptor 1*
chz	*chuzhoi*
Ci	*Cubitus interrupts*
Ck1	*Casein Kinase 1*
Co-IP	Co-Immunoprecipitation
Cos2	*Costal2*
Crc	*Circletail*
Crsh	*Crash*
Ct	Cycle threshold
Daam1	Dishevelled-associated activator of morphogenesis
DBD	DNA binding domain
DEP	Disheveled, Egl-10, pleckstrin
DEPC	diethylpyrocarbonate
Dgo	*Diego*
DH	Dbl-homology
Dhh	*Dessert hedgehog*
DIG	Digoxigenin
DIX	Dishevelled and axin
DLHP	Dorsolateral hinge point
dNTPs	Deoxyribonucleotide triphosphate
Ds	Dachsous
Dsh	*Dishevelled*
DV	Dorsoventral
Dync2h1	Dynein cytoplasmic 2 heavy chain 1
Dync2h1	Dynein cytoplasmic 2 light intermediate chain 1
E	Embryonic day
ENU	N-ethyl-N-nitrosourea
Fj	Four-jointed
Fmi	*Flamingo*
Ft	Fat
Fu	*Fused*
Fz	Frizzled

Gapdh	Glyceraldehyde 3-phosphate dehydrogenase
GCPS	Greig cephalopolysyndactyly syndrome
GDP	Guanosine diphosphate
GEF	Guaninenucleotide exchange factor
GEMS	Genotyping, Mutation detection and Sequencing Core Harwell
Gli1	*Glioma-associated oncogene homolog 1*
Gli2	*Glioma-associated oncogene homolog 2*
Gli3	*Glioma-associated oncogene homolog 3*
GPCR	G-protein coupled receptors
Gsk3	*Glycogen Synthase Kinase 3*
GTP	guanosine triphosphate
H&E	Hematoxylin and eosin
Hh	*Hedgehog*
hhkr	*hitchhiker*
HNP	Hindbrain neuropore
HPE	Holoprosencephaly
Hprt	*Hypoxanthine-guanine phosphoribosyltransferase*
HRP	Horseradish Peroxidase
IFT	Intraflagellar transport
IFTA	IFT complex A
IFTB	IFT complex B
IHCs	Inner hair cells
Ihh	*Indian hedgehog*
IMS	Industrial Methylated Spirit
JNK	Jun-N-terminal kinase
Kap3	*kinesin-associated protein 3*
Kif3A	*Kinesin family members 3A*
Kif3B	*kinesin family members 3B*
LB	Luria broth
Lp	*Loop-tail*
Lrp6	Low-density lipoprotein receptor related protein 6
LRRs	Leucine-rich repeats
MHP	median hinge point
M-MLV	Moloney Murine Leukamia Virus
NPC	Nucleopore complex
NT	Neural tube
NTDs	Neural tube defects
OHCs	Outer hair cells
OPT	Optimum cutting temperature
PBS	Phosphate buffered saline
PCP	Planar cell polarity
PCR	Polymerase chain reaction

PDZ	PSD-95, Dlg, ZO- 1
PFA	Paraformaldehyde
PH	Pleckstrin homology
PHS	Pallister-Hall syndrome
Pk	*Prickle*
PK	Proteinase K
PNP	Posterior neuropore
Ptc	*Patched*
Ptch1	*Patched homolog-1*
Ptch2	*Patched homolog-2*
Ptk7	*Protein tyrosine kinase-7*
qPCR	Quantative polymerase chain reaction
Rgnef	Rho-guanine nucleotide exchange factor
RhoA	Ras homolog gene family member A
RNA	Ribonucleic acid
RNAse	Ribonuclease
RPTK	Receptor protein tyrosine kinase
RQ	Relative Quantification
RT	Room temperature
RT-PCR	Reverse transcription polymerase chain reaction
SDS	Sodium dodecyl sulphate
Shh	*Sonic Hedgehog*
Smo	*Smoothened*
SNP	Single nucleotide polymorphism
Stk36	*Serine/threonine kinase 36*
T	*Brachyury*
TBS	Tris-buffer saline
Tulp3	*Tubby like prototein 3*
UV	Ultra Violet
Vang	*Van gogh*
Vangl2	*Vang-like 2*
WMISH	Whole-mount *in situ* hybridization
Wnt	*Wingless*
Y2H	Yeast 2-hybrid

CHAPTER 1

INTRODUCTION

1 Introduction

Neural tube defects (NTDs) result from a failure to close the neural tube during embryogenesis. In this thesis, I have investigated the genetic, cellular, and molecular causes of NTDs in mouse. To address various aspects of neural tube development I have used three mutant mouse lines, each exhibiting neural tube defects.

1.1 Neural tube defects

Neural tube defects (NTDs) are the second most common human birth disorder after congenital heart defects. The incidence of NTDs varies substantially between different populations, ranging from 0.5 per 1000 pregnancies in Switzerland to 5.6 per 1000 pregnancies in northern China (Botto et al., 1999). The most common types of NTD in humans are anencephaly (failure to close the cranial neural tube), and spina bifida (failure to close the lumbosacral spinal neural tube). A less common NTD, which occurs in around 10% of cases, is craniorachischisis, where the hindbrain and entire spinal region of the neural tube remains open. Incidences of anencephaly and craniorachischisis are invariably lethal and infants die upon birth. Some cases of open spina bifida are less severe and can be compatible with life up to young adulthood, though with severe disability.

Understanding how NTDs arise is the first step in preventing and managing these conditions. Due to ethical and practical constraints, direct analysis of human neural tube development is difficult. For this reason, the mouse is employed as a model to study developmental processes such as neural tube closure.

1.2 Formation of the neural tube

Neural tube closure is a complex developmental process, which results in the formation of the neural tube, the precursor of the brain and spinal cord. The sequence of

events that give rise to a neural tube is well understood from the study of various model organisms including mouse, chick and frog.

1.2.1 Neural induction

The first step of neurulation is the formation of the neural plate at the dorsal midline of the embryo. Initially, a mouse embryo is cup-shaped consisting of two cell layers; epiblast and endoderm (Tam and Behringer, 1997). At gastrulation a proportion of epiblast cells migrate through the primitive streak and form the mesodermal layers of the embryo (Tam and Behringer, 1997). The notochord, a midline mesodermal structure that is essential for the correct dorsoventral (DV) patterning of the neural tube, forms from the migrating epiblast cells (Klingensmith et al., 1999; Sadler, 2005b). The epiblast cells that do not migrate through the node form the ectodermal layer of the embryo. Through inhibition of Bone Morphogenetic Protein (BMP) signalling by *noggin* and *chordin*, the ectoderm differentiates into neuroepithelium to form the neural plate on the dorsal surface of the embryo (Harland, 2000; Sadler, 2005a).

Once the neural plate is formed, it then undergoes extensive remodelling to form an elongated structure that is broad at the cranial end and narrow in the spinal region of the developing embryo (Copp et al., 2003). This remodelling of the neural plate continues throughout neurulation. The mechanism that regulates this process has been identified as convergent extension (CE) which is regulated by the planar cell polarity (PCP) signalling pathway (see Section 1.3.4.1).

1.2.2 Neural tube closure

Formation of the neural tube is an early developmental process. In mice the period of gestation is 19 days and the initiation of neural tube closure occurs at E8.5 (5-9 somites) and primary neurulation is completed by E10.5 (Copp et al., 1990). This event is even

earlier in human development, where the formation of neural tube is completed by 28 days of gestation (DeSesso et al., 1999).

In mouse, neural tube closure is initiated at three independent positions (termed closure 1, closure 2 and closure 3) along the rostrocaudal axis(Copp et al., 1990). At around the five to seven somite stage (precise stage can vary slightly between strains), closure 1 occurs at the hindbrain/spinal cord boundary and closure progresses caudally to close the spine and cranially to close the hindbrain. Shortly after closure 1, at approximately the 11 somite stage, closure 2 occurs near the boundary between the midbrain and forebrain and, from this site, closure progresses rostrally to close the forebrain and caudally to close the midbrain. The exact position of closure 2 is variable between mouse strains. At the 12 somite stage, closure 3 initiates at the most rostral extremity of the embryo and from there progresses caudally to meet the rostrally spreading closure from the site of closure 2 to create the anterior neuropore (ANP). The complete closure of the forebrain occurs by approximately the 16 somite stage (Copp et al., 1990). Similarly, the cranially extending closure from the site of closure 1 meets the caudally extending closure from the site of closure 2 to create the hindbrain neuropore (HNP). The HNP closes by approximately the 17 somite stage, completing closure of the hindbrain (Copp et al., 1990). The formation of the spinal neural tube occurs by the extension of closure in a zippering fashion caudally from the site of closure 1, and is completed with closure of the posterior neuropore (PNP) at approximately the 29 somite stage (Copp et al., 1990). Once primary neurulation has completed, secondary neurulation occurs at the caudal end of the embryo. During secondary neurulation, mesenchymal cells in the tail bud undergo condensation and epithelialization to form an epithelial rod which then undergoes canalization to produce a secondary neural tube (Greene and Copp, 2009). The lumen of the secondary neural tube is continuous with the lumen of the primary neural tube.

Disruption to any processes of primary neurulation results in NTDs (Figure 1-1). Failure of closure 1 results in craniorachischisis, the most severe NTD where the entire

spinal region and the hindbrain remains open (Curtin et al., 2003; Murdoch et al., 2003; Lu et al., 2004) (Figure 1-1B). In mutants with craniorachischisis the cranial neural tube closes normally indicating that different mechanisms are involved in closure of the cranial and spinal neural tube. The failure of posterior neuropore closure results in spina bifida (Figure 1-1C). Disruption of closure 2 and/or closure 3, or incomplete closure of the ANP or HNP, results in exencephaly where the cranial neural tube remains open (Figure 1-1D). Defects in secondary neurulation leads to closed form of spina bifida (Greene and Copp, 2009).

In humans the exact number and positions of the sites of initiation of neural tube closure is not known; however, there is increasing evidence to support a multiple closure sites model, similar to that observed in mice (Seller, 1995; Ahmad and Mahapatra, 2009; Vashu and Liew, 2010).

1.2.3 Three modes of spinal neural tube closure

To enable the flat neural plate to form a closed neural tube, the neural folds elevate, bend and fuse at the dorsal midline. Bending of the neural folds can occur at three different sites; at the ventral midline, termed the median hinge point (MHP), and at the paired dorsolateral region of the neural folds, termed the dorsolateral hinge point (DLHP) (Figure 1-2 A-C). The combination of these bends has been interpreted as three modes of spinal NT closure: mode 1, mode 2, and mode 3. The MHP is present in the upper and intermediate spinal region and is absent from the lower spine. It functions to elevate the neural folds to form a 'V' shaped neural groove and is the only form of bending in the upper spine (Figure 1-2 A). The DLHPs are absent in the upper spine but present in the intermediate and lower spine (Figure 1-2 A-C). The MHP and DLHPs act to bring the opposing neural folds together which fuse in the midline creating a hollow tube. In mouse, the initiation of neural tube closure occurs at E8.5 and is completed by E10.5.

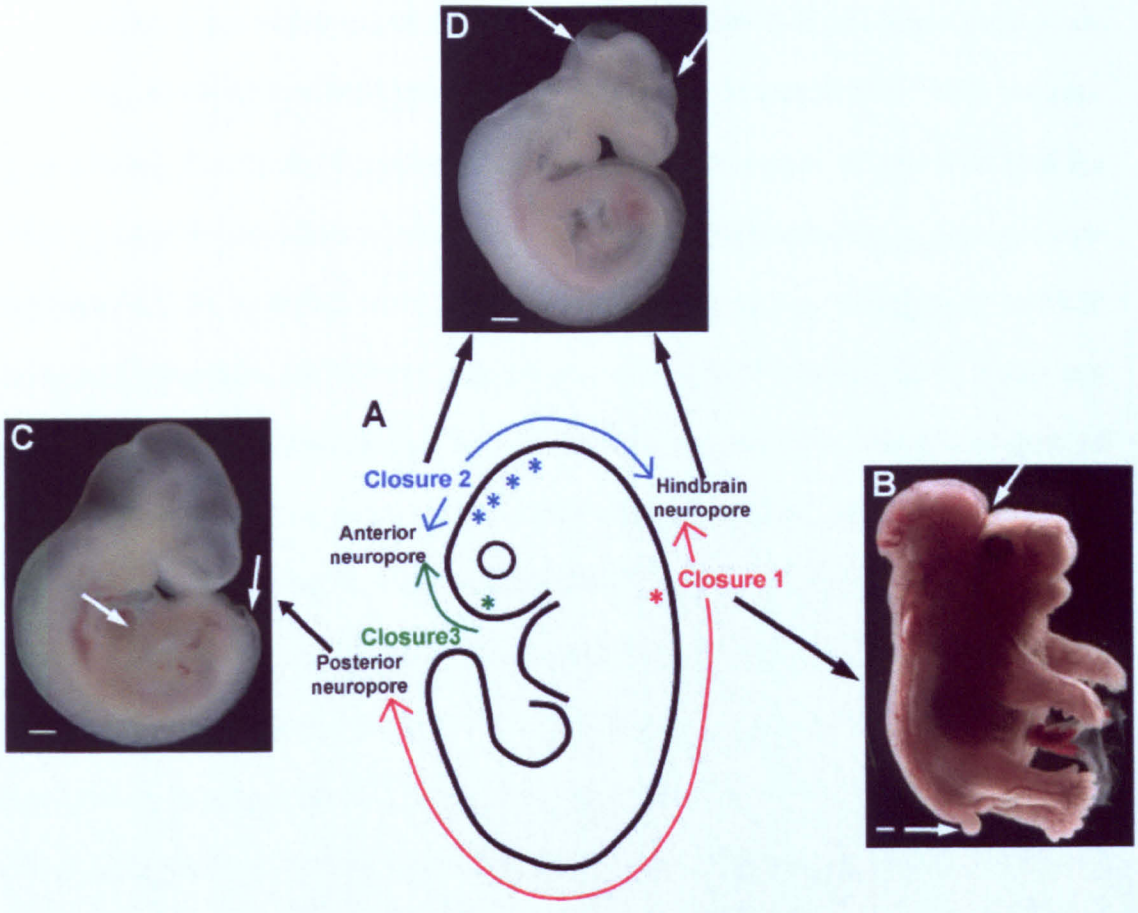

Figure 1-1: Closure of the neural tube is a multi-step process.
(A) Initiation of neural tube closure occurs at three *de novo* positions within the mouse embryo. First, closure 1 (red asterisk) occurs at the future cervical region and closure spreads from here both rostrally and caudally into the hindbrain and the spine, respectively (red arrows). Closure 1 is followed by closure 2 which occurs at or near the forebrain/midbrain boundary (blue asterisks), and from here closure progresses both rostrally and caudally (blue arrows). The position of closure 2 is varied among different strains of mice as indicated by multiple blue asterisks. Closure 3 occurs at the rostral extremity of the forebrain (green asterisk) and progresses caudally (green arrow). Caudally spreading closure from the site of closure 2 meets the rostrally extending closure from the site of closure 1 to create the hindbrain neuropore; similarly the rostrally extending closure from closure 2 meets the caudally extending closure from closure 3 to create the anterior neuropore. A defect in any one of these closure events give rise to neural tube defects. A failure to initiate closure 1 results in craniorachischisis (B) where the entire spine and the hindbrain remains open (open neural tube between white arrows). Failure to complete spinal closure gives rise to spina bifida (C) where the caudal neural tube (between white arrows) remains open. Defects in closure 2 and/or closure 3 and/or failure to close the anterior neuropore or hindbrain neuropore leads to exencephaly (D), where a part of the head remains open. The embryo shown in D has failed to complete closure 2, resulting in a failure to close the midbrain (between white arrows). (A) modified from Copp *et al.*, 1990); (B) E18.5 *chuzhoi* homozygous embryo, scale bar represents 1 mm; (C and D) E10.5 *hitchhiker* homozygous embryos, scale bars represent 500 μm.

At E8.5, the active site of spinal neural tube closure is at the upper spine level, where only the MHP is present (mode 1) (Figure 1-2 A). At around E9.5, when the mid-spine is being formed, the formation of DLHPs starts to take place. At this level both the DLHPs and MHP play a role in bending the neural tube thereby effecting its closure (mode 2) (Figure 1-2 B). At E10.0, when the spinal neural tube is nearing completion, the MHP completely disappears and only DLHPs are present (mode 3) (Figure 1-2 C) (Shum and Copp, 1996). This gradual change from MHP to DLHP correlates with the strength of Sonic Hedgehog (Shh) signalling from the underlying notochord, which weakens as the embryo grows. The formation of the DLHPs is negatively regulated by Shh signalling from the underlying notochord and positively regulated by BMP signalling from the surface ectoderm (Ybot-Gonzalez et al., 2002; Ybot-Gonzalez et al., 2007a). This model is further supported by experimental inhibition of Shh, which results in formation of the MHP and DLHPs ectopically at the upper spinal level. Moreover, mutants of negative regulators of Shh signalling, such as *Tulp3*, have reduced DLHPs in the caudal spinal region leading to failure of neural tube closure (Ybot-Gonzalez et al., 2002; Patterson et al., 2009).

1.2.4 Cranial neural tube closure

Cranial neural tube closure is a more sensitive process than closure of the spine as indicated by the fact that mouse mutants exhibiting exencephaly are much more common than those exhibiting spina bifida or craniorachischisis (Harris and Juriloff, 2007). During cranial neural tube closure, the MHP is not present; however, the neural folds are elevated as a direct consequence of increased proliferation of underlying mesenchymal cells, leading to expansion of underlying mesenchyme (Morriss and Solursh, 1978) (Figure 1-2 D). This is supported by the *Alx1/Cart1* mutant where the cranial neural tube fails to close as the underlying mesenchymal cells are removed by apoptosis, resulting in neural folds that fail to elevate (Zhao et al., 1996).

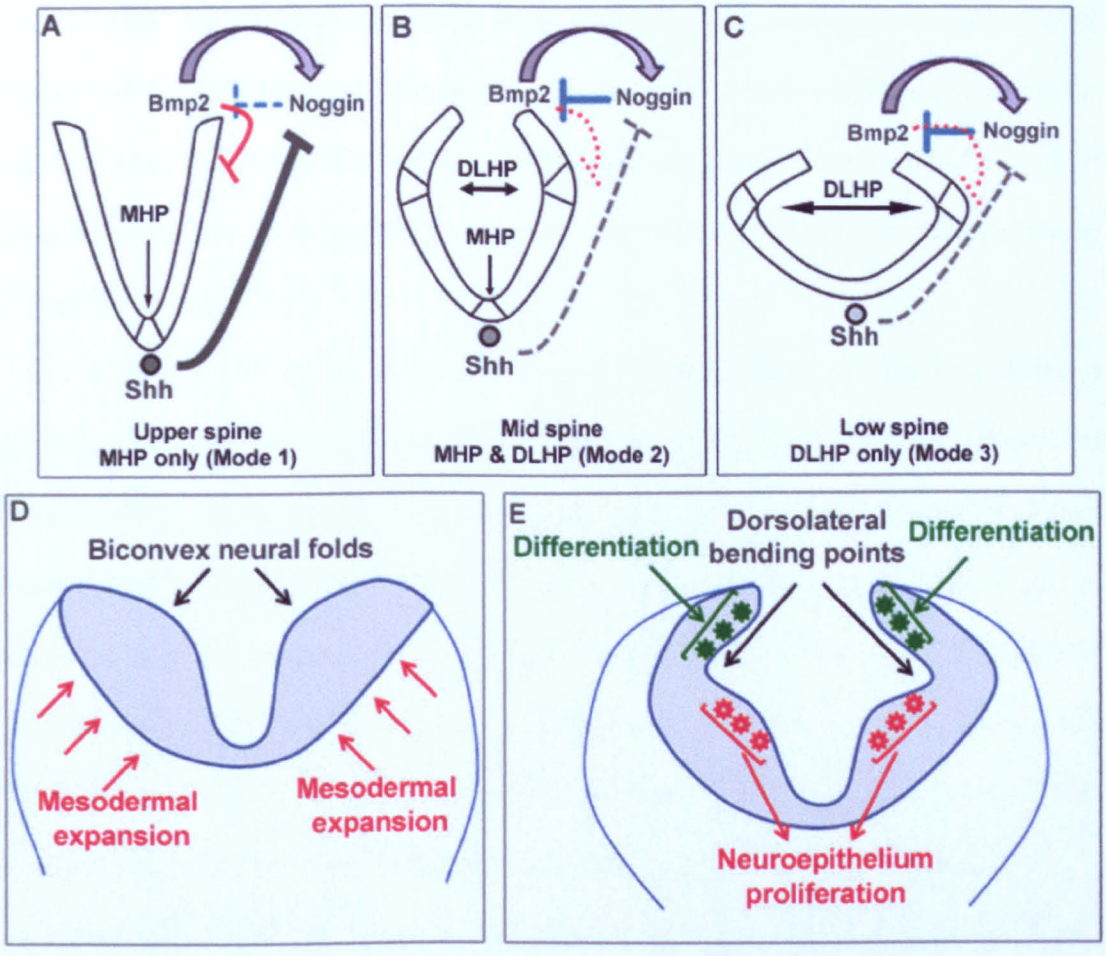

Figure 1-2: Morphology of neuroepithelium during the closure of spinal and cranial neural tube.

(A-C) Morphology of neural folds in the posterior neuropore, during closure of different axial levels; upper spinal level (A), mid spinal level (B) and lower spinal level (C). Bmp2 induces the expression of Noggin (purple arrows) which in turn inhibits BMPs. The function of Noggin is inhibited by Shh. At the upper spinal level (A), where the concentration of Shh from the notochord is high, Shh inhibits the function of Noggin (grey solid line) resulting in activation of Bmp2, which inhibits the formation of DLHPs (solid red line). During the closure of mid and lower spine (B and C), the concentration of Shh from the underlying notochord progressively weakens. This low level of Shh is insufficient to inhibit the function of Noggin (broken grey line), enabling Noggin to antagonize the function of Bmp2 (solid blue line), which results in formation of DLHPs. (D and E) Morphology of cranial neural folds during fold elevation (D) and formation of dorsolateral bending points (E). (D) Neural folds elevate and adopt a biconvex morphology resulting from expansion of underlying mesoderm (red arrows). Cells within the elevated neural folds undergo differentiation (green stars) and proliferation (red stars) to enable the formation of dorsolateral bending points, which are required to enable two neural folds to appose and fuse at the midline. Figure modified from Ybot-Gonzalez et al., 2007 (A-C) and Copp et al., 2003 (D and E).

Once the neural folds are elevated, the dorsolateral regions of the neural folds bend towards each other to bring the neural folds together at the midline to facilitate fusion (Figure 1-2 E). This bending of the neural folds at the dorsolateral region depends on the actin cytoskeleton, cell proliferation, and differentiation; mutations affecting any one of these processes lead to exencephaly in mouse, often without affecting spinal neural tube closure (Copp et al., 2003).

Although 70% of all mouse mutants with NTDs exhibit exencephaly alone, a smaller proportion of mutants (20%) display both exencephaly and spina bifida (Harris and Juriloff, 2007), suggesting that at least some parts of cranial and spinal neural tube closure are regulated by the same mechanisms. One of these mechanisms is Shh signalling, as mutants of negative regulators of this pathway such as *Rab23, Tulp3* and *Pka* all exhibit defects in both cranial and spinal neural tube closure (Gunther et al., 1994; Nagai et al., 2000; Ikeda et al., 2001; Huang et al., 2002; Norman et al., 2009; Patterson et al., 2009), giving evidence that Shh signalling is required for both cranial and spinal closure.

The final step in the formation of the neural tube is the fusion of apposing neural folds to create a hollow tube. This step of the neural tube closure is the least characterised process as mouse models available to study this process are limited. Currently there is only one mouse mutant, the *ephrin-A5* null, that has been described as giving rise to NTDs as a direct consequence of failure to fuse the two apposing neural folds after they have been elevated (Holmberg et al., 2000). Ephrin-A5 is a specific ligand for EphA7, a member of Eph tyrosine kinase receptors. These groups of proteins are well known for their involvement in cell repulsion during axonal guidance and cell migration; however, in contrast to this role it was found that an endogenously expressed truncated isoform of EphA7 shifted the repulsion cellular response to that of adhesion and this appears to be important for neural tube closure (Holmberg et al., 2000). The Holmberg et al study provided the first evidence that cell-cell adhesion is important for neural tube closure. More molecules with a similar mechanism must exist to close the spinal neural tube as

both EphA7 and Ephrin-A5 are expressed only in the cranial neural folds and give rise to defects in closure of the head. However, the identity of such molecules is currently unknown. There is also evidence for a role of glycoproteins during neural fold fusion. Glycoproteins are present on the surface of the neuroepithelium throughout neurulation but become restricted to the tip of the neural folds at the time of the fusion. The removal of these proteins by chemical treatments leads to neural tube defects (McLone and Knepper, 1985).

Additionally, it has been proposed that the intercalation of cellular protrusions, detected on the surface of the neuroepithelium cells at neural folds, initiates fusion of the neural folds by cell-cell interaction (Geelen and Langman, 1979). Once the neural folds are fused together, permanent intercellular connections between the neuroepithelium cells of the apposed neural folds are made to create a continuous tissue; however, the precise mechanism for this has not been determined.

1.3 The Wnt signalling pathway

There are three known Wnt signalling pathways which play critical roles during early embryonic development; Wnt/β-catenin (canonical), Wnt/Calcium and Wnt/PCP (planar cell polarity or non-canonical) signalling. These pathways are activated when a specific extracellular Wnt ligand binds to a specific membrane-bound Frizzled receptor resulting in recruitment of downstream proteins, which then triggers the appropriate intracellular Wnt pathway. Both Wnt and Frizzled proteins are encoded by large multigene families. The Frizzled family consists of four members in *Drosophila* and 10 members in human and mouse. Similarly, the Wnt family consists of seven members in *Drosophila* and 19 in human and mouse.

Functional studies of many Wnt ligands have shown that each of them has a distinct role and can effect development of different tissues. For example, mouse Wnt3a is

involved in tail bud development while Wnt4 is required for female gonad development (Greco et al., 1996; Kim et al., 2006). Although the Wnt ligand that activates PCP signalling is not yet known in *Drosophila*, there is some evidence to indicate that PCP signalling is activated by Wnt molecules in vertebrates. It has been reported that in zebrafish a mutation in *Wnt11* leads to defects associated with compromised PCP signalling (Heisenberg et al., 2000) and similarly mutations in mouse *Wnt5a* or *Wnt7a* result in PCP defects (Dabdoub et al., 2003; Qian et al., 2007).

Dishevelled is at the heart of both canonical and non-canonical Wnt signalling as it is required for both pathways. It is a large cytoplasmic protein with three main domains; the DIX, PDZ and DEP domains. It has been established that the DIX domain is required to signal through the canonical Wnt pathway; however, it is not required for non-canonical Wnt signalling. Conversely, the PDZ and DEP domains are both required for non-canonical PCP signalling while the DIX domain is dispensable (Boutros et al., 1998; Habas et al., 2001).

To activate the canonical Wnt pathway, a Wnt ligand binds to Frizzled and its co-receptor, low-density lipoprotein receptor related protein 6 (LRP6). This results in recruitment of Dishevelled leading to stabilisation of β-catenin which then accumulates and enters the nucleus and activates the transcription of Wnt responsive genes (MacDonald et al., 2009).

1.3.1 Planar Cell Polarity signalling in *Drosophila*

The planar cell polarity (PCP) (historically referred to as tissue polarity) signalling pathway was first described in Drosophila as a signalling cascade that is required to regulate the orientation of cells in the plane of an epithelial sheet (Gubb and Garcia-Bellido, 1982). PCP has been most studied using the organization of hairs on the wing of Drosophila as a model (Simons and Mlodzik, 2008), as this represents a beautiful example

of controlled orientation of cells in the plane of an epithelium. Each cell on the wing of Drosophila produces a hair which is orientated such that all hairs point toward the distal side of the cell in a uniform pattern; however, when PCP is disrupted this uniform pattern is disrupted. In 1989 the first PCP gene, frizzled (fz), was cloned and was found to be a large transmembrane protein with seven transmembrane domains, resembling a G protein coupled receptor (Vinson et al., 1989). This was followed by cloning of dishevelled (dsh) (Krasnow et al., 1995), van gogh (vang) (Taylor et al., 1998), prickle (pk) (Gubb et al., 1999), flamingo (fmi) (Usui et al., 1999) and diego (dgo) (Feiguin et al., 2001). These six genes are required for establishment of PCP in many systems such as hair cells in the wing and precise orientation of ommatidia in the eye, therefore are known as the core PCP molecules (Fanto and McNeill, 2004). Subsequently, it has been shown that Fz forms a complex with Dsh (Fz-Dsh) and Vang forms a complex with Pk (Vang-Pk) (Figure 1-3). During cell polarisation, these two complexes antagonize each other and become restricted to opposite sides of a cell (Simons and Mlodzik, 2008). Fz-Dsh localises to the distal side and conversely Vang-Pk localises to the proximal side of the cell (Figure 1-3). The mechanism underlying this asymmetric distribution is poorly understood. However, it has been established that Diego directly binds to Dsh and it is thought that this interaction promotes PCP signalling by protecting the Fz-Dsh complex from the antagonistic effect of Vang-Pk on the distal side of the cell (Figure 1-3) (Jenny et al., 2005). The role of Fmi is not very well understood, though it is thought to serve as a homophilic adhesion molecule (Simons and Mlodzik, 2008). It localises to both the proximal and distal side of the cell and is genetically required for the asymmetric distribution of both complexes (Strutt and Strutt, 2008). However, it has been reported that it preferentially interacts with the Fz-Dsh complex to promote its localisation to the distal side of the cell (Strutt and Strutt, 2008).

The PCP signalling pathway is activated by an unknown ligand resulting in interaction between Dishevelled and the PCP effector molecule, Dishevelled-associated activator of morphogenesis (Daam1) via PDZ and DEP domains of Dishevelled (Habas et

al., 2001). Daam1 then forms a complex with RhoA which is activated by a Rho-specific guaninenucleotide exchange factor (GEF) (Habas et al., 2001). Additionally, the DEP domain of Dishevelled is sufficient to activate Rac, a second member of the Rho family of GTPases, which in turn activates Jun-N-terminal kinase (JNK) (Habas et al., 2003). This activation of RhoA and JNK mediates the nuclear response and cytoskeleton reorganisation that is required for cellular polarization and movement (Figure 1-4). In addition, there is evidence to suggest that the core PCP molecules signal to downstream effectors which are known to be tissue specific, as mutants of these downstream effectors give rise to PCP phenotypes in a single system. For example, a mutation in the *nemo* gene encoding a kinase molecule appears to affect the establishment of polarity in the eye without affecting PCP in the wing, while a mutation in *fuzzy* or *inturned* results in a PCP defect specific to cytoskeleton rearrangements in the wing and the cuticle (Simons and Mlodzik, 2008).

A second group of genes affecting the *Drosophila* PCP signalling pathway in all tested systems has been described. There are three main components in this group: Fat (Ft); Dachsous (Ds); and Four-jointed (Fj). The relationship between Ft/Ds/Fj and Fz/Fmi/Vang PCP signalling is confusing. Originally it was suggested that the Ft/Ds/Fj signalling acted upstream of the Fz/Fmi/Vang to regulate the PCP signalling (Yang et al., 2002). More recently, evidence has emerged to suggest that these two signalling cascades may in fact act in parallel but independently to regulate PCP (Casal et al., 2006).

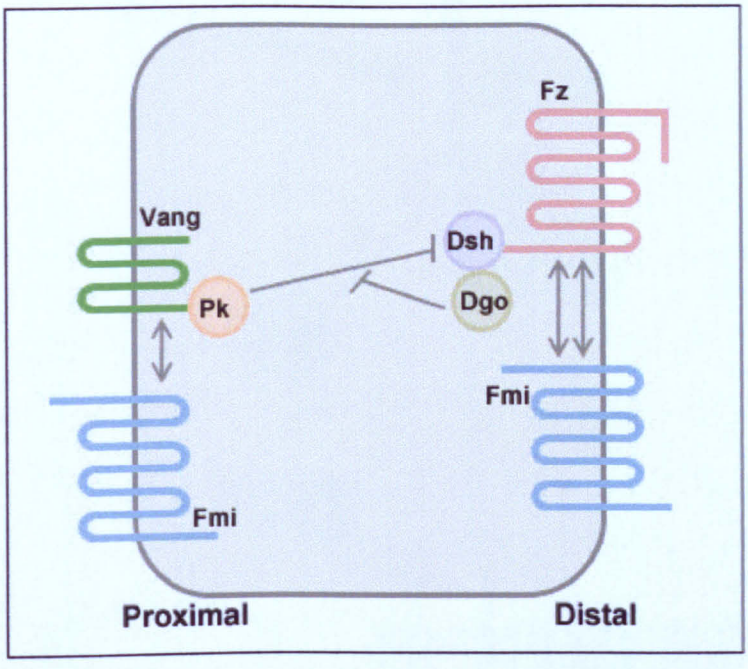

Figure 1-3: Subcellular localization and molecular interaction between core components of the *Drosophila* PCP pathway.
Apical view of the cell following asymmetric localization of the core PCP factors. Proximal is on the left and distal is on the right. On the distal side of the cell, Frizzled (Fz, pink), consisting of seven transmembrane domains, recruits the cytoplasmic protein Dishevelled (Dsh, purple) to the membrane via its cytoplasmic tail. Dsh binds to Diego (Dgo, brown). On the proximal side, another transmembrane protein Van gogh (Vang, green) recruits the cytoplasmic protein Prickle (Pk, orange) to the membrane. Pk can bind Dsh in a competitive manner, inhibiting the formation of Fz-Dsh complex. Dgo protects the Fz complex from Pk inhibition. The third transmembrane protein, Flamingo (Fmi, blue), localizes to both the proximal and distal side and is required for asymmetric distribution of both Vang-Pk and Fz-Dsh complexes. There is evidence to indicate that Fmi preferentially promotes the asymmetric localization of the Fz-Dsh complex to the distal side of the cell (indicated by double arrow) rather than Vang-Pk complex to the proximal side of the cell (indicated by single arrow). Figure modified from (Seifert and Mlodzik, 2007).

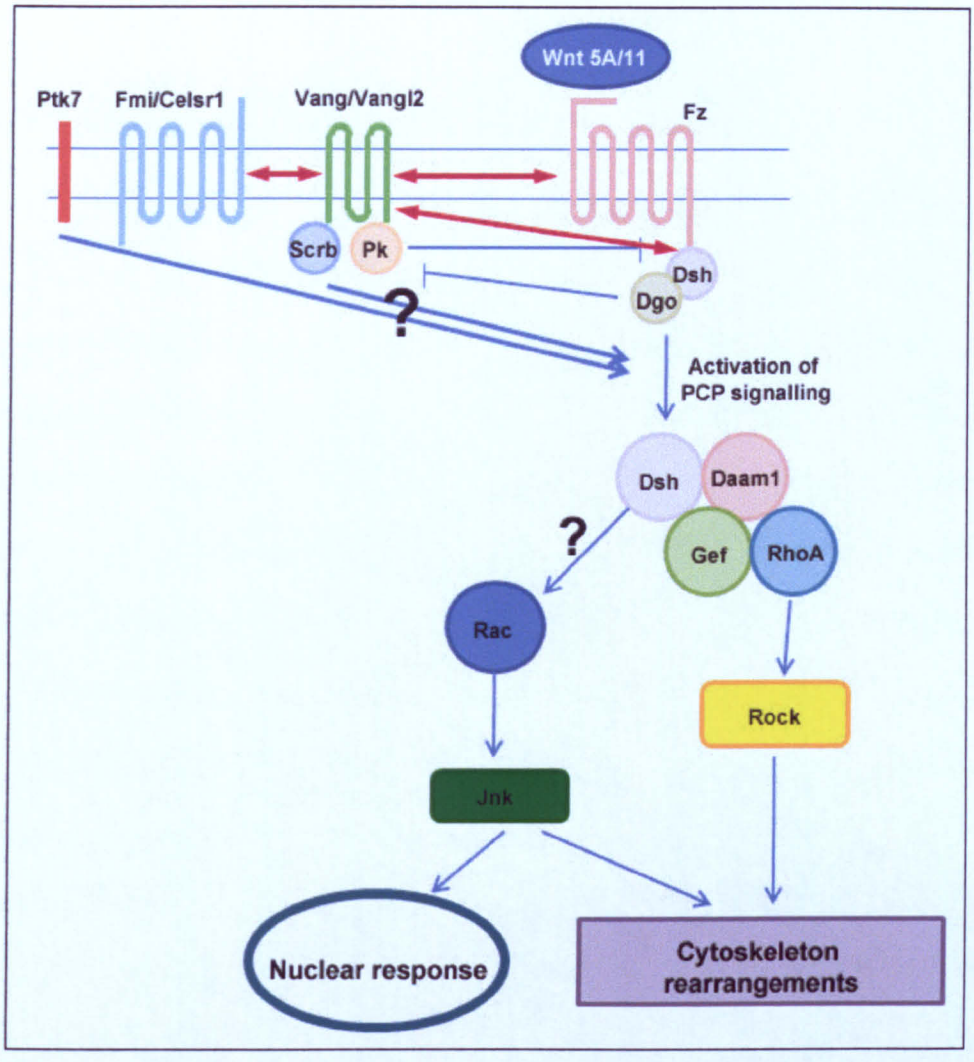

Figure 1-4: The Planar Cell Polarity signalling pathway: evidence from *Drosophila* and mice

A ligand binds to Frizzled (Fz, pink transmembrane protein) activating the PCP signalling pathway. Evidence from mice indicates that the ligand is a Wnt molecule (Wnt, blue). Upon activation of the pathway, Dishevelled (Dsh, purple) binds to Dishevelled-associated activator of morphogenesis (Daam1, pink) and activates it. Activated Daam1 forms a complex with RhoA (light blue) and Rho specific guanine nucleotide exchange factor (Gef, dark green) resulting in activation of RhoA. RhoA then signals through Rho associated kinase (Rock, yellow) to enable cytosketeleton changes. Dsh also signals through a second mechanism. Dsh activates another Rho family GTPase, Rac (dark blue) via an unknown mechanism. Activated Rac signals through Jun-N-terminal kinase (Jnk, green) which results in a nuclear response and cytosketeleton changes. The mechanism by which Ptk7 (orange transmembrane protein) and Scribble (Scrb light blue cytoplasmic protein) influence PCP signalling is unknown. Physical interactions between Vang/Vangl2 and Scrb, Vang/Vangl2 and Dsh, Fz and Vang/Vangl2, and Vang/Vangl2 and Fmi/Celsr1 have been reported (indicated by red double headed arrow).

1.3.2 Planar cell polarity signalling in vertebrates

Homologues of all *Drosophila* core PCP genes are found in vertebrates and many of them are functionally conserved. Analysis of vertebrate core PCP mutants indicates a crucial role for this signalling cascade during the establishment of epithelial planar cell polarity, analogous to that observed in Drosophila. The best example of epithelial PCP in vertebrates is the uniform orientation of the hair cell stereociliary bundles within the organ of Corti in cochlea. The organ of Corti consists of a single row of sensory inner hair cells (IHC), three rows of sensory outer hair cells (OHCs) and non-sensory supporting cells which are present around the sensory hair cells. On the apical surface of each hair cell, a single microtubule-based organelle, the kinocilium, and an actin-based stereociliary bundle, are present. The hair cell bundle consists of stereocilia of different lengths, which are arranged in a step-wise fashion to create a symmetrical "V" shape, with the single kinocilium located at the apex of the "V" (Figure 1-5) (Rida and Chen, 2009). All sensory hair cells are precisely oriented such that the apex of the stereociliary bundle points towards the lateral side of the cell (Rida and Chen, 2009). PCP signalling is responsible for this precise orientation of sensory hair cells, as mouse mutants carrying a mutation in a core PCP molecule such as Vangl2 (homologue of Drosophila van gogh) and Celsr1 (homologue of Drosophila Flamingo), exhibit a defect in orientation of these sensory hair cells (Figure 1-5) (Curtin et al., 2003; Montcouquiol et al., 2003). Other genes that are involved in regulating mammalian PCP, defined by showing a similar defect in orientation of sensory hair cells, are Frizzled 3/6 (homologue of *Drosophila* Frizzled) (Wang et al., 2006b), Dishevelled 1/2 (homologue of *Drosophila* Dishevelled) (Hamblet et al., 2002), Scribble (homologue of *Drosophila* Scribble) (Montcouquiol et al., 2003) and Ptk7 (homologue of *Drosophila* off-track) (Lu et al., 2004).

1.3.3 Molecular mechanism of Planar Cell Polarity signalling in vertebrates

The molecular mechanisms of vertebrate PCP have mostly been studied in the context of inner ear sensory hair cells. The distribution pattern and the interactions of many components of the core PCP molecules have been reported. It has been established that Dishevelled1/2, Vangl2 and Frizzled3/6 show an asymmetric localization where Vangl2 and Frizzled3/6 co-localise to the proximal side while Dishevelled1/2 localises to the distal side of side of the sensory hair cell (Montcouquiol et al., 2006; Wang et al., 2006a; Wang et al., 2006b). In contrast, Scribble does not show an asymmetric distribution; however, it both interacts with and is required for the asymmetrical localisation of Vangl2 (Montcouquiol et al., 2006). Vangl2 and Frizzled3 have been shown to physically interact and the asymmetric distribution of Frizzled3 is lost in the sensory hair cells of Vangl2$^{Loop\text{-}tail}$ mutants (Montcouquiol et al., 2006). Conversely, localization of Vangl2 is altered in *Frizzled3* and *Frizzled6* mutants (Wang et al., 2006b). Although Vangl2 and Dishevelled localise to opposite ends of the cell, the loss of Vangl2 severely disrupts the asymmetric localisation of Dishevelled in Vangl2$^{Loop\text{-}tail}$ sensory hair cells (Wang et al., 2005). The distribution pattern of Celsr1 has not been examined in mouse sensory hair cells, however it has been shown to physically interact with Vangl2, and loss of Celsr1 leads to loss of asymmetric localization of Vangl2 in *Celsr1*^{Crash} mutants (Montcouquiol et al., 2006; Devenport and Fuchs, 2008). Recently, a similar result was reported during branching morphogenesis in lungs where the localisation of Vangl2 was affected in *Celsr1*^{Crash} mutants; however, the distribution of Celsr1 was not changed in *Vangl2*$^{Loop\text{-}tail}$ mutants (Yates et al., 2010), suggesting that Celsr1 is upstream of Vangl2 during establishment of asymmetric localization. It remains to be seen whether the distribution pattern of Celsr1 is affected by loss of Vangl2 during the establishment of PCP in the inner ear.

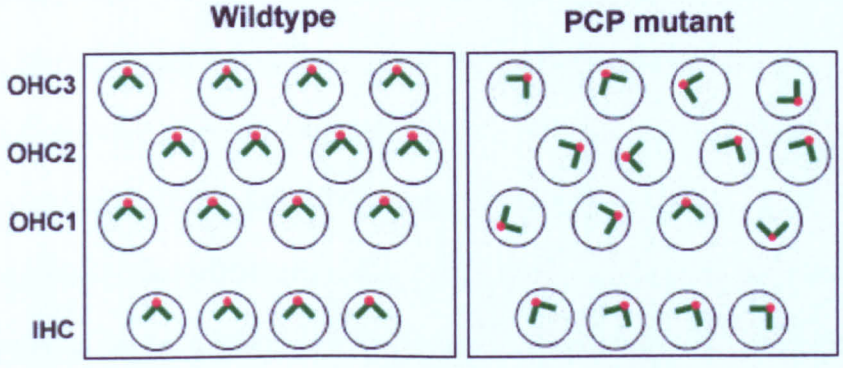

Figure 1-5: Planar cell polarity in establishment of orientation of the inner-ear sensory hair cells.
A diagrammatic representation of hair bundle orientation in sensory hair cell of the inner ear. Actin-rich stereocilias (green) are arranged in a "V" shape with a single tubulin-based kinocilia (red) at the apex of the "V". In wildtype, hair cells are uniformly aligned such that the stereocilias bundle point in one defined direction. In PCP mutants, hair cells lose their orientation therefore the stereocilia bundle no longer point in a defined direction. IHC, inner hair cells; OHC1, inner row of outer hair cells; OHC2, central row of outer hair cell; OHC3, outer hair cells. Figure adapted from (Wang and Nathans, 2007).

Although the asymmetric distribution of core PCP proteins has been conserved between *Drosophila* and vertebrates, one key difference is noticeable. In *Drosophila,* Dishevelled is recruited to the membrane by Frizzled and it co-localises with Frizzled at the distal side of wing cells, opposite the Vang-Pk complex (Simons and Mlodzik, 2008). In mouse sensory hair cells Vangl2 co-localises with Frizzled3/6 and Dishevelled is at the opposite side (Montcouquiol et al., 2006; Wang et al., 2006a; Wang et al., 2006b). This raises the question as to how Dishevelled is recruited to the membrane. It has been suggested that one of the other members of the Frizzled family may be involved in establishment of mammalian PCP and may be required to recruit Dishevelled to the distal side of sensory hair cells (Simons and Mlodzik, 2008).

1.3.4 Planar cell polarity signalling and neural tube closure

As well as displaying orientation defects in the sensory hair cells, mutants of PCP signalling also exhibit the severe neural tube defect, craniorachischisis. Although the

cellular mechanism of how PCP controls the closure of the neural tube is now quite well understood, the molecular mechanism is less clear. One of the key events required for proper neural tube closure is the shaping of the neural plate before and during elevation and fusion of the neural folds. During this event, the spinal neural plate and the underlying mesoderm narrows in the mediolateral axis and lengthens in the rostrocaudal axis allowing the neural folds to appose and fuse in the midline. In PCP mutants this process is affected and as a consequence the midline is wider preventing the neural folds from apposing and fusing at the midline (Greene et al., 1998; Kibar et al., 2001; Murdoch et al., 2001a). This results in a failure to initiate neural tube closure, leading to the severe neural tube defect, craniorachischisis. In mouse, this defect was first described in the *loop-tail* mutant, which carries a mutation in the core PCP gene *Vangl2* (homologue of *Drosophila Vang*) (Kibar et al., 2001; Murdoch et al., 2001a). Subsequently, it was shown that other mouse mutants that exhibit craniorachischisis also display a wider midline (Murdoch et al., 2003; Lu et al., 2004; Wang et al., 2006a). The cellular mechanism that is proposed for shaping the neural plate prior to its closure is convergent extension.

1.3.4.1 Convergent Extension

Convergent extension (CE) has been best defined in Xenopus as complex process which involves cells elongating mediolaterally and moving towards and intercalating into the midline to elongate and narrow the midline, without increasing the number of cells (Figure 1-6) (Keller, 2006). This cellular rearrangement was first described in the mesoderm of Xenopus as a process that was regulated by PCP signalling and was essential for the narrowing of the dorsal midline during neural tube closure (Wallingford and Harland, 2001, 2002). It was shown that when a dominant mutant form of *dishevelled* was injected into *Xenopus* embryos, the neural tube failed to close due to specific defects in the narrowing of the midline, although all other aspects of the neural tube closure, such as the

elevation and movement of the neural folds, were not affected. Subsequently, it was shown that *strabismus* (the homologue of *Drosophila Vang*) also regulated neural tube closure by mediating CE in the neural tissue and the underlying mesoderm in *Xenopus* embryos (Darken et al., 2002; Goto and Keller, 2002). Interestingly, in 2007 it was reported that Lrp6, a co-receptor of Frizzled that is required for canonical Wnt signalling, is also a key molecule required for convergent extension during *Xenopus* gastrulation (Tahinci et al., 2007). This study provides evidence to suggest Lrp6 negatively regulates PCP signalling while positively activating canonical Wnt signalling. More recently it was shown that CE also occurs during neural tube closure in mice and is regulated by PCP signalling (Wang et al., 2006a; Ybot-Gonzalez et al., 2007a; Yen et al., 2009).

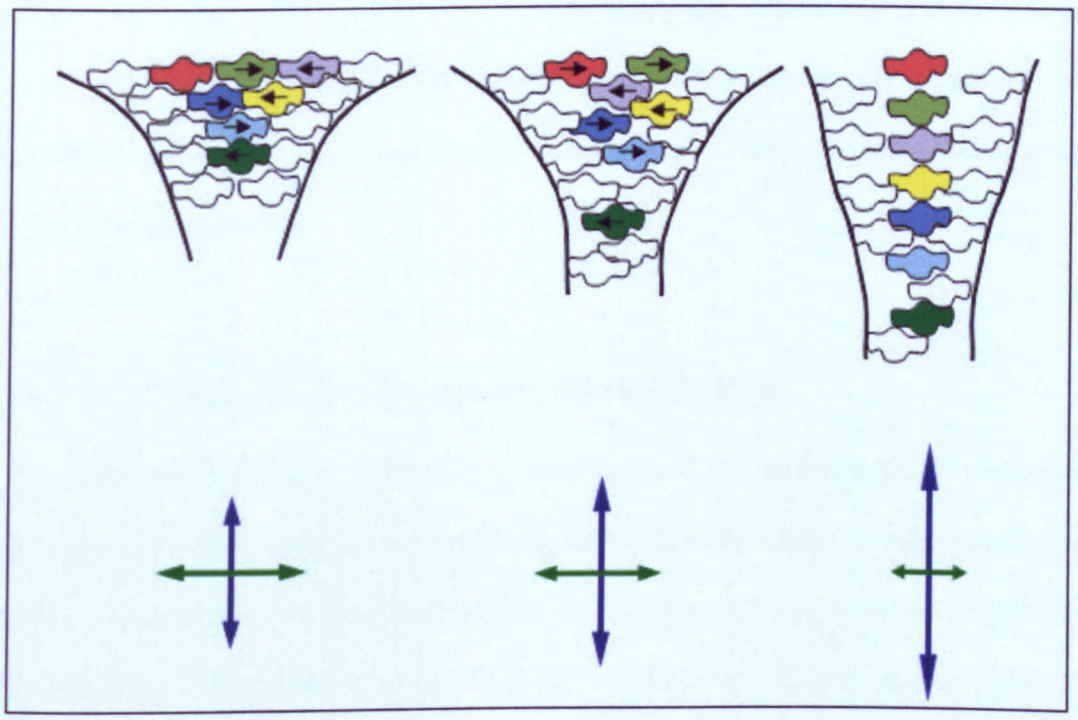

Figure 1-6: Cellular movement during convergent extension.
Convergent extension is a continuous process that occurs throughout the neurulation to remodel the neuroepithelium prior to its closure. During this process, cells on the dorsal surface of the embryo and the underlying mesoderm move towards the midline and intercalate resulting in a narrowing of the medio-lateral axis (green double headed arrow) and lengthening of the anterior-posterior axis (blue double headed arrow). In PCP mutants this process does not occur as effectively, resulting in embryos that are wider in the medio-lateral axis and shorter in the anterior-posterior axis.

The precise molecular mechanism underlying convergent extension remains poorly understood. It has been speculated that asymmetric localization of core PCP molecules is required for the process of convergent extension, but very little has been reported about the distribution pattern of core PCP proteins during CE. In mice, it has been reported that Dishevelled and Ptk7 localises to the plasma membrane of the neuroepithelium during CE, however they do not show an asymmetric distribution (Wang et al., 2006a; Yen et al., 2009). Similarly, in *Xenopus,* Dishevelled shows a symmetric localization to the membrane during convergent extension and lost of this membrane localization leads to defects in CE (Wallingford et al., 2000; Kinoshita et al., 2003). This suggests that the membrane recruitment of Dishevelled is essential for CE in *Xenopus*. Evidence from zebrafish shows that the distribution of Prickled is asymmetric, with its localisation enhanced in the anterior membrane of the notochord and neural keel cells during CE. This asymmetric distribution of Prickled is lost in zebrafish *trilobite* PCP mutants, which display phenotypes that are consistent with a defect in CE and carry a mutation in *Van gogh* (Hammerschmidt et al., 1996; Ciruna et al., 2006).

1.3.5 PCP signalling in *Drosophila* and vetrebrates

Although the majority of the core components of PCP signalling have conserved functions between *Drosophila* and vertebrates, some differences exist. Results from initial studies suggested major differences between the function of some of the PCP genes in *Drosophila* and vertebrates, however with recent data these different have reduced. In *Drosophila*, *off-track* (the homologue of Ptk7) is involved in axon guidance and homozygous mutants have not been reported to exhibit any PCP defects whereas, in mice, the *Ptk7* null is reported to show PCP defects (Winberg et al., 2001; Lu et al., 2004). More recently PCP signalling in mice has also been linked to axon guidance (Vivancos et al., 2009). The mouse *Prickled1* (homologue of *Drosophila prickled*) is described as a gene

that is required for the establishment of apical basal polarity in the epiblast (Tao et al., 2009). However, it has also been reported that a mutation in mouse E3 ubiquitin ligase Smurf1/2, whose targets include Prickled1, leads to defects associated with PCP (Narimatsu et al., 2009). Another difference in the role of core PCP component is displayed by *Scribble*. In *Drosophila, scribble* was originally identified as a gene required for the establishment of apical basal polarity (Bilder and Perrimon, 2000). More recently, *Drosophila Scribble* has been shown to affect PCP signalling and to interact genetically and physically with Vang during the establishment of PCP. *Scribble,* however is not required to establish the asymmetric localisation of Vang and similarly the function of Vang and Fz is not required for its localization (Courbard et al., 2009), suggesting that Scribble is not a core component of PCP signalling. In mouse, the role of *Scribble* in establishment of apical basal polarity has not been reported.

Another core component of *Drosophila* PCP signalling is *diego*. The vertebrate homologue of *diego, Inversin,* is involved in regulating both the canonical and the non-canonical Wnt pathways and co-localises with Dishevelled during zebrafish gastrulation (Simons and Mlodzik, 2008). In mice, it is involved in establishment of the left-right axis and in controlling nodal flow at the node (Morgan et al., 1998). More recently, analysis of the vertebrate homologues of *Drosophila Inturned* and *Fuzzy* (known to be tissue specific downstream effectors of *Drosophila* PCP signalling) have given surprising results. Initial work in *Xenopus* showed that mutation of these genes gave rise to phenotypes that were consistent with a defect in PCP and Hedgehog signalling (Park et al., 2006). Park et al further go on to give evidence that the observed Hedgehog phenotype is a secondary consequence of failure of ciliogenesis in these mutants, therefore providing a link between PCP signalling and ciliogenesis. Roles of *Inturned* and *Fuzzy* are conserved in mice as the mouse mutants of these two genes show similar defects in PCP signalling, ciliogenesis and Hedgehog signalling (Gray et al., 2009).

These differences suggest that although the components of PCP signalling are conserved between vertebrates and invertebrates, the function of some of the proteins have changed during evolution.

1.4 The Hedgehog signalling pathway

Hedgehog signalling is essential for many biological processes involved in embryonic development, such as patterning and regulating the closure of the developing neural tube. In addition this signalling pathway is also active in postnatal life and its misregulation is associated with several types of cancers.

1.4.1 The Hedgehog signalling pathway in *Drosophila*

Hedgehog (hh) encodes a secreted protein that acts as an extracellular morphogen. It was initially identified in a *Drosophila* genetic screen as a segment polarity gene that was involved in patterning and establishing polarity of the larval segments (Nusslein-Volhard and Wieschaus, 1980). Further mutants with similar segmentation phenotypes were identified and through genetic crosses between these mutants it was documented that *hh, patched (ptc), smoothened (smo), fused (fu)* and *cubitus interrupts (ci)* were all part of the same signalling pathway and that *smo, fu* and *ci* function downstream of *ptc* and *hh* (Ingham, 1998). Through various genetic and biochemical studies it was established that Hh binds to the transmembrane protein Ptc, releasing an inhibitory effect on a second transmembrane protein Smo, which then becomes activated and signals through Ci to transduce the Hh signal. Ci is an important component of Hh signalling and can exist as both an activator and a repressor to control the expression of Hh target genes (Methot and Basler, 1999). In the absence of Hh signal, the 155 kDa full length Ci is proteolytically cleaved to produce a 75 kDa repressor form which translocates to the nucleus to repress Hh

target genes (Aza-Blanc et al., 1997). In the presence of Hh signalling, the proteolytic cleavage of Ci is blocked and full length Ci enters the nucleus and acts as the transcriptional activator of Hh target genes (Methot and Basler, 1999). There is evidence to suggest that the full length Ci needs to be modified to become activated, in a Hh dependent manner, however the nature of this modification is currently unknown (Methot and Basler, 1999).

Many years ago, it was clear that regulation of Ci was essential for Hh signalling as indicated by accumulation of full length Ci protein in protein kinase A (PKA) and *Slimb* mutants, which exhibit phenotypes that are consistent with over activation of the Hh pathway (Jiang and Struhl, 1998). This led many researchers to study how Ci processing was regulated. In 1997 it was reported that Ci formed a large cytoplasmic complex involving the Kinesin related protein Costal2 (Cos2) and Fu, and this complex was found to bind to microtubules in the absence of Hh signal but to lose this association in the presence of Hh (Robbins et al., 1997). This result provided a mechanism whereby full length Ci protein is prevented from entering the nucleus, in the absence of Hh signalling. Then it was reported that Slimb targeted Ci for proteolytic cleavage into the repressor form (Jiang and Struhl, 1998) and that phosphorylation of Ci by PKA, Glycogen Synthase Kinase 3 (GSK3) and Casein Kinase 1 (CK1) was essential for the formation of the cleaved Ci repressor form in the absence of Hh (Price and Kalderon, 1999; Jia et al., 2002; Price and Kalderon, 2002). In 2005 it was published that Cos2 was essential for Ci phosphorylation and that it formed a complex with PKA, GSK3 and CK1, in the absence of Hh signalling. Furthermore, it was shown that Hh signalling inhibits the formation of complexes of Cos2 and these three kinases (Zhang et al., 2005). This result, in conjunction with the study reporting a physical interaction between Smo and the Cos2 complex (Lum et al., 2003), provided a mechanism by which Hh regulates the cleavage of Ci by signalling through Smo.

1.4.2 The Hedgehog signalling pathway in mammals

Many core components of the Hh signalling have been conserved between *Drosophila* and mammals; however there are some important differences. The first difference is that many single genes involved in Hh signalling in *Drosophila* have been replaced with multigenic families in mammals. In mammals there are three Hedgehog orthologues, Indian hedgehog (Ihh), Dessert hedgehog (Dhh) and Sonic hedgehog (Shh); two Patched orthologues, Patched homolog-1 and -2 (Ptch1, Ptch2) and three orthologues of Ci, glioma-associated oncogene homolog 1, 2 and 3 (Gli1, Gli2, Gli3). Mouse mutants of all these genes have been studied and reveal that each member of a family has a distinct role. Ihh is required for skeleton morphogenesis (St-Jacques et al., 1999) while Dhh is essential for male gonad development (Bitgood et al., 1996). Shh is the most studied member of the Hh family and is found to be essential for various aspects of mouse embryonic patterning. Mouse mutants of *Shh* show defects in specification and proliferation of the cranial midline, resulting in holoprosencephaly, and limb buds, resulting in narrow limbs with a single digit. *Shh* mutants also have severe defects in the dorsoventral patterning of the neural tube, whereby all ventral cell types, including the floor plate, are missing and the dorsal cell types expand ventrally to occupy the entire neural tube (Chiang et al., 1996). It has become well established over many years that Shh signalling is key for ventral patterning of the neural tube; consequently, the dorsoventral patterning of the neural tube is now commonly used to assess the level of Shh signalling in mouse mutants.

Ptch1 is essential for embryonic development and mouse *Ptch1* mutants die between E9.0 and E10.5. The mutant embryos display neural tube defects, whereby the cranial and the spinal neural tube fail to close, and a severe defect in dorsoventral patterning of the neural tube (Goodrich et al., 1997). In keeping with its role as a negative regulator of Hh signalling, the dorsoventral patterning of the neural tube is opposite to that seen in *Shh* mutants and the ventral cell types are expanded dorsally at the expense of the

dorsal cell types (Goodrich et al., 1997). Despite an essential role of *Ptch1* during embryonic development, *Ptch2* is dispensable for development as the mouse mutants for this gene are viable, fertile and developmentally normal (Nieuwenhuis et al., 2006).

In *Drosophila*, the regulation of Ci is essential for proper Hh signalling. This is also true for mammalian Hh signalling; however, the regulation of three separate proteins is more complicated than that seen in *Drosophila*. It has been shown that the function of Gli1, Gli2 and Gli3 are different. Gli1 functions only as a transcriptional activator, Gli2 mainly functions as an activator but can also have a repressor function, and Gli3 functions primarily as a repressor but also has an activator function (Sasaki et al., 1999; Bai et al., 2004). Similar to the case in *Drosophila,* in the absence of Shh ligand, Gli2 and Gli3 are proteolytically cleaved to produce the repressor form, which inhibits the transcription of Shh target genes. In the presence of Shh ligand, proteolytic processing of Gli2 and Gli3 is inhibited, and the full-length forms are modified to become transcriptional activators and induce the transcription of Shh target genes (Dai et al., 1999; Aza-Blanc et al., 2000).

Mutation in *Gli1* does not result in defective Shh signalling as the mutant mouse is viable, suggesting that Gli1 is not a primary target of Hh signalling (Bai et al., 2002). Gli2 and Gli3 are direct effectors of Hh signalling and mutations in these genes result in multiple disorders including defects in skeletal patterning, craniofacial defects and abnormal dorsoventral patterning of the neural tube (Mo et al., 1997; Matise et al., 1998; Persson et al., 2002) indicating a deficiency in signal transduction from all three Hh ligands.

The importance of proper regulation of Gli proteins is highlighted by the finding that many mutants that affect Shh signalling have an altered ratio of full length Gli3 to cleaved repressor form, the Gli3FL:Gli3R ratio. For example in *Ptch1* mutants, where the Shh signal is over-activated, the repressor form of Gli3 is totally absent; conversely in Smo mutants, where Shh signalling is not active, the level of Gli3 repressor is increased (Huangfu and Anderson, 2005).

Another difference between Hh signalling in *Drosophila* and mammals is that the roles of certain proteins are more prominent while other genes have lost their essential function. Examples include Fu and Sufu. In *Drosophila*, mutation in *fu* results in severe segmental defects, similar to those seen in the *Hh* mutant. In contrast, mutation in *Suppressor of fused* (*Sufu*) results in no phenotype; however, when the two mutations are combined, *Sufu* completely rescues the *fu* phenotype (Preat, 1992). Surprisingly, in mouse the function of *Serine/threonine kinase 36* (*Stk36*, homologue of *Drosophila fu*) is not required for Hh signalling (Chen et al., 2005) whereas a mutation in mouse *Sufu* gives rise to a phenotype that is very similar to that seen for *Ptch1* mutants demonstrating that *Sufu* is a strong negative regulator of Hh signalling in mammals (Svard et al., 2006).

1.4.3 The Hedgehog signalling in mammals takes place in primary cilium

In 2003 two mutants carrying a mutation in genes required for intraflagellar transport (IFT), *Ift88* and *Ift172*, were described as having a defect in Shh signalling (Huangfu et al., 2003). IFT proteins were first described in *Chlamydomonas reinhardtii* as essential components for assembly and maintainance of the flagella (Goetz and Anderson, 2010). Mutations in either *Ift88* or *Ift172* resulted in the absence of an organelle called the primary cilium, suggesting for the first time, the importance of this organelle during Hh signalling (Murcia et al., 2000; Huangfu et al., 2003).

The primary cilium is a microtubule based organelle that projects from the cell surface. The core of the primary cilium consists of a circular array of nine microtubule doublets, which serve as binding sites for microtubule based motors. There are two classes of motors, Kinesin-2 motor complexes and Dynein motor complexes, which are involved in IFT trafficking from the base of the cilium to the tip (anterograde trafficking) and from the tip of the cilium to the base (retrograde trafficking) (Figure 1-7) (Goetz and Anderson, 2010). Kinesin-2 motor complexes consist of three proteins; kinesin family members 3A

and 3B (Kif3A and Kif3B), and kinesin-associated protein 3 (Kap3), and associates with IFT complex B (IFTB) (Goetz and Anderson, 2010). Disruption of anterograde trafficking results in the absence of cilia formation as seen in mouse mutants of IFT88 and IFT172, which are part of the IFTB complex (Murcia et al., 2000; Huangfu et al., 2003). Dynein motor complexes consist of two proteins; dynein cytoplasmic 2 heavy chain 1 (Dync2h1) and dynein cytoplasmic 2 light intermediate chain 1 (Dync2h1), and associates with IFT complex A (IFTA). Disruption in retrograde trafficking results in formation of bulged and short cilia as seen in the *alien* mutant, carrying a mutation in *Ttc21b* (*Thm1*) (Tran et al., 2008).

All examined mouse mutants carrying a mutation in motor complexes or IFT genes have defective Hh signalling and abnormal cilia morphology (Goetz and Anderson, 2010). In general, mutations resulting in a defect in anterograde trafficking have reduced Hh signalling while defects in retrograde trafficking are associated with increased Hh signalling (Goetz and Anderson, 2010). Due to this correlation between defects in Hh signalling and abnormal cilia, several studies have been published which examine the localization of Hh signalling components in the cilia. It has been that shown that all key components of the Hh pathway examined are enriched in cilia. In the absence of Shh, Ptch1 localises to the cilia, preventing Smo entry (Figure 1-7 A). In the presence of Shh ligand, Ptch1 no longer localises to the cilia but Smo is found to be highly enriched in cilia (Figure 1-7 B) (Rohatgi et al., 2007). Furthermore this study also shows that in *Ptch1* mutants, where Shh signalling is constitutively active, Smo localises to the cilia in a ligand-independent manner. This result provides evidence to support the hypothesis that Ptch1 inhibits Smo by blocking its recruitment into the cilia in the absence of Shh ligand and that the localization of Smo to cilia is required for the transduction of Shh signalling, highlighting the importance of cilia in Shh signalling. Gli1, Gli2, Gli3 and Sufu also localise to the tip of the cilia (Figure 1-7) (Haycraft et al., 2005). Additionally, Gli2 accumulates in the cilia in response to the activation of Smo and this accumulation is

necessary to inhibit the cleavage of Gli2 and allow the accumulation of full length activator form in the nucleus (Kim et al., 2009). Ttc21b, Rab23 and Tulp3 are negative regulators of Shh signalling in mice and have recently been shown to be localized in the cilia (Eggenschwiler et al., 2001; Tran et al., 2008; Cameron et al., 2009; Norman et al., 2009; Boehlke et al., 2010). Although the mechanism by which Ttc21b and Tulp3 regulate Shh signalling is largely unknown, there is evidence to suggest that Rab23 is involved in recycling Smo within the cilia and when it is functionally inactive, the speed at which Smo is recycled is reduced (Boehlke et al., 2010).

1.4.4 Shh signalling and neural tube defects

Mouse mutants of many genes involved in Shh signalling have been analyzed and an interesting pattern has emerged involving the level of Shh signalling and the presence of NTDs (Murdoch and Copp, 2010). In mouse mutants where the level of Shh signalling is reduced, for example in *Shh* and *Smo* mutants, NTDs are not present; instead defects in cranial development leading specifically to holoprosencephaly and cyclopia are observed (Chiang et al., 1996; Zhang et al., 2001). Conversely, mutants with ectopic activation of Shh signalling exhibit both cranial and/or spinal NTDs. In *Ptch1* and *Sufu* mutants, both of which are strong negative regulators of Shh signalling, embryos exhibit very severe NTDs, where the entire cranial and most of the spinal neural tube remains open (Goodrich et al., 1997; Svard et al., 2006). Mutants of other negative regulators of Shh signalling, such as *Rab23, Fkbp8* and *Tulp3,* also exhibit cranial and/or spinal NTDs although these are less severely affected than *Ptch1* and *Sufu* mutants and only a proportion of embryos exhibit NTDs (Gunther et al., 1994; Ikeda et al., 2001; Shirane et al., 2008). Interestingly, in *Rab23, Fkbp8* and *Tulp3* mutants, Shh signalling appears to be increased in only the caudal region of the spinal cord and not along its entire length, as indicated by the dorsoventral patterning of the neural tube (Eggenschwiler et al., 2001; Ikeda et al., 2001; Bulgakov et

al., 2004; Wong et al., 2008; Cameron et al., 2009; Norman et al., 2009; Patterson et al., 2009). Although these mutants exhibit cranial NTDs the dorsoventral patterning in the cranial neural tube has not been analysed in these mutants so it is not yet known whether Shh signalling is also increased in this region.

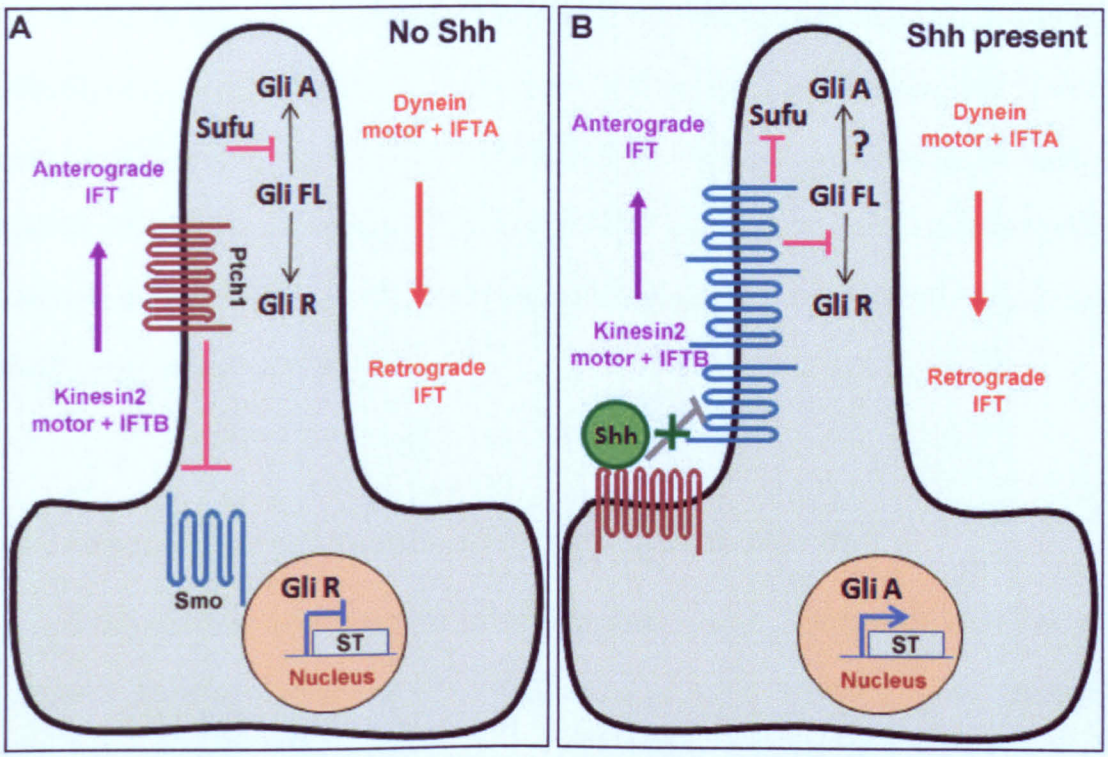

Figure 1-7: Main components of Shh signalling in mice.
(A and B) Shh signalling in mice takes place in primary cilia where Kinesin 2 motor and IFTB complexes are involved in transporting molecules to the tip of the cilia (anterograde IFT) and conversely Dynein motor and IFTA complexes transport molecules out of the cilia (retrograde IFT). (A) In the absence of Shh ligand, Ptch1 (red transmembrane protein) is present in the cilia and inhibits Smoothened (blue transmembrane protein) from entering the cilia. At the tip of the cilia, Sufu inhibits the processing of Gli full length protein (GliFL) to the Gli activator form (Gli A), allowing the processing of GliFL to the repressor form (GliR). GliR exits the cilia and enters the nucleus to inhibit the transcription of Shh target (ST) genes. (B) In the presence of Shh ligand, Shh binds to Ptch1 releasing its inhibitory effect on Smo. This enables Smo to enter the cilia, where it becomes enriched. Smo inhibits Sufu and the processing of GliFL to GliR. GliFL is processed to GliA via unknown mechanism, and GliA leaves the cilia and enters the nucleus to activate the transcription of specific target genes.

The presence of NTDs in mutants of negative regulators of Shh signalling indicates that an increased level of Shh signalling causes NTDs. During spinal neural tube closure the concentration of Shh from the underlying notochord and the floor plate play a role in the formation of DLHPs in the elevating neural folds, whereby the high concentration of Shh in the upper spine inhibits the formation of the DLHPs and low concentration of Shh in mid and caudal spine enables the formation of DLHPs (Ybot-Gonzalez et al., 2002; Ybot-Gonzalez et al., 2007a). In the mutants where the Shh signal is increased, it may result in inhibition of the formation of DLHPs in the mid and the caudal spinal region, which could explain the spinal NTDs observed in these mutants. Indeed this has been observed in *Tulp3*$^{hhkr/hhkr}$ mutant where sections through the caudal spine show reduced DLHPs (Patterson et al., 2009).

1.5 Mouse as models of human neural tube defects

Mice are an invaluable tool for studying the processes underlying neural tube closure and many genes have been identified to regulate this process. However, similar advances in the identification of genes that regulate human neural tube closure have not occurred. This is in part due to the differences between species as well as the ethical boundaries that surround the study of a developmental process in human.

The first difference seen between the mouse and the human neural tube closure is the prevalence of different NTDs. In human, the incidence of anencephaly and spina bifida are approximately equal (Au et al., 2010) however in mouse 90% of NTD mutants exhibit exencephaly (Harris and Juriloff, 2007). This increased susceptibility of mouse to disruption of cranial closure has been attributed to the morphology of the cranial neural tube as mouse embryos have a proportionally larger brain compared to the human embryo, therefore making the elevation of the cranial neural folds more "difficult" (Harris and Juriloff, 2007).

Another difference is the genetic contribution to the neural tube defects in mouse and human. In mice, large numbers of genes are identified as regulating neural tube closure however in human, despite large number of screens, no major causative gene for NTD has been identified (Kibar et al., 2007a). This observation has led to the suggestion that there might not be a major gene involved in human neural tube closure; instead the NTDs risk is likely to be multigenic involving more than one gene in an additive manner to increase the risk of human NTDs.

Additionally, in mice much of the work has been focused in characterising the NTD mutants where a homozygous form of the mutation in a particular gene gives rise to NTD with high penetrance and often these homozygous embryos also display other developmental defects such as abnormal formation of the heart and lungs. This does not represent the common NTDs in human, where the NTDs are not associated with other developmental defects (Harris and Juriloff, 2007). The main reason for this could be that the chance of finding an embryo that homozygous for a mutation in a randomly breeding human population is extremely low, so the majority of the human NTDs cases with a genetic basis are likely to be the result of compound heterozygous mutations. To model this aspect of human neural tube closure, a mouse mutant which gives rise to non syndromic NTDs in a compound heterozygous form with a low penetration would be needed and would represent a strong candidate gene for human NTDs.

1.6 Involvement of core planar cell polarity genes in human neural tube closure

The *loop-tail* mouse, the first PCP mutant identified as carrying a mutation in *Vangl2*, gives rise to craniorachischisis when homozygous and spina bifida, with a low penetrance, when heterozygous (Kibar et al., 2001; Murdoch et al., 2001a). This makes the *Vangl2* gene an extremely good candidate to model the human caudal NTD. In vertebrates,

there are two *Vangl* genes, *Vangl1* and *Vangl2,* both producing very similar proteins. A mouse mutant of *Vangl1* has been reported and was reported to be normal (Torban et al., 2008). Interestingly, embryos that are doubly heterozygous for *Vangl1* and *Vangl2* exhibit craniorachischisis, similar to that seen in *Loop-tail* mutants, suggesting that these two genes can genetically interact during neural tube closure (Torban et al., 2008). Both *VANGL1* and *VANGL2* have been screened in human NTD patients and some mutations were found to be linked to NTDs in both cases (Kibar et al., 2007a; Kibar et al., 2007b). In *VANGL2* three mutations were found to be disease specific; however, none of these mutations were predicted to affect the protein sequence, so how they are increasing the risk of human NTDs remains debatable. It could be hypothesised that these silent mutations may affect the rate of protein translation by changing the codon usage, which may result in reduced protein yield. Studies with *VANGL1* were more successful. Three mutations, all affecting evolutionarily conserved residues, were identified in human NTD patients (Kibar et al., 2007b). Furthermore it was found that one of these mutations (V239I) abolished the ability of VANGL1 to bind to DISHEVELLED, which is required for proper PCP signalling. This study links the PCP signalling to human NTDs and suggests that genes involved in the PCP pathway are good candidates for causing NTDs in a subset of patients.

More evidence for the involvement of PCP signalling in human neural tube defects comes from analysing human fetuses with craniorachischisis, where they present with a reduced anterior-posterior axis, increased mediolateral axis, and a wide/split notochord (Kirillova et al., 2000). These phenotypes are all features of mouse embryos carrying a mutation in a PCP gene (Greene et al., 1998). These observations suggest that the primary defects leading to craniorachischisis may be the same in mice and in human i.e. failure of PCP controlled convergent extension during the shaping of the neural plate.

More recently a screen has identified *PRICKLED2*, homologue of *Drosophila* core PCP component, as a potential modifier of the risk of spina bifida (Wen et al., 2010).

1.7 Shh signalling and human disease

Mutations in many components of Shh signalling have been linked to human development and disease. There are two main classes of defects associated with mutations in the components of Shh signalling. The first class are the developmental defects leading to holoprosencephaly (HPE), Greig cephalopolysyndactyly syndrome (GCPS) and Pallister-Hall syndrome (PHS). HPE results from a midline defect resulting in the failure to divide and form two hemispheres of the brain (Dubourg et al., 2007), GCPS affects the development of limbs, head and face and PHS results in many defects including polydactyly, syndactyly and kidney abnormalities. Mutations in *SHH*, *GLI2* and *PTCH1* are associated with holoprosencephaly (Villavicencio et al., 2000; Ming et al., 2002; Roessler et al., 2003) while mutation in *GLI3* leads to GCPS and PHS (Villavicencio et al., 2000). The second class of defects that are seen in humans harbouring a mutation in a component of the Shh pathway are the tumours of various tissues. PTCH and SMO function as tumour suppressors and their inactivation has been associated with basal cell carcinomas (skin cancer) and medulloblastomas (brain tumours) while the level of GLI1 is increased in tumours such as glioblastomas (brain tumours), osteosarcomas (cancers of the bone), rhabdomyosarcomas (cancers of connective tissue), B cell lymphomas (blood cancer) and basal cell carcinomas (Villavicencio et al., 2000). More recently, germline mutation of *SUFU* has also been linked to medulloblastomas (Brugieres et al., 2010).

Despite large numbers of mouse mutants showing a link between Shh signalling and occurance of NTDs, to date human NTDs have not been linked to any mutation in Shh pathway, again suggesting that there may not be a strong genetic contribution from one gene giving rise to NTDs in human.

1.8 Folic acid and neural tube closure

The link between maternal micronutrient levels in the serum during early pregnancy and the incidence of having babies with NTDs has been known since 1976 (Botto et al., 1999). Since then, multiple clinical trials have shown that women taking folic acid supplements prior to conception reduce the risk of recurrence of NTDs by as much as 50-70% (Padmanabhan, 2006). Although folic acid appear to play a major role in reducing the risk of human NTDs, in most NTD-affected pregnancies, the maternal folate level is within the "normal" range (Greene et al., 2009). This suggests that the low maternal folate level observed in some pregnancies may simply increase the susceptibility to NTDs rather than actually causing it (Greene et al., 2009). In addition, it was found that approximately 50% of the mouse mutants that have been tested, responded positively to folic acid with prevention of 35-85% of NTDs (Harris, 2009). This has led researchers into investigating genes that are involved in the folic acid pathway as candidate genes for human NTDs. Although many genes involved in folic acid metabolism have been studied, only a few have yielded positive results (Kibar et al., 2007a). Furthermore, of the 10 null mouse mutants for genes involved in folic acid metabolism that have been reported, none model the nonsyndromic NTDs observed in human patients (Harris, 2009), questioning the importance and significance of this pathway in neural tube closure.

1.9 Project Summary

In the present study, I have investigated the genetic, cellular and molecular defects leading to neural tube defects in mice. I have analyzed the phenotypes of three different mouse mutants, all exhibiting neural tube defects. *chuzhoi* is a novel allele of *Ptk7*, *Circletail* is a mutant of *Scribble* (Murdoch et al., 2003) and *hitchhiker* is a strong hypomorphic allele of *Tulp3* (Patterson et al., 2009). Phenotypic analysis suggests that the

neural tube defect observed in *chuzhoi* is consistent with a defect in convergent extension and results from failure of closure 1 during neural tube closure. I have shown that a mutation in the gene *Ptk7* is the causative mutation in *chuzhoi* and provide evidence to suggest that *Ptk7* can influence the planar cell polarity signalling pathway although it might not act directly in this pathway. *Scribble* in *Drosophila* is required for establishment of apical-basal polarity and controlling rate of proliferation. Here I have shown that the mouse *Scribble* is not required for establishment of apical-basal polarity or controlling rate of proliferation, during neurulation. *hitchhiker*, carrying a mutation in *Tulp3* also exhibits neural tube defects; however, its molecular function is largely unknown. My work provides evidence to suggest that Tulp3 is not a transcription factor but is involved in many protein-protein interactions, some of which may be of direct relevance to neural tube closure.

CHAPTER 2

MATERIALS AND METHODS

2 Materials and methods

2.1 Mouse lines

All mouse studies were conducted under the guidance issued by the Medical Research Council in 'Responsibility in the Use of Animals for Medical Research' (July 1993) and under the authority of Home Office Project Licence Number 30/2007 or 30/2469.

Loop-tail was imported from the Institute of Child Health (London) (Murdoch et al., 2001a) and was maintained as a congenic line on a C3H/HeH background. *Circletail* arose during construction of a transgenic line but rapidly segregated from the transgene (Rachel et al., 2002) and was maintained as a congenic line on the C3H/HeH background. *Crash* came out of an ENU screen (Curtin et al., 2003) and was congenic on BALB/c background. *Chuzhoi* and *hitchhiker* were derived from a G3 recessive screen at Harwell and were maintained on a C3H/HeH background. *Gli3*^{Xtj} *(Extra-toes)* was obtained from Thomas Theil, Edinburgh University and was maintained on a C3H/HeH background. All these lines were maintained as heterozygous stocks. Outbred strain CD1 was used to provide some wild-type embryos.

2.2 Dissection and tissue collection

Embryos were collected from timed matings between CD1 mice or between two heterozygous animals. Mice were kept in a controlled 12 hour light/dark cycle, where the light cycle begins at 7am and ends at 7pm. Midday on the day of finding a copulation plug was designated embryonic day (E) 0.5. Some mice were kept under a reverse light dark cycle, where the light cycle began at 4pm; under these conditions, midday on the day of finding a copulation plug was designated E1.0. Pregnant females were culled by cervical

dislocation and their uteruses containing the embryos were dissected out by making a small incision on the abdomen. Uteruses were dissected in 10% newborn calf serum in phosphate buffered saline (PBS) and embryos were dissected out under a Leica MZ6 dissecting microscope. For mutant litters, extra-embryonic membranes were removed and kept for genotyping. The somite number of the embryo was counted to determine the developmental stage of the embryo. Embryos past mid-gestation (E10.5) were terminated by decapitation or by immersion in ice cold fixative, as permitted under Home Office guidelines. Embryos were then rinsed in PBS and were collected for various experiments as described below.

2.2.1 Embryos for whole mount *in situ* hybridisation (WMISH)

E7.5 to E10.5 embryos were fixed in ice cold 4% paraformaldehyde (PFA) in PBS, overnight at 4°C on a rocking platform, washed twice in PBS at room temperature, dehydrated through methanol series of increasing concentration of 25%, 50%, 75% and 100% and were stored in 100% methanol at -20°C. Methanol series was made up in PBT (PBS plus 0.1% Tween-20).

2.2.2 Embryos for cryo-sections

E8.5 embryos and the caudal ends of E10.5 embryos were fixed in cold 4% PFA for 1 hour at 4°C, washed twice with PBS at room temperature, and cryo protected in 30% sucrose overnight at 4°C. Embryos were embedded in optimum cutting temperature (OCT) for transverse sections and frozen in dry ice. Sections were generated by the histology facility at Harwell. Sections were collected on charged slides.

2.2.3 Embryos for wax-sections

E8.5 embryos were fixed in cold 4% PFA, overnight at 4°C on a rocking platform, washed twice in PBS at room temperature and dehydrated in Industrial Methylated Spirit (IMS) of increasing concentration (30%, 50% and 70%) and were stored at 70% IMS at

room temperature (RT). Each wash and dehydration step was 10 minutes. Embryos older than E10.5 were terminated by decapitation under Home Office guidelines and were fixed in cold 4% PFA for one week at 4°C on a rocking platform. They were then washed twice in PBS at room temperature and dehydrated through an IMS series to 70% IMS. Each wash and dehydration step was 1 hour. Embryos stored in 70% IMS were processed for wax embedding and sectioning as described in section 2.13.

2.2.4 Fetuses for *chuzhoi* lung analysis

E18.5 embryos were terminated by decapitation under Home Office guidelines. The chest cavity was opened and the intact lungs were dissected out and examined for morphological defects. Each of the five lobes was separated and photographed using a Leica MZ16 microscope with a DFC420 camera attachment (Leica). For sections, lungs were fixed in cold 4% PFA, overnight at 4°C on a rocking platform, washed twice in PBS at RT and dehydrated through an IMS series and stored at RT in 70% IMS. Each wash and dehydration step was 10 minutes. Lungs stored in 70% IMS were processed for wax embedding and sectioning as described in section 2.13.

2.2.5 Embryos for oligreen staining

E8.5 and E8.0 embryos were fixed in cold 4% PFA and stored at 4°C.

2.2.6 Fetuses for interaction studies

E11.5 to E13.5 embryos were dissected in cold PBS. Gross phenotype was recorded. Those with a phenotype and the littermate controls were fixed in cold 4% PFA overnight at 4°C others were terminated by decapitation under Home Office guidelines.

2.2.7 Embryos for measuring embryo dimensions

Fresh E8.5 embryos (somite number 3-7) were flat mounted on a slide with a coverslip. Dabs of silicon grease at the corners of the coverslip were used to prevent the

coverslip from moving and to protect the embryo. The coverslip was gently pushed down on the silicon grease until it just touched the embryo to hold it in place. Photographs were taken using a Leica MZ16 microscope. Images were printed out and length and width measures were made using a ruler.

2.2.8 Embryos for protein and RNA extraction

Embryos ranging from E7.5 to E17.5 and adult tissue were frozen in dry ice and stored at -80°C.

2.3 Genotyping

Yolk sac and ear biopsies were digested in 50 µl of lysis buffer (0.05 M Tris-HCl pH 8.5, 1 mM EDTA pH 8.0 and 0.5 % Tween–20) and 5 µl of 10 mg/ml proteinase K (PK) at 55°C for 2-4 hours. PK was denatured by heating to 95°C for five minutes and 1-3 µl of digest was used for genotyping by PCR. *chuzhoi, hitchhiker, Loop-tail, Circletail* and *Crash* mice were genotyped using single nucleotide polymorphism (SNP) based allele determination by pyrosequencing assays (PCR conditions and primer sequence given in Table 2-1). Assays for *chuzhoi, Loop-tail, hitchhiker* and *Crash* genotype the mutated base directly while two SNPs flanking the mutation were used to genotype *Circletail.*

Extra-toes was genotyped using primer pairs that detect 51.5 kb deletion in the *Gli3* gene. This deletion gives rise to the *Extra-toes* phenotype. Two pairs of primers are used to genotype *Extra-toes* in the same PCR reaction. First set of primer is designed within the deletion to give a product size of 193 bp from the wildtype chromosome and the second set of primers is designed spanning the deletion breakpoints to give 580 bp from the mutant chromosome (Maynard et al., 2002). The second pair of primers can also anneal to the wildtype DNA but since the forward and reverse primers are designed to anneal at either ends of deletion points (of 51.5 kb) an amplification of this size is not possible during the

PCR (PCR conditions and primer sequence given in Table 2-2). PCR was carried out as described in section 2.6 and examined on 3% agarose gel as described in section 2.7.

2.4 RNA extraction

Total RNA from whole E7.5 to E17.5 embryos, adult tissues (liver, kidney, testis, and brain) and caudal ends of E9.5 embryos was extracted using the GenElute™ Mammalian Total RNA Purification Kit (Sigma) according to the manufacturers' instructions. Briefly, samples were lysed and homogenized in lysis buffer containing guanidine thiocyanate and 2-mercaptoethanol. Guanidine thiocyanate is a strong protein denaturant which releases RNA and 2-mercaptoethanol inactivates RNases by reducing their disulfide bonds which leads to conformational changes in the protein. For smaller tissue sample (E7.5-E12.5) 500 µl of lysis buffer was added and the tissue was passed through a 14G needle 10 times to break up the tissue. Lysates were then passed through a QIAshredder spin column (Qiagen) to homogenize the sample. With bigger samples (E13.5 – E17.5 and adult tissue) 1 to 3ml of lysis buffer was added and the tissue was homogenised using a 230V Ultra-Turrax T25 basic homogeniser. The lysate was filtered through a filtration column to remove cell debris and shear genomic DNA. Ethanol was added to the filtrate and mixture was applied to a high capacity silica column to bind total RNA. Contaminants were washed away and RNA was eluted in 50 µl of RNAse free water. The concentration of RNA was determined by absorbance at 260 nm using a NanoDrop ND-1000 spectrophotometer (Thermoscientific).

Table 2-1: Details of pyrosequencing assays used to genotype mouse lines.

Assay	Forward	Reverse	Sequencing	PCR program	Product size	Allele (WT/ Mut)
chuzhoi	NNNGGATGGCCCTGCCTCTTTCT	*GGAGGTGGCGTGAACTTGAG	CCTCCTCTCTTTCCCA	1	89 bp	A/G
hitchhiker	TGCAATTAGCCCATGGTAAC	*GCGACTCCTAAGTTCACACAGTA	GCTGAAGCTGGACAATC	1	264 bp	T/A
Loop-tail	*GTCCTGGCGCTTCAAGAGGA	NNNGGCCAAACAGTGGACCTTGG	CAGTGGACCTTGGTGA	1	87 bp	C/T
***Circletail* 76**	*GACAGTGGGCAAGGCTGACA	NNNGGCTGCACTTGTCGCTCAGA	GCTCAGAGGACTCTCATC	1	93 bp	A/C
***Circletail* 88**	NNNCATTGGAAAACATGGGGAGGA	*AGCATCAGGGACAGGCAAGG	AAAACATGGGGAGGAC	1	98	C/T
Crash	NNNGAGAACAGCCCTGTGGGTTCA	*CATTGCCCTCCACGATCTGA	GAATAAGGGCCAACG	1	111 bp	A/G

* denotes biotin label
PCR Program 1: 95°C for 5 minutes [95°C for 15 seconds, 62°C for 30 seconds, 72°C for 15 seconds] x 38 cycles, 72°C for 5 minutes

Table 2-2: Details for genotyping Gli3 mice.

Primer	Forward	Reverse	PCR program	Product size	Allele
Gli3-C3	GGCCCAAACATCTACCAACACATAG	GTTGGCTGCTGCATGAAGACTGAC	2	193 bp	C3H (WT)
Xt^J-580	TACCCCAGCAGGAGACTCAGATTAG	AAACCCGTGGCTCAGGACAAG	2	580 bp	Xt^J

PCR Program 2: 95°C for 5 minutes [95°C for 30 seconds, 67.2°C for 30 seconds, 72°C for 1 minute] x 35 cycles, 72°C for 5 minutes

2.5 cDNA synthesis

cDNA was synthesised using Moloney Murine Leukamia Virus (M-MLV) reverse transcriptase (Invitrogen). 0.5 - 1 μg of total RNA, isolated as describe in section 2.4, was mixed with 0.2 μg of random hexanucleotides (Invitrogen) and denatured by heating at 70°Cfor 10 minutes. The mixture was cooled on ice and spun to collect all the reaction mix at the bottom of the tube. 1 X First Strand Reaction Buffer (Invitrogen), 10 mM of each dNTPs and 0.01 M of Dithiothreitol (Invitrogen) was added to the reaction and mixed briefly by vortexing. The reaction was made up to 20 μl by addition of 20 units of RNAse inhibitor (Sigma), 200 units of M-MLV reverse transcriptase (Invitrogen) and RNAse free water. To synthesise cDNA, the reaction was incubated at 37 °C for one hour then was stopped by cooling on ice and addition of 80 μl of RNAse free water. This was stored at -20 °C and 1 μl was used in a PCR. For each cDNA synthesis reaction, a negative control with no reverse transcriptase was set up in parallel.

2.6 Polymerase chain reaction (PCR)

A wide variety of primer pairs and conditions were used to amplify sequences from genomic DNA and cDNA. Primers were designed using Primer3 software (http://frodo.wi.mit.edu/primer3/) and were synthesised by Sigma. Unless otherwise stated, all PCR was performed as 20 μl reactions and consisted of 1 X Buffer with 1.5 mM magnesium chloride (Abgene), 0.0125 mM of each dNTP (Roche), 0.4 μM of each primer, 0.7 units of Thermoprime Polymerase (Abgene) and ~ 25 ng of DNA. PCR reactions were carried out using a Tetrad thermocycler (MJ Research) or a G-storm thermocycler (GRI). DNA and primers were initially denatured at 95°C for 5 minutes, then were subjected to 30-40 cycles of 95°C for 15 seconds, annealing at 55 - 65°C for 30 seconds and extension at 72°C for 15 seconds to one minute; the program was finished with a final extension at

72°C for 5 minutes. Specific conditions for each of the primer pairs and the primer sequences are stated in the Appendix.

2.7 Gel electrophoresis

PCR reactions and RNA extractions were analysed by gel electrophoresis using 0.5-4% agarose (Sigma) : TBE (Biorad) gels containing either 0.001% ethidium bromide or 1 X SybrSafe (Invitrogen). Loading buffer containing 1 X TBE, 25% glycerol and orange G or Bromophenol blue was added to the sample prior to gel loading. To estimate the size of the PCR products being generated, a DNA ladder (500-12,000 bp: 1kb DNA ladder mix or 100-12,000 bp: 1kb Plus DNA ladder mix; both from Invitrogen) was also run. DNA or RNA was electrophoresed at 90 to 110 voltages for 30-40 minutes. DNA or RNA was visualised by using an Ultra Violet (UV) gel doc system (Biorad).

2.8 PCR Purification

PCR products generated from PCR reaction were purified using QIAquick PCR purification kit (Qiagen), according to the manufacturer's instructions. Briefly, PCR reaction was applied to a column containing a silica membrane in the presence of high salt concentrations, up to 10 μg of DNA of 100 bp to 10 kb can bind to the silica membrane while other components of the PCR reaction such as excess primers and enzyme pass through the membrane and can be discarded. The membrane containing the DNA is washed to remove any salt using washing buffer containing ethanol and DNA is then eluted in 50 μl of distilled water. The concentration of purified PCR product was determined by absorbance at 260 nm using NanoDrop ND-1000 spectrophotometer.

2.9 Sequencing

To get sufficient PCR product for sequencing, three 20 μl PCR reactions were performed for each primer pair. To make sure that all three reactions worked with the same

efficiency, a 5 µl aliquot was removed and run on 1% agarose gel. Three reactions were then combined and the PCR product was purified using the Qiaquick PCR purification kit from Qiagen, as described in section 2.8. The purified PCR product was used for sequencing by either GEMS (MRC Harwell) or Geneservice (http://www.geneservice.co.uk/services/sequencing/).

GEMS Core sequencing

Sequencing reactions were carried out as a 10 µl reactions as follows; 5 ng of PCR product was mixed with 2 µl of Big Dye (ABI) and 1 µl of 5 mM primer (that was used to amplify the PCR fragment). This was done with both the reverse and forward primers. The PCR conditions for sequencing involved initial denaturation at 94°C for 2 minutes, then 25 cycles of 94°C for 10 seconds, annealing at 50°C for 5 seconds, and extension at 60°C for 4 minutes. The reaction was precipitated by adding 10 µl of AnalaR water, 2 µl of 3 M sodium acetate and 50 µl of freshly aliquotted 100% ethanol. The reaction was incubated at room temperature for 15 minutes and was centrifuged at 2,000 g for one hour. The plate was inverted and centrifuged for 1 minute at 60 g. The sequencing product was given to the GEMS core for electrophoresis through ABI3000.

Geneservice

Geneservice carries out high throughput sequencing using an Applied Biosystems 3730 DNA Analyzers. PCR fragments and sequencing primers were sent by courier and sequences returned by e mail.

The result was analysed using NCBI blast and sequence alignment tools.

2.10 Cloning

2.10.1 TA cloning

PCR product was generated and purified as described in sections 2.6 and 2.8 and was ligated into a pGEM®-T Easy vector (Promega) according to manufacturer's instructions. Briefly, 50 ng of vector was combined with a 3 fold molar excess of PCR product in presence of 1 X Rapid Ligation Buffer and 3 units of T4 DNA ligase. Reaction was made up to the final volume of 10 µl by addition of ddH_2O (BDH) and was incubated either RT for 1 hour or at 4 °C overnight. This kit works on the principle that when the DNA is amplified by Taq polymerase during PCR, an 'A' overhang on the 3' end of DNA is produced. pGEM®-T Easy vector is a linear vector, with a 'T' overhang at the 5' terminal. So when the PCR product and the vector are combined the 'A' overhang and 'T' overhang hybridize and the DNA ligase seals the backbone of the DNA, resulting in insertion of the PCR product into the vector. 2 µl of ligation reaction was used during transformation.

2.10.2 Transformation

Electro-competent *Escherichia coli (E. coli)* cells (DH5α strain) and chemically competent *E.coli* cells (Top10, Invitrogen) were used for transformation. To ensure the viability of the electro-competent cells, eppendorfs and cuvettes used for the process were chilled on ice. 1 µl (~50 ng) of DNA or 2 µl of ligation reaction was pipetted into a chilled eppendorf. An aliquot of electro-competent *E. coli* cells were removed from -80 °C freezer and thawed on ice. For each transformation, 20 µl *E. coli* was added to the DNA, gently mixed by pipetting up and down, then quickly pipetted into a chilled cuvette. The outside of the cuvette was wiped clean of water/ice and was inserted between the electrodes in an electroporation chamber (Bio-rad). The electroporation was performed at 1.8 kvolts for 4 –

5 milliseconds; immediately 1 ml of Luria broth (LB) was added to the cuvette and was inverted to mix. To recover the cells, the suspension was transfered to a sterile tube and incubated with shaking at 37°C for one hour.

Chemically competent cells (Top10 Invitrogen) were removed from -80 °C freezer and were left to defrost on ice. 2 µl of ligation reaction or purified plasmid was added to 25 µl of cells and left to incubate on ice for 5 to 30 minutes. For transformation, the cells were heat shocked for 30 seconds in a 42 °C water bath. Immediately, cells were transferred back to ice and 250 µl of SOC medium (Invitrogen) was added to the cells. Cells were left to recover by incubating on a shaking platform at 37 °C for one hour.

To prepare the plates, LB agar was melted in a microwave and cooled to 55 °C before the addition of either 50 µg/ml ampicillin, 30 µg/ml kanamycin or 25 µg/ml zeocin, as appropriate. The agar was poured into sterile plates and then left to cool and set. To ensure well separated colonies, 10 µl and 100 µl of the culture was plated onto different plates and incubated overnight (O/N) at 37°C; the remainder of the culture was stored at 4°C.

2.10.3 Plasmid midipreparation

A single colony was picked from the LB agar with appropriate antibiotic plates using a sterile pipette tip, and inoculated into 5 ml LB with appropriate antibiotic. Cells were incubated at 37°C on a shaking (225 rpm) platform for six to eight hours. 100 µl of this starter culture was used to innoculate 35 ml of LB with appropriate antibiotic and cultured overnight on the shaking platform. Plasmids were purified from cultures using the Qiagen or Invitrogen midiprep kit according to manufacturer's instructions. The concentration of the DNA was determined by absorbance at 260 nm using a NanoDrop ND-1000 spectrophotometer.

2.11 *Riboprobe generation*

2.11.1 Plasmid linearization

10 µg of plasmid was digested with an appropriate restriction enzyme (Table 2-3) in a total volume of 200 µl, the completion of the digest was assayed by agarose gel electrophoresis of 1 µl of the reaction. DNA was precipitated by adding 1/20 vol 3M Sodium acetate and 2 volume of ethanol, and incubated at -20°C for 1 hour. This was then centrifuged at 15,000 g for 10 minutes at 4°C and precipitated salt was washed off with 200 µl 70% EtOH. The pellet was air dried and resuspended in 10 µl of RNAse-free water.

Table 2-3: RNA probes used for *in situ* hybridization

Probe	Linearization enzyme	RNA Polymerase	Description of template	Reference
Shh	*Hind*III	T3	Nucleotide 200-850 bp of *Shh* cDNA	(Echelard et al., 1993)
Brachyury	*Bam*HI	T7	Full length cDNA (~1.7 kb)	(Rivera-Perez and Magnuson, 2005)
Nodal	*Xho*I	T3	Nucleotide 330-660 bp of *Nodal* cDNA	(Conlon et al., 1994)
Ptk7	*Sal*I	T7	Nucleotide 981-1799 bp of *Ptk7* cDNA	
Sox10	*Sal*I	T7	Full length cDNA (~2.3 kb)	(Southard-Smith et al., 1998)
BC037112/ Fam193a	*Aat*II	SP6	Nucleotide 766-1332 bp of *BC037112/ Fam193a* cDNA	
Nup155	*Aat*II	SP6	Nucleotide 116-593 bp of *Nup155* cDNA	
Ibrdc1	*Aat*II	SP6	Nucleotide 27-602 bp of *Ibrdc1* cDNA	
Ktn1	*Aat*II	SP6	Nucleotide 514-1013 bp of *Ktn1* cDNA	
Tnks2	*Aat*II	SP6	Nucleotide 136-703 bp of *Tnks2* cDNA	
Rgnef	*Spe*I	T7	Nucleotide 118-705 bp of *Rgnef* cDNA	

2.11.2 Riboprobe synthesis

Digoxigenin (DIG) RNA labelling kit from Roche was used to label the probe. All the reagents used in this protocol are RNAse free. 20 µl reactions were set up with 1 x transcription buffer, 2 µl of DIG labelling mix, 1 µg of linearised plasmid, 20 Units of RNAse inhibitor and 10 Units of Sp6, T7, or T3 RNA polymerase (Table 2-3). The reaction was incubated at 37°C for 2 hours. The efficiency of the probe synthesis was tested by removing 1 µl aliquot and running on 1% agarose/TBE gel. The RNA band should be ~10X more intense than the plasmid band, indicating ~10 µg probe synthesised. The probe was precipitated by adding 100 µl TE, 10 µl of 4M LiCl and 300 µl EtOH. Reaction was mixed and incubated at -20°C for 2 hours or until needed. Final stage of probe synthesis included, centrifuging in a microfuge at 15,000 g for 20 minutes at 4°C and washing the pellet with ice-cold 70% EtOH to remove salt. The pellet was immediately resuspended in 100 µl of TE (RNAse free). The pellet was not allowed to dry as RNA is very difficult to redissolve once it is dry. For hybridisation mix, 10 µl probe per ml was used.

2.12 *Whole mount in situ hybridisation*

This protocol was designed to be used in 12 well disposable plastic plates.

2.12.1 Embryo pre-treatment and hybridisation

Embryos were rehydrated by taking them back through the methanol series (75%, 50%, 25% MeOH in PBT) followed by two washes in PBT (PBS with 0.1% tween 20). To inactivate endogenous phosphates, embryos were bleached in 6% Hydrogen peroxide (H_2O_2) in PBT for 1 hour, then washed in PBT three times. To allow the probe to penetrate, embryos were incubated in proteinase K (PK) at 10 µg/ml in PBT, at room temp

for 15 minutes. PK was inactivated by a five minute wash in freshly prepared glycine (2 mg/ml in PBT), then embryos were washed twice in PBT. Embryos were post-fixed in fresh 0.2% glutaraldehyde in 4% PFA in PBS for 20 minutes, washed twice in PBT then incubated in prehybridisation solution (50% formamide, 5X SSC pH 4.5, 50 µg/ml yeast tRNA, 1% SDS and 50 µg/ml heparin) at 70°C for at least 2 hours. Embryos were then hybridised, with prehybridisation solution containing 10 µl labelled riboprobe (~1 µg probe; Section 2.11.2), at 70°C overnight.

2.12.2 Post-hybridisation washes

Most of the hybridisation solution was removed and stored at -20°C for future use. (Hybridisation solution was reused twice). To remove non-specific binding, embryos were washed twice with solution 1 (50% formamide, 5X SSC pH 4.5 and 1% SDS) at 70°C, 30 minutes each and twice with more stringent solution 2 (50% formamide, 2X SSC pH 4.5 and 1% SDS) at 70°C, 30 minutes each. To prepare the embryos for blocking, they were washed three times with Tris-buffer saline tween-20 (TBST) (0.14 M sodium chloride, 3 mM potassium chloride, 25 mM Tris-HCl pH 7.5, 1 % Tween-20 and 1 mg/ml levamisole) for 5 minutes each at RT. Blocking was achieved by incubating embryos in 10% sheep serum in TBST for 60-90 minutes, with rocking at RT.

2.12.3 Preperation of embryo powder

E12.5-E14.5 embryos were collected and homogenised in a minimum volume of PBS. To dehydrate the tissue, four volume of ice-cold acetone was added to the homogenised tissue and the mixture was incubated for 30 minutes on ice. To separate the tissue from solution, the mixture was centrifuged for 20 minutes at 15 000 g. The supernatant was removed and the pellet was washed with ice-cold acetone. To pellet the tissue, the mixture was again centrifuged for 20 minutes at 15 000 g and the supernatant

was removed. The pellet was spread out on filter paper and ground into a fine powder. This was left to air dry. This embryo powder was stored in an air tight tube at -20°C.

2.12.4 Antibody preperation

1ml TBST was added to ~ 5 ng of embryo powder and heated at 70°C for 30 minutes. This was centrifuged at 15,000 g for 5 minutes, the supernatant was discarded and the pellet of embryo powder was chilled on ice. 1 ml of 1% sheep serum in TBST and the required volume of anti-DIG conjugated with alkaline phosphatase (AP) antibody (0.5µl per ml of final volume of 1% sheep serum required) were added to the embryo powder pellet and left to shake gently at 4°C for 1 hour to preabsorb the antibody. To remove the embryo powder, the tube was spun at 15,000 g and the supernatant was made up to the required volume in 1% sheep serum. To allow the binding of the antibody to the probe, the embryos were incubated in 1% sheep serum in TBST with preabsorbed antibody at 4°C overnight or over the weekend.

2.12.5 Post-antibody washes

To reduce non-specific antibody binding, embryos were washed three times with TBST for 5 minutes each and an additional five times for one hour each, then left rocking overnight or over the weekend in TBST at 4°C.

2.12.6 Developing

To prepare for the colour reaction, embryos were washed three times with alkaline phosphatase buffer (NTMT; 100 mM NaCl, 100 mM Tris-HCl pH 9.5, 50 mM $MgCl_2$ and 0.1% Tween-20) for 10 minutes each. They were then transferred to glass containers, as the colour reagents precipitate in plastic vessels. To allow the colour reaction to develop embryos were incubated in NTMT including Nitro-Blue Tetrazolium Chloride (NBT) and 5-Bromo-4-Chloro-3'-Indolyphosphate p-Toluidine Salt (BCIP) in a light-tight box. Embryos were checked frequently and once the signals were strong enough the colour

reaction was stopped by two washes in PBT; this could take between 30 minutes and 4 days. The embryos were left to wash overnight at RT in PBT.

2.12.7 Fixing and sectioning.

Embryos were refixed in 4% PFA in PBS for 1 hour at RT, then transferred back to PBT. Pictures were taken using a dissecting microscope and sectioning was either performed by the histology facility at Harwell for wax or cryosections or the embryos were processed for vibratome sectioning (section 2.12.8). Embryos that were not sectioned immediately were stored in 0.4% PFA in PBS at 4°C.

2.12.8 Vibratome sectioning

Embryos in PBT were coated with vibratome embedding mixture (0.56% Gelatine, 33.75% Albumin and 22.5% Sucrose in PBS). Depending on the size of the embryo, an appropriate embedding mould was filled with the embedding mixture and the embryo coated in the mixture was transferred to the side of the mould. To enable the mixture to set, 1/10 volume of 25% glutaraldehyde solution was added to the embedding mixture in the mould and was mixed thoroughly with a pipette tip. Immediately, the embryo was transferred into the mould and orientated as required. Blocks were allowed to set for at least 30 minutes before sectioning. If the sectioning was not done immediately, the blocks were immersed in PBS and stored at 4°C for several weeks. For sectioning, blocks were removed from the moulds and trimmed into a pyramid shape and mounted onto the mounting block with a drop of superglue. The mounting block was inserted into the vibratome (Leica VT 1000S) and sectioned at 40 µm. Sections were collected on glass slides and mounted with 50% glycerol/PBT mixture under a coverslip. Pictures of the sections were taken under DIC optics using a Zeiss AxioCam HRc camera attached to a Zeiss AxioPhot 2 microscope.

2.13 Wax embedding and sectioning

Embryos from the age of E10.5 were given to the Histology facility at Harwell to be further dehydrated and embedded in wax. Samples in 70% IMS were put in a Thermo Shandon tissue processor and were processed to 100% wax. All steps were performed under vacuum which ensures that wax penetrates the tissue. Embryos younger than E10.5 were hand processed to wax. Embryos in 70 % IMS were further dehydrated in 90% IMS for 20 minutes followed by three 30-minute washes in 100% Ethanol. Embryos were then transferred to a glass container as Histoclear used in the subsequent step melts plastic. To clear the embryo and allow wax penetration, they were washed twice in Histoclear (National Diagnostics) for 20 minutes each followed by a 30 minute incubation in 1:1 Histoclear:Wax mix in a 60°C oven. To make sure that wax fully penetrated the tissue, embryos were incubate in 100% molten wax three times for 30 minutes each in a 60°C oven. Final wax was removed and fresh wax was added before orientating the embryo under a dissecting scope (Nikon SMZ -U) to give either transverse or sagittal sections through embryo. The wax was allowed to set on ice. Once the wax was set, the glass container containing the embedded embryos was removed from ice and left to set further in room temperature over night or until required. To prepare for sectioning, the wax block containing the embryo was removed from the glass dish and was trimmed to create a pyramid shape block with a wide base and a narrow top where the embryo was orientated. This was done under a microscope as it is possible to see the embryo. The block of wax with the embryo was mounted onto a cassette which fitted into the microtome (Microm Heidelberg HM 320) and was sectioned with various thickness required for different experiment. For slide *in situ* hybridisation 12 μm sections were collected on RNAse-free polysine treated slides. For *chuzhoi* heart and lung histological staining 12 μm sections were collected on standard slides. For PPH3 immuno-histochemistry and E8.5 histological staining 5 μm sections were collected on charged slides.

2.14 Slide *in situ* hybridisation

E12.5, E14.5 and E16.5 embryos were embedded in wax and sectioned as described in section 2.13. Sections were collected on RNAse-free slides by floating on RNAse-free water. PBS, ddH_2O and 5 M NaCl used during prehybridisation steps were treated with 0.1% diethylpyrocarbonate (DEPC) overnight to inactivate all RNAse, then autoclaved to degrade the DEPC. Glassware and metal racks used in the experiment were wrapped in foil and baked at 200 °C for at least four hours to inactivate RNAse. All steps in this experiment were performed at room temperature unless otherwise stated.

2.14.1 Pre-hybridisation treatments

Sections were dewaxed and rehydrated by washing twice in Histoclear for 10 minutes each followed by three washes of 100% ethanol for three minutes each and IMS series of reducing concentration for two minutes each (90%, 70% and 50% IMS). Sections were then washed in PBS for two minutes before they were fixed in 4% PFA in PBS for 20 minutes. PFA was removed by two washes in PBS for two minutes each. To allow the probe to penetrate the tissue, slides were incubated in 20 μg/ml proteinase K (PK) in PBS, for eight minutes. Since PK partially digests the tissue, to avoid further damage to the tissue in the remainder of the protocol, it was refixed in 4% PFA for five minutes followed by two washes in PBS for two minutes each. Since RNA probes are negatively charged it is essential to remove any positive charge that is found in the tissue, to reduce the background signal. To do this, the rack containing slides was immersed in 0.1 M triethanolamine and 1 ml of acetic anhydride was drizzled over the slides, and the solution was magnetically stirred for 10 minutes. Acetic anhydride reduces positive charge by acetylation of the positively charged amino groups in the proteins present in the tissue. Slides were then washed in PBS twice for two minutes each and were dehydrated in IMS

series (50%, 70% and 90%) followed by three washes in 100% ethanol. For each slide, 1 µl/ml of RNAse inhibitor, 0.5 mg/ml yeast tRNA and 0.1 µg of RNA probe was added to 60 µl of HybMix (50 % deionised formamide, 0.3 M NaCl, 20 mM Tris-HCl pH 7.5, 5 mM EDTA pH 8.0, 10% dextran sulfate and 1 x Denhardts solution). This was denatured by heating to 70 °C for 10 mins, quenched on ice and applied to the slides. To have an even spread of the HybMix on the slide, a clean glass coverslip was placed on the HybMix. Slides were placed horizontally into a baked metal rack and placed in a humidified chamber (tissue soaked in 50% formamide in 2 x SSC (0.6 M sodium chloride and 30 mM tri-sodium citrate dihydrate, pH 7.0)) and hybridised overnight at 70°C in an oven placed in a fume hood.

2.14.2 Post-hybridisation washes

To get the coverslips off of the slides, the rack containing the slides was placed in warm 2 X SSC for 15 minutes and gently lifted up and down a few times during this incubation. Non-specific binding of the probe was washed away by incubating slides in 50% formamide in 2 x SSC, twice for 20 mins each, followed by two 30 minutes washes in 2 x SSC, and two additional 30 minute washes in 0.2 x SSC. All solutions used in these washes were heated to 70°C in a water bath and the incubations were performed in a 70°C oven. After the last incubation, 0.2 x SSC with slides was removed from 70 °C oven and was left to cool down to room temperature. Slides were then washed in buffer B1 (0.1M TrisHCl pH 7.6, 0.15 M NaCl) twice for 5 minutes each and were blocked for 1 hour using 10% Newborn Calf Serum in buffer B1. Anti-DIG antibody (Roche) was prepared in 2% Newborn Calf Serum in buffer B1. This antibody was used at 1:1000 dilution. 300 µl of antibody mix was applied to each slide in a humidified chamber and even spread was ensured by applying coverslip of parafilm. Applying parafilm coverslip also prevented the sections from drying out. Slides were incubated overnight at 4 °C.

2.14.3 Antibody detection and colour development

Parafilm coverslips were gently removed and slides were put back in a rack. To remove unbound antibody, slides were washed three times with buffer B1 followed by two washes in buffer B2 (0.1 M Tris-HCl pH 9.5, 0.1 M NaCl) for 10 minutes each. To allow the colour reaction to develop, slides were placed in a light-tight humidified chamber and 0.5 ml of 1 in 50 dilution of NBT/BCIP mix (Roche) was applied to each slide. This was left to incubate at room temperature and colour development was monitored every few hours. If the colour development was not strong enough by the end of the day, the reaction was left at 4°C over night. Once the development was complete, slides were put back into rack and reaction was stopped by standing a trough containing the slide rack under running tap water for 10 minutes. Slides were then dehydrated through IMS series (50%, 70% and 90% IMS) followed by 3 washes in 100 % ethanol. Each dehydration step was 10 seconds, as the stain is soluble in alcohol. Slides were placed in Histoclear, twice for five minutes 5 each and were mounted under a glass coverslip with a single drop of vectamount (Vector Laboratories). Images were taken using Zeiss AxioCam HRc camera attached to a Zeiss AxioPhot 2 microscope.

2.15 Immunohistochemistry

2.15.1 Day 1

Localisation studies for Ptk7, Scribble, Vangl2, Celsr1 and dorsal ventral patterning markers

Cryosections used for the experiments were thawed by removing them from -80°C freezer to RT. OCT was removed by two washes in PBS, five minutes each at RT. For some antibodies it was necessary to increase the permeability of the tissue hence slides were washed with PBS plus 0.5% Triton X-100 for 10 minutes at RT, then washed twice with PBS, 5 minutes each (see Table 2-4 for details). Non-specific binding was blocked

with appropriate blocking solution for one hour at RT (see Table 2-4 for details). Slides were laid in a humidified chamber and primary antibody, diluted in appropriate blocking solution (see Table 2-4 for details), was applied. Rabbit-anti-Ptk7 (X. Lu, University of Virginia (Lu et al., 2004)), rabbit polyclonal anti-Scribble-H300 (Santa Cruz), goat polyclonal anti-Vangl2-M13 (Santa Cruz) and rabbit polyclonal anti-Celsr1 (Formstone et al., 2010) antibodies are used at 1:5000, 1:50, 1:50, 1:1000 respectively. Mouse monoclonal antibodies against HB9, Nkx6.1, Pax6, Nkx2.2 and Msx1/2 were obtained from the Developmental Studies Hybridoma Bank and were used at 1:10 dilution. Rabbit polyclonal antibodies against Olig2 and Dbx2 were obtained from Abcam and were used at 1:500 dilution. To prevent sections from drying, slide were covered with coverslip made from parafilm. Ab was left to incubate O/N at 4°C.

Phospho-Histone H3 staining

Embryos were embedded in wax and 5 μm sections were collected on charged slides as described in section 2.13. Sections were deparaffinised, rehydrated and antigen retrieved by steaming in Declare (Sigma), diluted to 1:20 in distilled water. Sections were steamed for 40 minutes and Declare solution was replaced by warm fresh Declare , again diluted to 1:20. This was allowed to cool to room temperature. Sections were then bleached in 3% H_2O_2, for 10 minutes at RT and washed in PBS plus 0.1% Triton X-100, three times at RT. Sections were then blocked and primary antibody, Rat–anti-phospho-histone H3 (PHH3) ($pSer^{28}$) (Sigma) was applied at 1:500 dilution, as detailed above.

2.15.2 Day 2

Next day the coverslips were removed and slides were washed with appropriate washing solution (see Table 2-4 for details), twice, five minutes each at RT. The sections were again blocked with appropriate blocking solution (see Table 2-4 for details) for 30 minutes at RT. AlexFluor 594 donkey anti-rabbit (Invitrogen), AlexaFluor-594 donkey

anti-goat (Invitrogen), AlexFluor 594 donkey anti-mouse (Invitrogen), AlexaFluor-488 goat anti-rabbit (Invitrogen) or AlexFluor 594 donkey anti-rat (Invitrogen) secondary antibody was applied at the concentration of 1:250 in humidified chamber. To prevent sections from drying coverslip made from Parafilm was put on the slide. The chamber was wrapped in foil and was left at room temp for 2-3 hours. Slides were washed with appropriate washing solution, twice and were mounted with single drop Vectashield Plus DAPI (Vector Laboratories). Sections were photographed within 1 or 2 days using Zeiss AxioCam HRc camera attached to a Zeiss AxioPhot 2 microscope.

Table 2-4: Specific conditions for individual antibodies used during immunohistochemistry.

Antibody	Increased permeability	Blocking solution	Antibody Solution	Wash solution
α-Ptk7 **α-ScribbleH300** **α-Vangl2M13** **α-Celsr1**	Yes	10% newborn calf serum in PBS	2% newborn calf serum in PBS	PBS
α-HB9 **α-Nkx6.1** **α-Pax6** **α-Nkx2.2** **α-Msx1/2** **α-Olig2** **α-Dbx2**	No	10% sheep serum in PBS + 0.1% Triton-X100	1% sheep serum in PBS + 0.1% Triton-X100	PBS + 0.1% Triton-X100
α- PH3	No	10% fetal calf serum in PBS	1% fetal calf serum in PBS	PBS + 0.1% Triton-X100

2.16 *Oligreen staining*

PFA was removed and embryos were washed in PBS twice for five minutes each at RT. To increase the permeability of the embryo they were washed in PBS plus 0.1% Triton

X-100 three times five minutes each at RT. Oligreen (Invitrogen) was made up in 0.1% triton X-100 at a 1:400 dilution and was added to the embryos. To allow the oligreen to stain the chromosomes, embryos were incubated in oligreen solution O/N at 4°C on a rotator in the dark.

Next day, embryos were washed with PBS plus 0.1% Triton X-100 - 3 times, 5 minutes each, in the dark. To visualise the cells in the neuroepithelium, the embryos were flat-mounted on a slide, with the dorsal side on the top using a drop of fluorsave reagent (Calbiochem) and a coverslip. Nail varnish was applied around the coverslip to hold it in place and the embryos were viewed on a confocal microscope (Leica TCS SP5) at 40 times magnification.

Through confocal microscopy, it was possible to visualise the orientation of the cells division in the neuroepithelium because when the cells divide the DNA becomes condensed and appears brighter. To determine the orientation of cell division, a line was drawn between the chromatids of two daughter cells and the angle between this and the anterior posterior axis of the embryo was measured. For this purpose, embryos with two to five somites were used and the neuroepithelium just posterior to the second somite was examined, as this is the region which will undergo closure 1.

2.17 *Tissue culture*

HEK293T cell line (derived from human embryonic kidney) (Graham et al., 1977) was kindly provided by Chris Esapa (Medical Research Council, Harwell). All media and plastic ware used in this experiment were sterile, and experiments were performed in a class II hood (Microflow Peroxide). Cells were grown in full media consisting of Dulbecco's Modified Eagle's Medium (D-MEM) (Invitrogen), 1 x Antibiotic-Antimycotic (Invitrogen) and 10 % Fetal Calf Serum (Invitrogen). Media, PBS (Invitrogen) and trypsin

(Invitrogen) used in the experiment were pre-warmed to 37 °C in a water bath before they came in contact with the cells.

2.17.1 Growing cells

Frozen aliquots of cells were rapidly defrosted in a 37 °C water bath. They were then pipetted up and down to break off large clumps of cells and were pipetted into a 75 cm^2 flask (Greiner one bio) containing 35 ml of full media. Cells were left to recover and grown over night in a 37 °C incubator with 5 % CO_2 (Sanyo). Next day, cells were split in 1 to 10 dilution in a fresh 75 cm^2 flask and left to grow in a 37 °C incubator with 5 % CO_2, until they reached 90% - 95% confluency.

2.17.2 Splitting cells

Once the cells had grown to 90 % - 95 % confluency, full media was removed and cells were washed twice with 10 ml warm PBS. To detach cells from the flask, 4 ml of warm trypsin was added to the cells and incubated in a 37 °C incubator with 5 % CO_2 for 5 minutes. To make sure that all cells were detached, the side of the flask was gently tapped and viewed under a light microscope (Olympus CK2). To inactivate trypsin, 4 ml of full medium was added and cell aggregates were removed by pipetting up and down. Cell suspension was transferred to a 12 ml tube (SLS) and centrifuged at 1000 rpm for 5 minutes in a Beckman centifuge to pellet the cells. All but 1 ml of the supernatant was removed and cell pellet was resuspended in remaining 1 ml. 9 ml of full media was added and the cells were mixed by pipetting up and down. 1 ml of this resuspended cell mix was added to a fresh 75 cm^2 flask containing 35 ml of full media and incubated in a 37 °C incubator with 5 % CO_2 for two days.

2.17.3 Freezing Cells

Once the cells had grown to 90 % - 95 % confluency, full media was removed and cells were washed twice with 10 ml warm PBS before they were trypsinised and centrifuged as described in section 2.17.2. All the media and trypsin mixture was aspirated away and the pellet of cell was resuspended in 1 ml of freezing media (Invitrogen). Cell suspension was transferred to a 1.5 ml cryo tube (Nunc) and frozen in a -70 °C freezer in a box with polystyrene holders.

2.17.4 Transfecting Cells

Cells grown to 90% - 95% confluency in full media were trypsinised and centrifuged as described in section 2.17.2. The pellet was resuspended in 10 ml of media with 10% FCS but no antibiotics. 100 µl of cell suspension was added to 900 µl of media and this was used to establish the cell density using a haemocytometer. Six million cells were plated onto the 25 cm^2 flask containing 6 ml of media with 10% FCS and were incubated for 24 hours at 37 °C with 5 % CO_2 to give 90 % - 95 % confluency required for the transfection.

Transfections were carried using Lipofectamine 2000 Transfection Reagent (Invitrogen), following the manufacturer's instructions. Briefly, per transfection 30 µl of Lipofectamine 2000 was mixed with 720 µl of medium (no antibiotic or serum) and incubated at room temperature for 5 minutes. During this incubation, 5 µg – 10 µg of plasmid was mixed with medium (no antibiotic or serum) to make up to 750 µl. Once the 5 minute incubation was up, Lipofectamine 2000 mix was added to plasmid mix and left to incubate at room temperature for 30 minutes to allow the transfection complexes to form. In the meanwhile, cells incubating in medium with 10 % serum were prepared for transfection by removing medium and adding 6 ml of prewarmed fresh medium with no serum and antibiotics. Once the 30 minute incubation to generate transfection complexes was up, 1.5 ml of this mix was added to cells. Cells were left to incubate in 37 °C, 5 % CO_2

incubator for 4 hours and the basic medium was replaced with that containing 10 % FCS and left to incubate in 37 °C, 5 % CO_2 incubator for 24 or 48 hours. After 24 or 48 hours, cells were trypsinised and centrifuged as described in section 2.17.2. All the media and trypsin mixture was aspirated away and the pellet of cell was frozen in dry ice and was either stored at -80 °C or was used for protein extraction as described in section 2.18.1.

2.18 *Western blotting*

2.18.1 Protein extraction from embryonic sample

Protein was extracted from E8.5 and E11.5 embryonic tissue collected as described in section 2.2.8. Tissue required for the experiment was removed from -80 °C and was defrosted on ice. Once defrosted, E8.5 embryos of the same genotype was collected into a pre-chilled tube and 1 ml of chilled RIPA buffer (1% Nonidet P40 (Sigma), 1% SDS (Sigma) and 0.5 % sodium deoxycholate (Sigma) made in 1 X PBS) was added to the embryos. Embryos were homogenised using a pre-chilled syringe and series of increasingly fine needles (19G – 25G). To prevent protein degradation, 5 µl of protease inhibitor was added. The mixture was incubated on ice for 30 minutes, to allow the detergents in the RIPA buffer to lyse cells releasing the contents, including protein, into the solution. To pellet the cell debris and insoluble material, the mixture was centrifuged at 10 000 g for 10 minutes at 4 °C. The supernatant, containing the protein, was carefully removed and transferred into a fresh tube. To store, 50 µl aliquots were made and frozen at -20 °C.

2.18.2 Protein extraction from cells

Protein was extracted from transfected HEK 293T cells. The method of transfection and cell collection is described in section 2.17.4. Tubes containing cells were removed from -80 °C and were defrosted in ice. Once defrosted, cells were resuspended in 8 ml

RIPA buffer. To lyse the cells, 8 ml suspension of cells was taken through two cycles of freezing in IMS + dry ice bath and defrosting in 42 °C water bath. Next, DNA was sheared by passing the lysate through 18G needles attached to a syringe, three times. To pellet the cell debris and insoluble material, the mixture was centrifuged at 10,000 g for 15 minutes at 4 °C. Supernatant, containing the protein, was carefully removed and transferred into a fresh tube. Protein sample was stored at -20 °C until required.

2.18.3 Protein quantification

The concentration of protein was determined by DC Protein assay kit (Biorad). A series of bovine serum albumin (BSA) standards of known concentration was made by diluting the 1.5 mg/ml BSA stock (Sigma) in the buffer that was used to extract protein. The concentration is as follows 0, 0.25, 0.5, 0.75, 1.0, 1.25 and 1.5 mg/ml. The concentration of protein extracted from E11.5 embryo and the cells was likely to be more than 1.5 mg/ml hence outside the range. To avoid this, protein samples were diluted to 1 in 2 and 1 in 4 and these were used to determine the concentration of the protein stock. To account for technical variability between readings, each sample and standard was read as two replicates. 5 µl of each of the standards were pipetted into the first two columns of a 96 well flat bottom plates (Nunc) in replicates. Similarly, 5 µl of protein samples were also pipetted in two replicates into wells of the same plate. DC reagent A (an alkaline copper tartrate solution) was mixed with DC reagent S in a 1 to 5 ratio (S to A) and 25 µl of this mixture was added to each of the standards and the samples. Next, 200 µl of Folin Reagent (DC reagent B) was added and mixed by pipetting. This was incubated for 15 minutes to 1 hour and the absorbance of the samples was measured using µ Quant (Bio-tek instruments) at 750 nm. The principle behind this kit is the same as that of Lowry assay (Lowry et al., 1951) but has been modified to reduce the time for the reaction to take place and to make it detergent compatible. A reaction occurs between the protein and copper which in turn reduces folin reagent by releasing oxygen atoms. These reduced species have a blue colour

with maximum absorbance at 750 nm hence the intensity of the blue colour reflects the amount of protein in the sample.

A linear plot of concentration vs absorbance was created for the standards using Excel. Using the absorbance value of each of the samples, the concentration was determined using the linear plot.

2.18.4 Sample preparation for protein gels

Once the concentration of protein was determined, 1 μg to 3 μg of protein was loaded in each lane of a gel. The amount of protein loaded on the gel depended on the abundance the protein of interest in the sample and the quality of the antibody. For Ptk7, Scribble, Celsrl and Vangl2, 1 μg of protein was used for each lane. For Tulp3 and HA-Rgnef 3 μg of protein was used per lane. To prepare the samples for loading, 1 X reducing agent (Invitrogen), 1 X loading buffer (Invitrogen) was mixed with 1 μg to 3 μg of protein and this was made up to the required volume with water. The maximum volume that can be loaded in a lane in 10 well gel is 20 μl, in 12 well gel is 15 μl and in 15 well is 12 μl. Samples were denatured by heating at 70°C for 10 minutes and chilled immediately in ice. They were kept on ice until ready to load.

2.18.5 Running protein gels

Pre-made NuPAGE 3-8 % and 7 % Tris-Acetate gels (Invitrogen) were used throughout the experiments. Gels were prepared by a quick rinse with water to remove storage solution, removing combs and washing the lanes with 1 X TrisAcetate SDS Running Buffer (Invitrogen) three times. At the end of the wash, the lanes with filled with 1 X running buffer and gels were inserted into the running tank (Invitrogen). A sealed chamber in the middle was created with two gels and this was filled with 1 X running buffer, just covering the wells. To protect the protein during the run, 500 μl of NuPage Antioxidant (Invitrogen) was added to the inner chamber. Samples were prepared as

described in section 2.18.4 and loaded on to either 10-, 12- or 15-well gel. A HiMark protein ladder (Invitrogen) was also loaded on to a lane. The outside chamber in the tank was filled with 1 X running buffer and the gel was electrophoresed for 1 hour at 150 V (Invitrogen Power pack).

2.18.6 Western blotting

Following electrophoresis, the gel was removed from plastic cassettes and was trimmed. The gel and the required number of Hybond-ECL nitrocellulose sheets (GE Healthcare) were put into individual clean dishes filled with Transfer Buffer (25 mM Tris base, 0.2 M Glycine and 10 % Methanol) and left to soak for 10 minutes. Fiber pad and the filter paper used during the transfer were also fully soaked in transfer buffer. The blotting system was assembled by putting wet fiber pad and a filter paper on top of the negative side of the blotter. The gel was put on top of the filter paper and was overlaid with the Hybond-ECL sheet before applying another wet filter paper and wet fiber pad. To make sure there were no air bubbles which could disrupt the transfer, a plastic roller was used to roll out air bubbles. Finally the positive side of the blotter was flipped over the top of the fiber pad and was sealed. The whole cassette was inserted into the blotting tank half filled with transfer buffer. Next, a small ice pack and a magnet bar were also inserted into the blotting tank and the tank was filled up with more transfer buffer. To avoid overheating during high voltage transfer, the blotting tank was stood on a magnetic stirrer to ensure that the hot buffer generated was mixing well with buffer cooled by the ice pack. The transfer was performed at 100 V for 30 – 45 minutes.

2.18.7 Immunodetection on Western blots

The Hybond-ECL sheet containing transferred protein was removed from the blotter and was prepared for immunodetection by blocking non-specific binding with 2 % ECL Advance blocking powder (GE Healthcare) in TBST (0.14 M NaCl, 20 mM Tris-HCl pH

7.6 and 0.1 % Tween 20) for 1 hour at RT or at 4 °C O/N on a shaking platform. The blocking solution was removed and replaced by primary antibody made in block and incubated for 1 hour at RT or O/N at 4 °C on a shaking platform. Antibodies were obtained from various places. Rabbit polyclonal anti-Ptk7 antibody was obtained from X. Lu (University of Virginia) and used at 1:15000 dilution. Mouse anti-Scribble monoclonal antibody was obtained from P. Humbert and used at 1:500 dilution. Rabbit anti-Celsr1 polyclonal antibody was obtained from C. Formstone (Kings Collage London) and was used at 1:3000 dilution. Mouse anti-GFP B2 monoclonal antibody, goat anti-Vangl2 N13 antibody, mouse anti-Fatty acid synthase antibody and rabbit anti-Beta tubulin antibody were obtained from Santa Cruz Biotechnology and were used at 1:1000 dilution. Mouse anti-HA mono-clonal antibody was obtained from Covance and was used at 1:1000 dilution. Non-specific binding of primary antibody was reduced by two rinses in TBST followed by one 15 minute wash and three 5 minutes washes in TBST. Depending on the primary antibody used anti-mouse, -rabbit or -goat Horseradish Peroxidase (HRP) conjugated secondary antibody was applied to the blot and incubated at RT for 1 hour on a shaking platform. All secondary antibodies were obtained from DAKO and were used at 1:10,000 dilutions in blocking solution. Non-specific binding of secondary antibody was reduced by two rinses in TBST followed by one 15 minute wash and three 5 minutes washes in TBST on a shaking platform. Enhanced chemiluminescence (ECL) Advance Western Blotting Detection Kit (GE Healthcare) was used to detect the secondary antibodies on the membrane. ECL Advance Solution A and ECL Advance Solution B were allowed to equilibrate to RT and were mixed in 1:1 ratio and diluted in equal volume of TBST. ECL advance mixture was applied to the blot and incubated in the dark for 5 minutes. During this time HRP (conjugated to secondary antibody) and hydrogen peroxide (present in solution A) oxidize luminol (present in solution B), which then luminesces. This light can be detected by exposing and developing X-ray films. ECL mixture was drained off and blots were mounted between two acetate sheets into a light proof cassette.

When anti goat HRP secondary was used, prior to mounting, the blots were rinsed very quickly in 0.1 M Tris pH 9.5. This step was essential to remove the background signal. X-ray films (GE Healthcare) were exposed to the blots in the dark and developed (Xograph Compact X4). Various exposure times (1 second – 10 minutes) were tested to obtain optimal results.

2.19 Co-Immunoprecipitation

Protein from doubly transfected HEK293 cells and from mock transfected cells were extracted and quantified as described in section 2.18.2 and 2.18.3. These were used to perform Co-Immunoprecipitation (Co-IP) with protein G sepharose beads (Sigma) or Dyanbeads protein G immunoprecipitation kit (Invitrogen).

2.19.1 Protein G Sepharose beads

20 µl of protein G sepharose beads (Sigma) was washed with 500 µl of RIPA buffer and 600 µg of protein was added to the beads. Protein sample was mixed with the beads and incubated on rotation for 1 hour at 4°C. Beads were separated from the protein lysate by centrifuging at 1,000 g for 2 minutes at 4°C. Supernatant was transferred into a fresh tube and beads were kept as a control for non-specific bead-only binding control. 2 µg of antibody (mouse anti V5 antibody (Invitrogen) or mouse anti HA antibody (Covance)) was added to 250 µg of pre-cleared protein lysate; a further 250 µg of protein was used as no-antibody control. The remaining 100 µg of pre-cleared protein lysate was kept to run on a protein gel as a control for the starting material of the Co-IP. Protein lysate with or without antibody was incubated O/N at 4°C with rotation. The next day, a further 20 µl of protein G sepharose beads per co-IP reaction were washed with RIPA buffer and protein lysate with or without antibody were added to the beads. Protein lysate and beads were incubated for 1 hour at 4 °C on rotation. At the end of this incubation, the beads were spun down and the

supernatant containing unbound protein was removed and kept. The beads were washed twice with 500 µl of RIPA buffer, and supernatant from both washes were kept for gel analysis. To elute and denature bound proteins, 40 µl of SDS loading buffer (Invitrogen) and 4 µl of reducing agents (Invitrogen) was added to the beads and incubated at 70 °C for 10 minutes. 1 to 5 µl of the eluted sample was run on a protein gel, blotted and probed with either rabbit anti-Tulp3 antibody or mouse anti-HA antibody as described on sections 2.18.5 - 2.18.7 .

2.19.2 Dynabeads Protein G immunoprecipitation kit

25 µl of resuspended dynabeads (Invitrogen) was separated on a magnetic rack and the supernatant was removed. To obtain pre-cleared protein lysate, 600 µg of each protein sample was applied to the beads and incubated at RT for 30 minutes with rotation. In parallel, further 25 µl of beads per co-IP reaction were prepared and 2 µg antibody (mouse anti-V5 antibody (Invitrogen) or mouse anti-HA antibody (Covance)) was mixed with 200 µl of antibody Binding and washing buffer and applied to the beads. For no-antibody control, 200 µl of antibody Binding and washing buffer without any antibody was applied. This was incubated on rotation at RT for 10 – 30 minutes.

Pre-cleared protein lysate was separated from the beads on a magnetic rack and transferred into a fresh tube. Dynabeads with non-specific binding was kept for gel analysis. Once the antibody binding step was complete, beads were separated and 250 µg of pre-cleared lysate was applied to the dynabeads conjugated with or without the antibody. To allow the antibody bound to the dynabeads to bind to specific antigen, the reaction was incubated on rotation for either 2 hours at RT or ON at 4 °C.

Next, dynabeads were separated on a magnetic rack and the supernatant was kept as the unbound fraction for gel analysis. The dynabeads with the bound proteins were washed four times with Washing Buffer and during the final wash; dynabeads were transferred into

a new tube to avoid any protein bound non-specifically to the wall of the tube. The supernatants from the first and the last wash were analyzed on a gel.

To elute and denature proteins bound to the dynabeads, 40 µl of SDS loading buffer (Invitrogen) and 4 µl of reducing agents (Invitrogen) were added and this was incubated at 70°C for 10 minutes. 1 to 5 µl of the eluted sample was run on a protein gel, blotted and probed with rabbit anti-Tulp3 or mouse anti-HA antibody as described in sections 2.18.5 - 2.18.7 .

2.20 Microarray

2.20.1 Tissue collection and RNA extraction

E9.0 embryos (16-18 somite) from matings between two *hitchhiker* heterozygous animals were dissected out as described in section 2.2. For this experiment only the caudal end of the embryo was used, defined as tissue caudal to the 11^{th} somite. Caudal ends were dissected using a sharp pair of forceps, washed in PBS and immediately frozen in dry ice and stored as described in section 2.2.8. Total RNA from caudal ends of seven wildtype and seven mutants was extracted individually using the RNeasy Plus Mini Kit (Qiagen) according to manufacturer's protocol. The principle behind this kit is as described in section 2.4.

2.20.2 SMART cDNA synthesis

cDNA was synthesised using 1 µg of pooled RNA for WT and mutant samples. SMART™ PCR cDNA Kit (Clontech) was used according to manufacture's instructions. 1 µg of RNA was mixed with 2 µl of 10 µM of 3' SMART CDS Primer IIA ($^{5'}$AAGCAGTGGTATCAACGCAGTACT$_{(30)}$VN$^{3'}$) and 2µl of 10 µM SMART IIA Oligonucleotide ($^{5'}$AAGCAGTGGTATCAACGCAGAGTACGCGGG$^{3'}$). Secondary structure that may have formed in oligonucleotides or in RNA template was removed by

heating the mixture at 70 °C for 2 minutes and quenching on ice for further two minutes. 1 X first-strand buffer, 20 mM DTT, 10 mM dNTP and 1 µl of PowerScript reverse transcriptase (Clontech) was added to the RNA and primer mixtures and was incubated at 42 °C for 1 hour. During this incubation poly T sequence at the 3' end of 3' SMART CDS Primer IIA hybridises with poly A sequence at the 3' end of the RNA and the reverse transcriptase extends this oligonucleotide using the RNA as template. Once reverse transcriptase reaches the 5' end of RNA, it adds a few extra nucleotides, primarily deoxycytidine (C) to the 3' end of cDNA. This stretch of C at the 3' end of first strand cDNA is used to hybridise with poly G present at the 3' end of SMART IIA Oligonucleotide. Reverse transcriptase then extends this oligonucleotide using first strand cDNA as template resulting in full length cDNA. Reaction was terminated by placing on ice.

2.20.3 cDNA amplification by LD PCR

As a control for the cDNA amplification step, two separate reactions were performed for both WT and mutant samples. For each reaction, 4 µl of first strand reaction was transferred to a prechilled tube. To this 80 µl of dH_2O, 1 X advantage 2 PCR buffer, 10 mM dNTP, 1 X advantage polymerase mix and 2 µl of 10 µM 5'PCR Primer IIA ($^{5'}$AAGCAGTGGTATCAACGCAGAGT$^{3'}$) was added and mixed. The reaction was placed in a preheated thermocycler and subjected to the following program – denature at 95 °C for 1 minute, and 17 cycles of 95°C denature for 30 seconds, 65°C annealing for 30 seconds and 68°C extension for 6 minutes. To remove excess dNTP, primer and enzyme, this reaction was processed through a Qiagene PCR purification Column as described in section 2.8. To ensure that cDNA of all sizes amplified equally, 3 µl of purified PCR product was run on an agarose gel as described in section 2.7.

2.20.4 Klenow labeling

cDNA was labeled using Bioprime kit (Invitrogen) with modifications. For each genotype three arrays were performed. For the first array, WT sample was labeled with Cy3 and mutant sample was labeled with Cy5. For the second array, same cDNA sample was used, but the dye was reversed i.e. WT was labeled with Cy5 and mutant was labeled with Cy3. As two dyes do not get incorporated in the same way, this is essential in order to account for non specific differences in the intensity of signals between WT and mutant samples. The third array is a control for the cDNA amplification process. Here, the second set of cDNA for WT and mutant is labeled with Cy3 and Cy5, respectively. To label cDNA, 10 µl of purified cDNA was added to 10 µl of dH_2O and 1 X random primer/reaction buffer mix (125 mM Tris-HCl pH 6.8, 12.5 mM $MgCl_2$, 25 mM 2-mercaptoethanol and 750 µg/ml oligodeoxyribonucleotide primers). To remove secondary structure, the mixture was boiled for 5 minutes and then cooled on ice. While on ice, 1 X dNTP mix with low concentration of dC (1.2 mM of each dATP, dGTP, dTTP and 0.6 mM of dCTP), 2 mM of Cy5-dCTP or Cy3-dCTP and 60 Units of Klenow were added to the reaction. The reaction was made up to 50 µl by addition of dH_2O and was incubated at 37 °C for 3 hours.

To remove excess nucleotides, the reaction was passed down a Sephadex G50 spin column (GE Healthcare). Next, differentially labeled WT and mutant samples for each array are mixed together and desiccated using a speedvac. This was resuspended in 50 µl of microarray hybridization solution (40 % deionised formamide, 5 X Denhart's, 5 X SSC, 1mM Na pyrophosphate, 50mM Tris pH 7.4 and 0.1% SDS) and incubated at 85 °C for 5 minutes.

2.20.5 Hybridisation

A spotted array with 25000 mouse oligos (one oligo per gene and controls) was used (Le Brigand et al., 2006). The array was placed inside a humidified hybridisation

cassette and incubated at 42 °C for 30 minutes. The labeled cDNA mixture (prepared in section 2.20.4) was incubated at 42 °C for 30 minutes in parallel. Following this incubation, the mixture was centrifuged for two minutes to remove any precipitates. The supernatant was applied to the array slide ensuring no bubbles were formed. Slides were covered with coverslips and were placed inside the humidified hybridization cassette. Hybridization took place overnight at 48°C. Next day, the slides were washed to remove any non-specific binding of the probes. Washing was done by placing slides in a slide rack and washed in wash solution A (2 X SSC) until coverslips fall off. They were then washed vigorously in wash solution B (0.1 X SSC, 0.1 % SDS) for 5 minutes and then in wash solution C (0.1 X SSC) for 2 minutes. Slides were dried by being placed in a 50 ml falcon tube and spun at 600 rpm for 5 minutes. The dry slide is ready for scanning using Perkin Elmer ProScanArray HT.

2.20.6 Scanning

Fluorescent reading for each spot per dye was taken at seven photomultiplier tube (PMT) voltage ranging from 45 to 75 PMT for Cy3 and 40 to 70 PMT for Cy5. This range of PMT voltage is appropriate to avoid both: signal saturation from a highly expressing gene and lack of signal from lowly expressed genes. ImaGene from BioDiscovery converts these images into numerical data and also flags spots with poor quality data. MAVI analyses the values from seven readings per spot per dye and draws a regression line. The middle fluorescent value from the linear part of the regression is taken as the value of expression for each gene in WT and mutant. This information is fed onto Agilent's GeneSpring software. The software compares data from the WT to data from the mutant. It then draws a list of potential candidate genes which showed a significant difference between the WT and mutant expression values.

2.21 Quantitative Real Time PCR

SYBR Green based quantitative real assays were used to validate results from the microarray experiment. Individual caudal ends of E9.0 embryos from *hitchhiker* timed mated were collected and RNA was extracted as described in section 2.20.1. cDNA for individual RNA samples was synthesized as described in section 2.5. To optimize PCR reaction cDNA generated form pooled caudal ends of E9.0 CD1 embryos were used. To avoid signals from any contaminating genomic DNA that may be present in the cDNA sample, primers for candidate genes and endogenous controls were designed so that they overlap the introns using Primer Express V3 software (ABI). All the primers were chosen to have annealing temperature of 60 °C. Reactions were performed in triplicate and cDNA from seven individual WT and mutant *hitchhiker* embryos were processed individually. Initially, for each primer pairs a standard curve and dissociation curve was obtained from six cDNA concentrations ranging from 0 ng to 50 ng. Standard curve is used to calculate the efficiency of the reaction $[(10^{(-1/\text{Slope})} - 1)*100]$ and the dissociation curve gives an indication of the number of products being amplified. For each reaction 1 X SYBR Green PCR master mix (ABI) was mixed with 900 nM of reverse and forward primer, 0 ng to 50 ng of cDNA and dH_2O to bring final volume up to 20 µl. PCR were set up in a MicroAmp(R) Fast Optical 96-Well plates (ABI) and sealed with MicroAmp(R) Optical Adhesive Films (ABI). PCR was ran on 7500 FAST system (ABI) using a standard protocol of 95 °C for 10 minutes to activate emzyme, then 40 cycles of denature at 95 °C for 15 seconds and annealing and extension at 60 °C for 1 minute. Results were analyzed using 7500 system software (ABI).

2.22 Standard Stock solutions

ddH_2O (BDH)

20% SDS (Fisher)

10% Tween 20 (Sigma)

10x TBE (Biorad)

Ethylenediamineteraacetic Acid (EDTA): Stock solution 0.5M, pH8.0 (Sigma)

Tris- HCl: 121.1g Tris base in 800ml H_2O, Adjust to desired pH by adding concentrated HCl, Make up volume to 1L using ddH_2O.

TE: 10mM Tris HCl (pH8), 1mM EDTA,

Phosphate buffered Saline (PBS): 137mM NaCl, 2.7mM KCl, 10mM Na_2HPO_4, 2mM KH_2PO_4.

20xSSC (pH 4.5): 3M NaCl, 0.5M NaCitrate, adjust pH with citric acid.

Luria Broth (LB): 10% tryptone, 5% yeast extract, 10% NaCl, In 950 ml H_2O, adjust to pH7.0 using NaOH, make volume up to 1L with H_2O.

CHAPTER 3

CHUZHOI IS AN ENU-INDUCED MUTANT CARRYING A MUTATION IN PTK7 GENE

3 *chuzhoi* is an ENU-induced mutant carrying a mutation in *Ptk7* gene

3.1 *Introduction*

3.1.1 ENU mutagenesis

N-ethyl-N-nitrosourea (ENU) is one of the most powerful mutagenic chemicals (Russell et al., 1979) often resulting in a point mutation affecting one nucleotide every 1-2 Mb. The exact rate of mutation is dependent upon the dose of ENU (Kile and Hilton, 2005). ENU works by transferring its ethyl group to oxygen or nitrogen radicals in DNA leading to mispairing of the base which results in a point mutation and predominantly (in 87%) affects AT base pairs (Justice et al., 1999). This results in an unbiased random mutagenesis which has the potential to identify novel genes giving rise to a phenotype under study. In addition, this technique is particularly powerful as it can also give rise to a series of alleles for a particular gene in a totally unbiased way, which is essential to completely understand the function of a particular gene.

At Harwell, ENU mutagenesis programs are used to identify both dominant and recessive genes involved in various biological processes (Nolan et al., 2000; Bogani et al., 2005; Goldsworthy et al., 2008; Ermakov et al., 2009; Patterson et al., 2009). The dose of ENU used at Harwell results in one mutation every 1.01 Mb of which 1 in 1.82 Mb are potentially functional (Quwailid et al., 2004).

3.1.2 Detection of an ENU induced mutation

To study the complete function of a gene, it is essential to identify the mutated gene that is giving rise to the phenotype under study. As ENU is a random mutagen and often results in a point mutation affecting one nucleotide every 1-2 Mb, sequencing the whole

genome to find the mutation in an affected individual will not reveal the mutation linked to the phenotype. Since the founder of any colony carries approximately 30 loss-of-function mutations (Kennedy and O'Bryan, 2006), it is necessary to segregate the mutation linked to the phenotype of interest from those mutations which are not involved. This is achieved through out-crossing and backcrossing the mutagenised line to another inbred strain, allowing recombination between genomes to occur. When selecting for a phenotype, the mutated region will be retained on the original strain DNA while the rest of the genome is gradually replaced by DNA from the new strain. There are several differences in the genome of different inbred strains which can be used as markers to differentiate between strains, and hence identify the origin of a sequence of DNA in the progeny. These sequence differences could be a single nucleotide polymorphism (SNP), difference in the number of tandem repeats (microsatellite markers) or sequence differences affecting the restriction map. To initially link the mutation to a part of the genome, DNA from several individuals exhibiting the phenotype under study is extracted and a panel of markers covering the entire genome is tested on each DNA sample. The region of genome where the least amount of recombination between two genomes is detected is most likely to be the genomic region where the mutation giving rise to the phenotype under study is located. Depending on the size of the critical interval and the availability of further markers, this genomic region is usually further defined. Once the minimal region is achieved through mapping, a list of potential candidate genes based on the published literature about the function of the gene are identified for sequencing to detect the mutation. The colony is then maintained using this mutation as a selection.

3.1.3 Confirmation of ENU induced mutation

To confirm an ENU induced mutation, it is necessary to exclude the possibility that the phenotype under study is achieved by a mutation in a gene closely linked to the gene

where initial mutation is found. This is often achieved in several different direct and indirect ways. There are two direct way to confirm an allele. Firstly, rescuing the phenotype by adding a functional copy of the gene of interest (e.g. BAC rescue), and secondly, by showing failure of complementation by crossing the putative allele to a previously known allele of the same gene (Kile and Hilton, 2005). These direct routes are not always possible hence indirect evidence is employed to verify the mutation. This evidence includes an availability of a published allele of the same gene showing identical phenotypes, an altered level or localization of the protein product of the gene in the mutant, and expression of the gene in tissue where a phenotype is observed (Kile and Hilton, 2005).

3.1.4 *chuzhoi*: an ENU induced mutant exhibiting severe neural tube defects

The *chuzhoi* mutant was identified in an ENU G3 recessive screen carried out by D. Norris at Harwell (Ermakov et al., 2009). Briefly, male BALB/c mice were mutagenised with ENU and were out-crossed to C3H/HeH female to produce G1 progeny. Male G1 progeny were further out-crossed to C3H/HeH females to produce G2 progeny. Female G2 progeny were backcrossed to G1 male and the litters (G3) from this cross were examined at E13.5 for any developmental defects (Figure 3-1 A). A mutant line exhibiting left-right defects and craniorachischisis was identified. These two phenotypes were subsequently segregated into two different lines. The line displaying craniorachischisis was named *chuzhoi*. As well as displaying the severe neural tube defect, in which entire neural tube from the midbrain/hindbrain boundary throughout the spinal cord remains open (Figure 3-1 C,D), *chuzhoi* also exhibited other developmental defects, which include open eyes at birth (Figure 3-1 F), failure to close the ventral body wall (observed in 48% fetuses, N= 27) (Figure 3-1 C), polydactyl (observed in 7% fetuses, N= 27) (Figure 3-1 L-N) and fused or bifurcated ribs (Figure 3-1 H,J).

Figure 3-1: Identification of *chuzhoi*.
(A) G3 recessive screen used to identify *chuzhoi*. Male BALB/c mice were mutagenised with N-ethyl N-nitrosourea (ENU) and were out-crossed to C3H/HeH females to produce G1 progeny. G1 males were crossed to C3H/HeH females to give G2 progeny. G2 females were backcrossed to G1 males and the litters (G3) from this cross were examined at E13.5 for any developmental defects. (B) Lateral view of an E17.5 wildtype embryo showing a fully closed neural tube. (C and D) Lateral view (C) and a dorsal view (D) of E17.5 *chuzhoi* embryo showing craniorachischisis, where the neural tube remains open from the midbrain/hindbrain boundary throughout the spinal region (C and D), and an open ventral body wall resulting in protrusion of the liver and guts (C). (E and F) Lateral view of the eye in E17.5 wildtype embryo (E) and in E17.5 *chuzhoi* (F) embryo, showing that the eyelids are closed in the wildtype but they remain open in *chuzhoi*. (G-N) Skeletal preparations of E17.5 wild-type (G, I and K) and *chuzhoi* mutant (H, J, L-N) fetuses stained with alcian blue for cartilage and alizarin red for bone. (G and H) Dorsal view showing the splayed vertebrae in *chuzhoi* mutants. (I and J) Lateral view showing the fused and bifurcated ribs in *chuzhoi* mutants. (K-N) *chuzhoi* mutants also show polydactyly. Scale bar represent 2 mm in B-D and G-J, 6 mm in E and F, and 4 mm in K-N.

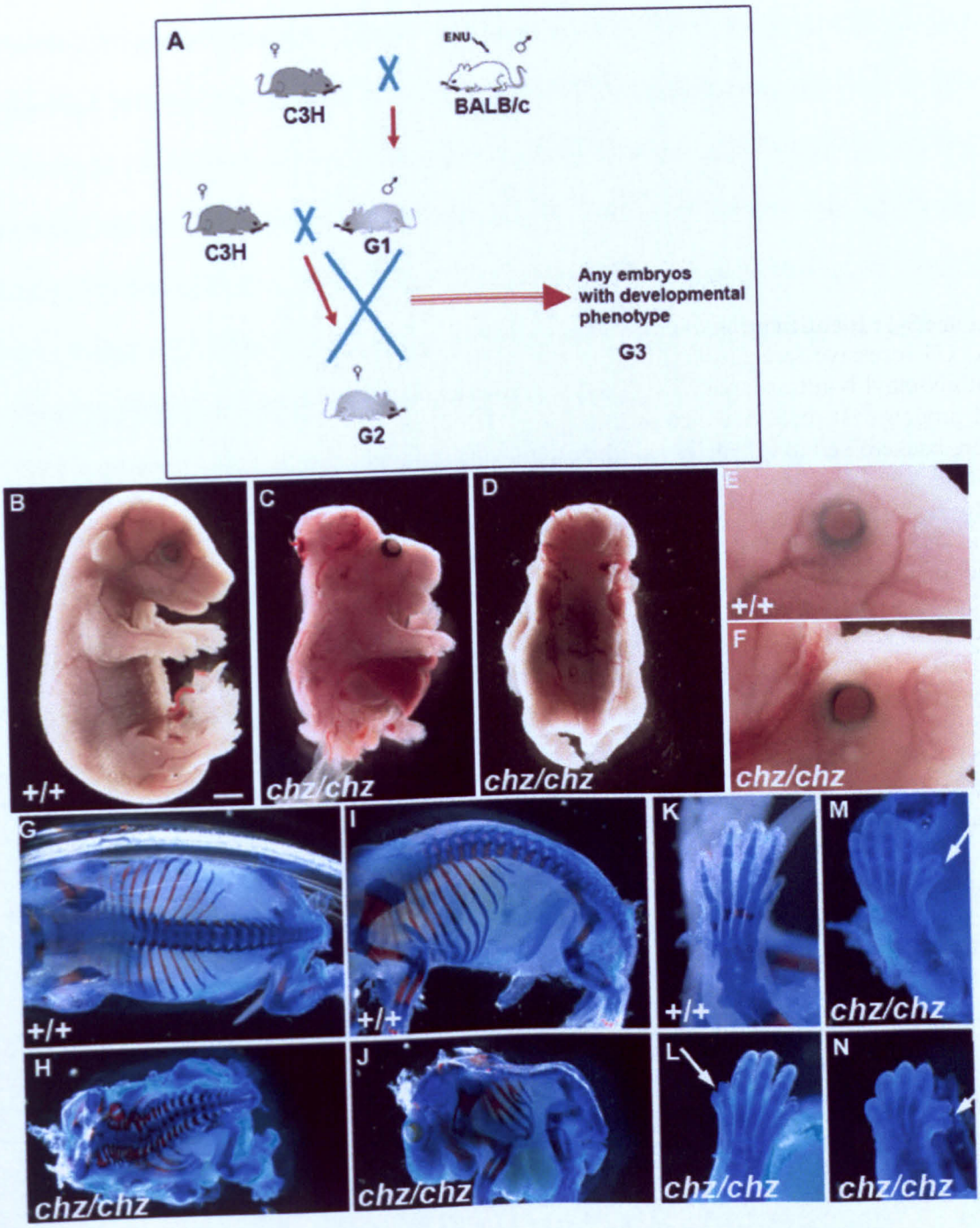
A
ENU
C3H
BALB/c
C3H
G1
G2
Any embryos
with developmental
phenotype
G3
B
+/+
C
chz/chz
D
chz/chz
E
+/+
F
chz/chz
G
+/+
I
+/+
K
+/+
M
chz/chz
H
chz/chz
J
chz/chz
L
chz/chz
N
chz/chz

3.1.5 Length to width ratio: an indication of a disturbance in convergent extension

Initial work on *Xenopus* has shown that the process of convergent extension is essential for proper neural tube closure and that it is controlled by the planar cell polarity signalling pathway (Wallingford and Harland, 2001; Wallingford and Harland, 2002). Convergent extension is a complex process which involves cells elongating medio-laterally, moving towards and intercalating into the midline to elongate and narrow the embryo (Wallingford et al., 2002; Keller, 2006). Convergent extension has been shown to occur during neurulation in mice and to be regulated by the planar cell polarity pathway (Ybot-Gonzalez et al., 2007b; Yen et al., 2009).

Failure of convergent extension results in an embryo that is short at the anterior posterior axis and wide at the medio-lateral axis (Wallingford and Harland, 2002; Wang et al., 2006a). This widening of the midline means that the neural folds are too far apart to oppose and fuse at the midline, resulting in neural tube defects (Kibar et al., 2001; Murdoch et al., 2001a; Murdoch et al., 2003; Wallingford and Harland, 2002).

Direct measurements of the length and width of embryos undergoing neurulation has shown that convergent extension is a continuous process that occurs during neurulation. It gives rise to a consistently increasing length to width ratio (Wallingford and Harland, 2002; Wang et al., 2006a). When convergent extension is disrupted, the rate at which the length to width ratio increases during neurulation is significantly slower (Wallingford and Harland, 2002; Wang et al., 2006a).

3.1.6 Remodeling of the outflow tract during heart development

For the development of a functional heart, a proper remodeling of the outflow tract is essential. Remodeling of the outflow tract is essential for ventricular septum, giving rise to four chambers of the heart which are separated by a muscular wall. The pulmonary

artery exits from the right ventricle and is involved in carrying oxygen depleted blood from the heart to the lungs. The aorta exits the left ventricle and carries oxygenated blood from the heart to the systemic circulation. Studies in chick have shown that the cranial neural crest cells are required for the proper remodeling of the outflow tract and removal of these cells results in failure of formation of the ventricular septum and double outlet right ventricle (Kirby et al., 1983), where both aorta and pulmonary artery exit from the right ventricle. More recently, another group of cells arising from the primary heart tube have been shown to have a role to play in the development of the outflow tract and disruption of these endocardial and myocardial cells also gives rise to similar outflow tract defects (Mjaatvedt et al., 2001).

The ventricular septum results from muscularization and fusion of mesenchymal swellings (referred to as cushions) that are present within the outflow tract (Mjaatvedt et al., 2001). Throughout development, the endocardial cells originating from the primary heart tube and the cells of neural crest origin invade the outflow tract cushion resulting in expansion and fusion of the cushion. Additionally at this stage, cardiomyocytes present in the outflow tract migrate in a polarized fashion into the cushion (Phillips et al., 2005). This results in muscularizaton of fused cushions leading to ventricular septum.

3.2 Results

3.2.1 Genetic mapping of *chuzhoi*

To determine the position of the mutation affecting *chuzhoi* within the genome, genomic DNA samples from 12 fetuses with craniorachischisis were given to the GEMS core at Harwell for a SNP-based whole genome scan. Since the BALB/c strain was ENU mutagenised and backcrossed to C3H/HeH, a panel of SNP makers that distinguished between BALB/c and C3H/HeH was used to determine the genomic region where the least amount of recombination took place between two genomes. This region will have high level of BALB/c genome and will contain the causative mutation. The initial scan showed a strong linkage to Chromosome 17 (Figure 3-2A), with a large critical interval between markers at positions 31 Mb and 71 Mb. To further refine the position, I added additional microsatellite markers and this reduced the critical interval to the region between markers at 37.5 Mb and 65.6 Mb (Figure 3-2B). The mutation showed a 100% linkage to *D17Mit115* at 45 Mb. No further informative microsatellite or SNP markers between BALB/c and C3H/HeH were identified in the region hence narrowing this large critical interval was not possible. This is an extremely gene rich region of the mouse genome (containing 268 genes) however, in the middle of this large critical interval, at 44 Mb, an extremely good candidate gene, *Protein tyrosine kinase-7* (*Ptk7*), was present. *Ptk7* was a good candidate because previous work had shown that a gene trap allele of *Ptk7* gave rise to craniorachischisis (Lu et al., 2004) and it is also located very close to *D17Mit115* which showed 100% linkage to the mutation (Figure 3-2B).

3.2.2 Identification of mutation in *Ptk7*

In order to test the hypothesis that *Ptk7* is the gene mutated in *chuzhoi,* I amplified *Ptk7* from mutant and wildtype cDNA using ten pairs of overlapping primers within the

transcript, see appendix Table 10-1 for primer details. The PCR products were purified and sequenced. Sequencing cDNA revealed that *chuzhoi* had an insertion of nine base pairs between exon eight and nine (Figure 3-2C). Since *chuzhoi* is an ENU-induced mutant, a single nucleotide substitution was expected; therefore finding an insertion of nine extra base pairs was puzzling. Sequence analysis of these extra bases showed that they were part of intron eight suggesting that *chuzhoi* may carry a mutation that affects the splicing of the *Ptk7* gene. To verify this, I designed a new primer pair to sequence intron eight from genomic DNA. This showed a single nucleotide substitution, A → G, at the splice junction on the 3' end of intron 8 (Figure 3-2D,E). This nucleotide change appears to induce an early splice acceptor site, resulting in the nine nucleotide insertion in the cDNA, which in turn results in the insertion of three extra amino acids in the *Ptk7* protein (Figure 3-2F). The parental strains (BALB/c and C3H/HeH), and other inbred mouse strains (129, DBA2 and C57BL/6) were also sequenced in this region and all strains tested had the 'A' nucleotide at the site. This provided evidence that this change was unique to *chuzhoi* mutant. Furthermore, the *chuzhoi* embryos are genotyped directly using the SNP and the phenotype and the genotype show a 100% correlation (N= 74 embryos at E9.5 or older).

3.2.3 The level of Ptk7 protein is reduced in *chuzhoi*

To provide further evidence that *Ptk7* is the gene mutated in *chuzhoi,* I performed immunohistochemistry and western blots using *chuzhoi* and wildtype tissue at the time of neural tube closure. Both immunohistochemistry and western blots showed that Ptk7 protein was produced; however level of the protein was dramatically reduced in the mutant (Figure 3-3A-D). Furthermore, immunohistochemistry showed that while the level of Ptk7 protein was reduced in *chuzhoi,* its ability to localize to the membrane was not affected (Figure 3-3C-D). As reported previously (Lu et al., 2004), western blot analysis showed that Ptk7 protein exists in two isoforms; full length and a shorter (likely cleaved) isoform.

While the levels of both isoforms were reduced in *chuzhoi* mutants, it was striking that the smaller form of the protein was reduced to a much greater extent (Figure 3-3A,B).

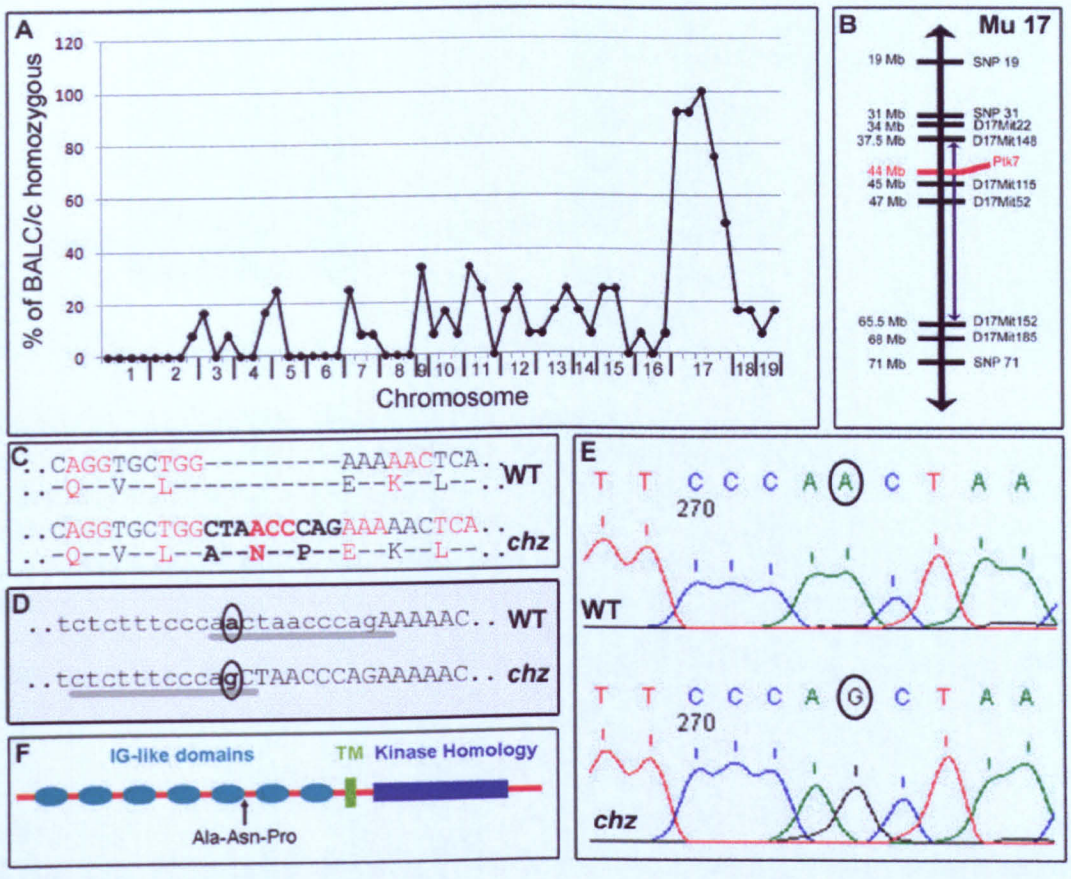

Figure 3-2: *chuzhoi* carries a mutation in *ptk7*.
(A) Result from whole genome scan using 56 SNP markers and 12 fetuses with craniorachischisis, showing percentage of fetuses genotyping as homozygous BALB/c at each marker. *chuzhoi* shows a strong linkage to Chromosome 17. (B) Genetic map of mouse Chromosome 17 following addition of microsatellite markers. Numbers on the left are the positions of each marker on the Chromosome. The blue arrow shows the critical region for *chuzhoi* between 37.5 Mb and 65.5 Mb, containing *Ptk7,* a candidate gene. (C) cDNA sequence from wildtype and *chuzhoi* showing an insertion of nine extra base pairs in *chuzhoi* between exon eight and nine; resulting in addition of three extra amino acids in the protein. (D) gDNA sequence from wildtype and *chuzhoi* at eighth intron reveals a nucleotide substitution from A in wildtype to G in *chuzhoi* (circled), resulting in the creation of a novel splice acceptor site 9 bp upstream of the wildtype site. The grey underlines represent the consensus splice sequence in wildtype and *chuzhoi.* (E) Sequence trace from wildtype and *chuzhoi* showing a nucleotide substitution (circled). (F) Protein structure of Ptk7 showing an extracellular domain with seven immunoglobulin-like domains, a single transmembrane domain and an intracellular domain with kinase homology. *chuzhoi* has an additional three extra amino acids in the extracellular domain, at the end of the fifth immunoglobulin-like domain.

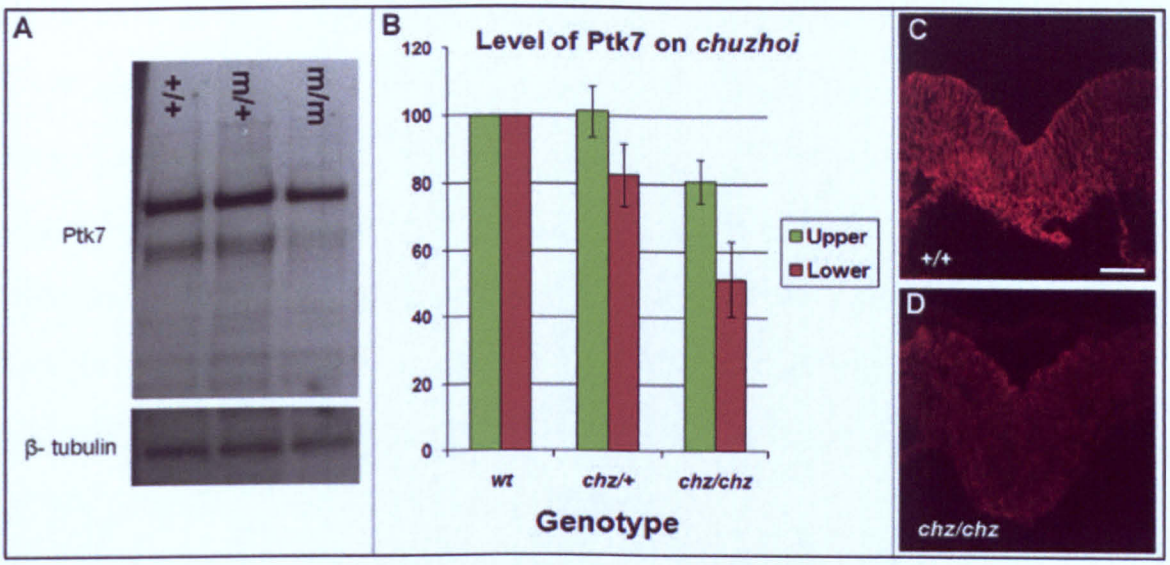

Figure 3-3: Level of Ptk7 is reduced in *chuzhoi*.
(A) Western blot on total cell lysate from E8.5 wildtype, heterozygous and homozygous *chuzhoi* embryos using anti-Ptk7 antibody. Ptk7 is found in two isoforms and the level of each isoform, particularly the smaller isoform, is reduced in *chuzhoi*. For a loading control anti-β-tubulin antibody was used. (B) Quantification of level of upper and lower isoform in wildtype, heterozygous and homozygous *chuzhoi* embryo, normalized to β-tubulin. (C,D) Localization of Ptk7 in E8.5 wildtype and *chuzhoi* embryos. Ptk7 localises to the plasma membrane in both wildtype and *chuzhoi* but the level of protein is reduced in *chuzhoi*. Scale bar represents 5 μm.

3.2.4 The *chuzhoi* phenotype is consistent with a defect in convergent extension

Previous work on other mutants displaying craniorachischisis has identified the fundamental defect giving rise to this phenotype as the failure to narrow and lengthen the midline of the embryo during neurulation (Greene et al., 1998; Murdoch et al., 2003). Since other craniorachischisis mutants exhibit a broadened midline owing to disruption of convergent extension (Section 1.3.4), I examined *chuzhoi* mutant embryos to see if they revealed similar midline defects.

1. *Chuzhoi* has a wider midline

To examine whether the midline of *chuzhoi* mutant embryo is wider compared to wildtype littermates, transverse sections through the spinal region of E8.5 embryos were

stained with hematoxylin and eosin (H&E) and examined. In the wildtype and heterozygous embryos, the neuroepithelium formed a V-shaped grove with a compact hinge at the midline. In contrast, the midlines of the mutants were wider and the neuroepithelium had a U-shaped morphology at the midline (Figure 3-4 C compare to D). Additionally, analyzing the sections further, it appeared that the neural folds failed to elevate in the *chuzhoi* mutants, a process which is thought to be normal in other mutants with craniorachischisis (Murdoch et al., 2001b). This suggests that the mechanism giving rise to craniorachischisis may be different in *chuzhoi.*

To confirm the finding that *chuzhoi* mutants have a wider midline, whole-mount *in situ* hybridization (WMISH) with probes for *sonic hedgehog* (*Shh*) and *brachyury* (*T*) was carried out. At E8.5, the time of initiation of neural tube closure, both *Shh* and *T* are expressed at the notochord, a midline structure of the embryo. The results showed that the notochord was wider in the mutant embryos compared to the wildtype littermates (Figure 3-4 E-L). In addition to the wider notochord, a subset of the mutant embryos had a split notochord (Figure 3-4 M-O).

2. Embryonic length to width ratio is smaller in *chuzhoi* mutant

A defect in convergent extension results in an embryo that is wider and has a shorter anterior posterior axis compared to wildtype embryos. With H&E stained sections and WMISH I have shown that the midline of the *chuzhoi* embryos is wider compared to wildtype littermates. To investigate whether or not the defect in *chuzhoi* mutant is consistent with a defect in convergent extension, I measured the width and the length of the anterior-posterior axis of the embryo. Briefly, embryos were harvested at E8.5 and were accurately staged by counting the number of the somites. Embryos were flat-mounted with the dorsal side up and a picture was taken under a microscope to measure the length and the width of the embryo. The embryonic width measurement was taken at the level of the third somite as this is the position within the embryo that will undergo the initiation of

neural tube closure, closure 1. The length of the embryo was measured from the site where the two head folds meet to the end of the embryonic body (Figure 3-5 A,B). Numbers of embryos analyzed for each genotype and somite numbers are given in appendix Table 10-2. Data suggests that the mutant embryos at each stage have a shorter body axis and a wider body compared to heterozygous and wildtype littermates. This gives rise to a lower length to width ratio in the mutant embryos at all stages (Figure 3-5 C). Furthermore, the difference in the ratio between the wildtype and the mutant increases as the embryos grow older suggesting that the defect is having an effect throughout the neurulation stages of the embryo and not only at the earlier stage. This result also shows that by the time embryos reach the 3 somite stage, the *chuzhoi* mutants are already significantly different compared to the wildtype littermates (Figure 3-5 C).

1. The node of *chuzhoi* is abnormal by head fold stage

To determine when defects are first seen in the *chuzhoi* mutants, WMISH using nodal probe was carried out on E7.5 and E8.0 embryos. Nodal is expressed by the cells surrounding the node, so it acts as a marker for the shape of the node. The node is a particularly important structure of an embryo at this stage as the cells migrating through the node give rise to the notochord which is an important midline structure and is abnormal in *chuzhoi* mutants. The results show that the shape of the node at E7.5 is normal in *chuzhoi* mutants compared to the wildtype (Figure 3-5 D,E), however by the headfold stage the node appears to be shorter and wider (Figure 3-5 F,G), again a phenotype that is consistent with a defect in the process of convergent extension.

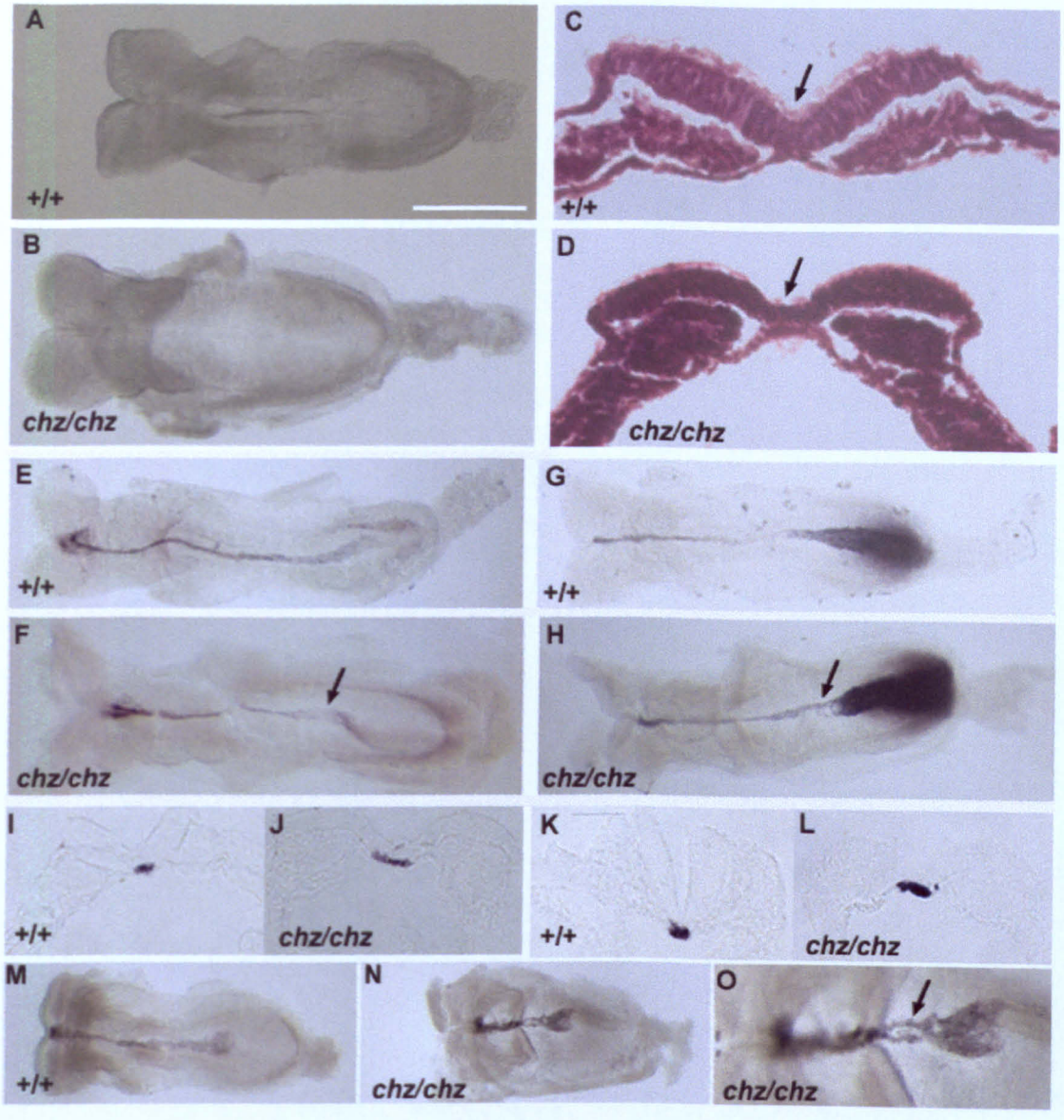

Figure 3-4: *chuzhoi* has a wider midline.
(A,B) Dorsal view of wildtype (A) and *chuzhoi* (B) embryos with six pair of somites, showing wildtype has undergone closure 1 to initiate neural tube closure while this has failed in *chuzhoi*. (C,D) Haematoxylin and eosin staining of transverse sections through the spinal region of wildtype (C) and *chuzhoi* (D) embryos with five somites, showing a compact midline in wildtype and a broadened midline in *chuzhoi* (arrows). (E-H) E8.5 embryos showing the expression pattern of *shh* (E,F) and *brachyury* (G,H) in wildtype (E,G) and *chuzhoi* (F,H) embryos. The domain of expression for both genes is wider in the posterior region of the *chuzhoi* embryo (arrow in F & H). (I-L) Transverse sections through the posterior region of embryos in panel E-H, showing a broader notochord in *chuzhoi* (J,L) compared to wildtype (I,K). (M) Wildtype embryo with four somites, showing expression domain of *shh*. (N) *chuzhoi* embryo with four somites showing expression domain of *shh* revealing a split notochord. (O) Higher magnification of embryo in panel (N), showing a split notochord (arrow). Scale bars represent 500 μm (A, B, E-H), 10 μm (C and D), 20 μm (I-L), 330 μm (M and N) and 165 μm (O).

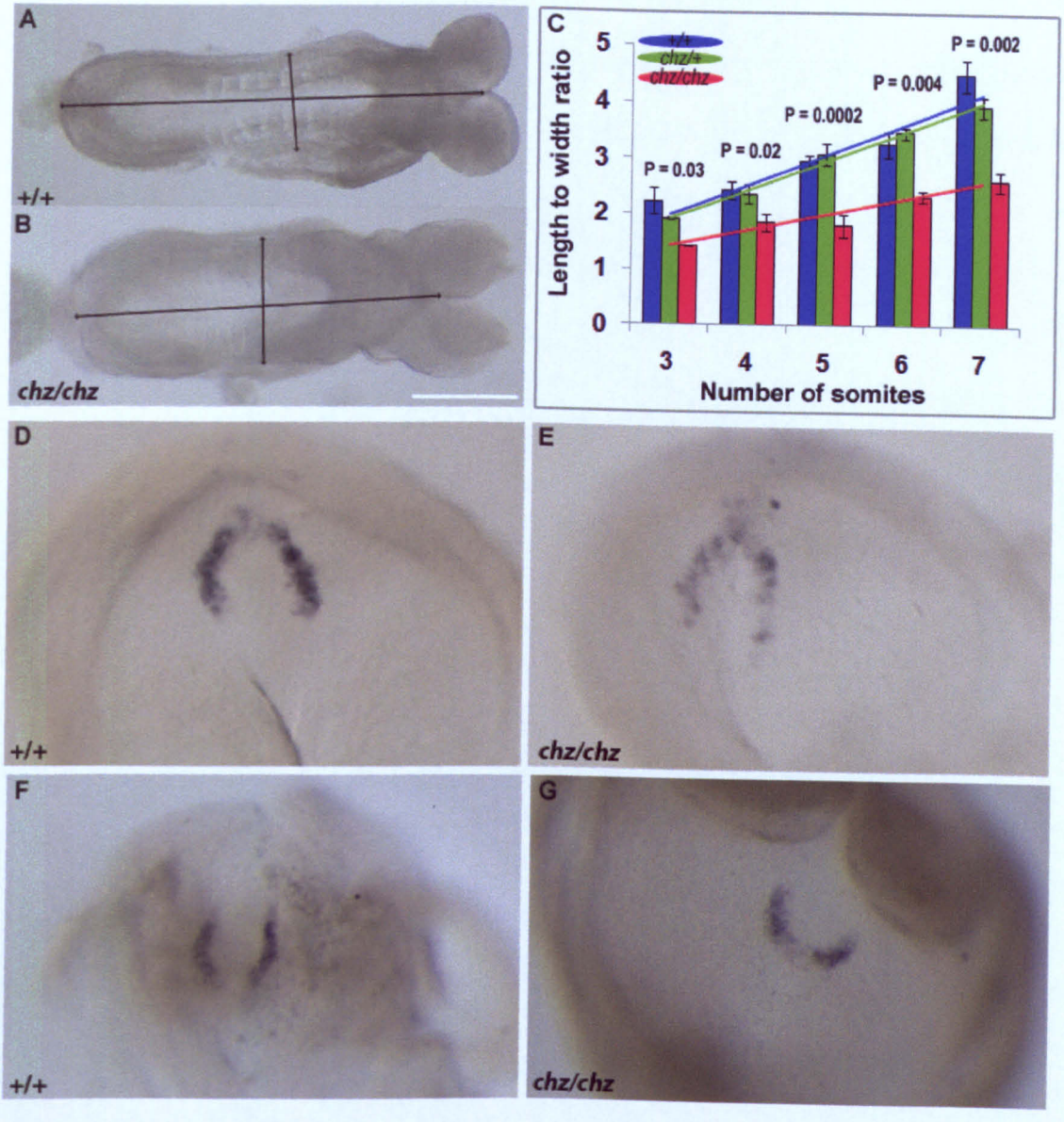

Figure 3-5: *chuzhoi* phenotype is consistant with a defect in convergent extension. (A,B) Dorsal view of a wildtype (A) and *chuzhoi* (B) embryo with seven somites. Lines indicate the position within the embryo where measurements for length and width were taken. (C) Comparison of length to width ratio of wildtype (blue), heterozygous (green) and *chuzhoi* mutant (red) embryos over three to seven somite stage. This shows a reduction in the increase of length to width ratio in *chuzhoi* mutant compare to wildtype and heterozygous. P value is obtained from a two tailed T-test between the wildtype and the mutant (D,E) Expression of *nodal* at E7.5 in wildtype (D) and *chuzhoi* (E) embryos, showing no differences in the expression domain of *nodal*. (F,G) Expression of *nodal* at E8.0 in wildtype (F) and *chuzhoi* (G) embryos, showing an altered expression domain in *chuzhoi* compared to wildtype. In *chuzhoi* the node appears shorter and broader compared to the wildtype node. Scale bar represents 500 μm (A and B), 250 μm (D and E) and 375 μm (F and G).

3.2.5 Expression of *Ptk7* during early development

The expression of *Ptk7* during neurulation (E7.5 to E9.5) was examined by WMISH using a *Ptk7* probe (Figure 3-6 A-C). In all stages examined, *Ptk7* was expressed robustly at the primitive streak and in the somites (when present). Interestingly, at the RNA level there appears to be only low intensity expression in the neuroepithelium at the site of closure 1; however when looking at the protein expression, there is a detectable level of Ptk7 protein present in the neuroepithelium at the site of closure 1 (Figure 3-3C). As expected from the nature of the mutation in *chuzhoi,* the *Ptk7* RNA expression pattern is not changed in the *chuzhoi* mutant embryos, compared to the wildtype littermates (Figure 3-6 D,E).

3.2.6 Expression of *Ptk7* during late development and associated phenotypes

To gain an insight into the function of *Ptk7* during later developmental stages, slide *in situ* hybridization was done on sections of E12.5, E14.5 and E16.5 wildtype embryos. The staining pattern shows that *Ptk7* is expressed robustly in the epithelium of developing lungs, gut and in the closing eyelid at E12.4 and E14.5 (Figure 3-6 F-K). By E16.5 the expression level of *Ptk7* appears to fall dramatically and very little expression is observed in lung and gut at this stage (Figure 3-6 L,M).

High levels of *Ptk7* expression in lung epithelium at E12.5 and E14.5, and an observation that other mouse mutants with craniorachischisis exhibited lung defects (Yates et al., 2010), led to examination of developing lungs in the *chuzhoi* mutant embryos. Briefly, lungs from E18.5 *chuzhoi* mutants and wildtype littermates were dissected and analyzed under a dissecting microscope. They were then processed for wax embedding and sectioned.

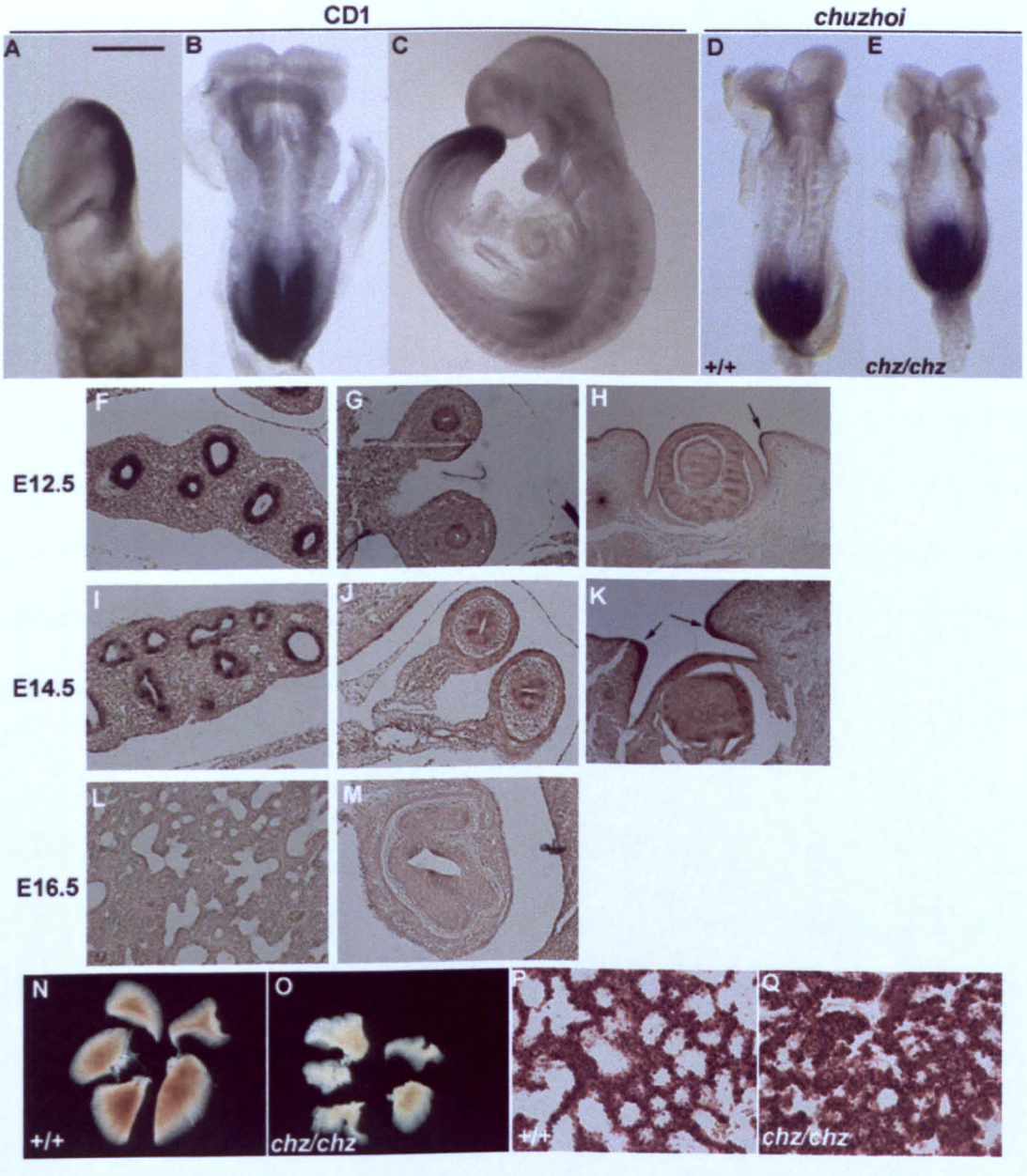

Figure 3-6: Expression of *ptk7* and lung phenotype.
(A-E) Whole mount *in situ* hybridisation with *Ptk7* probe. (A-C) Expression domain of *Ptk7* at E7.5 (A), E8.5 (B) and E9.5 (C) in CD1 embryos revealing that *Ptk7* is expressed robustly in the primitive streak and in somites. (D,E) Expression domain of *Ptk7* in wildtype (D) and stage matched *chuzhoi* (E) embryo, demonstrating that the expression domain does not change in *chuzhoi* compared to wildtype. (F-M) Slide *in situ* hybridisation with *Ptk7* probe to look at the expression domain of *Ptk7* during late development. (F-K) Expression of *Ptk7* in lung (F,I), gut (G,J) and in the eye (H, K arrow) at E12.5 (F-H) and E14.5 (I-K), showing that *Ptk7* is expressed most robustly in the epithelium. (L,M) Expression of *Ptk7* in lung (L) and gut (M) at E16.5, revealing a dramatic reduction compared to E12.5 and E14.5. (N,O) Gross morphology of lung from E18.5 wildtype (N) and *chuzhoi* mutant (O) embryo, revealing abnormalities in the shape and size of lung lobes. (P,Q) Haemotoxylin and eosin stained sections through the left lobe, showing thickened interstitial mesenchyme and fewer airway spaces in *chuzhoi* mutants (Q) compared to wildtype (P). Scale bar represent 400 μm (A), 250 μm (B), 1.2 mm (C), 650 μm (D,E), 20 μm (F-M), 4 mm (N,O) and 10 μm (P,Q).

Sections were stained with H&E and photographed. The gross morphology of *chuzhoi* lung is abnormal compared to the wildtype; namely lobes were reduced in size and were highly mishapen (Figure 3-6 N,O). Examination of histological sections revealed that the formation of airways in the lungs was severely compromised in the mutants compared to wildtype as mutants showed a thickened interstitial mesenchyme with occasional septation (Figure 3-6 P,Q). Correlating with Ptk7 expression on the closing eyelid, *chuzhoi* fetuses are born with open eye lid (Figure 3-1 E,F). This phenotype is similar to other mutants with craniorachischisis (Murdoch et al., 2003). Although no attempt was made to investigate whether or not there was an abnormal phenotype in the gut system of *chuzhoi* mutants, expression of Ptk7 was expected in the gut system because Ptk7 in human was originally identified as a suppressor of colon cancer (Mossie et al., 1995).

3.2.7 Heart development in *chuzhoi* is abnormal

Other mouse mutants with craniorachischisis also exhibit cardiovascular defects resulting from defective remodeling of the outflow tract during heart development (Henderson et al., 2001; Henderson et al., 2006; Phillips et al., 2007). To investigate whether or not *chuzhoi* exhibited heart defects, I collected and sectioned E17.5 *chuzhoi* and wildtype embryos to produce histological sections through the heart and sent them to a collaborator for analysis. The analysis showed that *chuzhoi* displayed various cardiovascular abnormalities resulting from defects in outflow tract development. In wildtype heart, the aorta exits from the left ventricle (Figure 3-7A) and pulmonary artery exits from the right ventricle (Figure 3-7C) and the two ventricles are separated by a muscular wall, the ventricular septum (Figure 3-7E). Of the seven *chuzhoi* mutants examined, three individuals displayed double outlet right ventricle, where both, the aorta and pulmonary artery, exit from the right ventricle (Figure 3-7 B, D) and a ventricular septal defect (Figure 3-7F) was observed. In another two cases the great arteries were

parallel rather than spiraling round one another but resulted in correct placements of the aorta and pulmonary artery.

3.2.8 Neural crest migration is unaltered in *chuzhoi*

The heart abnormalities observed in *chuzhoi* could arise from defects in neural crest migration (Kirby et al., 1983). Additionally, Ptk7 in *Xenopus* is required for neural crest migration (Shnitsar and Borchers, 2008). *Sox10* was used as a marker to visualize the migration of neural crest cells (Southard-Smith et al., 1998) at E10.5 in *chuzhoi* and wildtype embryos.

The result showed that the migration of the neural crest was not grossly disturbed in *chuzhoi* mutants but their distribution was slightly affected. In wildtype, Sox10 is expressed by neural crest cells at the cranial and dorsal root ganglia. In *chuzhoi* mutants, Sox10 is expressed at both cranial and dorsal root ganglia but the pattern of expression is disrupted. The trigeminal ganglion in *chuzhoi* mutants is of abnormal shape compared to wildtype and the ninth and tenth cranial ganglia appear to be fused. In dorsal root ganglia the normal V shape of stained cells is lost in mutants (Figure 3-8 A-C compare to D-F).

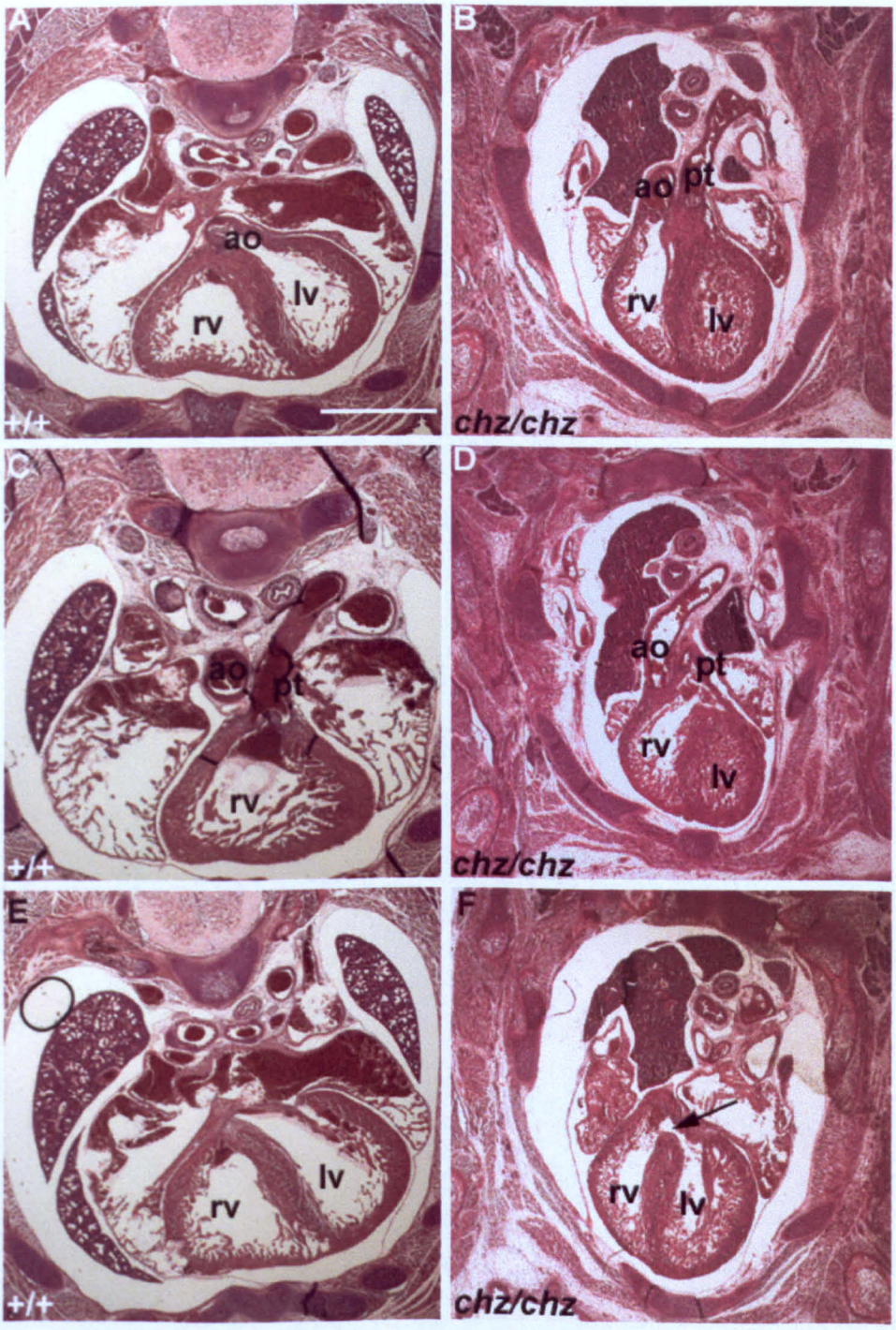

Figure 3-7: Heart defects displayed by *chuzhoi*.
(A-F) Haemotoxylin and eosin stained transverse sections through E17.5 wildtype (A,C,E) and *chuzhoi* (B,D,F) heart. (A,B) The aorta in wildtype (A) exits from the left ventricle; in *chuzhoi* heart (B) aorta exits from the right ventricle. (C,D) In both wildtype (C) and *chuzhoi* mutant (D), pulmonary trunk exits from the right ventricle. (E,F) In wildtype heart (E) two ventricles are completely separated by a muscular wall; in *chuzhoi* heart (F) the muscular wall is not completed (arrow) giving rise to a ventricular septum defect. ao, aorta; rv, right ventricle; lv, left ventricle; pt, pulmonary trunk. Scale bar represents 1 mm.

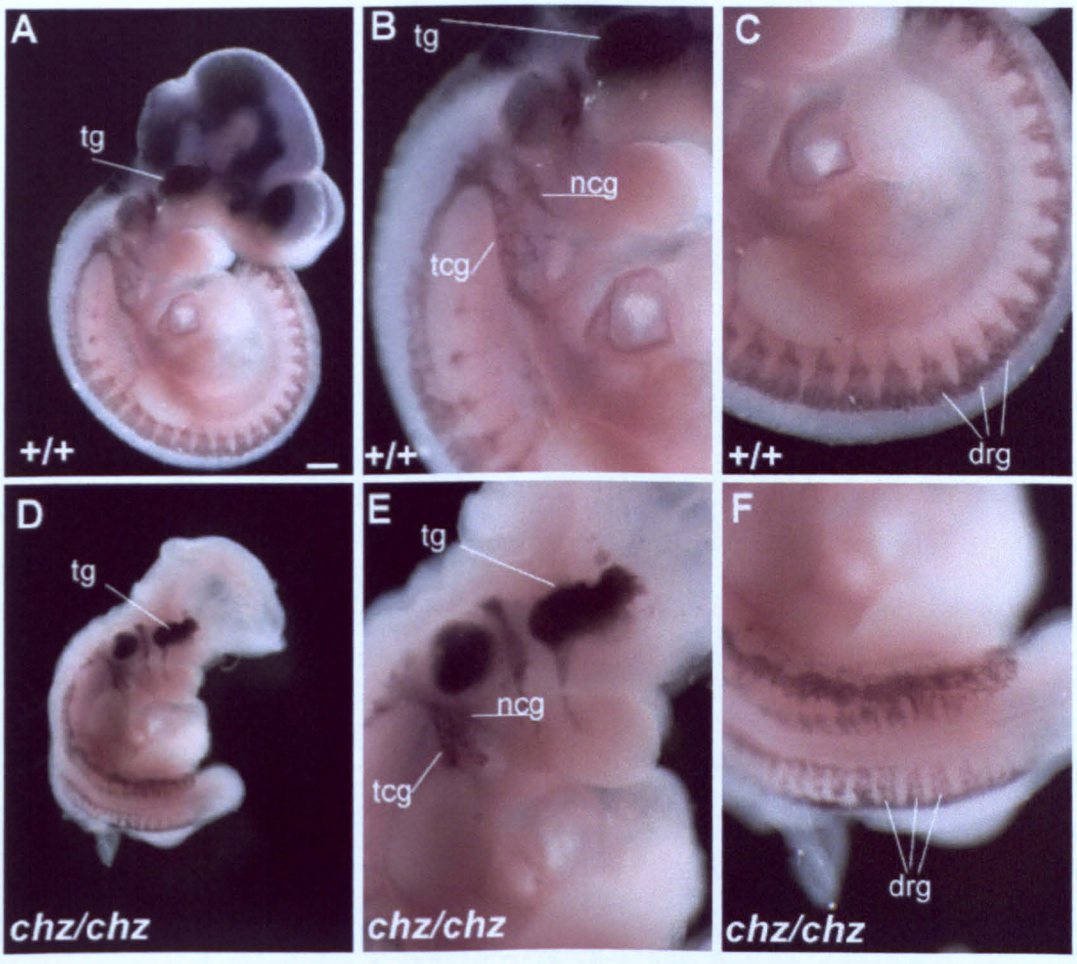

Figure 3-8: Neural crest migration is normal in *chuzhoi*.
(A-F) Wholemount *in situ* hybridisation for *Sox10* expression at E10.5 in wildtype (A-C) and *chuzhoi* mutant (D-F) embryos. Neural crest migration in *chuzhoi* is not affected as cells are found at both cranial ganglia (tcg, ncg and tg) and dorsal root ganglia (drg) (D-F) similar to that in wildtype (A-C). However the distribution of these cells is altered in *chuzhoi*. The shape of trigeminal ganglia (tg) is altered in *chuzhoi* (D,E), compared to wildtype (A,B). The ninth (ncg) and tenth (tcg) cranial ganglia appear fused in *chuzhoi* compared to wildtype (compare B with E). Distribution of neural crest cells at dorsal root ganglia is also affected in *chuzhoi* compare to wildtype (compare C with F). In wildtype *Sox10* positive cells form a V shape arrangement (C), while in *chuzhoi* this V shape is lost (F). Scale bar represent 500 μM in A and D, and 250 μM in B,C,E and F.

3.3 Discussion

3.3.1 *chuzhoi* carries a defect in Ptk7

A mutation in an intronic region of *Ptk7,* giving rise to a defect in the splicing of the gene, has been identified in *chuzhoi* as the causative mutation for the severe neural tube defect, craniorachischisis. Although the direct routes of confirming the mutation was not used in this study, several indirect evidences suggest that *Ptk7* is indeed the gene mutated in *chuzhoi.* Firstly, the gross phenotype of *chuzhoi* is identical to the phenotype reported for the gene trap allele of *Ptk7.* Both of these alleles display craniorachischisis with 100% penetrance, failure to close the ventral body wall and polydactyly ((Lu et al., 2004) and (Figure 3-1). Although craniorachischisis and failure to close ventral body wall have been reported for other mutants of severe neural tube defects (Curtin et al., 2003; Kibar et al., 2001; Murdoch et al., 2001a; Murdoch et al., 2003), the limb defect observed in the *Ptk7* mutant has not been reported in other mutants, giving evidence to support that the gene mutated in *chuzhoi* is that same as that in the gene trap allele of *Ptk7.*

Further evidence comes from the fact that the level of Ptk7 protein is reduced in *chuzhoi.* Furthermore, level of the lower isoform of Ptk7 protein appears to be disrupted in the mutant.

The third line of evidence comes from analyzing the expression domain of Ptk7 at RNA level and looking at the phenotypes displayed by *chuzhoi.* During early development Ptk7 is expressed most robustly at the caudal end of the embryo and at the somites. However, low level of Ptk7 is detected everywhere. Other genes giving rise to craniorachischisis when mutated are expressed most robustly at the site of closure 1 and at the caudal end (Kibar et al., 2001; Curtin et al., 2003; Murdoch et al., 2003). Since all the genes required for closure 1 are expressed most robustly at the caudal region of the embryo suggests that the primary defects leading to craniorachischisis may actually arise in the

caudal region. Indeed, a recent study has identified that the cells at the caudal end of *Loop-tail* embryos are abnormal (Ybot-Gonzalez et al., 2007b). *chuzhoi* also displays abnormal somite morphology and goes on to develop abnormal ribs, with fusions and bifurcations (Figure 3-1). While it is possible that abnormal somite morphology is a secondary consequence of the abnormal embryonic phenotype, it is also possible that Ptk7 is involved in regulating somite morphology as it is expressed in the somites of developing embryos. During late development, *Ptk7* is expressed in lungs and eye lid. A corresponding phenotype is observed in both lungs and eye lid development in *chuzhoi* mutants.

One of the direct routes that could be used to definitely confirm that *chuzhoi* carried a mutation in *Ptk7* is to do a complementation cross between *chuzhoi* and gene trap allele of *Ptk7* and show that they fail to complement each other.

3.3.2 The phenotype of *chuzhoi* is consistent with a defect in convergent extension

To date, all mutants displaying craniorachischisis show an identical early phenotype that precedes closure 1. In all of these mutants, the midline is broader placing the neural folds too far apart to oppose and fuse at the midline. A broader midline is now known to be a consequence of a failure in convergent extension. During convergent extension, cells of the neuroepithelium and the underlying mesoderm move towards and intercalate at the midline, contributing to narrowing and lengthening of the embryo. This process was first described in *Xenopus* (Wallingford and Harland, 2001), but since then it has also been demonstrated in mice (Wang et al., 2006a; Ybot-Gonzalez et al., 2007b; Yen et al., 2009). Furthermore, a defect in convergent extension has been reported in *Looptail* and the *Ptk7* gene trap allele (Ybot-Gonzalez et al., 2007b; Yen et al., 2009).

chuzhoi displays a broader midline with an expanded domain of *Shh* and *Brachyury* expression and a reduced rate of increase in length-to-width ratio. Both of these phenotypes are consistent with disruption of convergent extension.

3.3.3 Two bands are detected with an antibody against Ptk7

Ptk7 is a transmembrane protein, belonging to the receptor protein-tyrosine kinase family of proteins with an inactive kinase homology domain. Western blots to detect mouse Ptk7 protein using an antibody raised against the extracellular domain of Ptk7, detects two bands of approximately 100 kDa and 140 kDa (Lu et al., 2004) and (Figure 3-3). There are three main ways that these two isoforms can be formed; through alternatively spliced transcripts, through post translational modification of a proportion of full length protein or through cleavage of the full length protein. Although the organization of the *Ptk7* cDNA between human and mice is very similar and five alternatively splice variants have been reported for human PTK7, there is no evidence to indicate that alternatively spliced transcripts exist in mice (Jung et al., 2002; Jung et al., 2004) and Ensembl), giving no evidence to support the idea that the two isoforms of mouse Ptk7 are produced by this mechanism. Posttranslational modification of a proportion of Ptk7 protein could account for these two isoforms. The predicted molecular weight of mouse Ptk7 protein is 117.56 kDa however it has been reported that it runs at approximately 140 kDa in a western blot due to posttranslational modification (Jung et al., 2004). Indeed, Ptk7 is predicted to be post-translationally modified by phosphorylation at 4 residues (predicted with DisPhos 1.3) and by glycosylation at two different sites (predicted with DictyoGlyc 1.1). It could be hypothesized that the top band (of approximately 140 kDa) is the post-translationally modified Ptk7 while the bottom band (of approximately 100 kDa) is the full length Ptk7 protein without the posttranslational modifications. To determine whether or not this hypothesis is correct, mouse protein lysate could be treated with Trifluoromethanesulphonic acid to remove glycosaminoglycan chains and with Lambda protein phosphatase to remove phosphate groups from phosphorylated residues within Ptk7 protein. This treated lysate can then be run on a protein gel. If the hypothesis is correct then there would just be one band of approximately 100 kDa detected. However, if it is not correct then the antibody will still detect two bands but both of these bands are likely to be

smaller than that seen in untreated lysate. Another alternative is cleavage of Ptk7 protein. There is evidence to suggest that transmembrane proteins are cleaved to produce soluble fraction which can then function as a ligand to transduce signals (Schneider and Wolf, 2009). Interestingly, it has been reported that the extracellular domain of human PTK7 runs at approximately 100 kDa (Shin et al., 2008), supporting the hypothesis that the smaller isoform detected in the mouse lysate could result from cleavage of the protein close to the transmembrane region. However, both isoforms of mouse Ptk7 are detected in the membrane fraction (personal communication with Dr J. N. Murdoch) suggesting that, even if the protein is cleaved then it may be cleaved at the intracellular domain or the cleaved extracellular fragment may remain associated with the membrane by binding to the remaining fragment of the Ptk7 protein as seen with Notch receptor (Lai, 2002).

To determine whether the two isoforms of mouse Ptk7 protein result from post translational modification or from cleavage of the protein, a construct encoding full length Ptk7 with two unique tags (e.g. FLAG and V5) at either end of the protein could be expressed in a mouse cell line (where cellular machinery to cleave the protein and post-translationally modify the protein exits) and protein lysate from these cells could be run on a protein gel and detected with antibodies against the two tags (Figure 3-9). If the protein is cleaved, then the tag at the N terminal (e.g. FLAG) will detect a band of 140 kDa and 100 kDa, while the C terminal tag (e.g. V5) will detect a band of 140 kDa and 40 kDa. However if the protein is not cleaved and the two isoforms result from a posttranslational modification, then both C and N terminal tags will detect a band of 140 kDa and 100 kDa and treatment to remove posttranslational modifications should lead to detection of a single band of approximately 100 kDa (Figure 3-9).

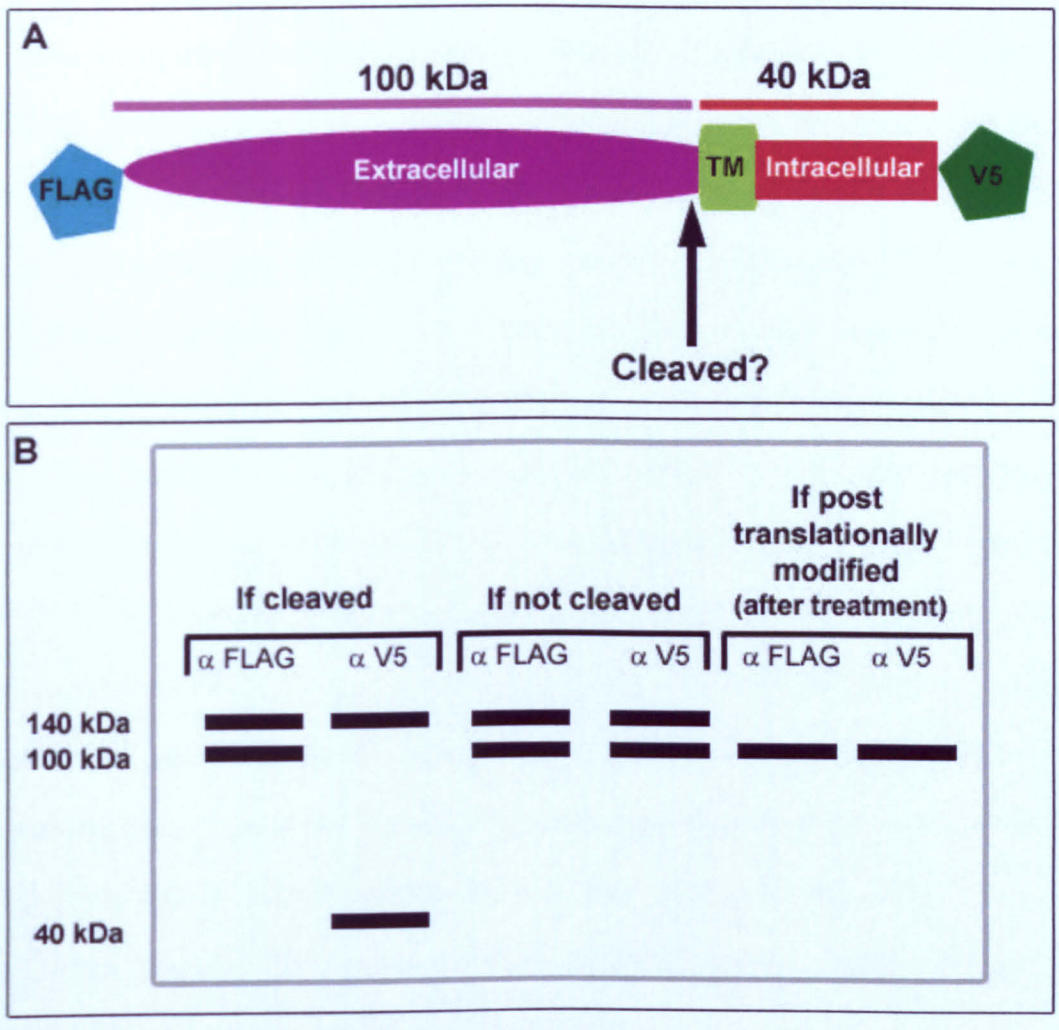

Figure 3-9: Proposed experiment to determine whether or not Ptk7 is cleaved.
(A) Structure of Ptk7 with a FLAG tag at the N-terminal and a V5 tag at the C-terminal. The full length mouse Ptk7 runs at 140 kDa on a western blot and the extracellular domain of human PTK7 runs at 100 kDa on a western blot. (B) Construct in (A) is expressed in a mouse cell line, protein is extracted and run on a protein gel. Antibody specific to two tags are used to determine the size of Ptk7 bands. Different size bands are detected by two different antibodies if Ptk7 is cleaved.

3.3.4 Ptk7 in *chuzhoi*

The mutation carried by *chuzhoi* results in addition of three extra amino acids at the end of the 5th immunoglobulin like domain. These extra amino acids appear to make the mutated protein less stable than the wildtype form as both isoforms of Ptk7 are reduced in *chuzhoi* mutants. Although both isoforms are reduced, the reduction level of the smaller isoform is more severe than the larger isoform. The precise mechanism by which this is achieved is not known. If Ptk7 is undergoing cleavage then it appears that the three extra amino acids present in *chuzhoi* Ptk7 are hampering the cleavage, presumably through a change in the overall structure of the mutated protein. However if the two isoforms result from post translational modification, where the larger band is the post-translationally modified form and the smaller band is the unmodified form, then in *chuzhoi* mutants the level of Ptk7 produced is low (as indicated by reduction in both isoform i.e. overall reduced level of Ptk7). However most of the protein that is produced is post-translationally modified so the level of lower isoform is dramatically reduced as it is not allowed to remain in a post-translationally unmodified form. In *chuzhoi* mutants, although both the isoforms are significantly reduced compared to the wildtype, the smaller isoform is more dramatically reduced than the larger isoform suggesting that the smaller isoform of the protein may be the active form during neurulation.

3.3.5 Heart defects in *chuzhoi*

The heart defects observed in *chuzhoi* are similar to those described in other mutants with craniorachischisis (Henderson et al., 2001; Hamblet et al., 2002; Phillips et al., 2005; Henderson et al., 2006; Phillips et al., 2007; Etheridge et al., 2008). In *Loop-tail*, an abnormality in muscularization of the outflow tract cushion was observed as a direct consequence of the failure of cardiomyocytes to migrate in a polarized fashion into the outflow tract cushion (Phillips et al., 2005). It has been suggested that this failure of

muscularization could account for the ventricular septum defect present in *Loop-tail* mice. *chuzhoi* exhibits a similar ventricular septum defect to *Loop-tail* mutants suggesting that the primary defect may be similar between these two mutants. To test this hypothesis, it is necessary to study the distribution of cardiomyocytes during muscularization of the outflow tract in *chuzhoi* mutants.

The link between the defects in neural crest migration and cardiovascular abnormalities have been known since 1983 (Kirby et al., 1983). Furthermore, a recent publication revealed a critical role for Ptk7 in neural crest migration in *Xenopus* (Shnitsar and Borchers, 2008). This led to an investigation of neural crest migration in *chuzhoi.* However, the role of Ptk7 does not appear to be conserved between *Xenopus* and mouse, as no neural crest migration abnormality was observed in *chuzhoi.* This result is in agreement with the result obtained for *Loop-tail*, where heart defects similar to *chuzhoi* are observed but no neural crest migration defect was found (Henderson et al., 2001).

The abnormal distribution of *Sox10* positive cells in *chuzhoi* is likely to be a secondary defect due to the severely disrupted phenotype. *chuzhoi* mutants at E10.5 are morphologically very different from the wildtype littermates. The organization of somites throughout *chuzhoi* embryo is malformed, which is likely to be a secondary consequence of the open neural tube and convergent extension defects, but could account for the differences observed in the dorsal root ganglia.

Another defect that can lead to the cardiac phenotypes observed in *chuzhoi* is the defect in aligning the great arteries with the ventricles. This could arise from incomplete axial rotation of the embryo, a phenotype that has been associated with *Loop-tail* (Smith and Stein, 1962), disruption of the laterality, as seen in *cited2* mouse mutant (Bamforth et al., 2004) or disruption in embryonic head flexure, as seen in chick embryos (Manner et al., 1993). These are all possibilities that remain to be examined in *chuzhoi.*

CHAPTER 4

INVESTIGATING GENETIC AND MOLECULAR ROLES OF PTK7

4 Investigating genetic and molecular roles of *Ptk7*

4.1 Introduction

4.1.1 Mutants of the Planer Cell Polarity (PCP) signalling pathway display craniorachischisis

Currently there are seven genes known to give rise to craniorachischisis when mutated in mice; *Vangl2* (mutated in *Loop-tail*) (Kibar et al., 2001; Murdoch et al., 2001a), *Celsr1* (mutated in *Crash* and *Spincycle*) (Curtin et al., 2003), *Disheveled 1/2* (Hamblet et al., 2002), *Frizzled 3/6* (Wang et al., 2006b), *Protein tyrosine kinase-7 (Ptk7)* (Lu et al., 2004), *Scribble* (mutated in *Circletail*) (Murdoch et al., 2003) and *Smurf1/2* (Narimatsu et al., 2009). Homologues of these genes are found in *Drosophila*, and homologues of *Vangl2, van gogh/strabismus; Celsr1, flamingo/starry night, Dishevelled1/2, dishevelled,* and *Frizzled3/6, frizzled* are considered to encode the core components of the planar cell polarity (PCP) signalling pathway. *Smurf1/2* is not a direct component of the PCP pathway but it is an ubiquitin ligase whose targets include Prickle1 (Narimatsu et al., 2009). *Prickle1* (*prickle*) is a component of the core PCP pathway. In *Drosophila Scribble* was originally identified as a gene required for setting up apical basal polarity and controlling proliferation rate (Bilder and Perrimon, 2000). Recently it has been shown that Drosophila *Scribble* is also a component of the PCP pathway and it genetically and physically interacts with *Drosophila* strabismus (Courbard et al., 2009). Genetic and physical interaction between mouse *Scribble* and *Vangl2* have also been reported (Murdoch et al., 2001b; Kallay et al., 2006; Montcouquiol et al., 2006). Although a homologue of *Ptk7* is present in *Drosophila, off-track,* to date this protein does not have any definitive link to the *Drosophila* PCP pathway. *off-track* is involved in axon guidance during development (Winberg et al., 2001) and more recently other members of the core PCP signalling, such as mouse Dishevelled, have also been linked to axon guidance (Zhang et al., 2007). The

mouse mutant *Ptk7* show signs of a defect in the vertebrate PCP pathway, as indicated by loss of uniform orientation of the hair cell stereociliary bundles within the inner ear and failure of closure 1 during neurulation (Lu et al., 2004) and Chapter 2; however its role in axon guidance has not yet been examined.

Furthermore, genetic tests have shown that the *Ptk7* gene trap allele shows genetic interactions with *Loop-tail* (the mutant carrying a mutation in *Vangl2*), producing double heterozygotes with neural tube defects (Lu et al., 2004) indicating that *Ptk7* may act in the same pathway as *Vangl2*.

4.1.2 Ptk7 and its homologues

Homologues of *Ptk7* are present throughout evolution, and are found in *Hydra* (*lemon*) (Miller and Steele, 2000), *Drosophila* (*off-track*) (Pulido et al., 1992), chickens (*klg*) (Chou and Hayman, 1991), mice (*Ptk7*) (Jung et al., 2004) and humans (*CCK4 / PTK7*) (Mossie et al., 1995). At the peptide level the similarity observed between mouse Ptk7 and the *Drosophila* homologue, off-track, is 43.7 %, while the similarity between mouse Ptk7 and human PTK7 is 94.7% (sequence obtained from Ensembl genome browser at http://www.ensembl.org/index.html and aligned using the EMBL-EBI align tool at http://www.ebi.ac.uk/). Despite the low level of similarity at the peptide level between mouse Ptk7 and *Drosophila* off-track, the overall structure of the protein is conserved, consisting of immunoglobulin like extracellular domains (six in *Drosophila* and seven in mouse and human), a transmembrane domain and an intracellular inactive tyrosine protein kinase domain (Pulido et al., 1992; Jung et al., 2004). The known functions of this protein differ widely. In *Drosophila* off-track is involved in axon guidance during neuronal development (Winberg et al., 2001) while PTK7 in human is involved in either the establishment or progression of colon carcinoma (Mossie et al., 1995). In *Xenopus* it is required for neural crest migration (Shnitsar and Borchers, 2008) and in mice, Ptk7 is

required to control the planer cell polarity signalling pathway (Lu et al., 2004; Yen et al., 2009).

Ptk7 is a member of the receptor protein tyrosine kinase (RPTK) family, and has an inactive kinase domain (Jung et al., 2004). RPTKs are a group of transmembrane protein that transduce extracellular signals into the cells and are important for various cellular functions such as regulating proliferation, cell migration and differentiation (Park et al., 1996). There are two different mechanisms by which RPTKs with inactive kinase domains can transduce extracellular signals.

The first mechanism is dimerization with other RPTKs containing active kinase domains able transduce the signal. One such example is ErbB3, a member of the vertebrate EGFR family. The kinase activity of ErbB3 is impaired; however it forms a complex with ErbB2, a second member of the EGFR family, which carries an active kinase domain and together they transduce mitogenic signals (Pinkas-Kramarski et al., 1996). The transmembrane domain of Ptk7 and its homologues is highly conserved suggesting a functional importance of this domain for the proper function of the protein (Miller and Steele, 2000). It has been suggested that it could be involved in driving protein-protein interactions (Kobus and Fleming, 2005), possibly leading to dimerization with other RPTKs. However, thermodynamic studies suggest that this motif in Ptk7 is not capable of driving a strong protein-protein interaction (Kobus and Fleming, 2005). This finding does not rule out the possibility that these proteins are functioning by dimerizing with other RPTKs via other domains.

The second mechanism by which RPTKs are known to transduce signals is by acting as a substrate for other RPTKs with active domains (Jung et al., 2004). However, a kinase assay showed that Ptk7 was not phosphorylated at tyrosine residues in the presence of other RPTKs, leading to the conclusion that Ptk7 is not a substrate of RPTKs (Jung et al., 2004).

As these proteins are likely to function by interacting with other proteins, it is essential to identify the interacting partners to fully understand the function of Ptk7.

4.1.3 Yeast 2 hybrid screen

The yeast 2-hybrid system is an established technique to identify novel protein-protein interactions in a cellular setting. First developed by Fields and Song in 1989 to study interaction between two proteins (Fields and Song, 1989) it has since been used in many different studies as a powerful tool to identify novel interacting partners of a protein of interest. This technique is based on the fact that transcription factors possess two distinct domains required for successful transcription of a gene (Keegan et al., 1986). The first domain, the DNA binding domain (DBD), is required to bind to the operator sequence present upstream of a gene and the second domain, the activation domain (AD), is required to recruit the RNA polymerase II complex to initiate transcription. The transcription factors commonly used in yeast 2-hybrid experiments are LexA and Gal4.

In a classic yeast 2-hybrid screen, the protein of interest is fused to the DBD to create a 'bait' protein which is used to screen the 'prey' cDNA library, which has been constructed by fusing a cDNA library with the AD. The bait and prey are co-transfected into a yeast cell. Protein synthesis takes place resulting in production of the protein of interest fused to the DBD of the transcription factor, as well as the protein encoded by a specific cDNA fragment from the cDNA library fused to the AD of the transcription factor. Due to the nuclear localization sequence present in both the DBD and AD, both the proteins are transported into the nucleus. In the nucleus, if the two proteins encoded by the prey and bait physically interact, then they bring the DBD and AD of the transcription factor into close proximity resulting in activation of transcription (Figure 4-1).

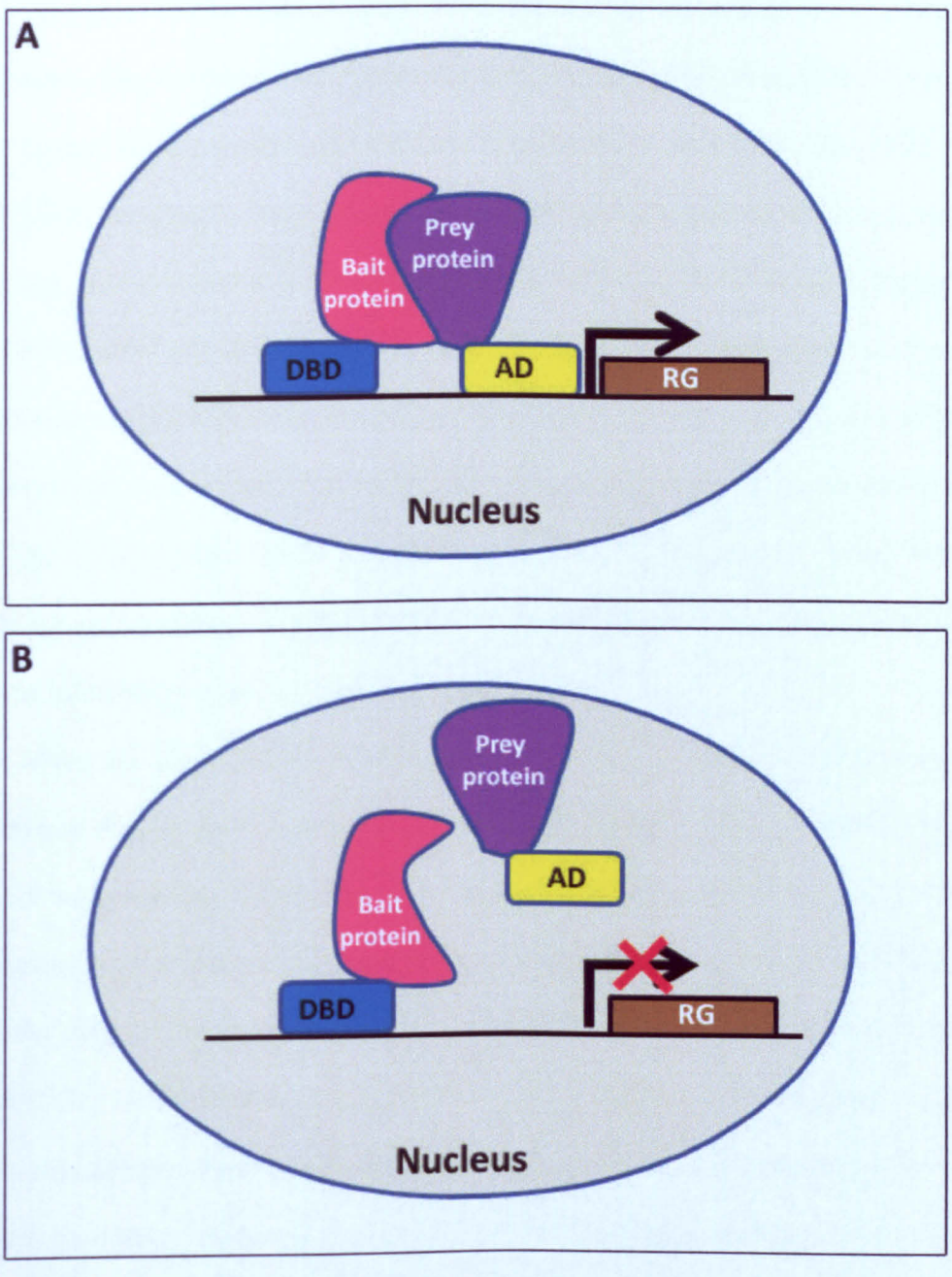

Figure 4-1: An overview of yeast 2-hybrid screen.
The protein of interest (bait protein, pink) is fused to the DNA binding domain (DBD, blue) of a transcription factor. A library is constructed by fusing proteins (prey protein, purple) to the activator domain (AD, yellow) of a transcription factor. When the bait protein and the prey protein interact, the DNA binding domain and the activator domain of the transcription factor come into close proximity which then function as a functional transcription factor and activates the transcription of reporter genes (RG, brown). If the bait protein does not interact with the prey protein (B), the reconstruction of a functional transcription factor fails to occur and the reporter gene is not transcribed.

In a yeast 2-hybrid screen, transcriptional activation of a number of reporter genes is measured. Two or more reporter genes are stably integrated in the genome of yeast used in the screen. Each reporter gene consists of an operator site, where the DBD of the transcription factor binds (the sequence of the operator site is specific to the transcription factor used during the screen), a minimal promoter region and the sequence of the reporter gene. The reporter gene is usually a gene that enables yeast to grow on medium lacking a certain amino acid, for example the His3 and Ade2 gene, which encode enzymes that allow the yeast to grow in medium lacking histidine and adenine respectively. Another reporter gene that is widely used in this technique is the LacZ gene. LacZ is a bacterial gene encoding β-galactosidase, an enzyme which reacts with X-gal to produce detectable levels of a blue insoluble product.

Since the yeast 2-hybrid system is now a standard technique, various companies can perform the screen for researchers. Dualsystems Biotech (www.dualsystems.com) is one such company that will undertake the entire screen from cloning the gene of interest into a vector used in the screen, to generating a list of candidate genes. Scientists can also clone the gene of interest into a vector provided by the company and then hand the construct over to the company to perform the screen. Before a screen is performed there are various steps that need to be successfully completed for each potential bait protein.
The first requirement is that the protein of interest is expressed correctly in the yeast. To test this, the bait is transformed into a yeast strain allowing protein expression. This is followed by western blot analysis of total cell extracts. An antibody raised against the DBD is used to detect the fusion protein. The second step is to test the bait for self activation. If the bait on its own is able to induce transcription of reporter genes, then it cannot be used in the screen without further modification. Further modifications may include reversing the orientation of the DBD, removal of certain amino acids, especially if the protein contains a large stretch of acidic amino acids, or splitting the protein of interest into domains. Once the self activation issues have been resolved, the bait is ready for a

pilot screen. This is an important step in the screening protocol as the outcome from this screen will define the conditions that will be employed to do the final screen. During the pilot screen, a bait-carrying yeast strain is transformed by empty library vectors and plated onto selective medium of increasing stringency. The lowest stringency condition, where no growth takes place, is the condition used for screening as this avoids many false positives without compromising the ability to detect weak interactions. This is usually a media lacking histidine (SD-His plate) with a low concentration of a histidine inhibitory compound, 3-aminotrazole (3-AT). 3-AT is usually required as the *HIS3* gene is slightly 'leaky', resulting in growth in SD-His medium.

Finally the bait is ready for screening the cDNA library to identify genes of interest. During this step, the bait-bearing yeast strain is transformed with a library of cDNA fused to the AD of the transcription factor. Several aliquots of cDNA library are used in many independent transformation reactions to make sure that a wide range of cDNA is tested for interaction. Transformed cells are then plated on selective medium as optimized in the pilot screen. Clones growing on this selection medium are picked and grown in another selective medium (usually SD-ade) and assayed for *LacZ* activity. The plasmid is isolated from all clones that give positive results for all three selection criteria, and is transferred into E-coli for amplification.

To remove some false positives, a bait dependency test is done. Here the DBD-bait and a negative control are transformed into a mating type 'α' yeast strain and the AD-prey that came out of the screen is transformed into a mating type 'a' yeast. The strains of yeast are allowed to mate and transferred to selective medium. Only those AD-preys that are positive for all selection criteria when co-expressed with the original bait and not with the negative control bait are true positives.

4.2 Results

4.2.1 *chuzhoi* genetically interacts with *Loop-tail* and *Crash* but not *Circletail*

To determine the involvement of *Ptk7* in the PCP pathway, I set up crosses to determine the genetic interaction between *chuzhoi* and *Loop-tail, Crash* or *Circletail*. Heterozygous *chuzhoi* mice were crossed with heterozygous *Loop-tail, Crash* or *Circletail* mice, and I examined the resulting embryos between E11.5 and E13.5 for any neural tube defects. Both males and females from each line were used during the crosses. In all crosses, the proportion of differentially genotyped embryos followed expected Mendelian ratios (Table 4-1), suggesting that all genotype groups of embryos were surviving until the stage examined.

Table 4-1: Intercross between *chuzhoi* and *Circletail, Crash* and *Loop-tail* heterozygous mice generates different classes of embryos with expected Mendelian ratios.
Chi-square test performed with 3 degrees of freedom.

Cross: *Crc/+; chz/+*					***Total***	***Chi*** ^{2}
Genotype	*+/+;+/+*	*Crc/+;+/+*	*+/+;chz/+*	*Crc/+;chz/+*		
Observed (expected) number of embryos	50 (39.5)	37 (39.5)	40 (39.5)	31 (39.5)	**158**	**4.8 (P>0.05)**
Cross: *Crsh/+; chz/+*						
Genotype	*+/+;+/+*	*Crsh/+;+/+*	*+/+;chz/+*	*Crsh/+;chz/+*		
Observed (expected) number of embryos	44 (38.25)	43 (38.25)	33 (38.25)	33 (38.25)	**153**	**2.9 (P>0.05)**
Cross: *Lp/+; chz/+*						
Genotype	*+/+;+/+*	*Lp/+;+/+*	*+/+;chz/+*	*Lp/+;chz/+*		
Observed (expected) number of embryos	39 (32.75)	30 (32.75)	27 (32.75)	35 (32.75)	**131**	**2.6 (P>0.05)**

The results obtained from these crosses were surprising. In all three crosses the majority of the compound heterozygous embryos were phenotypically normal. In the cross between *chuzhoi* and *Loop-tail*, 23% of doubly heterozygous embryos displayed spina bifida while a further 6% displayed craniorachischisis (Figure 4-2 C and D). The interaction between *chuzhoi* and *Crash* was even weaker, with only 6% of the doubly heterozygous displaying spina bifida (Figure 4-2 B and D) and none exhibiting craniorachischisis. No genetic interaction was observed between *chuzhoi* and *Circletail* mice as all the compound heterozygous embryos appeared normal (Figure 4-2 D). To test whether the compound heterozygous (*Crc/+;chz/+*) mice were viable, some of the females from intercrosses were allowed to litter down. The litter included doubly heterozygous animals which survived to adulthood. To determine if these doubly heterozygous animals were fertile, six doubly heterozygous females were crossed to doubly heterozygous males. This resulted in plugged females, which were pregnant suggesting that the compound heterozygous mice were both viable and fertile. These pregnant females were harvested between E10.5 and E12.5, however no doubly homozygous embryos were present in the litter (n = 30) suggesting that doubly homozygous embryos died early on in the development.

4.2.2 Mutation in Ptk7 does not affect the stability of Vangl2, Celsr1 or Scribble

In an attempt to examine the molecular nature of the genetic interaction between both *chuzhoi* and *Looptail*, and *chuzhoi* and *Crash*, and the lack of interaction between *chuzhoi* and *Circletail*, I carried out a western blot analysis to test whether or not mutation in Ptk7 affected the stability of Vangl2, Celsr1 or Scribble (Figure 4-3). For these experiments, I extracted total protein lysate from E8.5 embryos which had just undergone closure 1 (7-9 somites) and used this to study stability of Vangl2, Celsr1 and Scribble.

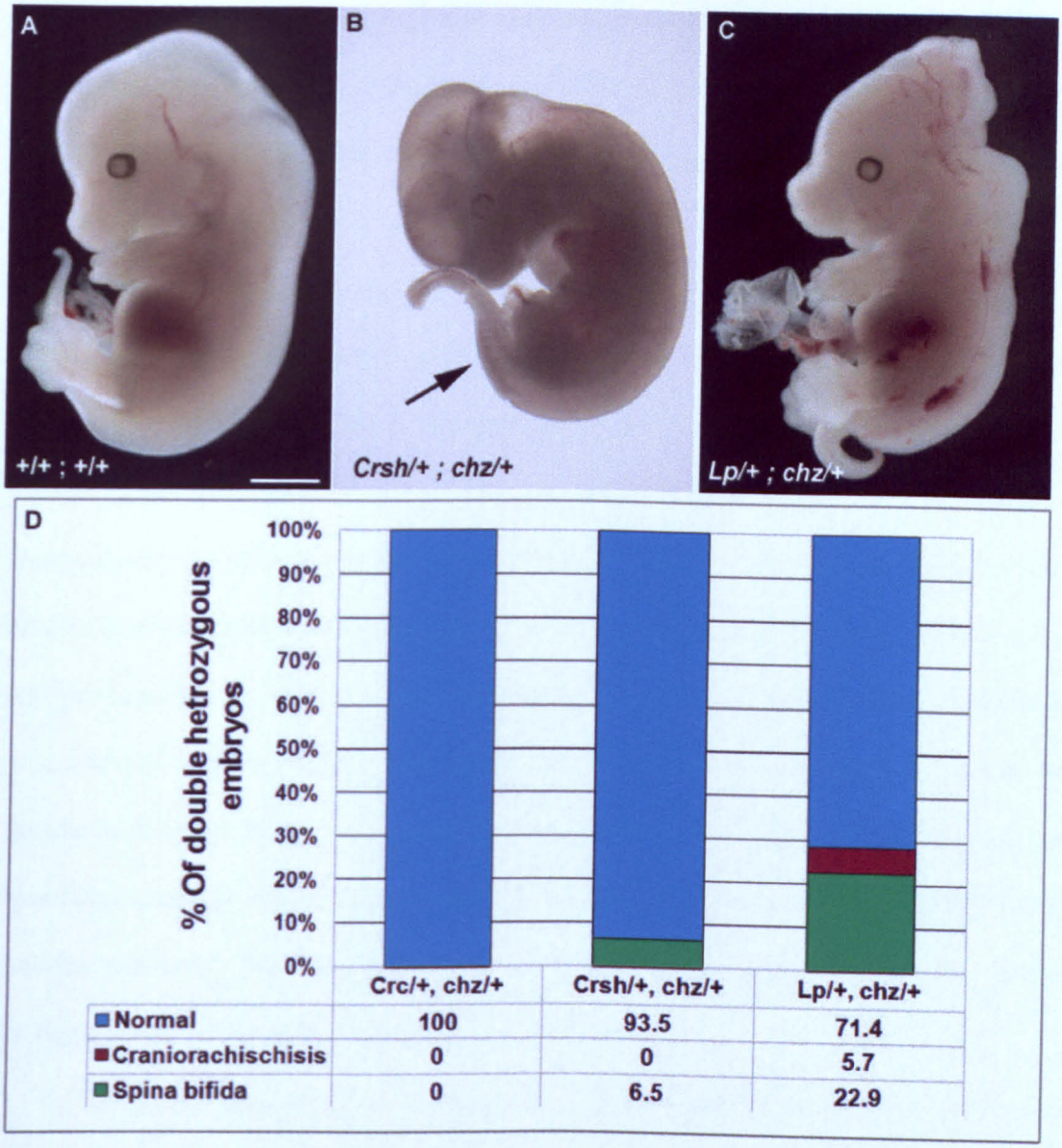

Figure 4-2: Genetic interaction between *chuzhoi* and *Circletail, Crash* and *Looptail.* (A) E13.5 wildtype embryo showing closed neural tube. (B) E11.5 *Crsh/+; chz/+* doubly heterozygous embryo, exhibiting spina bifida (arrow). (C) E13.5 *Lp/+; chz/+* doubly heterozygous embryo, displaying craniorachischisis. (D) The bar chart shows the percentage of double heterozygotes displaying normal (blue), spina bifida (green) or craniorachischisis (red) phenotypes, for each genotype as labeled in the X axis. Scale bar represent 2.5 mm in A and C, and 1.25 mm in B.

Protein extracts from *chuzhoi* mutant, heterozygous and wildtype littermates ($n \geq 3$ in all cases) were loaded onto a gel, blotted and probed with antibody raised against Vangl2, Celsr1 or Scribble. To make sure that the amount of protein loaded in each well was similar, the same blots were probed with antibody against fatty acid synthase as a loading control. The stability of Vangl2, Celsr1 and Scribble appears to be unaltered in *chuzhoi* mutants. The antibodies raised against Vangl2 gives multiple bands when used to probe a western blot. To determine the correct band corresponding to this protein, I ran the protein lysate from *Loop-tail* mutants on blots and probed for Vangl2 (Figure 4-3 A). It has been previously reported that Vangl2 is unstable in *Loop-tail* (Montcouquiol et al., 2006). Vangl2 gives two distinct bands with a smear between them. The top band is approximately 65 kDa and is the expected size of Vangl2. In *Loop-tail* lysate, the two distinct bands are absent but the smear between the two bands is still present (Figure 4-3 A). This suggests that the two distinct bands are Vangl2 protein but the smear in between is non-specific signal. Analysis shows that both the bands corresponding to Vangl2 are present in *chuzhoi* mutants at a similar level to that of the wildtype (Figure 4-3 A). For quantification purpose only the top band, which is most likely to represent the full length protein, was used. The quantification result shows that the level of protein in *chuzhoi* mutants is similar to that found in wildtypes (Figure 4-3 A).

The Celsr1 antibody gives a single band of the expected size (approximately 350 kDa) in all three genotypes. Quantifying this band in the three genotypes suggests that there is similar level of Celsr1 in *chuzhoi* mutants compared to wildtype littermates (Figure 4-3 B). Antibodies against Scribble give multiple bands when used to probe western blots. To determine the correct band corresponding to Scribble, I ran the protein lysate from *Circletail* mutants on blots and probed for Scribble (Figure 4-3 C). *Circletail* carries a mutation in *Scribble*. The nature of the mutation is such that it truncates the protein so full length *Scribble* is not formed (Murdoch et al., 2003). Scribble antibody gives three individual bands of approximately 185 kDa, 170 kDa and 130 kDa all of which are absent

in *Circletail* lysate suggesting that all three bands are part of the Scribble protein (Figure 4-3 C). In *chuzhoi* mutants, all three bands are present at similar levels to the wildtype lysate. For quantification purpose only the top band was used as it is most likely to represent the full length form of the protein and other lower bands are likely to be either cleaved or degraded forms of the protein. The quantification shows that the level of protein in *chuzhoi* mutants is similar to that found in wildtypes however the level of Scribble in *chuzhoi* hetrozygous is significantly higher compared to the wildtype (Figure 4-3 C)

4.2.3 Mutation in Vangl2, Celsr1 or Scribble does not affect the stability of Ptk7

Conversely, I also did the experiment to test whether or not mutation in Vangl2, Celsr1 and Scribble affected the stability of Ptk7 (Figure 4-4). For this experiments, I extracted total protein lysate from E8.5 embryos which had just undergone closure 1 (7-9 somites) and used this to study stability of Ptk7. Protein extracts from mutant, heterozygous and wildtype littermates from *Looptail, Crash* and *Circletail* ($n \geq 3$ embryos for each genotype) were loaded onto a protein gel, blotted and probed with Ptk7 antibody (Figure 4-4 A). The expression level of Ptk7 appears to be unaltered in all three mutants, compare to the wildtyoe. For each of the mutant lines, both the cleaved form of Ptk7 and the full length form are present in each of the mutants and wildtype littermates. To determine the level of full length and the cleaved from of Ptk7, I quantified the bands. This analysis shows that in the mutant the expression level of both of these forms of Ptk7 is comparable to that of the wildtype (Figure 4-4 B and C).

Together, these results suggest that the genetic interaction observed between *chuzhoi* and either *Looptail* or *Crash* is not mediated through a change in the levels of Ptk7, Vangl2 or Celsr1 proteins.

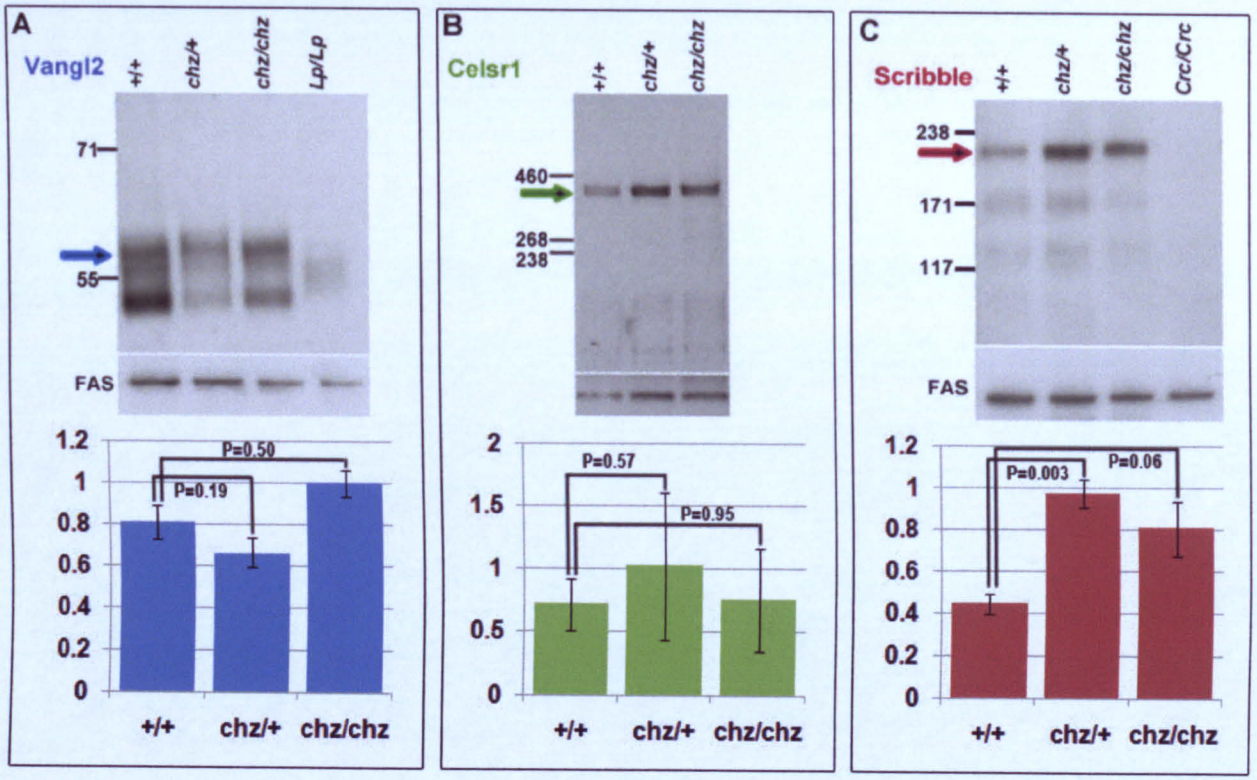

Figure 4-3: Western blots show that levels of Vangl2, Celsr1 and Scribble are unaltered in *chuzhoi* mutants
Western blot of total cell lysate from E8.5 wildtype, heterozygous, and mutant embryos, using antibodies against, Vangl2 (A) Celsr1 (B) and Scribble (B). *Loop-tail* and *Circletail* total cell lysate (A and C, respectively) is used as a control for the Vangl2 and Scribble antibody. In each case anti-FAS is used as a loading control. The bar charts represents the quantification of the level of full length Vangl2 (A, blue arrow), Celsr1 (B, green arrow) and Scribble (C, red arrow) in wildtype, heterozygous, and mutant *chuzhoi* embryos. P value is obtained from a student t-test. P values suggest that the levels of Vangl2, Celsr1 and Scribble are not altered in *chuzhoi* mutant compared to wildtype littermates, however the level of Scribble in *chuzhoi* heterozygous is significantly higher compared to the wildtype.

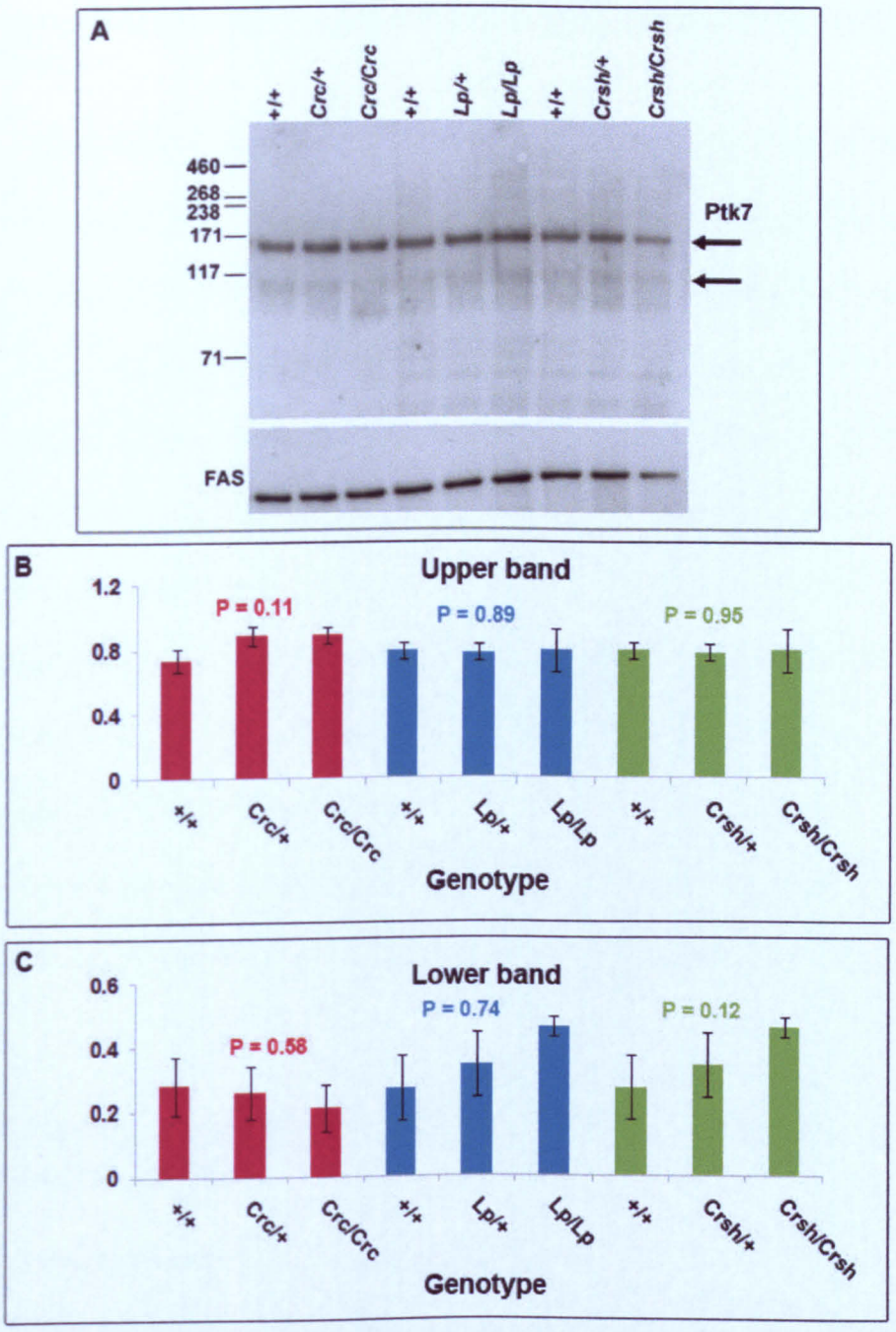

Figure 4-4: Western blots show that the level of Ptk7 is unaltered in *Circletail, Looptail* and *Crash* mutants.

(A) Western blot of total cell lysate from E8.5 wildtype, heterozygous, and mutant embryos from *Circletail, Loop-tail* and *Crash* line, using rabbit anti-Ptk7 antibody. The levels of both the full length Ptk7 and the cleaved form are similar in all three mutants compared to wildtype littermates. Anti-FAS antibody is used as a loading control. (B and C) Quantification of upper (B) and lower (C) Ptk7 bands (arrows in A) in wildtype, heterozygous, and mutant embryos from *Circletail,* (red), *Loop-tail* (blue) and *Crash* (green) lines, normalized to FAS. P value is obtained from a T-test between the wildtype and the mutant. Colors of letters correspond to the color of bars. P values suggest that the level of Ptk7 is not altered in *Loop-tail* and *Crash* mutant compared to wildtype littermates

4.2.4 Mutation in *Ptk7* does not affect the localization of Vangl2, Celsr1 or Scribble

Since there was no change in the levels of Valgl2, Celsr1 or Scribble in *chuzhoi* mutants, the next step was to test whether or not there was a difference in the subcellular localization of these proteins in *chuzhoi* mutants. To do this, I performed immunofluorescence experiments using antibodies against Vangl2, Celsr1 and Scribble on E8.5 *chuzhoi* and wildtype littermate tissue. Vangl2 protein localizes to the plasma membrane of the neuroepithelial cells with enrichment along the apical surface of cells (Figure 4-5A). The same distribution was observed in *chuzhoi* mutants (Figure 4-5B). Celsr1 protein localizes to the plasma membrane of the neuroepithelial cells in the wildtype (Figure 4-5C); this distribution of Celsr1 was observed in *chuzhoi* mutants (Figure 4-5D). Scribble is a cytoplasmic protein; however, through its interaction with Vangl2 (Kallay et al., 2006), it localizes to the plasma membrane. In wildtype sections, Scribble is enriched at the plasma membrane (Figure 4-5E) and this distribution of Scribble is maintained in *chuzhoi* mutants (Figure 4-5F).

4.2.5 Mutation in *Vangl2*, *Celsr1* or *Scribble* does not affect the localization of Ptk7

To determine whether or not the subcellular localization of Ptk7 depended on Vangl2, Celsr1 or Scribble, I performed an immunofluorescence experiment using antibodies against Ptk7 on E8.5 *Loop-tail, Crash* and *Circletail,* mutant embryos and wildtype littermates. In wild-type embryos, Ptk7 localizes to the cell membrane of both the neuroepithelium and underlying mesoderm (Figure 4-6 A,C,E). A similar distribution of Ptk7 was detected in *Loop-tail, Crash* and *Circletail* mutants (Figure 4-6 B,D,F).

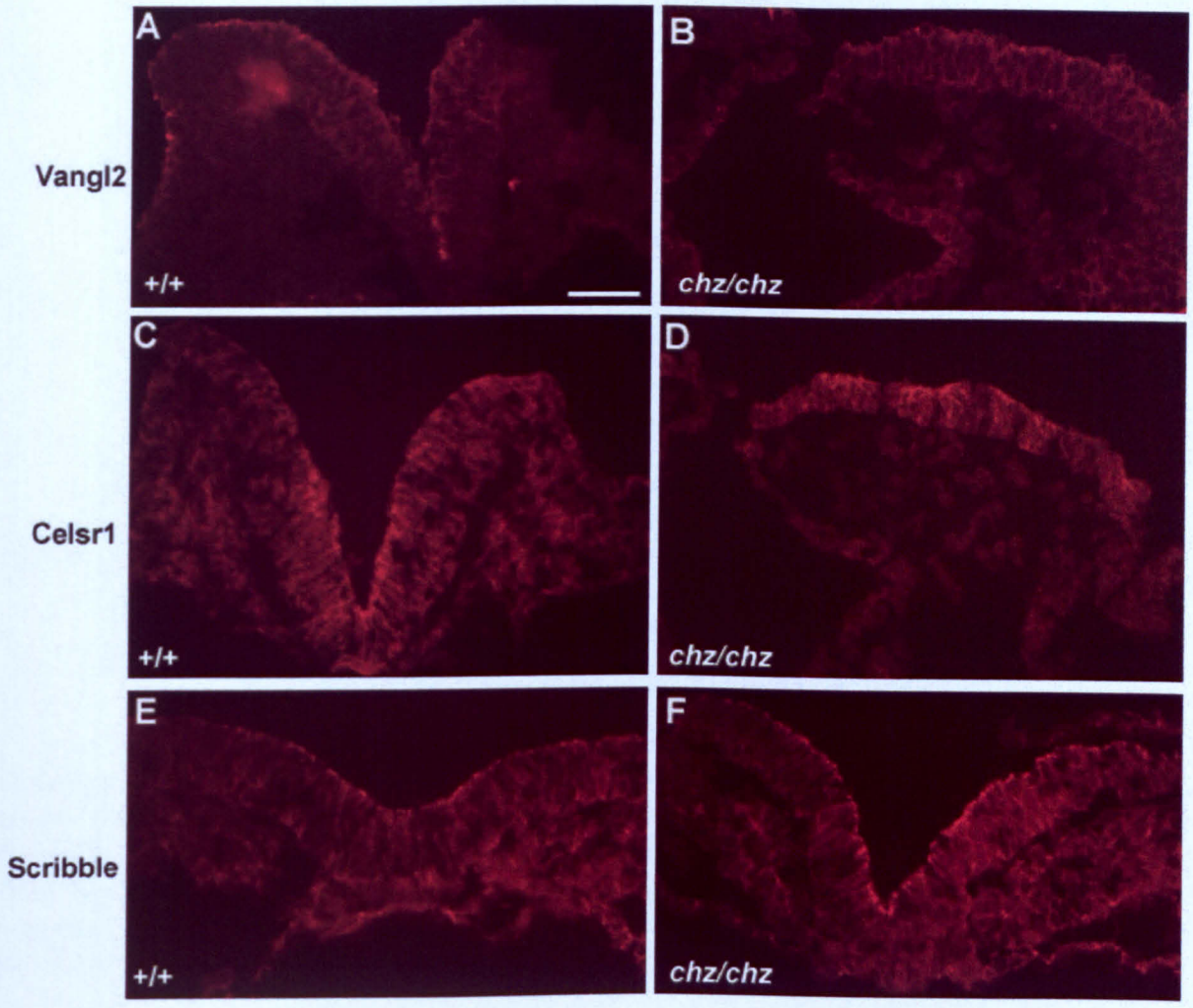

Figure 4-5: Localization of Vangl2, Celsr1 and Scribble are not altered in *chuzhoi*.
(A-F) Transverse sections through E8.5 wildtype (A,C,E) and mutant (B,D,F) *chuzhoi* embryos stained with of Vangl2 (A,B), Celsr1 (C,D) and Scribble (E,F). Vangl2, Celsr1 and Scribble localize to the plasma membrane of the neuroepithelium and underlying mesoderm cells in wildtype tissue, with an enrichment at the apical surface of neuroepithelium (A,C,E). The wildtype distribution of Vangl2 (A), Celsrl (C) and Scribble (E) is not disrupted in *chuzhoi* mutants (B,D,F). The scale bar represents 5 μm.

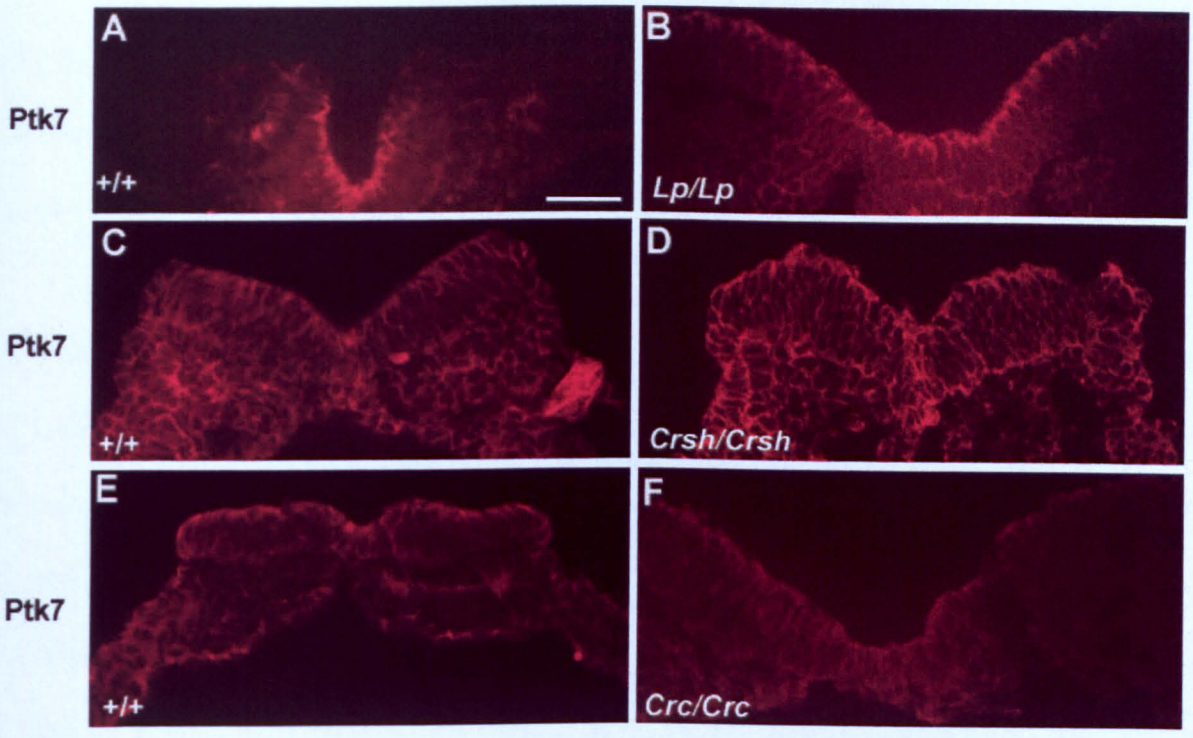

Figure 4-6: Localizations of Ptk7 is not altered in *Looptail, Crash* and *Circletail* mutants. (A-H) Transverse sections through E8.5 *Loop-tail*, *Crash* and *Circletail* mutant (B,D,F) embryos and their wildtype littermates (A,C,E) stained with an antibody against Ptk7 (A-F) . Ptk7 localizes to the plasma membrane of cells of the neuroepithelium and underlying mesoderm in wildtype tissue. This distribution of Ptk7 is not changed in *Loop-tail, Crash* or *Circletail* mutants. The scale bar represents 5 μm.

Together, these results suggest that the genetic interaction observed between *chuzhoi* and either *Looptail* or *Crash* is not mediated through gross alteration of the subcellular localization of Ptk7, Vangl2 or Celsr1 proteins.

4.2.6 Closure 1 is not delayed in *chuzhoi*

It has been previously reported that *Loop-tail* heterozygous embryos show a slight delay in initiation of neural tube closure and these embryos can develop craniorachischisis when

cultured in suboptimal conditions (Copp et al., 1994). To determine whether or not closure 1 was also delayed in *chuzhoi*, *Circletail* and *Crash* heterozygous embryos, I calculated the proportion of heterozygous and wildtype littermates where the initiation of neural tube closure has occurred. For this experiment embryos with 5 to 8 somites were analyzed and were grouped into 5-6 and 7-8 somites ranges (Figure 4-7).

My result also shows closure 1 is not delayed in *chuzhoi* heterozygous as it is present in approximately equal percentage of heterozygous embryos compared to wildtype littermates at both 5-6 and 7-8 somite stages (Figure 4-7 A). Slightly fewer proportion of *Circletail* heterozygous (38%), compared to wildtype littermates (52%), have undergone closure 1 at 5-6 somite stage, however by 7-8 somite stage a similar proportion of *Circletail* heterozygous and wildtype littermates close their neural tube (Figure 4-7 B). This suggests that although closure 1 may be slightly delayed in *Circletail* heterozygous, they successfully initiate their neural tube closure by 7-8 somite stage. *Crash* heterozygous embryos show a substantial delay in onset of closure 1. At 5-6 somite stage only 25% of *Crash* heterozygous show an initiated of neural tube closure, compared to 53% of wildtype littermates. Even by 7-8 somite stage, 30% of *Crash* heterozygous embryos have not undergone closure 1, compared to 8% for wildtype littermates (Figure 4-7 C).

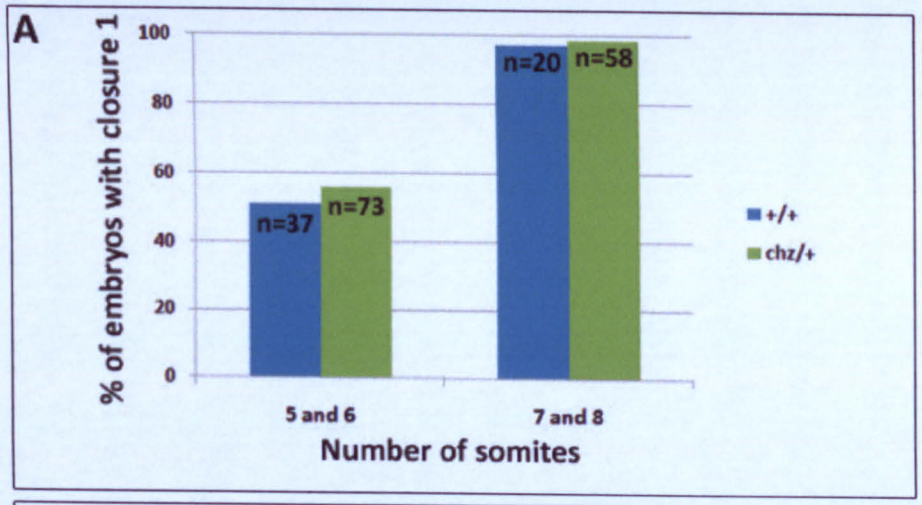

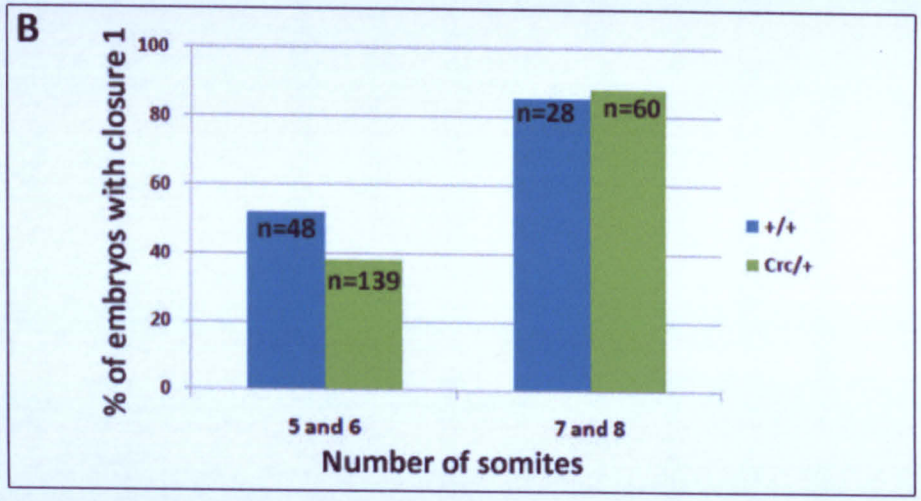

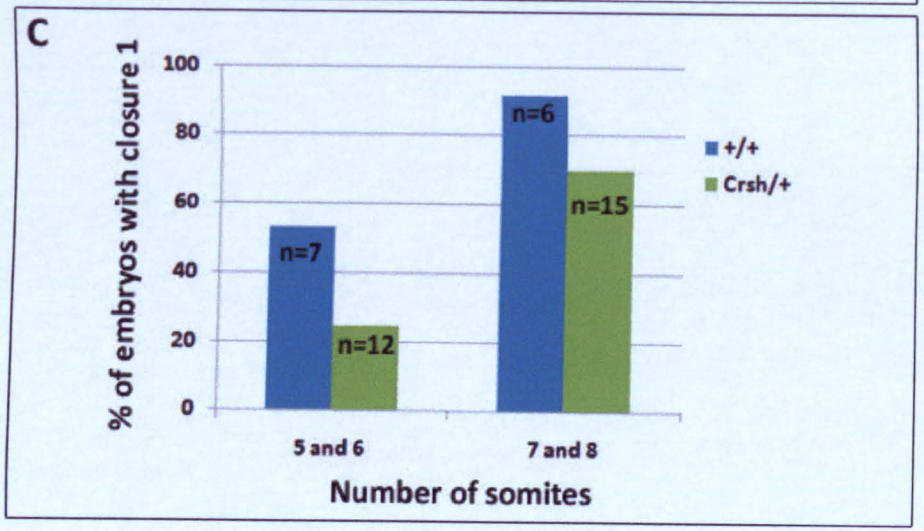

Figure 4-7: A delay in onset of closure 1 is not observed in *chuzhoi* and *Circelatil* heterozygous embryos but is observed in *Crash* heterozygous embryos.

(A and C) Bar chart showing the percentage of embryos where the initiation of neural tube closure has occurred. (A) The percentage of *chuzhoi* heterozygous embryos (green) where closure 1 has occurred is similar to that observed for wildtype littermates (blue) at both 5-6 and 7-8 somite ranges. (B) The percentage of *Circletail* heterozygous embryos (green) where closure 1 has occurred is slightly lower than that observed for wildtype littermate (blue) at 5-6 somite range however by 7-8 somites similar percentage *Circletail* heterozygous undergo closure 1 compared to wildtype littermates. (C) The percentage of *Crash* heterozygous embryos (green) where closure 1 has occurred is lower than that observed for wildtype littermates (blue) at both 5-6 and 7-8 somite ranges.

4.2.7 Yeast 2-hybrid screen using the intracellular domain of Ptk7

Ptk7 is a transmembrane protein; hence it is not possible to use the entire protein as the bait. This is because, for the yeast 2-hybrid screen to work, the bait protein and the interacting protein are required to enter the nucleus of the yeast to enable the transcription of a reporter gene. The mutation carried by *chuzhoi* gives evidence that the extracellular domain is required for the function of Ptk7 and previous work has shown that the removal of the intracellular domain of Ptk7 also leads to craniorachischisis (Lu et al., 2004), suggesting that this domain is equally important. To determine interacting partners of Ptk7 during signal transduction, the intracellular domain was chosen for a yeast 2-hybrid screen.

4.2.7.1 Cloning the intracellular domain of *Ptk7* into pLexA-C vector

A restriction map of the *Ptk7* cDNA showed that, although there are multiple restriction sites present within the sequence, none of these could be used to clone precisely just the intracellular domain of *Ptk7* into the pLexA-C vector. There is no suitable restriction site at the position where the intracellular domain starts (Figure 4-8A). To overcome this problem, I designed primers containing restriction sites to amplify the intracellular domain of *Ptk7*. The 5' end of the forward and reverse primers contained an *Eco*RI and *Sal*I site respectively, while the 3' ends of the primers contained *Ptk7* intracellular domain sequence (Figure 4-8B). Amplification from this set of primers produced the intracellular domain with an *Eco*RI site on the 5' end and a *Sal*I site on the 3' end (Figure 4-8C). Two different restriction sites were used to ensure that the PCR product was inserted into the vector in the correct orientation. *Eco*RI and *Sal*I enzymes were used to cut both the PCR product and the pLexA-C vector which were then ligated to generate pLexA-C vector with the intracellular domain of *Ptk7* inserted in-frame with LexA (Figure 4-8D).

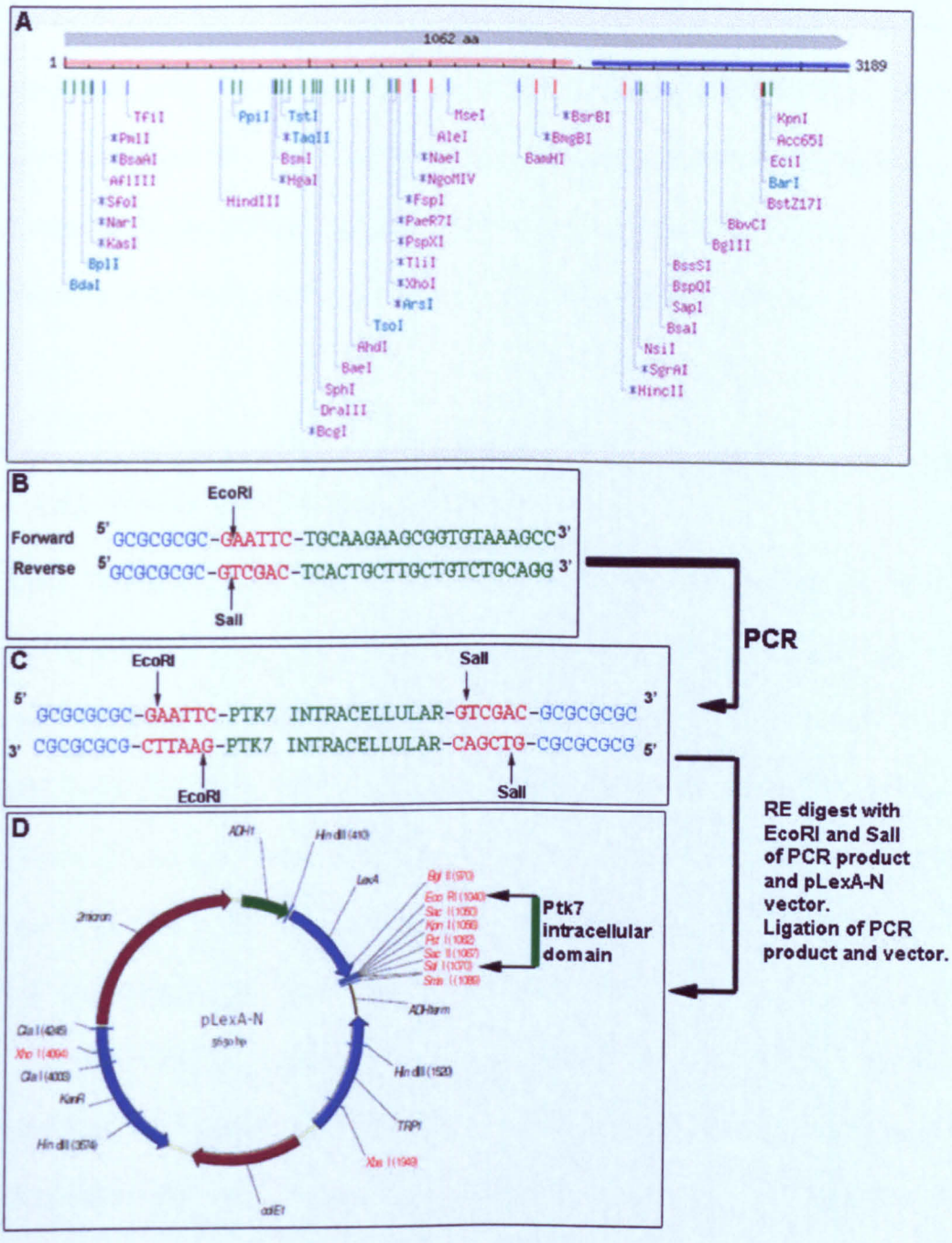

Figure 4-8: A flow diagram of steps involved in the generation of the bait used in the *Ptk7* yeast 2-hybrid screen.

(A) Restriction map of Ptk7 showing restriction sites within the extracellular domain (red line) and the intracellular domain (blue line). (B) Primer design to amplify the intracellular domain of *Ptk7* with *EcoRI* restriction site on the 5' and *SalI* restriction site in the 3'. The blue sequence at the 5' end is required for the restriction enzyme to attach prior to digestion. The red sequence is the restriction site for *EcoRI* and *SalI* as marked. Green sequence is complementary to the intracellular domain of *Ptk7*. (C) PCR product obtained from the primers in (B). The *Ptk7* intracellular domain is flanked by *EcoRI* on the 5' side and *SalI* in the 3' end. Double digestion of PCR product (C) and pLexA-N vector with *EcoRI* and *SalI*, followed by ligation leads to production of pLexA-N vector with the *Ptk7* intracellular domain inserted between the *EcoRI* and *SalI* sites (arrows) (D).

I transformed this plasmid into *E. coli* for amplification and extracted the plasmid DNA using midi prep. I next sequenced the plasmid to make sure that there was no PCR generated mutation present in the *Ptk7* intracellular domain and that the coding region of *Ptk7* was in frame with the coding region of LexA. This construct was given to Dualsystems Biotech to carry out a yeast 2-hybrid screen using E11.5 embryonic library.

4.2.7.2 A yeast 2-hybrid screen with Ptk7 intracellular domain identified only weakly interacting partners

Initial experiments performed by Dualsystems Biotech showed that the construct was suitable to be used in a yeast 2-hybrid screen as it was suitably expressed in yeast and there was no self activation. The pilot screen showed that the optimum selection medium was SD-his + 1mM 3-AT. The initial screen was performed using an E11.5 embryonic mouse cDNA library. From this initial screen, five clones were identified as showing an interaction as determined by growth on SD-his + 1mM 3-AT selective medium. However when these clones transferred into SD-ade selective medium they failed to grow and the assay for β-galactosidase activity was also negative, suggesting that these interactions were weak and unlikely to be real. Due to these disappointing results the same bait was used to screen a mouse adult brain library. From this screen, no interacting prey was found. This result is not typical of a yeast 2-hybrid screen, so the main concern was that the nuclear localization signal in the vector pLexA-N vector was not strong enough. To overcome this concern, the intracellular domain of Ptk7 was cloned into the pDS-Bait vector, which contains a stronger nuclear localization signal, by Dualsystems Biotech. This bait was used to screen a mouse adult brain library and a human brain library. From the screen with the mouse adult brain library, five clones were identified as showing a weak interaction with Ptk7. From the screen with the human brain library, 50 clones were isolated but again all interactions were classified as weak interaction.

Of these 50 clones, nine were sequenced to identify the gene (Table 4-2). Based on an extensive literature search, none of the genes in the list stood out as a good candidate for promoting neural tube closure by interacting with Ptk7. However, seven genes with different cellular functions were chosen for further analysis (Table 4-3).

Table 4-2: Proteins showing a weak interaction with the intracellular domain of Ptk7.

Prey clone	Gene / chromosome location	Name
Ptk7_prey_01-1	*Zinc finger CCCH-type containing 14*	*ZC3H14*
Ptk7_prey_02-1	*Chromosome 13 genomic contig*	*n/a*
Ptk7_prey_03-1	*Na+/H+ exchanger domain containing1*	*NHEDC1*
Ptk7_prey_04-1	*Chromosome 8 genomic contig*	*n/a*
Ptk7_prey_04-2	*DENN/MADD domain containing 4A*	*DENND4A*
Ptk7_prey_05-2	*Sodium bicarbonate cotransporter, member 4*	*SLC4A4*
Ptk7_prey_06-2	*Coatomer protein complex, subunit beta 1*	*COPB1*
Ptk7_prey_07-1	*Chromosome 15 genomic contig*	*OLFR1500*
Ptk7_prey_08-2	*Chromosome 18 genomic contig*	*SLC25A16*

4.2.7.3 Reverse transcription PCR shows the four genes identified in Ptk7 yeast 2-hybrid are expressed during mouse development

To assess the possibility that these seven genes may be interacting with Ptk7 during development, I performed reverse transcription PCR (RT-PCR). For a gene to interact with Ptk7 during development, the first requirement is that it must be expressed during development. In order to analyse gene expression over development, I extracted RNA from CD1 embryos collected at each day of embryonic development between E7.5 and E17.5. To

provide a positive control tissue, I also extracted RNA from adult kidney, brain and testis, since most of the seven genes are known to be expressed in one or more of these tissues, as determined using BioGPS: The Gene Portal Hub, an online resource (http://biogps.gnf.org/) (Table 4-3). One of the genes, Olfr1500, is expressed only in the nasal cavity. It was not possible to get this tissue from the adult mouse due to difficulty in dissecting out this tissue hence a positive control for this gene was missing. Following RNA extraction, I performed reverse transcription with MMLV-RT and primed with random hexamers, to synthesise first strand cDNA. I also generated a no-RT control, that is, a cDNA synthesis reaction without the RT enzyme, in order to provide a control to detect amplification from genomic DNA contamination. To determine the integrity of synthesised cDNA I performed PCR with a primer designed to detect *Hypoxanthine-guanine phosphoribosyltransferase* (*Hprt*), which is a housekeeping gene that is expressed in all tissues. To design primers specific for each gene, I first identified the mouse homologue of each gene and obtained its full coding sequence. For most of the genes several alternatively spliced transcripts were present (Table 4-3). I designed primers to identify most of the splice variants for each gene and to amplify a product of approximately 600 bp (Table 4-4). All primers were designed to flank at least one intron.

The RT-PCR results showed that four out of the seven genes were expressed in embryos during development (Figure 4-9). *Zc3h14, Nhedc1* and *Olfr1* were not expressed at any stage during mouse development however a band of approximately 600 bp was detected for both *Zc3h14* and *Nhedc1* in Testis, suggesting that the PCR had worked. *Dennd4a, Slc4a4, Copb1* and *Slc25a16* were all expressed during mouse embryonic development. *Dennd4a* and *Copb1* were expressed at all stages examined and more importantly they were all expressed at the stages when neurulation is taking place (E7.5-E10.5). Expression for *Slc4a4* was not detected at E11.5 and E17.5. Similarly, expression of *Slc25a16* was absent at E14.5.

As these interactions were weak and consequently unlikely to be real, and any further analysis would have involved substantial investment of time and funds a decision was taken not to pursue this project further at this time.

Table 4-3: Details of mouse orthologues of genes that were identified during the yeast 2-hybrid screen with the intracellular domain of mouse Ptk7.

Human gene	Mouse orthologue	Number of alternative transcripts in mouse	Analysis	+ve control
ZC3H14	*Zc3h14*	6 (6 are protein coding)	Yes	Testis
Chromosome 13 genomic contig	*N/A*	n/a	No	n/a
NHEDC1	*Nhedc1*	3 (3 are protein coding)	Yes	Testis
Chromosome 8 genomic contig	*N/A*	n/a	No	n/a
DENND4A	*Dennd4a*	2 (2 are protein coding)	Yes	Brain
SLC4A4	*Slc4a4*	9 (8 are protein coding)	Yes	Kidney
COPB1	*Copb1*	1 (protein coding)	Yes	Kidney
OLFR1500	*Olfr1500*	1 (protein coding)	Yes	Nasal cavity
SLC25A16	*Slc25a16*	4 (2 are protein coding)	Yes	Kidney

Table 4-4: Details of primers used to amplify fragments of mouse genes that were identified during the yeast 2-hybrid screen with the intracellular domain of mouse Ptk7.

Mouse gene	Forward primer (5'→3')	Reverse primer (5'→3')	Fragment size
Zc3h14	GTCCCAGAACGAAGCAAAAA	AATCCATTTCAAGGCGTGTC	688 bp
Nhedc1	CAAGAAGGATGATGGTTTCCA	TGACAAGCGCAGACAGACTC	691 bp
Dennd4a	TGTGTTCACTGCTGGGAAAG	TCCGACTTGCAAAGTGCATA	596 bp
Slc4a4	GCACCTCCTCAGCTCTTCAC	GAAGTCAACCTCCCCAACAA	572 bp
Copb1	GGAGAAAGGCGATGTGAAGT	TTCAACAATAACCAACTGTAGAATG	598 bp
Olfr1500	CCACACCCCAATGTACTTCC	GGAGGCACATGTTGAGAAGG	567 bp
Slc25a16	CCTCACGCCGAGACTTCTAC	AGGGCAGGAGCATAGGAAAG	586 bp

PCR condition: 95 °C for 5 minutes [95 °C for 30 seconds, 60 °C for 30 seconds, 72 °C for 30 seconds] x 29 cycles, 72 °C for minutes.

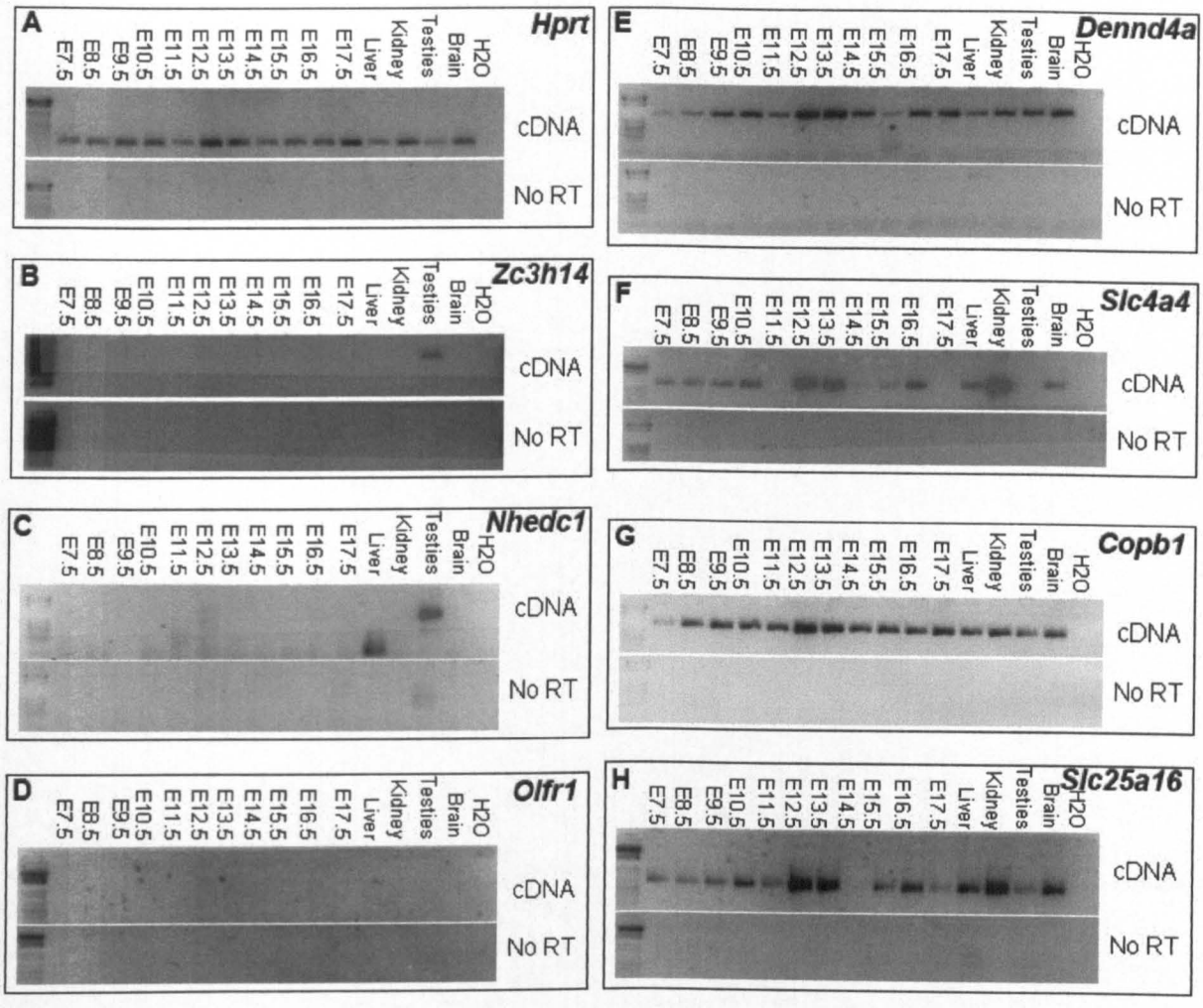

Figure 4-9: Reverse transcription PCR of genes identified by a *Ptk7* yeast 2-hybrid screen.

(A-F) PCR using primers for *Hprt* (A), *Zc3h14* (B), *Nhedc1* (C), *Olfr1* (D), *Dennd4a* (E), *Slc4a* (F), *Copb1* (G) and *Slc25a16* (H). In each case cDNA synthesis and a no reverse transcriptase control (No RT) was performed. RNA from E7.5 to E17.5 embryos, adult liver, adult kidney, adult testes and adult brain was used as template. *Hprt* (A) is expressed in all tissue examined and negative in all No RT negative controls. (B-D) *Zc3h14* (B), *Nhedc1* (C) and *Olfr1* (D) are not expressed during mouse embryonic development (E7.5-E17.5); *Zc3h14* (B), *Nhedc1* (C) are expressed in adult testis. (E-H) *Dennd4a* (E), *Slc4a* (F), *Copb1* (G) and *Slc25a16* (H) are expressed during neurulation (E7.5-E10.5) and throughout embryonic development as well as in range of adult tissues. No PCR product is observed in any No RT negative controls.

4.3 Discussion

4.3.1 Genetic interaction cross

Previous experiments have shown that *Loop-tail* genetically interacts with *Circletail* (Murdoch et al., 2001b) and *Dishevelled1/2* (Wang et al., 2006a) to produce *Lp/+, Crc/+* and *Dvl1+/–; Dvl2–/–; Lp/+* embryos which display craniorachischisis. Crosses between *Loop-tail* and *Crash,* and between *Crash* and *Circletail* have shown similar results, where a proportion of doubly heterozygous embryos exhibit craniorachischisis (C.Damrau and J. Murdoch, unpublished data). These results give strong evidence that the genes disrupted in each of these mutants influence the same signalling pathway.

The genetic interaction data presented in this report demonstrated an interaction between *chuzhoi* and *Loop-tail* and between *chuzhoi* and *Crash.* However no interaction between *Circletail* and *chuzhoi* was observed. Genetic interaction between *Loop-tail* and the gene trap allele of *Ptk7* has also been reported; however, the compound heterozygous embryos do not display craniorachischisis but 94% of the doubly heterozygous embryos exhibit spina bifida (Lu et al., 2004). In this study I have presented data to show that a cross between *chuzhoi* and *Looptail,* results in a smaller proportion of doubly heterozygotes embryos display spina bifida (24%) while 6% display craniorachischisis. This significant difference could be due to either the differences in the genetic background of the mice and/or the differences in the nature of the mutation between *chuzhoi* and the gene trap allele of *Ptk7.*

The gene trap allele of *Ptk7* was maintained on a C57BL/6 background and was crossed to *Loop-tail* mice of the LPT/Le stock obtained from the Jackson Laboratories (Lu et al., 2004). *chuzhoi* is congenic on a C3H/HeH background and was crossed to *Loop-tail,* which has also been bred to congenicity on the C3H/HeH background..

The nature of the mutation in the gene trap allele of *Ptk7* is different from that of *chuzhoi.* The gene trap allele appears to be a complete null allele of *Ptk7* as western blots using protein lysate from the mutant embryo and the antibody raised against Ptk7 protein fails to detect any protein (Lu et al., 2004). This is in contrast to *chuzhoi* mutants, where the same antibody detects a reduced but significant level of both the cleaved and full length forms of Ptk7 protein (Figure 3-3 G,H). However, no wildtype cDNA is detected in *chuzhoi* mutants during sequencing, suggesting that all Ptk7 protein detected in *chuzhoi* is the mutated form hence likely to be non-functional. To determine whether or not Ptk7 present in *chuzhoi* is functional or not, it is necessary first to identify the molecular function of Ptk7 and subsequently to test whether this is dirupted in *chuzhoi.*

These genetic interaction results suggest that *Ptk7* may be acting in the PCP pathway; however, the level of wild-type Ptk7 protein required for proper neural tube closure appears to be significantly lower than the required level of Scribble, Vangl2 and Celsr1, so one functional copy of *Ptk7* may produce enough Ptk7 protein to allow the initiation of neural tube closure to take place even in the present of reduced levels of functional Valgl2, Celsr1 or Scribble. This is supported by the observation that both *Loop-tail* and *Crash* show an adult heterozygous phenotype while none is observed in *chuzhoi* heterozygous animals. Furthermore, it has been reported that *Loop-tail* heterozygous embryos show a slight delay in initiation of neural tube closure and these embryos can develop craniorachischisis when cultured in suboptimal conditions (Copp et al., 1994). My observation also shows a delay in onset of closure 1 in *Crash* heterozygous embryos while this delay is not observed in *chuzhoi* heterozygous embryos (Figure 4-7).

Another possibility may be that Ptk7 is not directly acting on the PCP pathway; instead it might be involved in another pathway which influences PCP signalling. The lack of genetic interaction between *Circletail* and *chuzhoi* is exciting. This suggests that they may not be

functioning in the same signalling cascade implying that these two proteins may influence the PCP pathway through distinct mechanisms.

While it is obvious that the majority of compound heterozygotes from all three crosses closed their neural tube successfully, it would be interesting to look at the orientation of the inner ear sensory hair cells to determine whether there is any sign of a defect in the PCP signalling pathway. There is some evidence to indicate that the PCP pathway may not function in the same way during convergent extension as during regulation of the orientation of the inner hair cells. Evidence for this comes from analysis of the distribution of Dishevelled2 in *Loop-tail* mutants, in the neuroepithelium and in stereocilia. In the absence of Vangl2, Dishevelled2 loses its ability to localize in a polarized manner in stereocilia (Wang et al., 2005). However, during neurulation the localization of Dishevelled2 is not altered (Wang et al., 2006a) in *Loop-tail* mutants.

The nature of the molecular mechanism for the observed interaction is not clear. I have found that the level of expression and membrane localization of Ptk7 were not obviously affected when Vangl2 or Celsr1 are disrupted, and conversely the expression levels and subcellular localization of Vangl2 and Celsr1 were not affected when Ptk7 was mutated. In *Xenopus* it has been reported that Ptk7 binds to Dishevelled and Frizzled complex however more recently it was shown that a mutation in mouse Ptk7 does not lead to mis-localisation of Dishevelled 2 (Shnitsar and Borchers, 2008; Yen et al., 2009) suggesting that mouse Ptk7 is not required for membrane recruitment of Dishevelled 2. It could be hypothesized that Ptk7 may form a complex with an unknown protein and modulate the function of Vangl2 and Celsr1 during neural tube closure. To determine whether or not this hypothesis is correct, it is necessary to identify interacting partners of mouse Ptk7. Although no genetic interaction between *chuzhoi* and *Circletail* was observed, it is interestingly to find that the Scribble protein is significantly increased in *chuzhoi* heterozygous embryos. This result may suggest

that reduction in level of Ptk7 in *chuzhoi* heterozygous may increase the level of Scribble. It would be interesting to determined whether or not embryos that are doubly heterozygous for *chuzhoi* and *Circletail* also have an increased level of Scribble as it may explain the lack of genetic interection observed between these two mutants as increased level of Scribble may compensate for the lack of Ptk7 and ensure a successful neurulation.

4.3.2 Yeast 2-hybrid screen

A yeast 2-hybrid screen to identify interacting partners of Ptk7 was performed by Dualsystems Biotech. Only weakly interacting prey proteins were identified from this screen, despite the use of two bait vectors and several different libraries, and these were deemed by DualSystems Biotech to be likely false positive results. There are several factors that could account for the lack of positive results obtained.

1. Ptk7 is not an ideal protein for a yeast 2-hybrid screen

The first unavoidable factor is the nature of the Ptk7 protein. The fact it is a transmembrane protein means there is a large hydrophobic region in the protein which will hamper its ability to localize to the nucleus, a requirement for the yeast 2-hybrid screen. For this reason, full length Ptk7 could not be used as bait leaving a choice of either the extracellular or the intracellular domain to be used to screen the library. There are problems associated with using extracellular domains as they often have a high levels of posttranslational modifications such as N-glycosylation and addition of disulfide bonds, both of which are not expected to occur in the yeast nucleus (Fields and Sternglanz, 1994). Despite this problem, there are some examples where an extracellular domain has been successfully used as bait in a yeast 2-hybrid screen (Young and Ozenberger, 1995; Kajkowski et al., 1997).

The success of these experiments could be due to the types of posttranslational modifications that are required for the extracellular domain to correctly interact with a partner so the success of the experiment will depend on the protein used. The types of posttranslational modifications present in Ptk7 are unknown; however, there are seven N-glycosylation sites predicted in the extracellular domain of Ptk7 (predicted using ExPASY, an online resource www.expasy.ch/tools/#ptm).

The intracellular domain was chosen as the bait in this study, as we were particularly interested in identifying the proteins that function downstream of the Ptk7 (intracellularly) during neurulation. There are several examples in the literature where the intracellular domain of a protein has been used as bait to successfully identify interacting partners (Hopkinson and Jones, 2000; Torban et al., 2004). One of these examples is a PCP molecule, Vangl2, which was shown to interact with Dishevelled, another member of the PCP pathway, via its intracellular domain (Torban et al., 2004).

Despite a large collection of publications where the intracellular domain of a protein has successfully been used as the bait in a yeast 2-hybrid screen, no positive results came out of the Ptk7 intracellular domain screen. A reason for this could be that the intracellular domain of Ptk7 requires a signal from the extracellular domain before it can interact with a partner. Normally receptor protein tyrosine kinases (RPTKs) are involved in transduction of extracellular signals. When an extracellular ligand binds to the extracellular domain, it causes conformational changes resulting in activation of the intracellular domain. In RPTKs where the active kinase domain is present e.g. Fibroblast Growth Factor Receptor 1, the activated intracellular domain phosphorylates one or more tyrosine residues resulting in the recruitment of downstream proteins to form a complex (Mohammadi et al., 1996; Hubbard et al., 1998; Weiss and Schlessinger, 1998). Ptk7 is a member of a group of RPTKs without an active kinase domain and has been shown in culture that it cannot be phosphrylated by other RPTKs

(Jung et al., 2004); however the intracellular domain may still require a signal from the extracellular domain to become active in some as yet unknown way before it is able to interact with a partner.

It is also worth considering that the extracellular or transmembrane domain of Ptk7 are involved in protein-protein interactions. The extracellular domain of Ptk7 consists of immunoglobulin domains which are commonly involved in protein-protein interactions. It could be hypothesized that this extracellular interaction is both necessary and sufficient for the function of mouse Ptk7. In contrast to this hypothesis it has been reported that the intracellular domain of Ptk7 is required for the neural tube closure in *Xenopus* (Lu et al., 2004) however there is now evidence to suggest that the molecular functions of Ptk7 may not be conserved between *Xenopus* and mice (Shnitsar and Borchers, 2008; Yen et al., 2009). There is also some evidence to suggest that the transmembrane domain of Ptk7 may be functionally active. It has been reported that the transmembrane domain of Ptk7 and its orthologues are highly conserved throughout evolution (Kobus and Fleming, 2005), supporting a role for this domain.

2. cDNA libraries

The main aim of this study was to find interacting partners of Ptk7 that are involved in shaping the neural plate and neural tube closure. Neurulation in mice starts at E8.0 and is completed by E10.5 hence the ideal cDNA to screen for Ptk7 interaction partners would be whole mouse embryonic library between the age of E8.0 and E10.5. There is no such library available commercially and making such a library was out of the scope of this study. However, genes involved in neural tube closure such as *Scribble, Vangl2, Celsr1* and *Ptk7* continue to be expressed at later ages, supporting the argument that although neural tube closure is completed by E10.5, proteins interacting with Ptk7 during neural tube closure are likely to be expressed at later stages as well.

cDNA libraries derived from E11.5 embryo, mouse adult brain and human brain were screened using the intracellular domain of Ptk7. It has been reported that Ptk7 is expressed robustly in mice at E11.5 and less robustly in adult brain (Jung et al., 2004). The human expression pattern of PTK7 has not been reported. Since Ptk7 is present at E11.5 and in adult brain in mouse, presumably it must be interacting with other proteins to carry out its function. These interactions could be very transient providing an explanation for only the observed weak interactions coming out of three screens.

The human cDNA library was screened with the mouse Ptk7 intracellular domain. From this screen 50 clones were identified as weak interacting partners of Ptk7. The intracellular domain of mouse Ptk7 and human PTK7 is highly conserved (94.2% identity and 97.1% similarity, sequence obtained from Ensembl and aligned using EMBOSS Pairwise Alignment Algorithms), providing an argument that the interacting partner of mouse Ptk7 may also be present in the human cDNA library. However, the function of Ptk7 in mice and humans may be different; in human PTK7 has been linked with colon cancer (Mossie et al., 1995) and in mouse it has been linked to the PCP pathway (Lu et al., 2004). This apparent functional difference may indicate that, despite the structural similarity, the proteins interact with different molecules, determined by the different proteins present in the mouse and human genomes. Four out of seven genes that came out of the yeast 2-hybrid were expressed during mouse development suggesting a role for these genes during development.

Slc4a4 has been knocked out in mice however neural tube defects have not been reported, instead these mice show a defect in renal function and die before the age of weaning (Gawenis et al., 2007). Mouse mutants of other three genes, *Dennd4a, Copb1* and *Slc25a16,* are not available. *Dennd4a* is a member of protein containing Dennd domain. Dennd domain in other proteins have been shown to function as guanine nucleotide exchange factors (GEFs) for the Rab family of small GTPases (Marat and McPherson, 2010). This link between Ptk7 and small

GTPases is exciting since another family of small GTPases, Rac and Rho, are known to be downstream targets of the PCP pathway. *Copb1* is potentially an interesting gene. It encodes for a subunit of coatomer protein complex, which are involved in intracellular protein transport. More recently it has been discovered that a mutation in one of these coat proteins, CopII, leads to craniorachischisis in mice resulting from a failure to transport Vangl2 protein to the plasma membrane (Wansleeben et al., 2010). It could be hypothesized that Copb1 is required to transport Ptk7 to the membrane. In humans, members of Slc25 are involved in transport of small molecules in and out of mitochondria and Slc25a16 in particular has been linked to Graves' disease as it appears to be highly enriched in patients with this disease (Palmieri, 2004). Nothing has been reported for the function of mouse *Slc25a16*.

3. Analysis of clones

To assess the true reliability of the yeast 2-hybrid screen carried out in this study, it would have been ideal to identify the genes present in each clone of all three screens. This would identify any genes that were represented in more than one clone and may represent a true interaction partner of Ptk7.

4.3.3 Yeast 2-hybrid screen for membrane proteins

Owing to difficulties in studying interacting partners of membrane proteins, a system similar to that of the classic yeast 2-hybrid has been designed (Johnsson and Varshavsky, 1994). This modified technique is termed Split-ubiquitin membrane yeast 2-hybrid. This technique takes advantage of the fact that the N-terminal and C-terminal domains of an ubiquitin ligase can be separated. A protein of interest is attached to the N-terminus of the C-terminal domain of the ubiquitin ligase, and a transcription factor is fused to the C-terminus of

the same domain. The prey library is constructed using the N-terminus of the ubiquitin ligase. In the cell there is an ubiquitin specific protease, which recognizes the full form of the ubiquitin ligase and cleaves at the C-terminal domain. When the two proteins attached to the N- terminal (prey) and the C-terminal (bait) domains interact together, a full ubiquitin ligase is formed. This results in cleavage of the transcription factor attached to the C-terminus of the ubiquitin ligase. The transcription factor enters the nucleus and activates the transcription of reporter genes (Figure 4-10).

This technology has been successfully used to find interacting partners of membrane proteins (Thaminy et al., 2003). To find true interacting partners of Ptk7, this technology would have been more appropriate; however, at the time of study, appropriate libraries using this technique were unavailable.

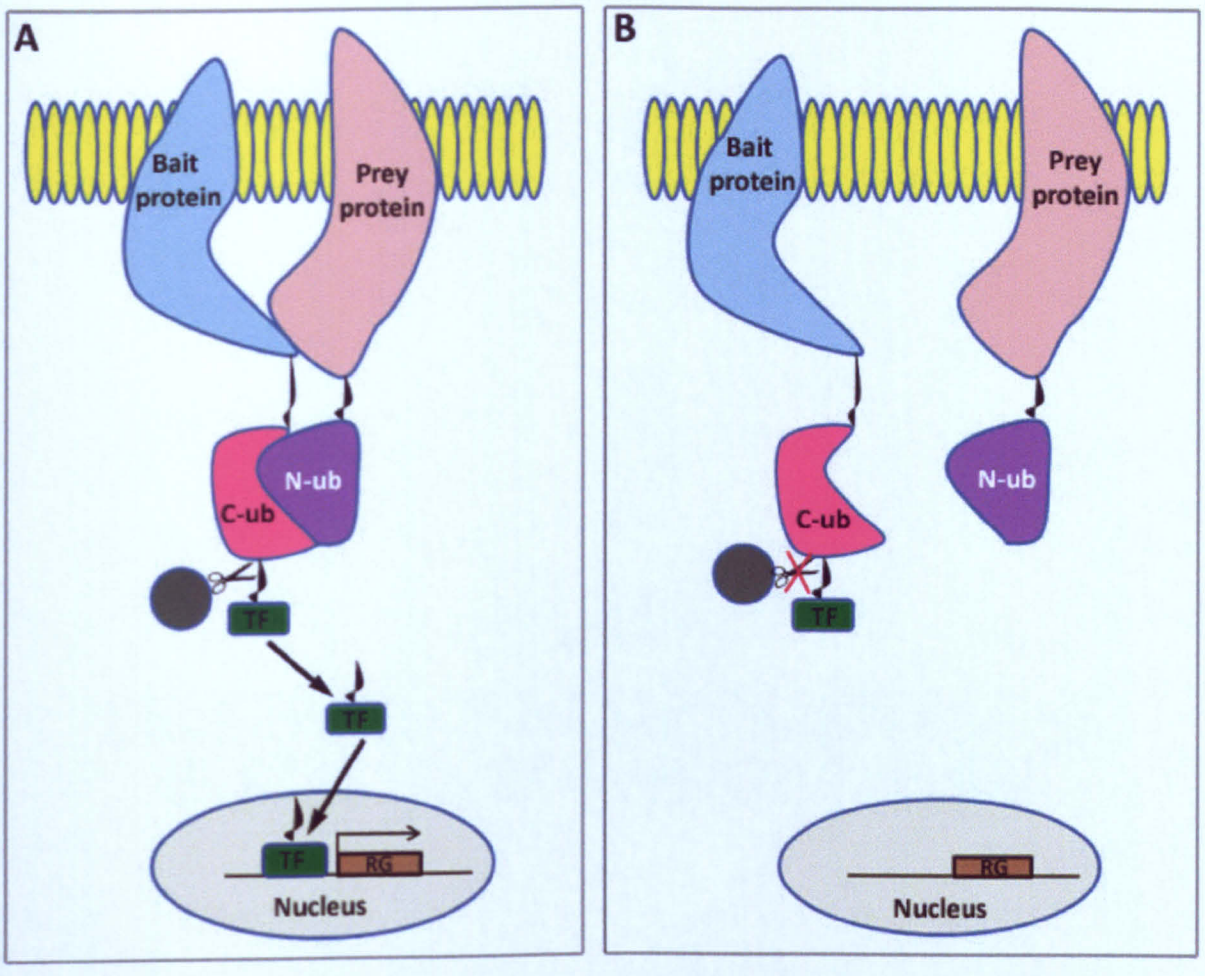

Figure 4-10: An overview of split-ubiquitin membrane yeast 2-hybrid.
The protein of interest (bait protein, blue) is fused to the N-terminus of C-terminal domain (C-ub, Pink) of an ubiquitin ligase and a transcription factor (TF, green) is fused to the C-terminus of C-terminal domain of an ubiquitin ligase. A library is constructed by fusing both transmembrane (prey protein, red) and cytoplasmic proteins to the N-terminal domain (N- Ub, purple) of the ubiquitin ligase. When the bait protein and the prey protein interact, the C-terminal and N-terminal domain of the ubiquitin ligase come together resulting in reconstruction of the ubiquitin ligase (A), an ubiquitin specific protease (black) cleaves at the C-terminal of the ubiquitin ligase, releasing the transcription factor, which enters the nucleus (grey) and activates the transcription of reporter genes (RG, brown). If the bait protein does not interact with the prey protein (B), then reconstruction of the ubiquitin ligase fails to occur and the protease fails to cleave at the C-terminal therefore the transcription factor is not released and the reporter gene is not transcribed. Figure modified from (Thaminy et al., 2003).

CHAPTER 5

CELLULAR ANALYSIS OF *CIRCLETAIL* DURING NEURAL TUBE CLOSURE

5 Cellular analysis of *Circletail* during neural tube closure

5.1 Introduction

5.1.1 *Circletail* carries a mutation in *Scribble* and is a model for craniorachischisis

Circletail carries a mutation in the *Scribble* gene. Mouse *Scribble* is a large gene with 38 exons covering 23 kb of genomic DNA. It encodes a cytoplasmic protein of 1665 amino acid with a molecular weight of 180 kDa and consists of 16 leucine-rich repeats (LRRs) and four PSD-95, Dlg, ZO- 1 (PDZ) domains. *Circletail* carries an insertion of a single base pair in exon 21, resulting in a frame shift which leads to the formation of a premature stop codon (Murdoch et al., 2003). This truncated Scribble protein is predicted to retain the 16 LRRs and the first two PDZ domains (Murdoch et al., 2003) and our western blot analysis shows that it is likely to be unstable as an antibody raised against the N-terminal domain of Scribble fails to detect any protein (personal communication with Dr J. Murdoch). Two other alleles have been reported for *Scribble, rumpelschtilzchen* (originally known as line 90) and *51206.* (Zarbalis et al., 2004; Dow et al., 2007; Wansleeben et al., 2010). Both of these lines are ENU induced mutants and result from point mutations. *rumpelschtilzchen* carries a missense mutation which results in an isoleucine-to-lysine substitution in the third LRR domain of *Scribble*; this leads to a five-fold reduction in the protein level (Zarbalis et al., 2004; Dow et al., 2007). The *51206* allele of *Scribble* carries a nonsense mutation towards the C terminal domain of the protein and truncates the protein by 158 amino acids. This mutation also results in 65% decrease in the expression of *Scribble* mRNA (Wansleeben et al., 2010). Homozygous mutation in scribble causes failure of closure 1, leading to craniorachischisis. This phenotype

is seen in all three mutant alleles (Murdoch et al., 2001b; Murdoch et al., 2003; Zarbalis et al., 2004; Wansleeben et al., 2010).

5.1.2 Roles of *Scribble* during epithelial morphogenesis: evidence from other species

Scribble is a conserved protein, found throughout evolution from *Drosophila* to Human. Mouse Scribble shares 88% identity with human SCRIBBLE and 44% identity with *Drosophila* Scribble, at the amino acid level (Murdoch et al., 2003). *Scribble* was originally studied in *Drosophila* and was found to have multiple roles in epithelial morphogenesis (Bilder and Perrimon, 2000). Initial studies using mutants showed that *Scribble* was involved in controlling three main cellular processes in the epithelium; establishment of apical basal polarity, rate of proliferation and rate of differentiation (Bilder and Perrimon, 2000). In *Drosophila* there are three protein complexes that are required for the proper establishment of apical-basal polarity and formation of the adherens junction: the Crb-complex, Baz-complex and Scrib-complex. Crb-complex, consisting of a transmembrane protein Crumbs and a cytoplasmic protein Stardust, localizes to the apical domain of the epithelial cell and is both required and sufficient for the establishment of this domain (Bilder et al., 2003). Baz-complex, consisting of Bazooka, Partitioning defective gene6 (PAR6) and an atypical protein kinase (aPKC), localizes to the adherens junction and the region that is just apical to this junction. The domain of Baz-complex partly overlaps with the domain of Crb-complex, and Baz-complex is required for restriction of Crumbs to the apical domain and Crb-complex is required for the maintenance of Baz-complex to the adherens junction (Bilder et al., 2003). Furthermore a direct protein interaction between Crumbs and PAR6 has been reported (Kempkens et al., 2006), providing a molecular basis for the interaction between Crb-complex and Baz-complex. Scrib-complex, consisting of Scribble, Discs-large (Dlg) and Lethal giant

larvae (Lgl), localizes to the basal domain of the epithelial cell (Bilder et al., 2003). In *Drosophila scribble* mutants, the integrity of the adherens junction is lost leading to unrestricted localization of normally apically restricted proteins to both apical and basal regions of the cell. In contrast, proteins normally restricted to the basolateral membrane show a normal distribution. This suggests that the Scrib-complex is required for the maintenance of the adherens junction and therefore the apical domain, however it is not required for the formation or maintenance of the basal domain (Bilder et al., 2003).

More recently *Drosophila Scribble* has also been shown to play a role in the planar cell polarity signalling pathway, a pathway determining the orientation of cells in the plane of an epithelium (Courbard et al., 2009).

In mice, mutation in *Scribble* results in defects associated with loss of the planar cell polarity as defined by failure of closure 1 during neural tube development and misalignment of stereociliary bundles within the inner ear (Montcouquiol et al., 2003; Murdoch et al., 2003; Wansleeben et al., 2010). To date, mouse *Scribble* has not been linked to either the establishment of apical basal polarity or controlling the rate of proliferation.

5.1.3 Orientation of cell division drives tissue elongation

The craniorachischisis observed in *Circletail* and in other mutants of the PCP signalling pathway is believed to arise as a consequence of defects during the process of neural plate shaping. During this process, the neural plate on the dorsal surface of the embryo undergoes extensive remodeling to produce a structure that is narrow in the medio-lateral axis and elongated in the anterior-posterior axis of the embryo. The main mechanism that has been proposed to drive this remodeling is convergent extension, a process that is controlled by the PCP pathway (Wallingford and Harland, 2002; Wang et al., 2006a; Ybot-Gonzalez et al., 2007b; Yen et al., 2009). This process has been discussed in section 1.3.4.1.

A second mechanism implicated in elongation of a structure is the orientation of cell division (Keller, 2006). This mechanism of axis elongation has been extensively studied in *Drosophila* and is known to play an important role during extension of the germband, and in specifying the shape of the wing and eye (Baena-López et al., 2005; da Silva and Vincent, 2007). During these processes in *Drosophila*, core PCP signalling does not appear to play a role; however when *dachsous* and *fat* are mutated the orientation of cell division is lost in wing and eye resulting in a structure that is rounder and shorter compared to wildtype (Baena-López et al., 2005). Dachsous and fat are PCP molecules reported to act either upstream of or in parallel with the core PCP signalling system (Fanto et al., 2003; Casal et al., 2006). The orientation of cell division is also important in mammalian systems. It plays an essential role during the maturation of nephrons in kidney development, which involves high levels of cell proliferation. During this process the majority of cells divide along the tubule axis which results in lengthening of the renal tubules without affecting its diameter (Fischer et al., 2006). Mice carrying a mutation in *Fat4*, a gene that affects PCP signalling in mice, have disrupted orientated cell division and show a genetic interaction with *Vangl2* (Saburi et al., 2008).

Furthermore, a study in Zebrafish has demonstrated that the core PCP pathway is involved in regulating the orientation of cell division during gastrulation, and this plays a role in axis elongation (Gong et al., 2004). In wildtype embryos when a cell in the neural plate divides, the daughter cells are oriented so that they are parallel to the anterior-posterior axis of the embryo, which results in overall increase in the body length. When the PCP pathway is blocked by injection of a mutant construct of *Dishevelled*, the daughter cells are randomly aligned resulting in a shorter anterior-posterior axis and a wider medio-lateral axis (Gong et al., 2004). The importance of this mechanism has not been examined in mice during neurulation.

5.1.4 The cell cycle

There are two main stages in the cell cycle; interphase and mitosis. Interphase is divided into four distinct phases; Gap 0 (G0), Gap 1 (G1), Synthesis (S) and Gap 2 (G2). During G0 phase cells are quiescent. Fully differentiated cells and cells that are no longer dividing (e.g. neurons) remain in this phase. During G1 phase the cell synthesizes various enzymes and molecules required for S phase, where duplication of the chromosomes takes place. Once the duplication of chromosomes is completed, cells enter the G2 phase, where the various proteins required for mitosis (such as microtubules) are synthesized by the cell. Once interphase is completed, cells are ready to enter mitosis and divide into two daughter cells. There are five distinct stages in M phase; prophase, prometaphase, metaphase, anaphase and telophase. During the first step in mitosis, prophase, the chromosomes begin condensing and centrioles begin moving to the opposite poles of the cell. This is followed by prometaphase, where the nuclear membrane dissolves releasing the condensed chromosomes into the cytoplasm. Microtubules from the centrosomes at the opposite pole of the cell emerge and bind to the kinetochore protein complex present in the centromere of each chromosome. During metaphase the chromosomes line up at the centre of the mitotic spindle and are attached to the microtubules from two opposing centrosomes via the kinetochore protein complex. This is followed by anaphase where the two sister chromatids are separated and move towards the opposite poles. During telophase, chromosomes arrive at the opposing ends of the cells and the nuclear membrane forms around daughter nuclei. At this stage the chromosomes de-condense and two new cells begin to form.

Studying the rate of cell division is essential for understanding functions of many genes. Various techniques have been used to determine the rate of proliferation in a tissue. These include studying the rate of Bromodeoxyuridine (a synthetic analogue of the thymidine nucleotide) incorporation into the newly synthesied DNA during S phase of the cell cycle,

counting the number of cells that are positive for markers of the cell cycle, such as phosphorylated Histone H3, and visualizing the structure of DNA within the cell to determine the phase of cell cycle.

Histone H3 is a member of a large histone family involved in packaging the DNA into chromatin. During mitosis the N terminus of histone H3 becomes phosphorylated at serine 10 and 28. Phosphorylation is initiated at the end of G2 phase and is seen at the pericentromeric heterochromatin region. Throughout prophase it spreads throughout the chromosome and it is completed by the end of prophase. It is then maintained throughout metaphase. During anaphase, dephosphorylation of Histone H3 begins and this ends at the beginning of telophase (Goto et al., 1999; Hans and Dimitrov, 2001).

During mitosis the chromosomes condense. When condensed they appear brighter than the non-condensed DNA when stained with a fluorescent dye that binds to DNA e.g. Oligreen. This can be used as a method to identify cells undergoing mitosis. Furthermore, by looking at the structure of the stained chromosome it is also possible to distinguish cells into two main groups; prophase-metaphase and anaphase-telophase. During prophase and metaphase chromosomes are condensed but appear at the center of the cell as one structure however at anaphase and telophase, the condensed sister chromatids are being pulled apart so they appear as two separate structures. This information can also be used to study the orientation of cell division.

5.1.5 Apical basal polarity in epithelial tissue

The hallmark of epithelial cells is that they exhibit apical-basal polarity and strong cell-cell contact with the neighboring cells to create a sheet of epithelium. The apical surface of an epithelial cell is in contact with a lumen while the basal surfaces of the cells are in

contact with the extracellular matrix. Lateral surfaces of the cells are involved in cell-cell contacts with the neighboring cells. On the lateral surface of these cells there are groups of protein complexes that hold the cells together and enable cell-cell communication; these are known as junctions. In vertebrates, there are three main types of junctions, gap junction, adherens junction and tight junction. Gap junctions are composed of proteins encoded by the Connexins gene family and these enable ions and small molecules (less than 1 kDa) to pass freely in between cells (Lampe and Lau, 2004). An adherens junction gives mechanical support to the cells and holds the cells together. It is composed of two groups of proteins, Cadherins and Catenins. Cadherin is a transmembrane protein whose extracellular domain interacts with the extracellular domain of Cadherin from the adjacent cell and the intracellular domain interacts with the Catenins which in turn are connected to the actin filament of the cytoskeleton (Yamada et al., 2005). Tight junctions are located towards the apical region of the cell and consists of a large group of transmembrane proteins and cytoplasmic proteins which interact with the proteins bound to the membrane. These proteins are distributed so that they surround the cell to form a tight barrier between the apical and basolateral domains of the cell, across which molecules are unable to pass. A tight junction consists of two main groups of proteins, Occludins and Claudins in addition to other molecules including ZO2. Claudin is a multigene family and members of this family show tissue specific expression (Morita et al., 1999). There are at least two functions defined for tight junctions. First, they serve as a barrier between the protein complexes present in the membrane of the apical domain and the membrane of the basolateral domain of the cell hence they are critical for maintaining the apical basal polarity of the cell. Second, they regulates transcription of genes that are involved in cell proliferation and differentiation (Balda and Matter, 2000; Metais et al., 2005).

In invertebrates, the analogue of the tight junction is the septate junction. Studies in *Drosophila* have revealed that *Scribble* localizes to septate junctions, which is found at the

more basal level to the adheren junction. Furthermore, it appears that *Scribble* specifies the site of the septate junction as it localizes to the site of future septate junctions, prior to junction formation (Bilder and Perrimon, 2000). In keeping with the role of the septate junction in restricting the distribution of proteins to their apical or basolateral domain within the cell, the consequence of a mutation in *Scribble* results in mislocalisation of normally apically restricted proteins throughout the apical and basolateral region of the cell. However, in *Scribble* mutants the proteins normally localizing to the baslolateral region of the cell are not mis-localized suggesting that the role of the *Scribble* is to restrict the localization of the apical proteins to the apical region without affecting the distribution of proteins in the basolateral domain of the cell (Bilder et al., 2000; Bilder and Perrimon, 2000). More recently human SCRIBBLE has also been shown to localize to the tight junctions of intestinal epithelium and is required for the assembly of the tight junction in an intestinal epithelial cell line (Ivanov et al., 2010).

5.1.6 *Scribble* has a tumor suppressor role in *Drosophila* and Human

Scribble in *Drosophila* has been described as a neoplastic tumor suppressor gene of epithelial tissue. Mutation of *Scribble* results in over-proliferation giving rise to cells that have lost their ability to form an organized epithelial sheet and to differentiate (Bilder et al., 2000; Bilder and Perrimon, 2000). These features are also hallmarks of many human cancers. It has been reported that the expression level of Scribble is reduced in the epithelium of various human cancers, such as breast cancer, cervical cancer and colon cancer (Gardiol et al., 2006). Furthermore, human SCRIBBLE has been identified as one of the targets of the E6 oncoprotein of Human Papilloma Virus (a major risk factor of human cervical cancer), leading to its ubiquitin-mediated degradation (Nakagawa and Huibregtse, 2000).

These results suggest a role for *Scribble* in negatively regulating the cell cycle. This has been demonstrated for both *Drosophila* and human Scribble (Brumby et al., 2004; Nagasaka et al., 2006). These studies report that both *Drosophila* Scribble and human SCRIBBLE negatively regulate the transition from G1 to S phase of the cell cycle.

5.2 Results

5.2.1 The rate of proliferation in the neuroepithelium of *Circletail* is unaffected during neurulation

Drosophila Scribble has role as a tumor suppressor whereby the mutation results in over-proliferation of epithelial cells (Bilder et al., 2000; Bilder and Perrimon, 2000). To examine if this function of *Scribble* is conserved in mice during neurulation, I measured the rate of proliferation in the neuroepithelium of *Circeltail* and wildtype littermate embryos, using two different methods.

Firstly, I sectioned embryos undergoing neurulation to obtain transverse sections through the spinal region of embryos and performed immunohistochemistry. Cells undergoing proliferation were marked by an antibody raised against phosphorylated Ser-28 histone H3 (PHH3), which marks cells in prophase, metaphase and early anaphase (Figure 5-1 A), and sections were counter-stained with DAPI (Figure 5-1 B,C). Cells positive for PH3 in the neuroepithelium were counted and, to calculate the rate of proliferation, the total number of cells in the neuroepithelium, as marked by DAPI, was also counted (Figure 5-1 D).

Secondly, I counted the number of cells with and without condensed chromosomes using the composite obtained from the oligreen staining of whole embryo (Figure 5-3). By looking at the structure of the condensed chromosomes, it is possible to group proliferating cells into two classes; cells in prophase to metaphase and cells in anaphase to telophase (Figure 5-1 D and Figure 5-3).

Results from both experiments show that the rate of proliferation in the neuroepithelim of *Circletail* is not significantly different to that of wildtype littermates for any part of mitosis analyzed (Figure 5-1 E).

5.2.2 The apical basal polarity in the neuroepithelium of *Circletail* is unaffected during neurulation

Scribble in *Drosophila* was initially identified as a gene required to maintain the apical-basal polarity in epithelial tissue (Bilder et al., 2000; Bilder and Perrimon, 2000). To examine whether this function of *Scribble* is conserved in mice and affects the neuroepithelium during neurulation, I examined the distribution of F-actin and the localization of the tight junction on transverse sections of E8.5 *Circletail* and wildtype littermates. F-actin is a component of the cytoskeleton and is apically enhanced during neurulation (Ybot-Gonzalez and Copp, 1999). Fluorescently conjugated phalloidin was used to visualize F-actin distribution and antibodies raised against ZO-2 and Claudin-6 were used to visualize the tight junctions. The distribution of ZO-2 and Claudin-6 in *Circletail* is comparable to that seen in wildtype littermates (Figure 5-2). The overall distribution of the F-actin is not changed in *Circletail* mutant as it is still enriched towards the apical surface of neuroepithelium cells, however the organization of the neuroepithelium looks disorganized compared to the wildtype tissue (Figure 5-2 C and D). F-actin and ZO-2 are present in the neuroepithelium of E8.5 embryos; however, Claudin-6 is absent from neuroepithelium but is present in ectoderm (Figure 5-2).

5.3 *Orientation of cell division at the site of closure 1 is random in mice*

Previous work has shown that the correct orientation of cell division during gastrulation in zebrafish contributes to anterior-posterior axis elongation and this orientated cell division is regulated by the planar cell polarity pathway (Gong et al., 2004). Mouse mutants of PCP fail to elongate the anterior-posterior axis during neurulation (section 3.2.4).

Figure 5-1: Rate of proliferation in *Circletail* and wildtype littermates.
(A) Four main phases of mitosis. The red line indicates the phases of mitosis which can be detected by rat anti-PH3 and the green line indicates the phases of mitosis that can be detected by oligreen staining. (B,C) Transverse section through the spinal region of E8.5 wildtype (B) and *Circletail* (C) embryos, showing cells undergoing mitosis as marked by anti-PH3 antibody (red) and counterstained with DAPI. (D) Table showing numbers of cells counted in five wildtype and *Circletail* embryos using two separate methods. Total number of cells and cells in different phases of mitosis as determined by PH3 staining and oligreen staining were counted. (E) A bar chart showing the percentage of proliferating cells in wildtype and *Circletail* embryos as marked by PH3 antibody and oligreen. The error bars are the standard errors of the data. P values are calculated using two-tailed T-test. Scale bars represent 5 μm.

A

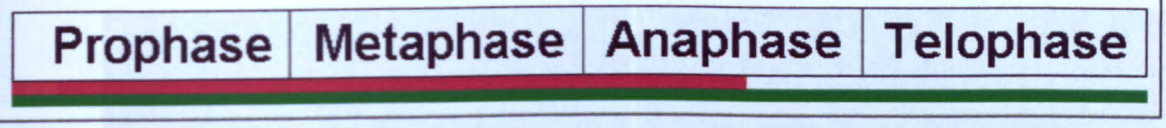

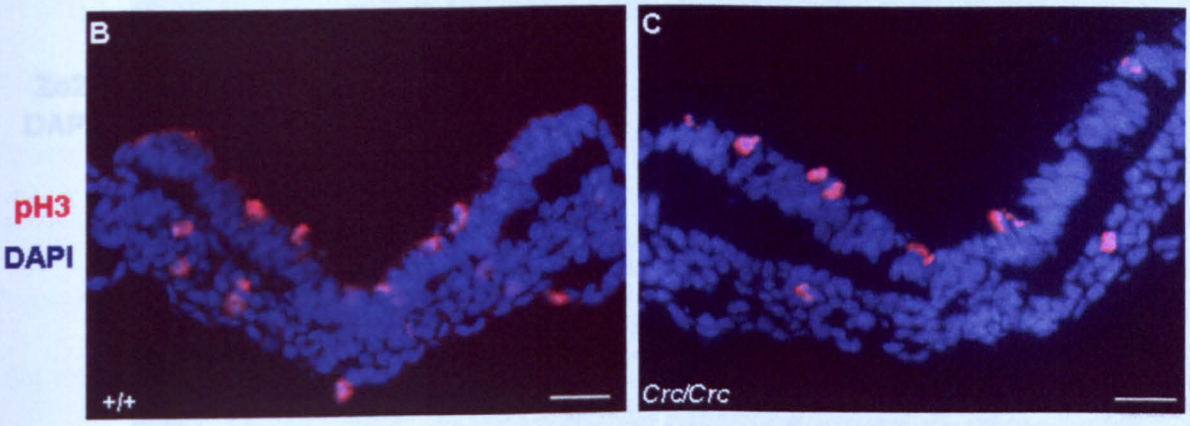

D

		+/+ (N=5)	*Crc/Crc* (N=5)
PH3	Total number of cells counted	7855	7691
	Number of cells in prophase-mid anaphase	346	281
Oligreen	Total number of cells counted	8108	8253
	Number of cells in prophase-metaphase	399	442
	Number of cells in anaphase-telophase	98	147

E

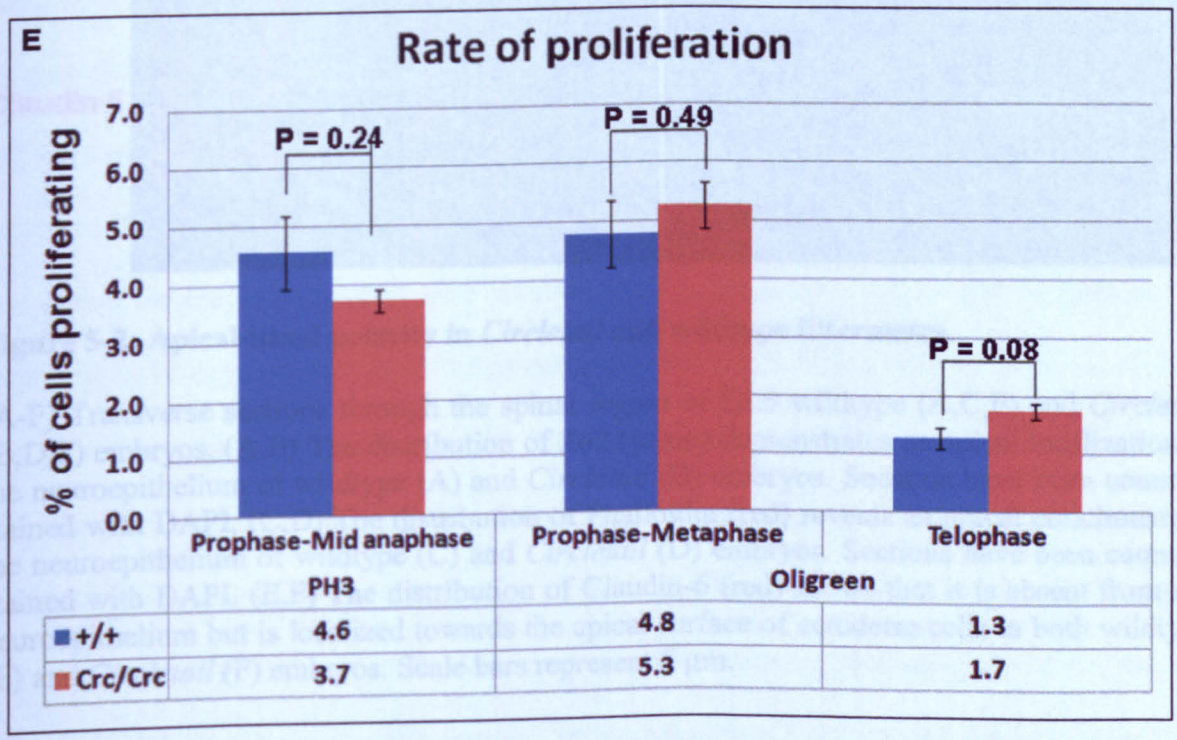

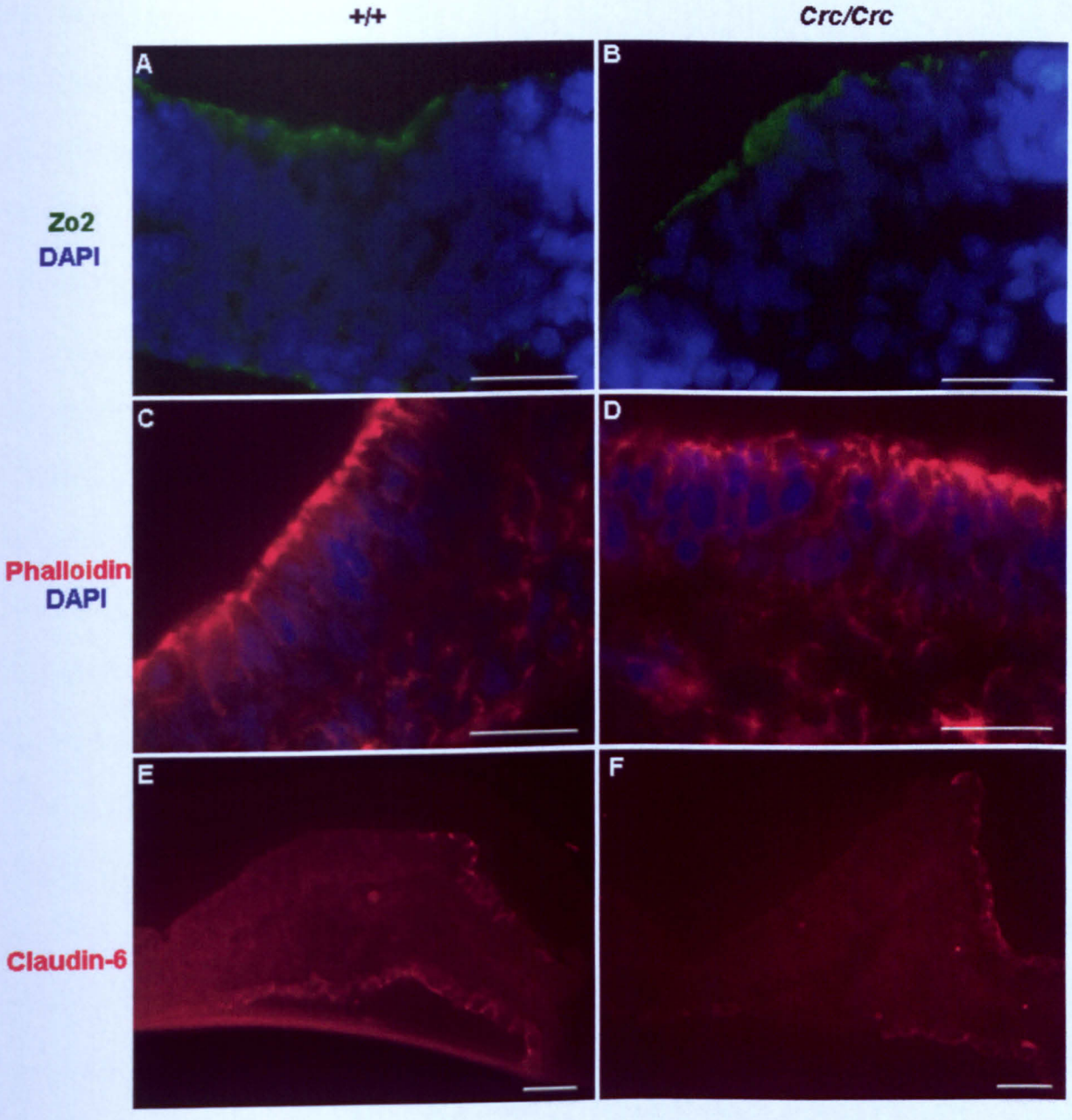

Figure 5-2: Apical-basal polarity in *Circletail* and wildtype littermates.

(A-F) Transverse sections through the spinal region of E8.5 wildtype (A,C,E) and *Circletail* (B,D,F) embryos. (A,B) The distribution of Zo2 (green) demonstrates an apical localization in the neuroepithelium of wildtype (A) and *Circletail* (B) embryos. Sections have been counter-stained with DAPI. (C,D) The distribution of Phalloidin (red) reveals an apical enrichment in the neuroepithelium of wildtype (C) and *Circletail* (D) embryos. Sections have been counter-stained with DAPI. (E,F) The distribution of Claudin-6 (red) shows that it is absent from the neuroepithelium but is localized towards the apical surface of ectoderm cells in both wildtype (E) and *Circletail* (F) embryos. Scale bars represent 5 μm.

To test the hypothesis that orientation of cell division is important during initiation of neural tube closure at the site of closure 1, and that it is controlled by the PCP pathway, I measured the angle of cell division in CD1 embryos (a wildtype strain) and in *Circletail* mutants and wildtype littermates. E8.0 embryos, with 3-5 somites, were stained with oligreen to stain the chromosomes and were viewed under a confocal microscope. 5 μm optical sections through the neuroepithelium at the level of third somites (where the closure 1 occurs) were photographed and were overlaid using Photoshop software to create a composite (Figure 5-3). Oligreen stains the DNA and when the cells divide the chromosomes condense and appear brighter (Figure 5-3). During telophase of the cell cycle, the chromosomes remain condensed as two daughter cells are formed. To measure the angle of cell division I drew a line between nuclei of two daughter cells and measured the angle relative to the anterior-posterior axis of the embryo (Figure 5-3). Zero degree is parallel to the anterior posterior axis and 90 degrees is perpendicular to the anterior-posterior axis. The angles of division were divided into 10 groups and the percentage of cells dividing at angles within each group was plotted as a bar chart (Figure 5-4). For the orientation of cell division to play a role in elongating the embryo, the majority of cells must divide parallel or with a low angle to the anterior-posterior axis, as observed in zebrafish. In CD1 embryos, 72 cells undergoing telophase were analyzed and it was found the majority of cells were dividing with an angle between 21 and 50 degrees and between 81-90 degrees, relative to the anterior posterior axis. The lowest proportions of cells divide with an angle of 0-20 and 51-80 degrees (Figure 5-4A). This pattern of orientation is not observed in *Circletail* mutant embryos or their wildtype littermates. In wildtype littermates, 93 cells undergoing telophase of the cell cycle were analyzed and the majority of cells were dividing with an angle between 0 and 10 degrees or between 31 and 60 degrees (Figure 5-4B). In *Circletail* embryos, 287 cells undergoing telophase of the cell cycle were analyzed and there is an even distribution of percentage of cells dividing with angle between 0

and 90 degrees (Figure 5-4C). These results suggest that the orientation of cell division in the neuroepithelium at the site of closure 1 does not play a role in elongating the anterior-posterior axis of the embryo during initiation of neural tube closure.

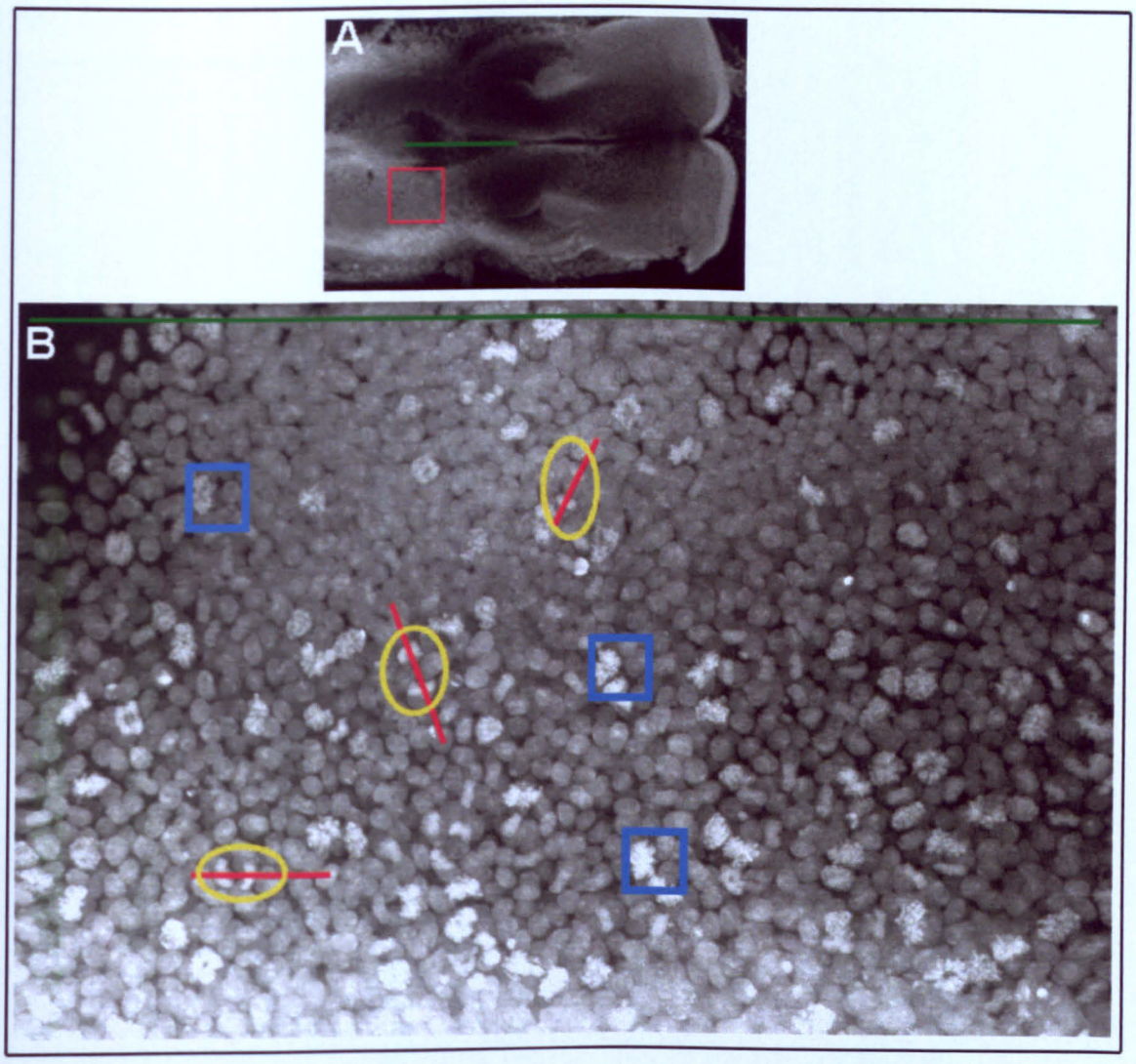

Figure 5-3: Measuring the orientation of cell division and rate of proliferation from oligreen stained whole embryos.

(A) A low power confocal image of a *Circeltail* wildtype littermate embryo with three somites. Anterior is to the right and posterior to the left. The green line represents the anterior-posterior axis of the embryo and the red box highlights the area within the embryo where higher magnification images were taken to study the orientation of the cell division and the rate of proliferation. The corresponding area on the other side of the midline was also studied. (B) Overlay of high magnification confocal optical sections from the area highlighted in (A). Yellow circles highlight examples of the cells during anaphase/telophase of the cell cycle and blue boxes emphasise examples of cells in prophase and metaphase of the cell cycle. The red line represents the orientation of cell division and the green line represents the anterior posterior axis of the embryo. The angle between the red and green lines was measured to obtain the angle of cell division. Both cells with condensed chromosomes and the total number of cells were counted to obtain the rate of proliferation.

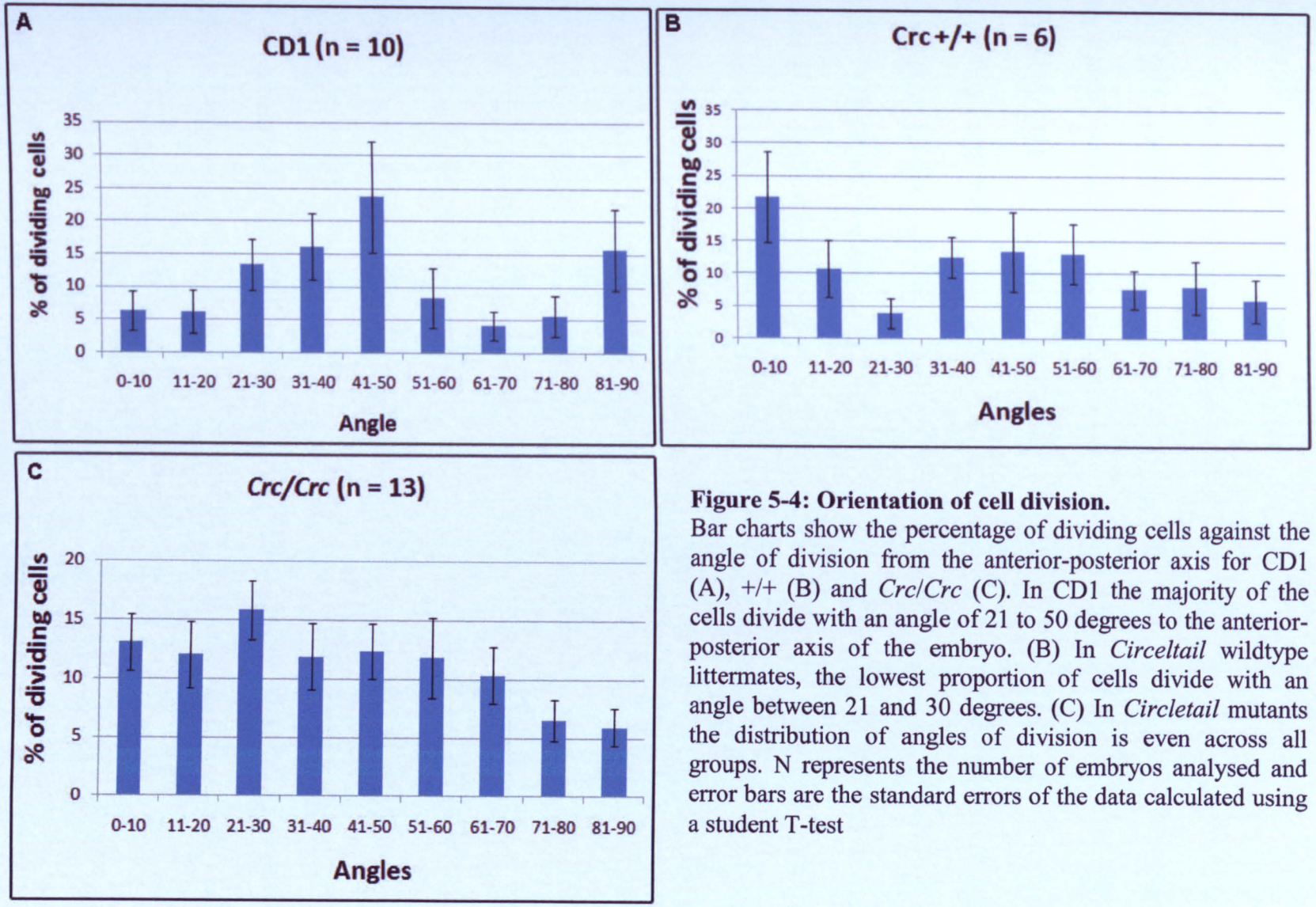

Figure 5-4: Orientation of cell division.
Bar charts show the percentage of dividing cells against the angle of division from the anterior-posterior axis for CD1 (A), +/+ (B) and *Crc/Crc* (C). In CD1 the majority of the cells divide with an angle of 21 to 50 degrees to the anterior-posterior axis of the embryo. (B) In *Circeltail* wildtype littermates, the lowest proportion of cells divide with an angle between 21 and 30 degrees. (C) In *Circletail* mutants the distribution of angles of division is even across all groups. N represents the number of embryos analysed and error bars are the standard errors of the data calculated using a student T-test

5.4 Discussion

5.4.1 The role of *Scribble*

It had originally been published that mouse *Scribble* functions to control the PCP signalling pathway while the homologous gene in *Drosophila* is involved in specification of apical-basal polarity and controlling the rate of proliferation (Bilder et al., 2000; Bilder and Perrimon, 2000; Montcouquiol et al., 2003; Murdoch et al., 2003). Recently it has been established that, similar to mouse, *Drosophila Scribble* also has an additional function in controlling the PCP signalling pathway (Courbard et al., 2009). To establish whether mouse *Scribble* functions to specify apical-basal polarity and control the rate of proliferation during neurulation, apical-basal polarity and the rate of proliferation were examined in *Circletail* mutant and wildtype embryos. Data presented in this thesis show that the rate of proliferation and apical-basal polarity are not altered in mouse embryos during neurulation when *Scribble* is mutated; however, the cellular organization of the neuroepithelium appears to be disrupted. Disruption in organization of neuroepithelium cells is consistent with the known role of Scribble as it has been previously reported that mouse Scribble is required for the cell-cell adhesion in cultured kidney epithelial cells and that *Circletail* mutants show a cellular disturbance of cardiomyocyte organization during early heart development (Qin et al., 2005; Phillips et al., 2007).

Recent studies have demonstrated a link between PCP signalling and apical-basal polarity (Dollar et al., 2005; Tao et al., 2009; Vandenberg and Sassoon, 2009). These studies show that components of the core PCP signalling pathway, such as *Prickle*, *Dishevelled* and *Vangl2*, have a role in regulating apical-basal polarity in mice and *Xenopus*. Using *Xenopus* as a model system, Dollar *et al* show that the PCP core protein, Dishevelled forms a complex with Lethal Giant Larvae (Lgl) the apical-basal polarity determinant proteins and that the

function of Dishevelled is essential for localization of Lgl to the membrane and establishment of the apical basal-polarity in embryonic ectoderm (Dollar et al., 2005). Tao *et al* report a null allele of mouse *Prickle1* and show null embryos have a disrupted apical-basal polarity in the epiblast. Furthermore, they show that *Prickled1* genetically interacts with *Vangl2* to regulate the epiblast apical-basal polarity (Tao et al., 2009). These studies give evidence to support a link between apical-basal polarity and PCP. Vandenberg and Sassoon study the effect of a mutation in mouse *Vangl2* on the organisation of epithelial cells in female reproductive tract using *Loop-tail* as a model. They show that the overall organisation of the epithelium and the apical-basal polarity is disrupted as the cells lose their columnar morphology and the apical enrichement of actin and E-cadherin. Interestingly, the localization of Scribble is also altered in *Loop-tail* reproductive tract so it no longer localizes to the basolateral membrane of the uterine epithelial cells suggesting that Vangl2 is required for the correct localization of Scribble in these cells (Vandenberg and Sassoon, 2009). In contrast, the localization of Scribble is not affected in the neuroepithelium of *Loop-tail* mice (personal communication with Ms C. Damrau), giving evidence that the role of these genes may be tissue specific.

Loss or down-regulation of Scribble is associated with tumorogenesis in *Drosophila* and human (Bilder et al., 2000; Gardiol et al., 2006). Additionally, it has been shown that the human SCRIBBLE is a functional homologue of *Drosophila* Scribble and can rescue the polarity and overgrowth defects of *Drosophila Scribble* mutant (Dow et al., 2003). Studies in cell lines have also suggested that human SCRIBBLE inhibits proliferation by negatively regulating the progression of the cell cycle into S phase (Nagasaka et al., 2006). These results give evidence that *Scribble* is involved in controlling proliferation in both *Drosophila* and human. However this does to appear to apply to mice as the rate of cell proliferation is unaltered in *Circletail* mutant embryos and no growth abnormalities have been reported. It would be interesting to test for a genetic interaction between *Scribble* and *Prickled1* by

crossing animals that are heterozygous for each of the gene and determining whether or not *Scribble* genetically interact with *Prickled1*during the establishment of the apical-basal polarity. Another idea would be that mouse Scribble is a core component of the PCP pathway and is only required for in this pathway. One of the ways this hypothesis could be tested is by analyzing the distribution of other PCP core proteins such as Dishevelled, Vangl2 and Frizzled in *Circletail* mutant in a tissue where the polarity has already been established. This for example could be done on inner ear sensory hair cells of E18.5 *Circletail* mutant. If the Scribble is a core component of the PCP signalling then the asymmetric distribution of other core PCP molecules will be lost. In support for this hypothesis, it has already been published that the asymmetric distribution of Vangl2 requires the function of Scribble (Montcouquiol et al., 2006).

5.4.2 Orientation of cell division is random in mice

Previously it has been reported that, in the neuroepithelium, at the level of forebrain, hindbrain and the spine, of a mouse embryo undergoing neurulation (E7.5, E8.5 and E9.5), the mitotic spindles of dividing cells are preferentially orientated along the anterior-posterior axis of the embryo. This is predicted to result in cell division where two daughter cells end up parallel to the body axis, hence contributing to the overall lengthening of the embryo (Sausedo et al., 1997). Results reported in this chapter suggest that the orientation of cell division, at E8.0 (3-5 somites) at the site of closure 1, is random in mice. This contrasting result could be due to different methods of study as well as a difference in stage of the embryos and the positions within the embryo that the cells were analyzed. Sausedo *et al.* studied the orientation of the mitotic spindle of cells in metaphase of the cell cycle. In this study, I have analyzed the orientation of cell division by measuring the angle of cell division in anaphase/telophase,

where two daughter cells are beginning to segregate. There is evidence, from studies in rat and *Xenopus*, that suggests a significant variation in results between these two methods could be expected. In both rat and *Xenopus* neuroepithelium the mitotic spindle rotates substantially prior to onset of anaphase/telophase, giving rise to cell division where the orientation cannot be predicted by looking at the mitotic spindle (Adams, 1996; Kieserman and Wallingford, 2009). To verify whether this is the case in mouse cell division it is essential to study time lapse images of cells undergoing proliferation and determine whether or not the mitotic spindle rotates prior to cell division.

5.4.3 Evidence of orientated cell division during axis elongation and PCP signalling

Two separate studies suggest a role for orientated cell division in zebrafish during gastrulation. Both show that cell division on the dorsal surface of the embryo during gastrulation stage is oriented along the anterior-posterior axis of the embryo, the axis which is elongating during early development (Concha and Adams, 1998; Gong et al., 2004). During this stage not only are the cells dividing with anterior-posterior orientation but they are also actively moving in anterior-posterior direction (Concha and Adams, 1998). This anterior-posterior movement of cells appears to be different from the convergent extension movement where cells move and intercalate into the midline of the embryo, rather than moving along the anterior-posterior axis. Gong *et al.* further go on to show that this oriented cell division is downstream of PCP signalling, so when PCP signalling is blocked by injection of a mutated form of *Dishevelled* into the gastrulating stage embryo, the orientation of cell division is random and the embryo fails to elongate (Gong et al., 2004).

At later stages (3-6 somites) cells no longer divide along the anterior-posterior axis but switch to dividing along the medio-lateral axis. During this stage cell movement is also

altered, and cells move towards the midline of the embryo (Concha and Adams, 1998). This movement of cells towards the midline of the embryo appears to be similar to the movement observed during convergent extension, which is known to take place during zebrafish development and is controlled by PCP signalling (Heisenberg et al., 2000). Further detailed study has shown that PCP signalling during this stage is not required for oriented cell division, as cells still divide along the medio-lateral axis of the embryo when PCP signalling is altered; however PCP is required for integration of the daughter cell into the midline (Ciruna et al., 2006). These results suggest PCP signalling is involved in driving the axis elongation in zebrafish by initially controlling the orientation of cell division and, at later stages, by controlling the movement of cells.

During *Xenopus* gastrulation (stage 13), cells in the neural plate divide with a specific orientation but this is along the medio-lateral axis rather than the anterior-posterior axis. Furthermore, this oriented cell division is not controlled by PCP signalling (Kieserman and Wallingford, 2009). However, when PCP is disrupted the embryo fails to elongate due to a defect in convergent extension (Wallingford and Harland, 2002), a result similar to that described above for the late development of zebrafish *(Ciruna et al., 2006)*. These observations suggest that, in *Xenopus,* the orientation of cell division does not play a role during axis elongation and that axis elongation is dependent on convergent extension. The orientation of cell division in *Xenopus* is not random, suggesting that it has a specific role; what this role may be remains to be seen.

In mice the orientation of cell division at the site of closure 1 (at the level of 3rd somite) is random, which can suggest two things. Perhaps in mice the mechanism of axis elongation does not require oriented cell division and may just depend on the process of convergent extension. Alternatively, orientation of cell division at the site of closure 1 is random but may be regulated at different levels along the body axis. It is important to look at the orientation of

cell division at the caudal end of embryos undergoing neurulation as there is some evidence that the cells in this region are abnormal in mutants of PCP signalling (Ybot-Gonzalez et al., 2007b).

CHAPTER 6

IDENTIFYING TARGET GENES OF TULP3

6 Identifying target genes of *Tulp3*

6.1 Introduction

6.1.1 *hitchhiker* carries a mutation in *Tulp3*

hitchhiker came out of a G3 recessive ENU screen at Harwell and displays multiple developmental defects including spina bifida, exencephaly and polydactyly (Patterson et al., 2009). *hitchhiker* mutants carry a point mutation in the second intron of *Tubby-like protein 3* (*Tulp3*). This splice site mutation causes skipping of exon 2, creating a 52 bp deletion that leads to a frame shift and premature truncation of the Tulp3 protein. *hitchhiker* is considered to be a strong hypomorphic allele of *Tulp3,* rather than a complete null, as approximately 4% of the wild-type level of Tulp3 protein is detected in the mutant (Patterson et al., 2009). A null allele of Tulp3 has also been described and exhibits similar, but slightly more severe, neural tube defects (Ikeda et al., 2001; Norman et al., 2009; Patterson et al., 2009). Recent studies have revealed the role of Tulp3 in mice as a negative regulator of the Sonic Hedgehog (Shh) signalling pathway (Cameron et al., 2009; Norman et al., 2009; Patterson et al., 2009). Shh signalling is a fundamental pathway involved in many developmental processes including neural tube closure and dorsoventral patterning of the neural tube (Ybot-Gonzalez et al., 2002; Wilson and Maden, 2005). Both of these processes are affected in *Tulp3* mutants (Cameron et al., 2009; Norman et al., 2009; Patterson et al., 2009).

6.1.2 Dorsoventral patterning of the neural tube

The developing neural tube is patterned along the dorsoventral axis, where the progenitors of different neuronal subtypes are present in a precise spatial order. This

arrangement is determined by the actions of four different families of signalling molecules. Retinoic Acid (RA) produced by the paraxial mesoderm inhibits the Fibroblast Growth Factors (FGFs) in the neuroepithelium and promote its differentiation to produce different neuronal subtypes (Wilson and Maden, 2005). Bone morphogenetic proteins (BMPs), produced by the overlying surface ectoderm and the roof plate, induce the formation of the dorsal cell types while Shh, produced from the ventral midline, induces the formation of the ventral cell types (Wilson and Maden, 2005). Shh ligand, which is initially produced by the underlying notochord, is a secreted morphogen and a concentration gradient is established across the dorsoventral axis of the neural tube. Cells in the ventral-most region of the neural tube are exposed to the highest level of Shh ligand, and these become the floor plate, which then becomes the second centre of Shh ligand production (Roelink et al., 1995). Cells on the dorsal surface of the neural tube are exposed to the lowest level of Shh. Along the dorsoventral axis of the neural tube specific homeodomain transcription factors, combinations of which give rise to unique neuronal identity, respond to this Shh gradient (Briscoe et al., 2000). The distributions of cells expressing these specific homeodomain transcription factors are commonly used as markers to study dorsoventral patterning of the neural tube. High levels of Shh induce ventral markers such as Nkx2.2 in V3 neurons, adjacent to the floor plate. Progressively lower levels of Shh induce progressively more dorsal neuron types, revealed by expression of a number of markers such as HB9 in motorneurons, Olig2 and Nkx6.1. Expression of dorsal markers, such as Pax6, are inhibited by Shh but are induced by BMPs from the dorsal neural tube.

A number of mutants have been identified as showing a disruption in the dorsoventral patterning of the neural tube, as a result of altered Shh gradient. In the absence of Shh, the floor plate and ventral markers such as Nkx2.2 and HB9 are lost and the neural tube becomes completely dorsalized, with expansion of expression of dorsal markers (Chiang et al., 1996;

Norman et al., 2009; Patterson et al., 2009). In mutants where activation of the Shh pathway is increased, such as in *hitchhiker*, the expression domains of the ventral markers (such as Nkx2.2 and HB9) expand dorsally at the expense of more dorsal markers (Eggenschwiler et al., 2001; Bulgakov et al., 2004; Tran et al., 2008; Wong et al., 2008; Norman et al., 2009; Patterson et al., 2009).

6.1.3 Gli proteins and dorsoventral patterning of the neural tube

Gli proteins are zinc-finger containing transcription factors and function as mediators of Shh signalling. In vertebrates, there are three members of this family; *Gli1*, *Gli2* and *Gli3*. All three genes are expressed in the neuroepithelium during neural tube development (Lee et al., 1997), suggesting a role in neural tube patterning. There are two forms of Gli2 and Gli3; a repressor form and an activator form. In the absence of Shh ligand, Gli2 and Gli3 are proteolytically cleaved to produce the repressor form, which inhibits the transcription of Shh target genes. In the presence of Shh ligand, proteolytic processing of Gli2 and Gli3 is inhibited, and the full-length forms are modified to become transcriptional activators and induce the transcription of Shh target genes (Dai et al., 1999; Aza-Blanc et al., 2000). Gli1 exists only in the activator form as it cannot be cleaved (Dai et al., 1999). Analyzing dorsoventral patterning of the neural tube in null mutants has revealed different roles of each of these three proteins. Mutants of *Gli1* do not show a defect in dorsoventral patterning (Matise et al., 1998; Park et al., 2000). In *Gli2* mutants, the ventral-most cell types fail to be specified and as a result the floor plate is absent (Matise et al., 1998). These ventral-most cells are exposed to the highest level of Shh signalling and consequently to the highest level of activator form of Gli2, suggesting that the activator form of Gli2 is most important for the patterning of the neural tube. This idea is further supported by the rescue of Gli2 function by

Gli1 *in vivo*, which always exists as an activator form (Bai and Joyner, 2001). Gli3 primarily functions as a repressor form and is important in limb patterning such that both heterozygous and homozygous *Gli3* mutant embryos exhibit polydactyly (Sasaki et al., 1999; Wang et al., 2007). A subtle defect in dorsoventral patterning of the neural tube is also observed in *Gli3* mutants, where the intermediate cell types are expanded dorsally without affecting the ventral cell types (Persson et al., 2002). This phenotype is not detected in mice that lack the full length Gli3 but produce the cleaved form of the protein, suggesting that the repressor form of Gli3 is important for patterning of the neural tube (Persson et al., 2002).

Recent studies have shown that Tulp3 acts downstream of Shh and upstream of Gli2 during neural tube patterning (Norman et al., 2009; Patterson et al., 2009). In *Gli2/Tulp3* double mutants the dorsoventral patterning resembles that of *Gli2* single mutants; however a subtle difference was observed (Norman et al., 2009), suggesting that *Tulp3* may be partly functioning through another molecule during neural tube patterning. This molecule could be Gli3. We have found that *Tulp3* and *Gli3* genetically interact during limb patterning as introduction of one mutated *Gli3* allele into an embryo that is homozygous for the *Tulp3 hhkr* mutation results in more severe polydactyly than that observed in either *hhkr* homozygotes or *Gli3* heterozygous mice (Patterson et al., 2009). The molecular nature of the interaction between Tulp3 and Gli3 is not understood as the processing of Gli3 to the repressor form is not obviously affected in either *hhkr* or the *Tulp3* knockout (Norman et al., 2009; Patterson et al., 2009).

6.1.4 Roles of Tubby family

Tulp3 is a member of the Tubby family, consisting of Tubby, Tulp1, Tulp2 and Tulp3. The C-terminus of these proteins is conserved and consists of a Tubby domain (Nishina et al.,

1998; Boggon et al., 1999). The crystal structure of the Tubby domain has been resolved and shows a single hydrophobic helix surrounded by a 12-stranded β-barrel sheet (Boggon et al., 1999). Clusters of positively charged residues and a separate cluster of negatively charged amino acids on the surface of the Tubby domain indicate that it has the potential to bind to DNA and proteins. Indeed, it has been shown that this domain is capable of binding specifically to double stranded DNA *in vitro* (Boggon et al., 1999). The N-terminal domain of proteins within the Tubby family is less conserved but it contains a nuclear localization signal (NLS) and sequence that is reminiscent of a transactivation domain of a transcription factor (Nishina et al., 1998; Boggon et al., 1999). Furthermore, Tubby is predominantly found in the nuclear fraction of cell protein extracts and the N-terminal domains of Tubby and Tulp1 have been shown to activate transcription in reporter assays (Boggon et al., 1999). A recent study has reported that Tulp3 is also present in the nuclear fraction as well as the cytoplasmic and membrane fractions (Norman et al., 2009). Together these data strongly argue for a role of Tulp3 as a transcription factor.

6.1.5 Microarray analysis

Microarray analysis is a powerful technology which enables scientists to study and compare the expression profiles of many genes under various conditions. Since its first use in 1995 to study the expression profile of 45 cDNA clones from *Arabidopsis thaliana* (Schena et al., 1995), microarrays have become a widely used standard method of studying global gene expression in various systems. In the case of oligonucleotide microarray, this is achieved by immobilizing DNA sequences (usually 50-70 bp) representing individual genes from a genome onto a solid surface e.g. a glass slide. Oligonucleotides corresponding to each gene are represented as a single spot within the slide; therefore an array slide consists of thousands

of spots, each representing a single gene within the genome. To compare the level of gene expression between two biological samples, cDNA from each sample is synthesized and each is labeled with a different fluorescent tag, such as Cy5 and Cy3. These differentially labeled samples are mixed together and applied to the array slides where they will compete to hybridize to the complementary probe present within the array. The level of fluorescence of each dye is measured for each oligonucleotide spot to determine the relative abundance of a specific transcript within the two biological samples.

During the course of this study an array consisting of 25,000 mouse oligonucleotides printed onto a glass slide was used to compare the gene expression profile between *hitchhiker* embryos and wildtype littermates.

6.1.6 SYBR green based real time PCR

Real time RT-PCR is often used to validate microarray results. There are four main types of real time RT-PCR that are regularly used to quantify expression level of a gene in a biological sample; TaqMan assays, Molecular Beacons, Scorpions and SYBR green. TaqMan, Molecular Beacons and Scorpions require the use of labeled probes specific to the gene of interest while SYBR green approach does not. All of these techniques allow detection of PCR products during the PCR reaction by emitting a fluorescent signal upon excitation with a laser beam. Among these four approaches SYBR green based real time RT-PCR is the most economical method for detecting and quantifying PCR products, therefore it is used most frequently when a large number of genes are under study. SYBR green PCR requires a pair of primers, similar to that of a regular PCR and a master mix containing SYBR green. During the PCR reaction, SYBR green binds to double stranded DNA and when excited with a laser beam it emits light, which is detected by a real time PCR machine. As the PCR product accumulates,

with increasing cycle number, more SYBR green binds to DNA resulting in an increased fluorescence level.

Because SYBR green binds to any double stranded DNA non-specifically it is essential to optimize individual PCR assays before use for quantification purpose. This is usually achieved by optimizing PCR such that only one product is amplified and that the efficiency of the PCR is approximately 100%.

There are two ways to determine if multiple PCR products have been amplified during the reaction. The first option is to electrophorese the final PCR product through an agarose gel and visualize the bands. The second option is to construct a dissociation curve at the end of the SYBR green PCR reaction using the real time machine. During this process the temperature of the reaction is gradually increased from 60°C to 95°C and the fluorescent signal generated by the SYBR green is recorded at each temperature point. At the beginning, the majority of the PCR products are double stranded hence SYBR green emits maximum level of light, however as the temperature increases the PCR product starts to denature into single stranded DNA and the signal from SYBR green gradually decreases. At a certain temperature this decline in fluorescence is very rapid as the majority of the product denatures. This is the melting temperature of the PCR product. The change in florescence is usually plotted as a derivative (change in fluorescence/change in temperature) against the temperature, which gives a peak at the melting temperature of the PCR product. The melting temperature of the amplicon depends on the base composition and the length of the PCR product, meaning that if more than one amplicon is present in the PCR reaction then more than one peak is detected in the dissociation curve.

The efficiency of the PCR reaction is calculated using a standard curve, which is generated by performing real time RT-PCR using serial dilutions of cDNA of known concentrations. For each concentration, the cycle threshold (Ct) value is determined and is

plotted against the log of cDNA concentration. Ct value is the number of PCR cycles which is required for the fluorescence level to reach a threshold value that is above the background signal, and is inversely proportional to the concentration of cDNA. Once the standard curve is plotted, the gradient of the slope is used to calculate the efficiency of the PCR reaction by using the following formula: Efficiency = $[10^{(-1/\text{gradient value})}-1]\text{x}100$. The optimum gradient is -3.32, which corresponds to an efficiency of 100%. A PCR efficiency of 100% means that the PCR product is doubling after every cycle; therefore the Ct value can be used to compare the levels of transcripts between two samples. An efficiency in the range of 90% - 110% is ideal to reliably compare between samples.

6.1.7 Relative quantification

There are two methods of quantification; absolute quantification and relative quantification. Absolute quantification determines the absolute quantity of a target gene in a sample by using a standard curve of known concentrations (Bustin, 2000). Relative quantification is used to determine abundance of a target gene in a sample relative to an endogenous control. For relative quantification is it absolutely mandatory that the expression level of endogenous control is constant in all biological samples under study. In addition, to account for the variability arising from reagents used during the PCR reaction, the assay for the endogenous control for each biological sample must be performed at the same time in a single plate. To obtain the relative expression value for each biological sample, the Ct value of a target gene is subtracted from the Ct value of the endogenous control giving rise to ΔCt. ΔCt values can then be used to compare the expression level of genes in two separate groups of biological samples e.g. between wildtype and mutant samples. One group of samples is defined as a calibrator (usually the wildtype) and the ΔCt value of the sample of interest

(usually the mutant) is substracted from the ΔCt value of the calibrator sample, to give ΔΔCt. Relative quantification is defined as $2^{-\Delta\Delta Ct}$. The error bars for the chart are calculated as RQmin and RQmax using the following formula: RQmin = $2^{-[\text{average } \Delta\Delta Ct + (\text{SE average } \Delta Ct \times t)]}$ and RQmax = $2^{-[\text{average } \Delta\Delta Ct - (\text{SE average } \Delta Ct \times t)]}$, where t is the t value from a Student's t-test table for a given degree of freedom. Degree of freedom is [(number of biological replicates for each genotype x 2) -2].

6.2 Results

6.2.1 Intercross between *hhkr* and *Gli3* mutants shows patterning defects are *Gli3* independent

Previously, data from our lab and others have shown that *Tulp3* acts downstream of *Sonic hedgehog* and *Smoothened* and upstream of *Gli2* during neural tube patterning (Norman et al., 2009; Patterson et al., 2009). To examine the relationship between Tulp3 and Gli3 in neural tube patterning, an intercross between *hhkr*/+ and *Gli3*/+ mice was set up. Doubly heterozygous mutants (*hhkr*/+;*Gli3*/+) were identified and intercrossed to generate compound homozygous embryos. The dorsoventral patterning of the caudal neural tube in embryos of the various genotypes (+/+;+/+, *hhkr/hhkr*;+/+, +/+;*Gli3/Gli3* and *hhkr/hhkr;Gli3/Gli3*) was examined.

As reported previously, *hhkr/hhkr*;+/+ embryos showed a ventralization of the caudal neural tube, where the ventral markers, such as Nkx2.2, Olig2 and Nkx6.1, are expanded to cover most of the neural tube at the expense of dorsal markers (e.g. Pax6) ((Norman et al., 2009; Patterson et al., 2009) and Figure 6-1). As reported previously, in *Gli3* mutants patterning in the ventral most region of the neural tube is not affected, as the domain of Nkx2.2 in *Gli3/Gli3* embryos appears to be comparable to that in the wildtype embryos (Figure 6-1 compare A with K). In *hhkr/Gli3* double mutants the Nkx2.2 expression is expanded dorsally, similar to that seen in *hhkr* mutant. This shows that Gli3 is not required for the ectopic activation of the Shh pathway, in *hhkr* mutants.

As mentioned earlier, Gli3 functions primarily as a repressor, rather than an activator, in patterning of the neural tube. Loss of Gli3R results in a subtle DV patterning defect, observed as dorsal expansion of markers in the intermediate region of the neural tube. As shown previously (Persson et al., 2002), *Gli3* mutants exhibited expansion of Olig2, Nkx6.1 and HB9 domains into more dorsal regions of the neural tube (Figure 6-1). If Gli3R is active

in *hhkr* mutants, then we would expect the double mutants to be more severely affected than either single mutant, as seen in the *Arl13b/Gli3* double mutants (Caspary et al., 2007). Close examination of the dorsal extent of marker expression domains in fact finds no difference between *hhkr* and *hhkr/Gli3* mutants. This suggests that Gli3R function is already disrupted, in *hhkr* mutants.

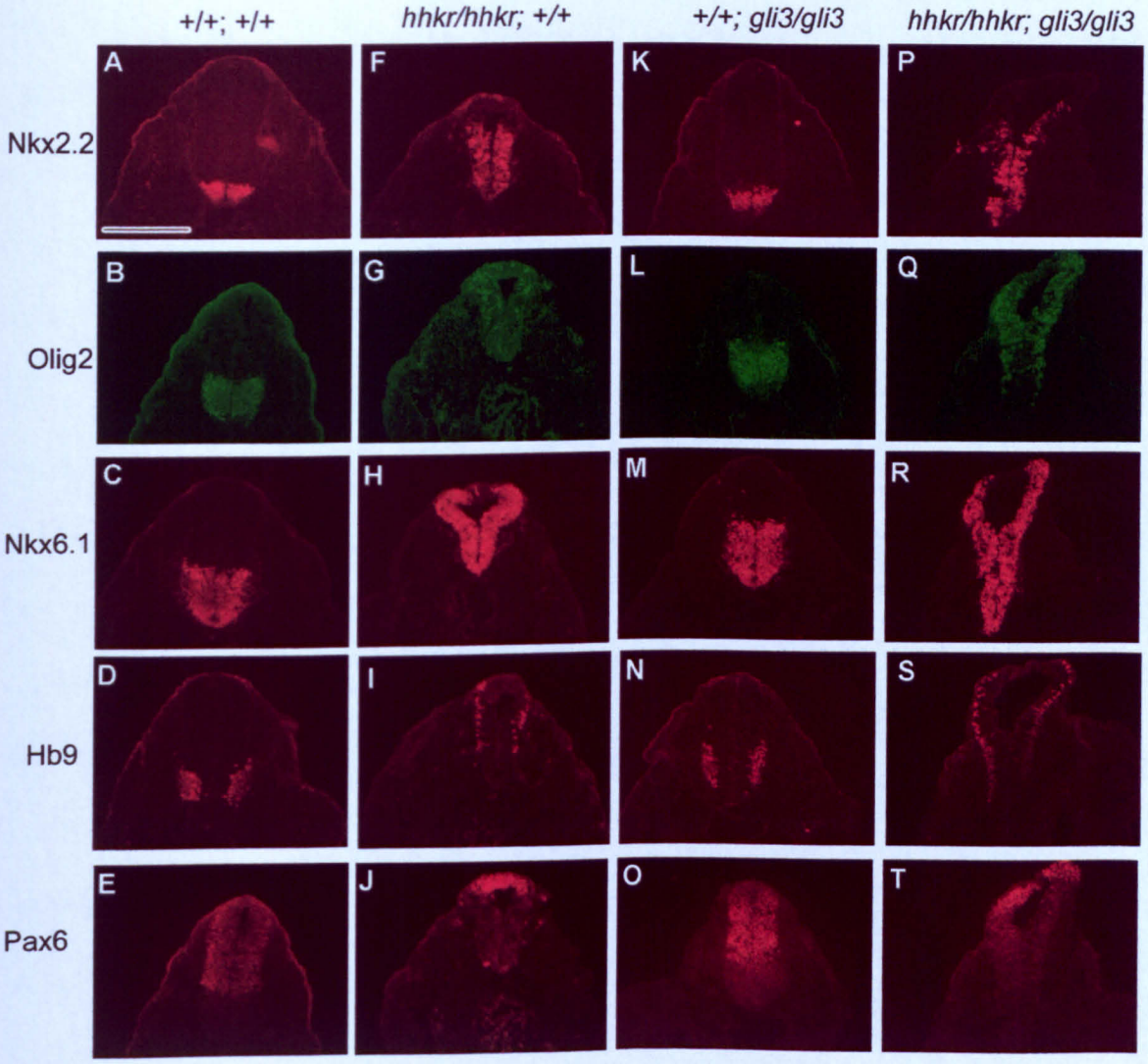

Figure 6-1: Intercross between Tulp3 and Gli3 mutants
(A-T) Immunostaining of transverse sections through the neural tube immediately anterior to the hindlimb bud of E10.5 embryos with antibodies against Nkx2.2 (A, F, K and P), Olig2 (B, G, L and Q), Nkx6.1 (C, H, M and R), HB9 (D, I, N and S) and Pax6 (E, J, O and T) in wildtype (A-E), *hhkr* (F-J), *Gli3* (K-O) and *hhkr/Gli3* double mutant (P-T). The immunostaining of the double mutant for all markers are similar to that for *hhkr*. Scale bar represents 300 μm.

6.2.2 A microarray screen to identify targets of *Tulp3* during neural tube patterning

The structure of Tulp3 consists of a nuclear localization signal in the N-terminal and a tubby domain in the C-terminal. N-terminal domains of Tubby and Tulp1 have been shown to activate transcription in gene reporter assays (Boggon et al., 1999). We hypothesised that Tulp3 is also a transcription factor, and conducted a microarray screen to identify genes regulated by Tulp3 during neural tube closure and patterning. The microarray screen used caudal ends of E9.0 (16 to 18 somites) *hhkr* and wildtype littermates. The caudal ends of embryos were used because *hhkr* shows a neural tube defect at the caudal end of the embryo therefore this is where *Tulp3* is likely to be functioning to pattern the neural tube and affect its closure. By 19 somites, the dorsoventral patterning defect in the caudal neural tube is detectable in *hhkr*. To avoid detecting genes that are differentially expressed as a secondary consequence of the defect in dorsoventral patterning, it was necessary to use tissue from embryos prior to this defect. However, it was also important not to use embryos at too early a stage of development, as the upper spinal region is normal in *hhkr* mutants, indicating that Tulp3 does not appear to play a significant patterning function at early stages. For this reason, embryos between the stages of 16 to 18 somites were chosen for this experiment. The same number of *hhkr* and wildtype embryos were used for each somite stage (Figure 6-2A). I extracted RNA from individual *hhkr* and wildtype caudal ends (n=7 for each genotype) and ran an aliquot of each sample on an agarose gel to make sure that the RNA was not degraded in any sample (Figure 6-2B). For each genotype, I pooled the seven RNA samples and synthesized and amplified cDNA in duplicate as described in section 2.20.2 and 2.20.3. An aliquot of each sample was electrophoresed on an agarose gel to ensure an even amplification of all sizes of cDNA fragments (Figure 6-2C-E). I then labeled the cDNA with Cy5 and Cy3 (Figure 6-2C and D) and used it to hybridize three spotted array slides containing 25000

mouse oligonucleotides. Three arrays were required to provide controls for the incorporation of two separate dyes and for the cDNA amplification step. For the first array, wildtype (WT) sample was labeled with Cy3 and mutant sample was labeled with Cy5. For the second array, the same cDNA sample was used, but the dye was reversed i.e. WT was labeled with Cy5 and mutant was labeled with Cy3. As the two dyes are not incorporated in the same way, this dye-swap is essential in order to account for non-specific differences in the intensity of signals between WT and mutant samples. The third array is a control for the cDNA amplification process. Here, the second set of cDNA for WT and mutant is labeled with Cy3 and Cy5, respectively. Hybridised slides were scanned and data was analysed by the Microarray facility at Harwell as described in section 2.20.

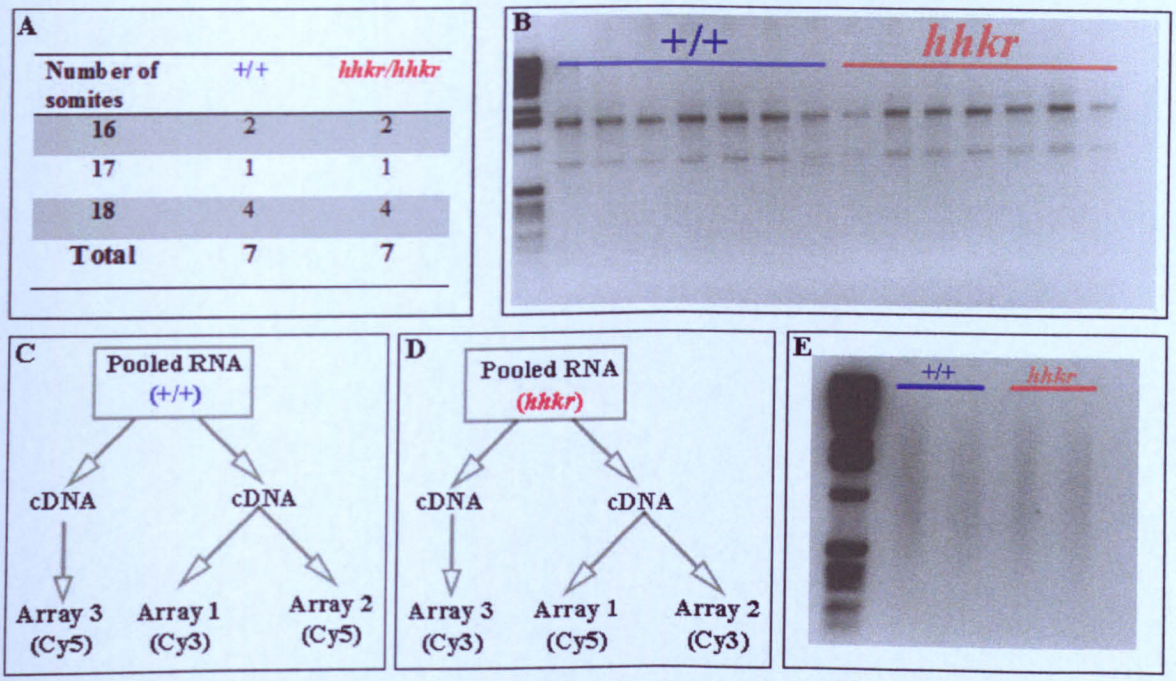

Figure 6-2: Generation of labeled cDNA used during the microarray experiment.
(A) Table showing the number of *hhkr* and wildtype embryos used for each somite number. For each genotype a total of seven embryos were used. (B) Agarose gel of RNA extracted from seven wildtype and seven *hhkr* embryos, showing that RNA has not degraded in any sample. (C and D) RNA from seven wildtype (C) and seven *hhkr* (D) individuals was pooled and cDNA was synthesized and amplified in duplicate for each sample. For each genotype, cDNA was labeled in triplicate and used to hybridize three arrays. (E) Gel analysis of wildtype and *hhkr* cDNA amplification, showing that cDNA fragments of all sizes were amplified giving an even smear on the gel.

The analyzed result shows that there was only one gene that was down-regulated by greater 2-fold and no genes that were up-regulated by 2-fold or more in *hhkr* compared to the wildtype. This was taking all three arrays into account. Ten genes were 1.5-fold or more up-regulated in *hhkr* compared to wildtype littermates in all three arrays. Forty-two genes were down-regulated in *hhkr* by 1.5-fold or more compared to wildtype littermates, in two out of the three arrays. A list of 52 genes that were identified as being differentially expressed in *hhkr* compared to wildtype littermates is given in appendix Table 10-3 and Table 10-4. Based on a literature search for these 52 genes, 10 genes were chosen for validation using SYBR green based real time PCR. A list of these genes is given in Table 6-1.

Table 6-1: Genes identified during a microarray screen and selected for validation through qPCR.

Gene Symbol	Gene name	Average fold change in *hhkr* compared to WT
Yif1b	*Yip1 interacting factor homolog B*	1.8 (down-regulated)
Ccnd2	*Cyclin D2*	1.8 (down-regulated)
Podx1	*Podocalyxin-like*	1.6 (up-regulated)
Dscam	*Down syndrome cell adhesion molecule*	1.8 (up-regulated)
Srp14	*Signal recognition particle 14*	1.6 (up-regulated)
Flrt2	*Fibronectin leucine rich transmembrane protein 2*	1.6 (up-regulated)
Dmrt2	*doublesex and mab-3 related transcription factor like family A2*	1.8 (up-regulated)
Nkx2.9	*NK2 transcription factor related, locus 9*	1.7 (up-regulated)
Fkbp8	*FK506 binding protein 8*	1.8 (up-regulated)
Gaparapl2	*Gamma-aminobutyric acid (GABA) A receptor-associated protein-like 2*	1.5 (up-regulated)

6.2.3 Validation of Microarray result using SYBR green based real time PCR

Primers to amplify 10 candidate genes (Table 10-5) and two endogenous controls (Hprt and Gapdh) were designed as described in section 2.21. Sequences of these primers can be found in appendix Table 10-5.

6.2.3.1 Optimization of real time RT-PCR

I extracted RNA from E9.0 CD1 caudal ends (n=6 embryos) and synthesized cDNA as described in sections 2.4 and 2.5. This cDNA was used to optimize real time RT-PCR to validate microarray results. To determine the specificity and efficiency of the PCR reaction for each of the primers, a dissociation curve and a standard curve was generated. Five dilutions of starting cDNA (50 ng, 10 ng, 1 ng, 0.1 ng and 0.01 ng) were used per reaction and to account for technical variability, each reaction was performed in triplicate. As SYBR green binds to any double stranded DNA in a non-specific way, it was essential to make sure that the primer pair used in the PCR amplified only one product and that primer dimers were absent. To verify this, a dissociation curve was obtained for each of the reactions. The dissociation curves showed that a single product was amplified at cDNA concentrations between 1 ng and 50 ng for *Yif1b, Ccnd2, Srp14, Dmrt2, Fkbp8* and *Gaparapl2* (Figure 6-3 shows the dissociation curve for three repeats using 10 ng of cDNA) when a primer concentration of 900 mM was used. Using the same concentration of primers (900 mM) to amplify *Podx1, Flrt2* and *Nkx2.9* resulted in amplification of more than one product (Figure 6-4A-C). To optimize these, I carried out the reactions using different concentrations of primers and found that for all three assays the primer concentration of 500 mM gave a single peak in the dissociation curve (Figure 6-4D-F). To optimize the reaction for *Dscam* I designed two separate primers, however both of these primers amplified multiple products (Figure 6-5) hence neither could be

used. In a standard PCR, it is most common to vary the annealing temperature of the primers to optimize the PCR. This is not possible for the qPCR because the annealing temperature of the assay needs to be identical to the annealing temperature of the endogenous control as both assays have to be run on the same plate to calculate the relative quantification.

To calculate the efficiency of the PCR reaction for each primer pair, a standard curve was generated by plotting the Ct value against the log of the cDNA concentration (Figure 6-6). Reactions using cDNA concentration of less than 1 ng resulted in either non-specific amplification or a high Ct value and in some cases the fluorescence failed to reach the threshold level, so data from these were not used to draw the standard curve. Efficiencies for each of the assays together with the average Ct value when using 10 ng of cDNA is given in Table 6-2. The majority of assays, with the exceptions of *Dscam* and *Flrt2*, show an efficiency in the range of 90% - 110%. The efficiency of both *Dscam* and *Flrt2* are over 110%, which suggests that the primers are either amplifying more than one product or that the primer dimmers are present in the reaction. To improve the efficiency of *Dscam* and *Flrt2* assays, I designed a second set of primers and used them to construct the dissociation curve and the standard curve. The dissociation curve showed that for both assays multiple products are amplified and, as a consequence, give rise to a PCR efficiency that is outside the 90% - 100% range. For this reason the first set of primers for *Flrt2* was used to verify the microarray result. The assay for *Dscam* was not performed as both sets of primers amplified many different products (Figure 6-5).

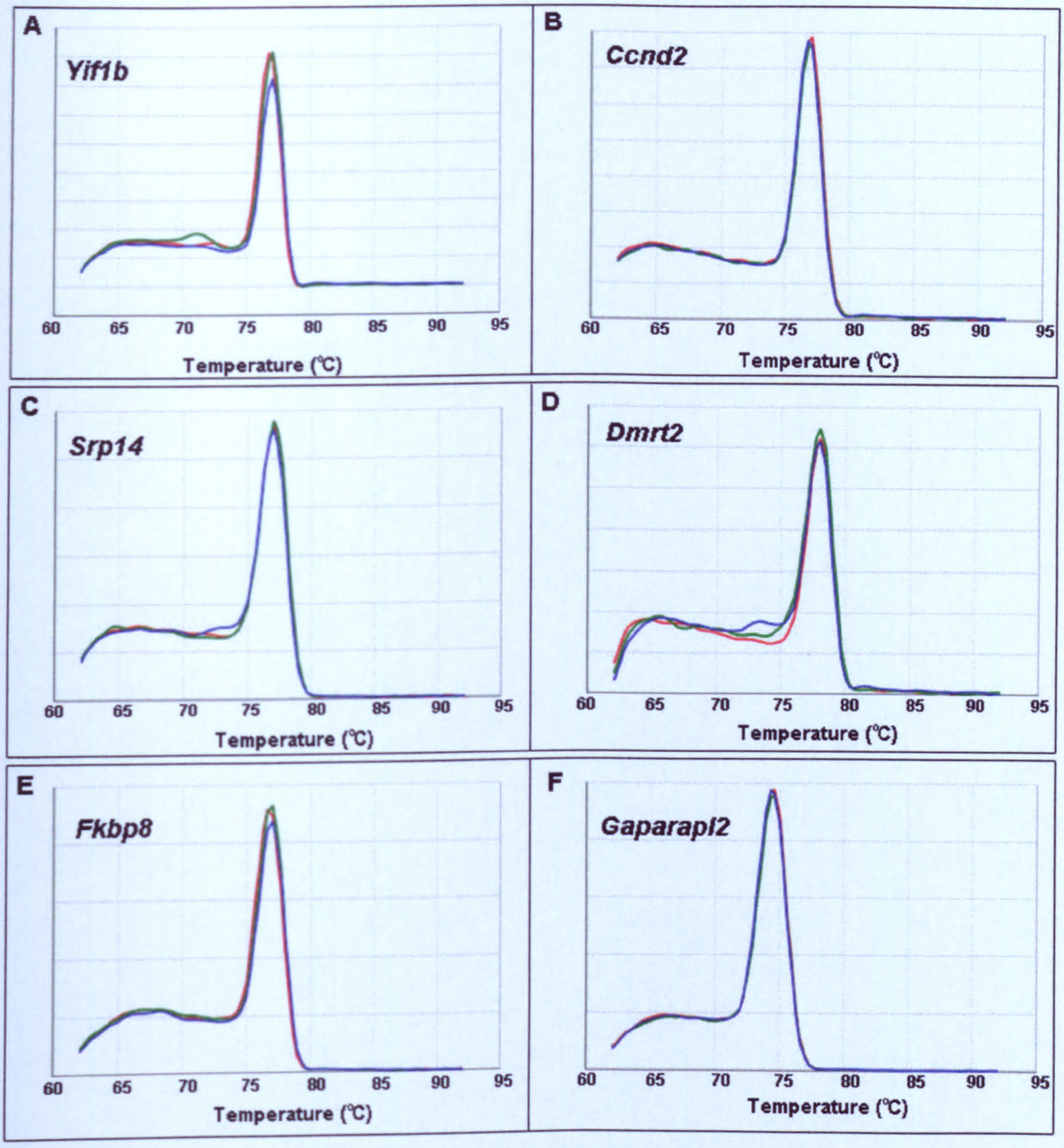

Figure 6-3: Dissociation curve from PCR product obtained using 10 ng of cDNA and 900 nM primer concentration.

(A-F) dissociation curve shows that a single product was amplified for *Yif1b* (A), *Ccnd2* (B), *Srp14* (C), *Dmrt2* (D), *Fkbp8* (E) and *Gaparapl2* (F). The curve is obtained by plotting the derivative of fluorescence change against the temperature. Three technical replicates are represented by three curves of different colors (red, green and blue).

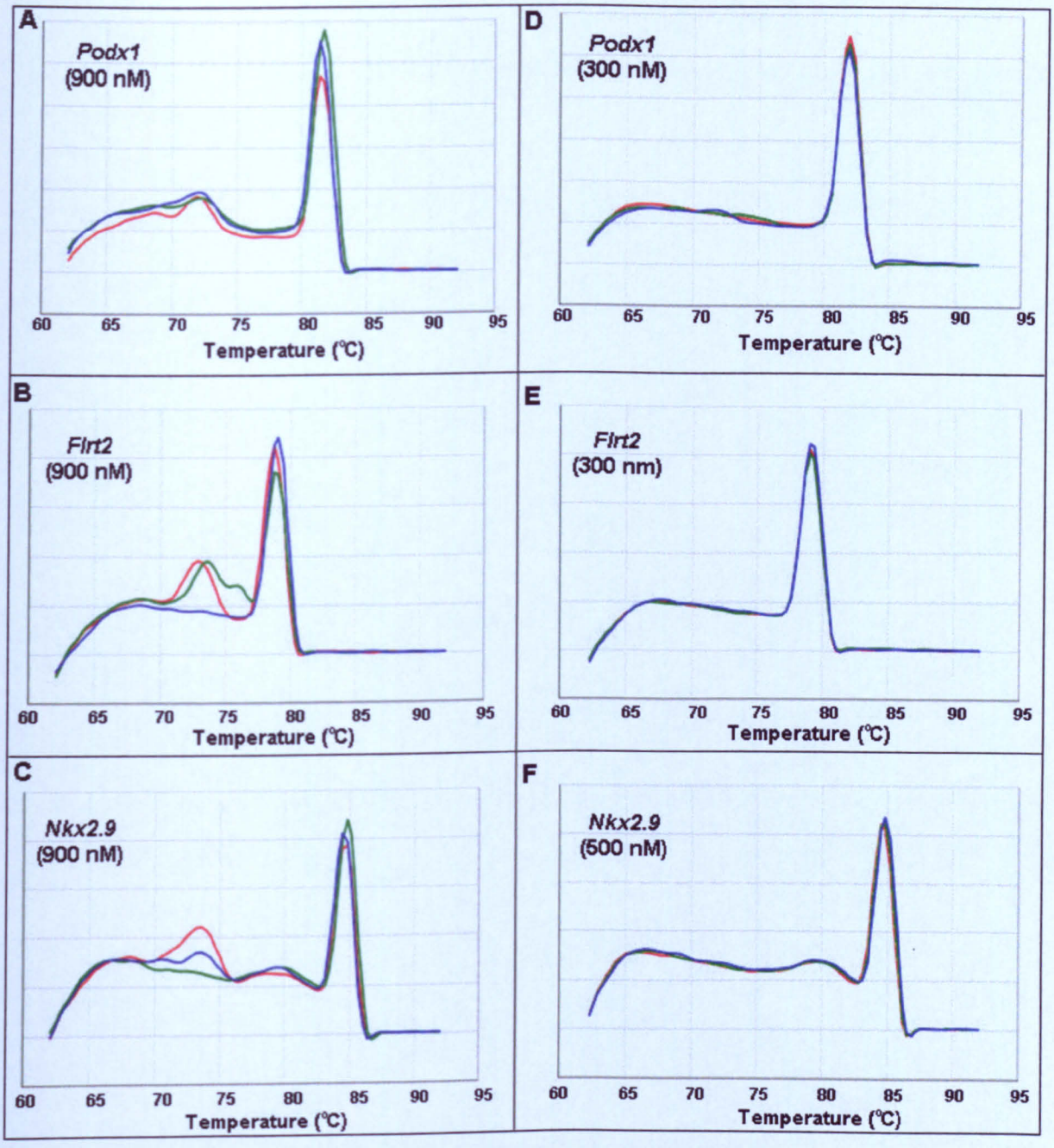

Figure 6-4: Optimization of PCR to generate a single product.
(A-F) Dissociation curve of PCR product generated using 10 ng of cDNA for *Podx1* (A and D), *Flrt2* (B and E) and *Nkx2.9* (C and F) showing that multiple products are amplified when 900 nM of primer concentration is used (A – C) as determined by multiple peaks in the dissociation curve. A single product is amplified for *Podx1* (D) and *Flrt2* (E) when the primer concentration is reduced to 300 nM. For the *Nkx2.9* (F) assay, a primer concentration of 500 nM results in amplification of a single product. The curve is obtained by plotting the derivative of fluorescence change against the temperature. Three technical replicates are represented by three curves of different colors (red, green and blue).

Table 6-2: Optimization of qPCR and results obtained from qPCR.

Gene Symbol	Average Ct value when using 10 ng of cDNA	PCR efficiency	Average fold change in *hhkr* compared to WT (qPCR)
Yif1b	25.31	97.6	2.4 (down-regulated)*
Ccnd2	22.96	101.3	1.8 (down-regulated)*
Podx1	23.85	100.1	2.2 (down-regulated)
Dscam	30.29	42713.3	N/A
Srp14	24.26	100.1	2.4 (down-regulated)
Flrt2	31.01	207.5	1.8 (down-regulated)
Dmrt2	32.99	100.5	3.1 (down-regulated)
Nkx2.9	29.28	98.1	2.4 (up-regulated)*
Fkbp8	25.34	99.3	2.8 (down-regulated)
Gaparapl2	26.58	101.3	2.7 (down-regulated)
Hprt	28.97	97.6	N/A
Gapdh	21.36	102.7	N/A

* donates assays for those genes where the direction of change was maintained between the microarray and qPCR.

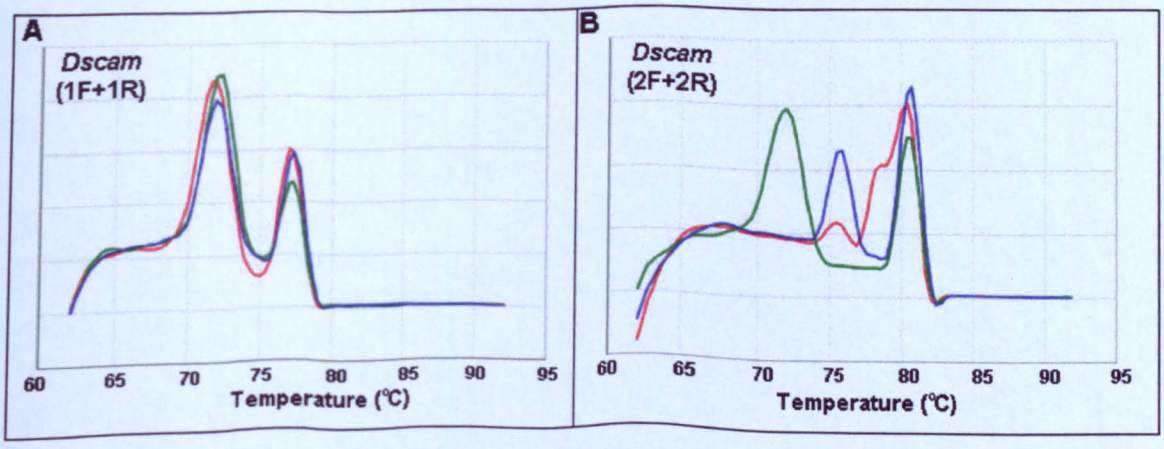

Figure 6-5: Both assays for *Dscam* result in amplification of multiple products.
(A and B) Dissociation curves for *Dscam* using two sets of primer pairs. First primer pair (A) amplifies two separate products and the second set (B) amplifies at least three separate products. 10 ng of cDNA and 900 nM of primer were used in each reaction. The curve is obtained by plotting the derivative of fluorescence value against the temperature. Three technical replicates are represented by three curves of different colors (red, green and blue).

Figure 6-6: Analysis of standard curve to calculate PCR efficiency.
(A-I) Standard curve obtained for *Yil1b* (A), *Ccnd2* (B), *Podx1* (C), *Srp14* (D), *Flrt2* (E), *Dmrt2* (F), *Nkx2.9* (G), *Fkbp8* (H) and *Gaparapl2* (I) using 1 ng, 10 ng and 50 ng of cDNA. For each assay the gradient of the slope and the R^2 values are given. Gradient value is used to calculate the efficiency of the PCR (Efficiency = $[10^{(-1/\text{gradient value})}-1]x100$) and R^2 value determines how well the individual Ct value fit into the linear line used to calculate the efficiency. The average Ct value is plotted againt the the log of cDNA concentration.

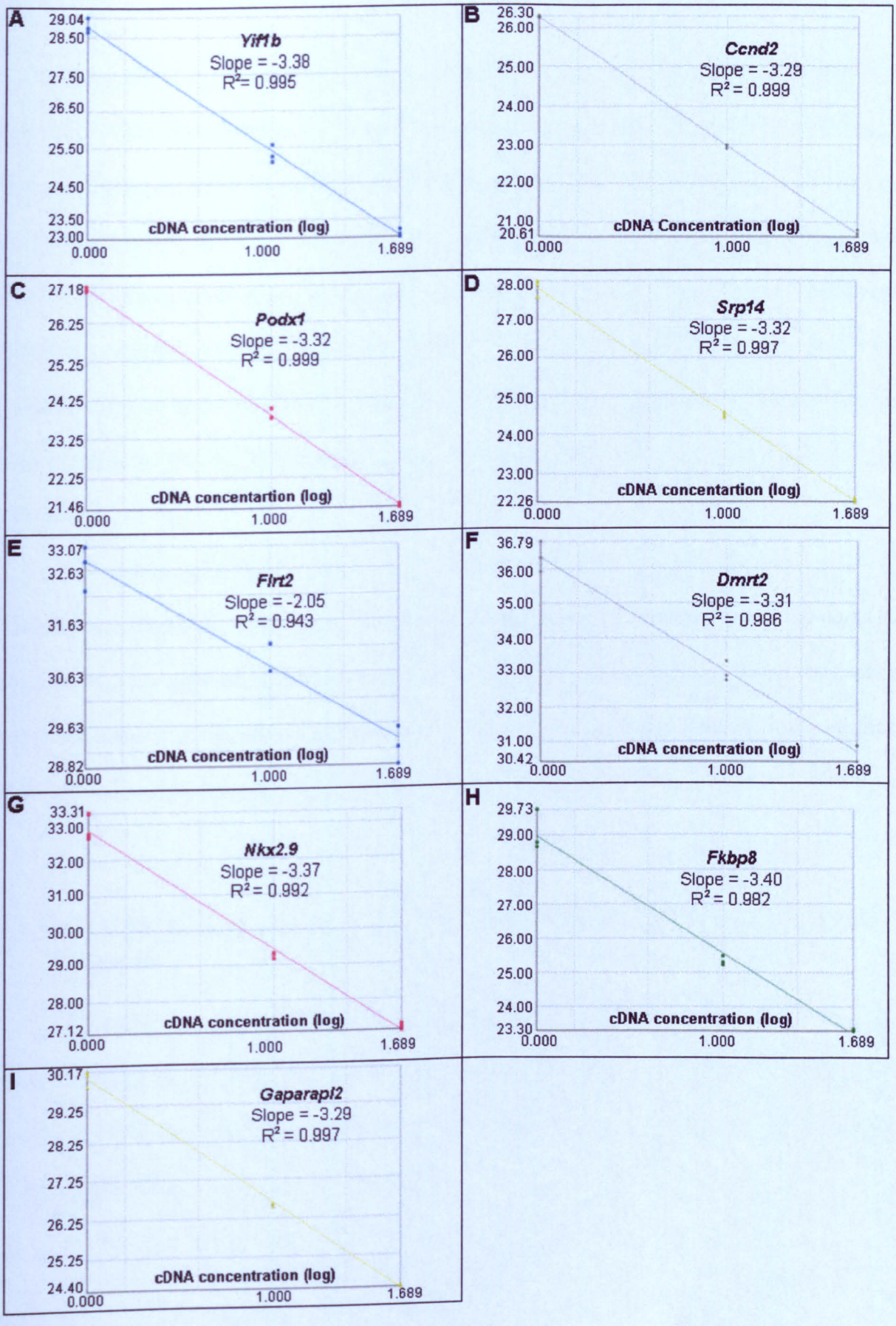
A
Yif1b
Slope = -3.38
R²= 0.995
cDNA concentration (log)
B
Ccnd2
Slope = -3.29
R² = 0.999
cDNA Concentration (log)
C
Podx1
Slope = -3.32
R² = 0.999
cDNA concentartion (log)
D
Srp14
Slope = -3.32
R² = 0.997
cDNA concentartion (log)
E
Flrt2
Slope = -2.05
R² = 0.943
cDNA concentration (log)
F
Dmrt2
Slope = -3.31
R² = 0.986
cDNA concentration (log)
G
Nkx2.9
Slope = -3.37
R² = 0.992
cDNA concentration (log)
H
Fkbp8
Slope = -3.40
R² = 0.982
cDNA concentration (log)
I
Gaparapl2
Slope = -3.29
R² = 0.997
cDNA concentration (log)

To perform a relative quantification, an endogenous control is required. This should be a gene for which the expression level does not change in the mutant compared to the wildtype. Hypoxanthine-guanine phosphoribosyltransferase (Hprt) and Glyceraldehyde 3-phosphate dehydrogenase (Gapdh) are well known genes that are frequently used as endogenous controls as they are housekeeping genes and their expression level shows little variation between samples. I designed primers for both of these genes and obtained a dissociation curve and a standard curve as described above. The result showed that both of the primers were amplifying a single product and the PCR efficiency was within the 90% - 100% range (Figure 6-7 and Table 6-2).

The dissociation curves for all assays, with the exception of *Dscam,* show that a single product was amplified when using 10 ng cDNA per reaction. Additionally the average Ct value is also low when using 10 ng of cDNA per reaction in all successful assays (Table 6-2). For these reasons 10 ng of cDNA per reaction was used in further experiments to compare ***hhkr*** and wild-type embryos, to validate the microarray results.

6.2.3.2 SYBR green based real time PCR does not support the microarray results

To verify the results obtained from the microarray experiment, I synthesized cDNA from individual caudal ends of seven E9.0 ***hhkr*** and seven wildtype littermates as described in section 2.5. The same RNA extraction that was used for the microarray experiment was used to synthesize cDNA.

Figure 6-7: Analysis of endogenous controls for qPCR.
(A – D) cDNA synthesized from caudal ends of CD1 wildtype embryos was used to obtain the dissociation curve (A and C) and the standard curve (B and C) for *Hprt* (A and B) and *Gapdh* (C and D). Dissociation curves were obtained using 10 ng of cDNA and standard curves were obtained using 1 ng, 10 ng and 50 ng of cDNA. The dissociation curve is obtained by plotting the derivative of the fluorescence value against the temperature. Three technical replicates are represented by three curves of different colors (red, green and blue). The standard curve is obtained by plotting the average Ct value against the log of cDNA concentration and the gradient of the slope is given for each assay. (E) Average Ct values for *Gapdh* and *Hprt* using 10 ng of cDNA extracted from caudal ends of seven *hhkr* and seven wildtype embryos. Error bars represent the standard error of the mean (SEM) observed between embryos. P values are calculated using the Student's two tailed T-test.

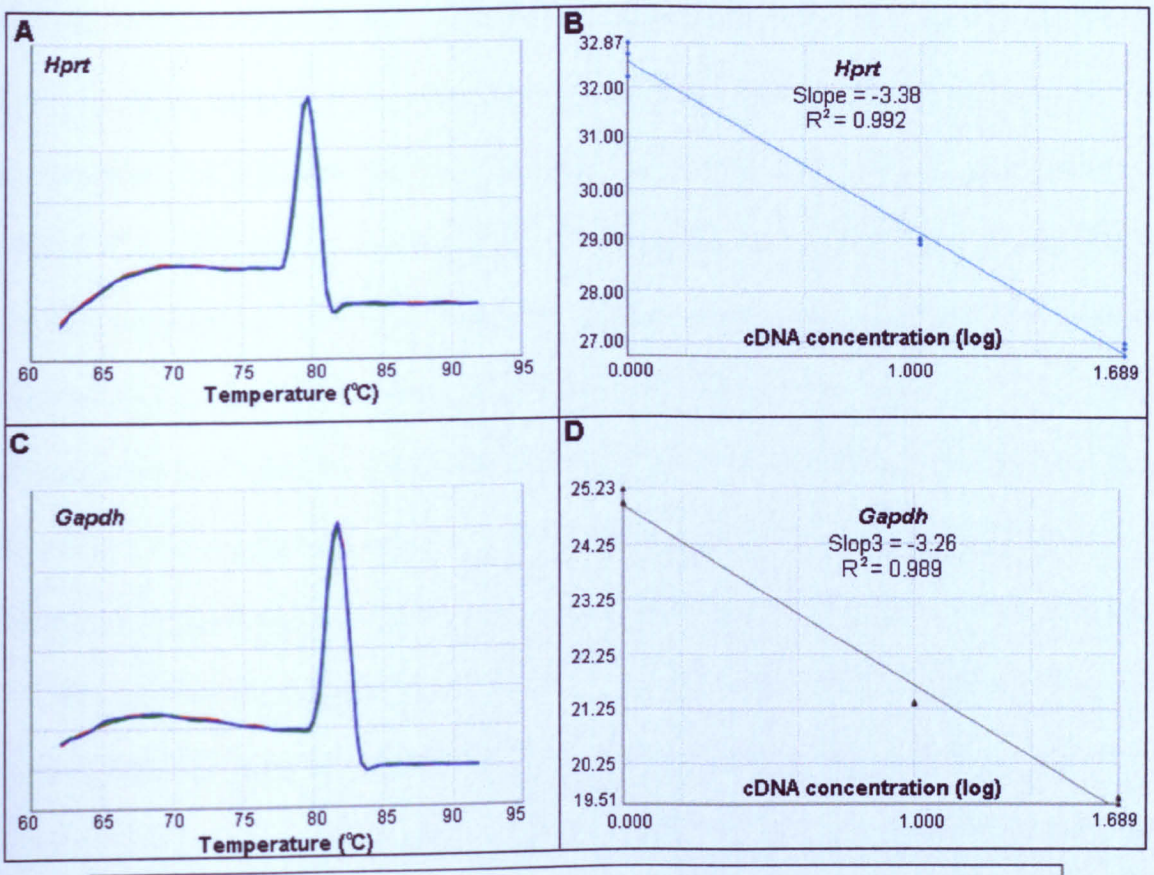
A
Hprt
60 65 70 75 80 85 90 95
Temperature (°C)
B
Hprt
Slope = -3.38
R² = 0.992
32.87 32.00 31.00 30.00 29.00 28.00 27.00
cDNA concentration (log)
0.000 1.000 1.689
C
Gapdh
60 65 70 75 80 85 90 95
Temperature (°C)
D
Gapdh
Slop3 = -3.26
R² = 0.989
25.23 24.25 23.25 22.25 21.25 20.25 19.51
cDNA concentration (log)
0.000 1.000 1.689

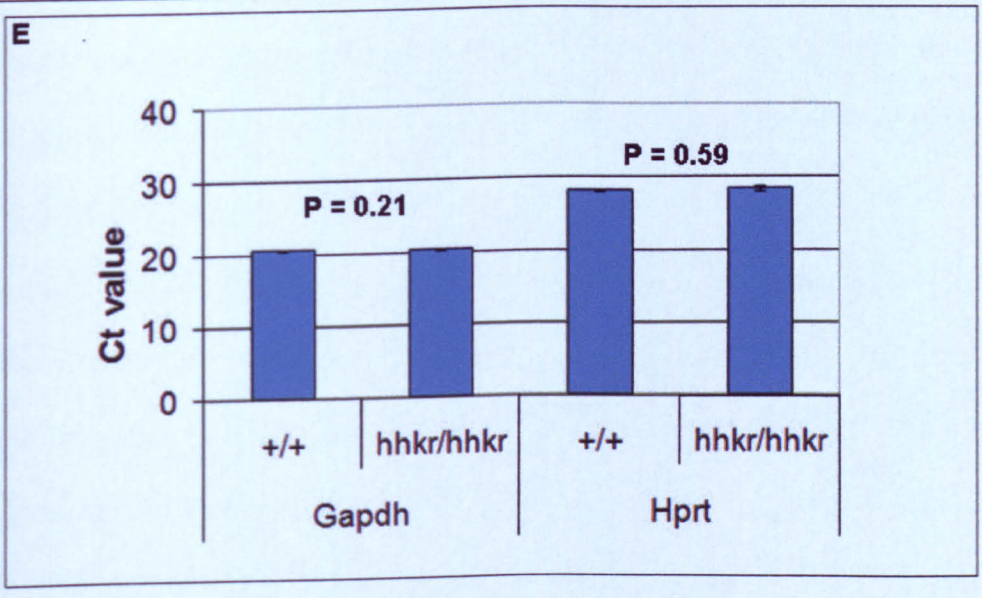
E
40 30 20 10 0
Ct value
P = 0.21
P = 0.59
+/+ hhkr/hhkr +/+ hhkr/hhkr
Gapdh
Hprt

Initially, to check whether or not the expression level of Hprt and Gapdh was consistent between hhkr mutant and wildtype littermates, I ran reactions with 10 ng of individual cDNA samples from hhkr and wildtype littermates and compared the Ct values across samples and between the two genotypes. As before, each reaction was performed in triplicate. The results show that the levels of both Hprt and Gapdh were not significantly altered between hhkr and wildtype littermate, as determined by the student's T-test (Figure 6-7). A small level of biological variation is observed between samples of the same genotype for both genes but this variation is less with *Gapdh* than *Hprt* in both genotypes (Figure 6-7). Additionally, the average Ct value of *Gapdh* was lower than that for *Hprt* (Figure 6-7 and Table 6-2). For these reasons *Gapdh* was chosen as the endogenous control for the experiment.

For each of the samples (seven ***hhkr*** and seven wildtype littermates), all nine assays and the endogenous control (*Gapdh*) were amplified on the same plate. To determine the fold change in the expression level in ***hhkr*** compared to the wildtype, relative quantification (RQ) was calculated in multiple steps. Average Ct value for each assays are given in appendix Table 10-6. First the Ct value of the three technical replicates was averaged for each biological samples (7 of each genotype) for each of the nine target genes and the endogenous control (*Gapdh*) to give a single Ct value for each biological sample and gene. For each biological sample, the Ct value of the endogenous control was subtracted from the Ct value for each gene to give ΔCt. The ΔCt values of the biological replicates (seven wildtype samples and seven ***hhkr*** samples) for each assay were averaged; the difference between the hhkr and wildtype average ΔCt values is given as the ΔΔCt value. The RQ value is then calculated as $2^{-\Delta\Delta Ct}$.

For each set of biological replicates, the standard deviation of the ΔCt values was calculated. This allowed the standard error of the mean for ΔCt (SEdCt), for each gene, to be calculated using the formula: SEdCt = $\sqrt{[(\text{Stdev of mutant samples})^2/n + (\text{Stdev of wild-type samples})^2/n]}$. RQmin and RQmax are calculated using the following formulas: RQmin = 2^-

$^{[\text{average } \Delta\Delta Ct+(SEdCt * t)]}$ and RQmax = $2^{-[\text{average } \Delta\Delta Ct-(SEdCt * t)]}$ where t is the t value from a Student's t-test table for a given degree of freedom at 95% confidence.

The data is presented as levels of transcript relative to the wildtype samples (Figure 6-8). This results shows that all genes with an exception of *Nkx2.9* were downregulated in *hhkr* compared to the wildtype, however since the RQmin and RQmax values on *hhkr* samples for all assays overlap with the RQmin and RQmax values on wildtype suggest that none of these genes are significantly altered in *hhkr* compared to the wildtype (Figure 6-8).

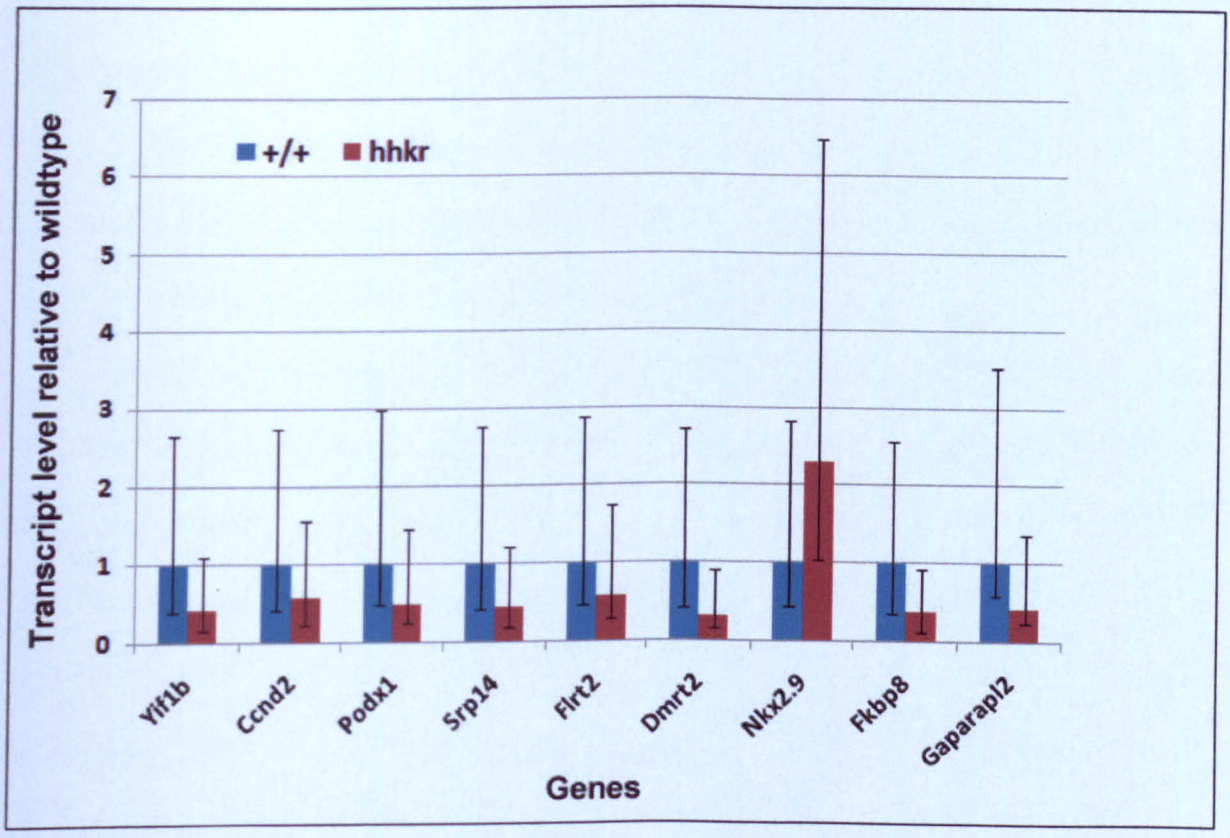

Figure 6-8: Results obtained from qPCR.
A bar chart showing the transcript level relative to the wildtype for each assay. The error bars are shown as RQ min and RQ max.

6.3 Discussion

6.3.1 Activation of Shh signalling in *hhkr* mutants occurs independently of Gli3

It has been published previously that Tulp3 is a negative regulator of *Shh* signalling and that it functions downstream of *Shh* and upstream of *Gli2,* during dorsoventral patterning of the neural tube (Norman et al., 2009; Patterson et al., 2009). A slight difference in the gene expression pattern in the neural tube of *Gli2* mutant and *Tulp3/Gli2* double mutant suggested that Tulp3 may be functioning through a second molecule. This second molecule could be Gli3 as it is expressed in the neural tube; mutants of *Gli3* exhibit exencephaly and subtle defects in dorsoventral patterning of the caudal neural tube (Lee et al., 1997; Persson et al., 2002). To test for an involvement of Gli3 in the action of Tulp3 in *Shh* signalling, a cross between doubly heterozygous *hhkr* and *Gli3* mice were set up and the dorsoventral patterning of the caudal neural tube was examined in the resulting embryos.

Gli3 can be processed to a cleaved repressor form (Gli3R) or the full length molecule can function as an activator (Gli3A). If Gli3A is required for ectopic pathway activation in *Tulp3* mutants, we would expect the phenotype to be reduced in the double mutant. Analysis of dorsoventral patterning of the neural tube in +/+;+/+, *hhkr/hhkr;*+/+, +/+;*Gli3/Gli3* and *hhkr/hhkr;Gli3/Gli3* embryos has given evidence that Tulp3 functions genetically downstream (independently) of Gli3A during dorsoventral patterning of the neural tube as the patterning defect observed in the *hhkr/Gli3* double mutant is identical to that of *hhkr* single mutant.
Gli3 functions predominantly as a repressor in NT patterning. If Gli3R is still active in *hhkr* mutants, as suggested by the western blot results from our lab, we would expect that the compound mutants would exhibit a more severe phenotype than either single mutant. This increased severity of phenotype is observed in compound mutants for *Gli3* and *Arl13b* (Caspary et al., 2007). Here, I have shown that the phenotype is indistinguishable between the

compound *hhkr/Gli3* double mutant and the *hhkr* single mutant. This result argues that Gli3R is already non-functional in the *hhkr* mutant.

Although the *hhkr* phenotype reported here is severe and the ventral cell types have expanded to cover most of the neural tube, an enhancement of this phenotype is possible. It has been reported that in *Arl13b/Gli3* double mutants, cells expressing HB9 are present throughout the neural tube, including the roof plate, at the dorsal extent of the neural tube (Caspary et al., 2007), giving evidence that these cell types can occupy the entire neural tube. In *hhkr/Gli3* double mutants, cells that are positive for Nkx6.1 and HB9 occupy most of the neural tube but are excluded from the roof plate, similar to that seen in *hhkr* single mutants.
It must be noted that the dorsoventral patterning phenotype reported here for *hhkr* is more severe that that reported previously by our lab (Patterson et al., 2009). This is likely to be due to the difference in the background of the mice used during these two experiments. In the previous study, we used *hhkr* mice that were congenic on the C3H/HeH background to generate embryos for analysis. During the present study, the *hhkr* embryos were obtained from a cross between *hhkr/+;Gli3* /+ mice, where *hhkr* was congenic on C3H/HeH and *Gli3* was in a mixed background of C57BL/6J and C3H/HeH. In the resulting embryos up to 25% of the genome was of C57BL/6J background. This result may indicate a presence of a modifier locus within the C57BL/6J genome. This hypothesis could be tested, by making *hhkr* congenic on the C57BL/6 background, or by re-examining the outcome of the interaction with *Gli3* congenic on the C3H/HeH background.

6.3.2 Microarray analysis

A microarray experiment to assess the changes in global gene expression in *hhkr* compared to wildtype littermates was performed. There were two main aims of this project;

first, to determine whether Tulp3 functions as a transcription factor and second, to identify genes that are differentially expressed in *Tulp3* mutants.

The microarray results showed that the expression of very few genes were altered in *hhkr* homozygous mutant embryos compared to the wildtypes. In a typical microarray experiment only those genes showing 2-fold or more differences in expression level between two experimental samples are selected for further verification. In this experiment only one gene (BC010711/Gm9580) showed a greater than 2-fold difference in *hhkr* compared to the wildtype. This gene was not investigated further because it is a pseudogene and not likely to be functional. A list of genes that showed at least a 1.5-fold difference in *hhkr* compared to the wildtype was obtained and some candidate genes were chosen for further verification.

There are at least three different possible reasons as to why only a small number of genes were identified as being differentially expressed between *hhkr* and wildtype, even after reducing the stringency of the selection method. First, this result may be genuine and there may be no substantial difference in the gene expression profile between wildtype and *hhkr* at E9.0 (16-18 somites). This stage was chosen with the intention to determine the primary genes that were regulated by Tulp3. At this stage the dorsoventral patterning of the caudal neural tube in *hhkr* is not significantly altered compared to wildtype at this stage (Patterson et al., 2009). Thus any genes that do show a change in expression level in *hhkr* compared to wildtype littermates are likely to be involved in the primary defect leading to dorsoventral patterning defects in *hhkr* and are likely to be a direct consequence of the mutation in Tulp3. However, it could also be that this stage was too early to see any consequence of the mutation in *Tulp3* as Tulp3 may be functionally active at a later stage.

Second, Tulp3 may not act as a transcription regulator therefore no substantial difference in gene expression exits in *hhkr* compared to the wildtype.

Finally, the entire caudal end of an E9.0 embryo, consisting of multiple cell types, was used as the starting material for the assay. This could be a problem because, although Tulp3 is expressed ubiquitously, the defect seen in *hhkr* is specific to the neuroepithelium of the caudal embryo so it is possible that differences in gene expression occur only in the neuroepithelium. Therefore, using caudal ends with heterogeneous population of cells could 'dilute' the real change in the gene expression in neuroepithelium, which makes up only a small part of the caudal embryo. To overcome this problem an attempt could be made to micro-dissect the neuroepithelium from the rest of the caudal end. However, this is technically challenging, especially because the tissue needs to be collected quickly to prevent degradation of the mRNA.

6.3.3 Verification of microarray result by SYBR green based real time PCR

Results obtained from a microarray experiment need to be validated using a separate method. The method usually used for this purpose is the quantitative real-time PCR (qPCR) as it can be both sensitive and reliable. In the present study I have used SYBR green based qPCR in an attempt to validate some of the candidate genes that came out of the microarray screen. Although qPCR results for all nine assays show that the expression levels of these genes were not significantly altered in *hhkr,* it was surprising that for the majority of the assays tested (six out of nine assays), the qPCR failed to confirm the overall direction of the change detected by the microarray. Rather, the qPCR analysis detected down-regulation of several genes in *hhkr*, in direct conflict to the up-regulation detected by microarray. This lack of correlation between the result obtained from microarray and that from qPCR has been documented (Morey et al., 2006). There are several factors that have been recognized to account for this lack of correlation; these include preparation of the tissue, the type of tissue used, the expression level

of genes and the fold-change observed between experimental samples. Some of these factors are directly relevant to my study.

The first difference was the cDNA used in these two experiments. For the microarray experiment, RNA from the caudal ends of seven embryos was pooled prior to cDNA synthesis and amplification. For qPCR, RNA from the individual biological samples was used to synthesise cDNA and there was no amplification step. Although the amplification of the cDNA is reported to be linear (Petalidis et al., 2003), it is an additional step where variations could potentially arise due to slightly suboptimal conditions resulting in biased amplification. Secondly, none of these genes showed a change in expression level of 2-fold or more suggesting that the validation of these results may be difficult (Rajeevan et al., 2001; Morey et al., 2006). This is because a change in expression level of 2-fold is seen as only one cycle difference in qPCR, so any change that is less than 2-fold will give rise to a difference that is less than one Ct value, which could easily arise due to technical and biological variations that are beyond the control of a scientist.

Finally, there is some evidence that a higher correlation between the microarray and qPCR may be obtained by using PCR primers that overlap or are close to (within 1000 bp of) the oligonucleotide used during the microarray (Etienne et al., 2004). It was not possible to design primers overlapping the oligonucleotide for the majority of the genes due to the location of the oligonucleotide within the gene. For qPCR it is required that the primers overlap the introns (to avoid amplification from contaminating genomic DNA) and to keep the efficiency of the PCR high, the amplicon should be short (50 – 150 bp). These requirements are in addition to those required for a standard primer such as the length of the primer, GC content and specificity to the gene of interest. The oligonucleotide for the majority of genes used in the array were designed in the middle of a large exon, so designing qPCR primers to overlap these sequences did not fulfill the criteria described above. Intriguingly, for all three

assays (*Yif1b*, *Ccnd2* and *Nkx2.9*) where the up- or down-regulation was maintained between the microarray and qPCR the distance between the 3' end of the amplicon and the 5' end of the array oligonucleotide was less than 1000 bp (Table 6-3). In contrast, this correlation was not seen for *Srp14*, *Fkbp8* and *Gaparapl2* where the distance between the amplicon and the array oligonucleotide was also less than 1000 bp, and for *Gaparapl2* the amplicon actually overlapped the array oligonucleotide (Table 6-3).

Table 6-3: Location of the oligonucleotide used during the microarray experiment and the primer used during qPCR for each assay.

Gene	Size of the coding region (bp)	Location of the amplicon (bp)	Location of array oligonucleotide (bp)	Distance between 3' end of the amplicon and 5' end of the array oligonucleotide (bp)	Up or down-regulation maintained between microarray and qPCR
Yif1b	1126	315-396	808-858	412	Yes
Ccnd2	1225	812-870	1036-1120	116	Yes
Podx1	5302	827-924	4754-4805	3927	No
Dscam	6369	347-418	6011-6061	5664	N/A qPCR failed
Srp14	749	117-178	576-626	397	No
Flrt2	1071	229-379	2746-2796	2366	No
Dmrt2	2947	861-921	2882-2932	1960	No
Nkx2.9	1254	262-384	940-990	555	Yes
Fkbp8	1799	903-964	1711-1787	746	No
Gaparapl2	960	345-409	320-359	-89 (overlap)	No

One interesting gene that was identified as being up-regulated in the microarray is *Fkbp8*. Similar to *Tulp3, Fkbp8* is a negative regulator of the Shh signalling pathway (Bulgakov et al., 2004; Wong et al., 2008). Despite it being a good candidate, the up-regulation of Fkbp8 detected from the microarray was not observed during qPCR as it shows a downregulation in *hhkr* although this was not statistically significant. This qPCR result fits in with the previous data from our lab which reported that the *Fkbp8* expression is not significantly altered in *hhkr* compare to the wildtype embryos at E9.5 by using TaqMan approach (Patterson et al., 2009).

Nkx2.9 is one of the genes which came out of the microarray screen as being up-regulated in *hhkr*. Although not statistically significant, an up-regulation for this gene was also seen with qPCR. *Nkx2.9* is a homeodomain transcription factor that is expressed in the ventral region of the neural tube and is likely to specify a neuronal subtype (Pabst et al., 1998). Since *hhkr* exhibits expansion of the ventral cell types in the neural tube (Patterson et al., 2009) it is likely that this gene is up regulated in *hhkr*. Although E9.0 stage embryos were specifically used because no significant dorsoventral patterning defect was present in *hhkr*, the expression for *Nkx2.9* was not analysed in *hhkr* giving rise to a possibility that expansion of this gene was already apparent in *hhkr* at E9.0. To confirm or to discard this possibility, the expression pattern of *Nkx2.9* needs to be analysed in the caudal neural tube of E9.0 *hhkr* and wildtype littermates by *in situ* hybridization or immunohistochemistry.

The microarray results reported here show that few genes were altered between wildtype and *hhkr* however qPCR shows expression level of these genes are not significantly altered between wildtype and *hhkr*. We conclude that Tulp3 may not be acting as a transcription factor.

CHAPTER 7

IDENTIFICATION OF INTERACTING PARTNERS OF TULP3

7 Identification of interacting partners of Tulp3

7.1 Introduction

7.1.1 Confirming a yeast 2-hybrid result

As described in chapter 4, a yeast 2-hybrid screen is a widely used molecular technique. Although it is used regularly to identify novel binding partners of a protein of interest, it is a high throughput technique that can give rise to many false positive results. Indeed it has been estimated that up to 50% of results obtained from this technique are false positives (Deane et al., 2002). There are many factors that can account for these results; during the screen two proteins are highly over-expressed in the cell and are forced into the nucleus, where they may bind non-specifically to give a false positive signal. Alternatively, two proteins that contain complementary domains but are not normally co-localised in an endogenous biological system may be brought together, allowing an interaction that may never happen endogenously. Finally, the folding of mammalian protein may be incorrect in the yeast cell, potentially causing two proteins to interact when they would not if they were correctly folded. Because of these reasons, the results obtained from a yeast 2-hybrid screen need to be validated by independent techniques. The most ideal technique is co-immunoprecipitation of endogenous proteins; however, this is usually not feasible as it requires a large amount of protein and specific antibodies for each of the proteins under study. Therefore a series of experiments are usually performed to validate an interaction.

First it is essential to make sure that the gene encoding the protein of interest and its putative interacting partner are expressed in the same tissue and that their expression domains overlap, spatially and temporally. This step is important even when the co-immunoprecipitation of endogenous proteins is possible because co-immunoprecipitation

involves extracting protein from lysed cells; therefore proteins from different tissues or cellular compartments are mixed together allowing potential for an interaction that does not occur physiologically. Expression analysis is usually achieved by reverse transcriptase PCR in combination with whole mount *in situ* hybridization or immunofluorescence. In cases where the gene of interest is ubiquitously expressed, examining the expression pattern of the gene encoding the putative interaction partner may be unhelpful in verifying the potential for interaction, or prioritising candidates. In this case, genes which are expressed in tissues that demonstrate a mutant phenotype following gene disruption are often prioritised, on the basis of playing a potentially important role during development.

Once it is established that both the protein of interest and the putative interacting partner are present in the same tissue, particularly where this tissue exhibits a defect following mutation of the gene of interest, further experiments to demonstrate an *in vitro* or *in vivo* interaction are set up. For *in vitro* studies, constructs are designed to over-express the two genes under study. In cases where specific antibodies against the proteins are unavailable, a unique tag (e.g. HA or V5) is added to each of the constructs to give differentially tagged proteins. These constructs are cloned into a plasmid containing a general promoter, such as the cytomegalovirus CMV promoter, and the plasmids are transfected into a mammalian cell line to allow co-expression. Total protein is extracted from the cells and the protein of interest and any interacting proteins are purified by immunoprecipitation using an antibody specific for the protein itself (where available) or for the tagged molecule. This purified complex is electrophoresed on a protein gel and a second antibody, specific to the putative interacting partner (where available) or to the second protein tag, is used to determine, through western blotting, whether the putative interacting partner was co-immunoprecipitated with the protein of interest. If the two proteins do co-immunoprecipitate, this is good evidence in support of an interaction.

7.1.2 A yeast 2-hybrid identified 11 proteins as putative interaction partners of Tulp3

As discussed in section 6.1.4, the structural analysis of Tulp3 suggests that it could bind to double stranded DNA and function as a transcription factor. The study described in chapter 6 has addressed the possibility that Tulp3 may be a transcription factor. Additionally, the Tubby domain present in Tulp3 has the potential to be involved in protein-protein interactions, suggesting that Tulp3 may interact with one or more proteins. To assess the possibility that Tulp3 functions via protein-protein interactions during neural tube closure, a yeast two-hybrid screen was performed by Hybrigenics. They tagged full length Tulp3 cDNA at the N-terminus with LexA or Gal4 and used both constructs to screen an E10.5 and E12.5 mouse brain cDNA library in parallel screens. From the two Tulp3 yeast 2-hybrid screens, 49 positive clones were identified. Sequencing of these clones revealed the identity of the proteins which could potentially interact with Tulp3. There were 16 genes and many of these genes are represented as multiple clones, increasing the chance that the interaction may be genuine. The identity of the genes and the number of clones representing each gene is given in Table 7-1. Out of these genes, five are known as false positives as they come out of many unrelated screens, and these have been excluded from further analysis. A further two genes have been identified from several unrelated screens performed by the company, hence may also be false positives and not true interacting partners of Tulp3. However, three genes came out of both Tulp3 screens, were not found in unrelated screens and are represented by multiple clones, suggesting that the interaction between these proteins and Tulp3 is independent of the tag. These proteins are likely to be true interacting partners of Tulp3. Six genes came out of only one of the screens and two of these are represented by two different clones and are

specific to the Tulp3 screen, suggesting that these too are likely to be true interacting partners of Tulp3. Different classes of genes are highlighted in Table 7-1.

Gene Symbol	Gene name	Number of clones
Fam193a	*Family with sequence similarity 193, member A*	10
Nup155	*Nucleoporin 155*	3
Trim71	*Tripartite motif-containing 71*	10
4931406P16Rik	*RIKEN cDNA 4931406P16 gene*	1
Alx1 / Cart1	*ALX homeobox 1 / Cartilage homeoprotein 1*	1
Ccnb1	*Cyclin B1*	2
Ibrdc1 / Rnf271	*Ring finger protein 217*	1
Ktn1	*Kinectin 1*	1
Rgnef	*Rho-guanine nucleotide exchange factor*	2
Tnks2	*Tankyrase 2*	1
Actn4	*Actinin alpha 4*	1
Fasn	*Fatty acid synthase*	1
Otx2	*Orthodenticle homolog 2 (Drosophila)*	1
Pax3	*Paired box gene 3*	3
Ranbp10	*RAN binding protein 10*	1
N-Taf1	*TAF1 RNA polymerase II, TATA box binding protein (TBP)-associated factor*	9

Table 7-1: List of genes identified from a Tulp3 yeast 2-hybrid screen as putative interaction partners of Tulp3.

Three genes, highlighted in pink, came out of both screens using LexA and Gal4 tagged Tulp3, therefore are independent of the tag. Six genes, highlighted in blue, came out of one of the two screens but are unique to the screen with Tulp3. Two genes, highlighted in green, are known to come out of other unrelated screens. Five genes, highlighted in grey, are the known false positives of a yeast 2-hybrid screen.

7.1.3 Rho-guanine nucleotide exchange factor (Rgnef) was chosen for verification

Based on published literature on each of the genes identified by the yeast 2-hybrid screen, a story can be made for how many of these proteins might interact with Tulp3 to affect neural tube closure or patterning. *Fam193a* is a novel gene and its function in mice has not been studied. In human, a high level of autoantibodies against *Fam193a/BC037112* is detected in patients with neurological disorder (Amin et al., 2001), suggesting a neuronal role for this protein. Nup155 is a part of the nucleopore complex (NPC) present in the nuclear membrane and is involved in bidirectional transport of molecules between the nucleus and cytoplasm (Xylourgidis and Fornerod, 2009) (Zhang et al., 2008). It could be hypothesized that Tulp3 may simply bind to Nup155 as it enters the nucleus. Alternatively, a more exciting scenario would be that Tulp3 binds to Nup155 to enhance the selective capacity of the NPC. Mouse mutants of both *Trim71* and *Alx1/Cart1* exhibit exencephaly; however, neither of these genes are expressed in the neural tube (Zhao et al., 1996; Lancman et al., 2005; Maller Schulman et al., 2008). This suggests that both Trim71 and Alx1 are unlikely to interact with Tulp3 to regulate the dorsoventral patterning of the caudal neural tube and its closure. However, *Tulp3* mutants also exhibit exencephaly giving a possibility that Tulp3 may interact with Trim71 and Alx1 to regulate cranial neural tube closure. Ccnb1 is an essential component of maturation promoting factor, which functions to promote cells into the mitotic phase of the cell cycle. In keeping with this fundamental role, mouse mutants of *Ccnb1* die by E10 (Brandeis et al., 1998). Both Trim71 and Ibrdc1 are proteins with RING finger domains, which are known to mediate protein-protein interactions. There is no study that reports the function of Ibrdc1; however, a subset of proteins containing RING fingers have been identified as having a role in E3 ubiquitin ligase activity (Freemont, 2000), suggesting a possible molecular role for Ibrdc1 and Trim71. Ktn1 is potentially a very good candidate as a binding partner of Tulp3 in

regulation of Shh signalling. Ktn1 binds to Kinesin motor proteins (Toyoshima et al., 1992), some of which are directly involved in Shh signalling by transporting vesicles containing components of Shh signalling up to primary cilia, where Shh signalling takes place (Simpson et al., 2009). Tulp3 may bind to Ktn1 to specify the correct Kinesin motor that is required for the Shh signalling.

However due to time constraints only one interaction could be verified in this study. Based on the expression profile during mouse neurulation (see below in Figure 7-2) and published literature, Rgnef was chosen as the best candidate to interact with Tulp3 during dorsoventral patterning of the caudal neural tube and regulation of its closure. Other members of the lab are pursuing verification of other interactions as most of the genes are very interesting and could potentially interact with Tulp3 to regulate different molecular events in which Tulp3 is likely to participate.

7.1.4 Rho-guanine nucleotide exchange factor (Rgnef)

Rho-guanine nucleotide exchange factor (Rgnef, also called p190RhoGEF) is a guanine nucleotide exchange factor which is required specifically to activate the Ras homolog gene family member A (RhoA). RhoA belongs to the Rho family of small G proteins (Rho GTPases), which are involved in many cellular processes such as cytoskeleton reorganization to regulate cell shape and cell movement, cell polarity gene expression and regulation of cell cycle (Schmidt and Hall, 2002). Rho GTPases cycle between an inactive guanosine diphosphate (GDP)-bound form and an active guanosine triphosphate (GTP)-bound state and this activation is stimulated by a member of the guanine nucleotide exchange factor (GEF) family, which catalyses the exchange of GDP to GTP. There are over 70 GEF proteins and each has a unique specificity for a different class of Rho GTPase (Rossman et al., 2005).

There is evidence to suggest that the activity of some members of the GEF family are regulated by heterotrimeric G proteins, which act downstream of G-protein coupled receptors (GPCR) and receptor tyrosine kinases (Rossman et al., 2005; Schiller, 2006), providing a link between extracellular signalling and activation of Rho GTPases.

Rgnef was first identified in a yeast 2-hybrid screen that was designed to find binding partners of RhoA in controlling neuronal morphology (Gebbink et al., 1997). It was shown that Rgnef physically interacts with both the active and inactive form of RhoA and functions to activate RhoA to induce cell rounding and suppress neurite outgrowth (Gebbink et al., 1997). Furthermore, it was shown that Rgnef activates RhoA but not other members of the Rho GTPase family (Gebbink et al., 1997; van Horck et al., 2001). Rgnef is a large protein of 190 kDa with multiple domains, including a leucine rich domain, a Zinc finger domain, a Dbl-homology (DH) domain, a Pleckstrin homology (PH) domain and a C-terminal coiled-coiled domain (Gebbink et al., 1997). DH and PH domains are conserved in all members of the RhoGEF family and the DH domain has been identified as the catalytic domain required for exchange of GDP to GTP in other GEFs (Hart et al., 1994). Similar to other GEFs, studies using truncated Rgnef containing the DH/PH domain showed that this domain is sufficient to promote GDP/GTP exchange on RhoA *in vitro* (van Horck et al., 2001). Since these initial studies, Rgnef has been implicated in various cytoskeletal roles. It has been shown to bind directly to microtubules, focal adhesion kinase (which functions to regulate the formation of different actin cytoskeletal structures), and the 3' region of the light neurofilament subunit mRNA (which encodes a component of the neuronal cytoskeleton) to increase stability of the transcript (Canete-Soler et al., 2001; van Horck et al., 2001; Zhai et al., 2003).

7.2 Results

7.2.1 Reverse transcriptase PCR shows all potential interaction partners of Tulp3 are expressed during neurulation

Eight genes specific to the Tulp3 yeast 2-hybrid screen were analyzed further. To assess the possibility that these eight genes could interact with Tulp3 during neurulation and development I performed a reverse transcription PCR using cDNA synthesized from E7.5 – E17.5 embryos and some adult tissues. The result showed that all genes were expressed during neurulation (E8.5-E10.5) (Figure 7-1). All genes, with the exception of *Rgnef,* are also expressed at E7.5, which is the earliest stage examined and is just prior to initiation of neural tube closure. *Rgnef* is first detected at E8.5 and continues to be expressed throughout development (Figure 7-1H). The expression of *Nup115, Trim71* and *Ktn1* appears to be absent at E14.5, however these genes are expressed at detectable levels in all other development stages examined (Figure 7-1 B, C and G). All the other genes are expressed at all developmental stages examined.

7.2.2 *In situ* hybridization to reveal the expression pattern of potential interaction partners of Tulp3

The expression patterns of *Fam193a, Nup155, Ibrdc1, Ktn1* and *Rgnef* during mouse development have not been reported. To assess if any of these genes are expressed in tissues that are important for closure and patterning of the neural tube, I performed *in situ* hybridization on mouse embryos undergoing neural tube closure i.e. at E8.5, E9.5 and E10.5 ($n \geq 3$ at each stages). I cloned fragments of each cDNA into pGEM-T Easy vector, and used these fragments to generate gene-specific riboprobes. The size and the region of the gene used to generate probes are given in Table 2-3.

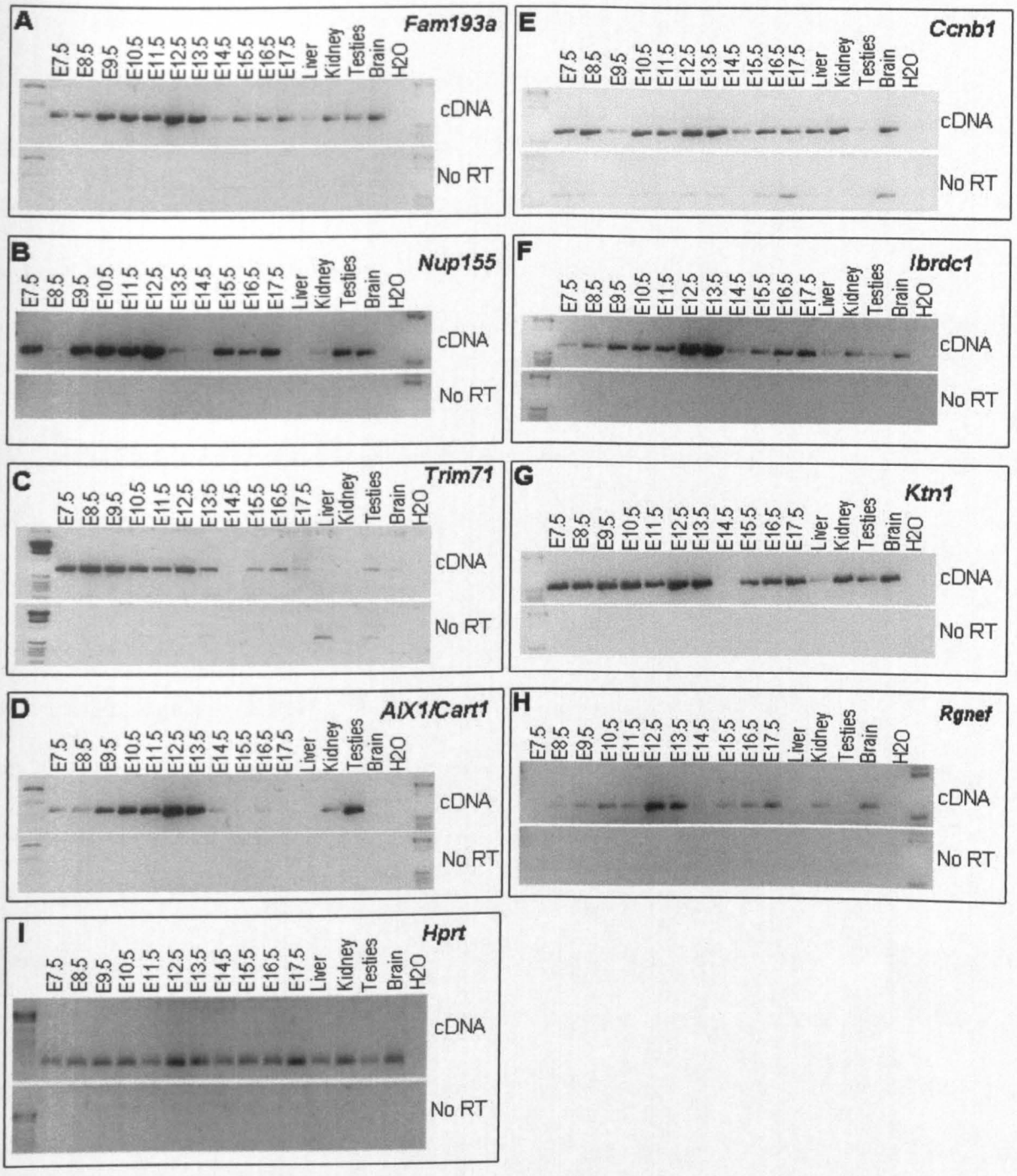

Figure 7-1: Reverse transcription PCR of genes identified by a Tulp3 yeast 2-hybrid screen.

(A-I) PCR using primers for *Fam193a* (A), *Nup155* (B), *Trim71* (C), *Alx1* (D), *Ccnb2* (E), *Ibrdc1* (F), *Ktn1* (G), *Rgnef* (H) and *Hprt* (I). RNA was extracted from E7.5 to E17.5 embryos, adult liver, adult kidney, adult testes and adult brain. PCR was performed following cDNA synthesis by reverse transcription from the RNA (cDNA) and from control reactions in which no RT enzyme was used (No RT) to test for amplification from contaminating genomic DNA. All genes are expressed during neurulation (E7.5-E10.5). No significant level of PCR product is observed in any No RT negative controls.

The results show that *Fam193a* is expressed at a low level throughout the embryo at all stages examined (Figure 7-2 A-C). *Nup155* is expressed at a low level at E8.5 and it appears to be enriched at the caudal and rostral ends of the embryo. At E9.5 and E10.5 *Nup155* shows a ubiquitous distribution pattern (Figure 7-2 D-F). *Ibrdc1* is widely expressed at E8.5; however, at E9.5 and E10.5 it becomes restricted to the somites (Figure 7-2 G-I). This somitic restriction of *Ibrdc1* is seen more clearly in the transverse sections through E9.5 and E10.5 embryos (Figure 7-3 C and D). *Ktn1* is expressed ubiquitously from E8.5 – E10.5. At E9.5 and E10.5 it appears to be enriched in the somites and developing limb buds (Figure 7-2 J-L). Transverse sections through E8.5 embryos probed for *Nup155* and *Ktn1* shows that these genes are expressed throughout the neuroepithelium; however, at E9.5 the expression domains of both *Nup155* and *Ktn1* become enriched in the dorsal half of the neural tube (Figure 7-3 A, B, E and F). *Rgnef* is expressed in the floor plate of the neural tube from E8.5 to E10.5. There is a difference in the rostrocaudal axis of the embryo, whereby it is expressed more strongly at the rostral end of the embryo compared to the caudal end (Figure 7-2 M-Q). This is confirmed by comparing the intensity of staining in the transverse sections at the level of the hindbrain (rostral) and the caudal end of an E8.5 embryo (Figure 7-3 compare G and H), where more intense staining is seen in the rostral sections compared to the caudal sections. At E9.5, sections through the caudal end of the embryo show that expression is weak but is detectable (Figure 7-3 I). Hybridization using a sense probe for ubiquitously expressed genes (*Fam193a*, *Nup155* and *Ktn1*) at E9.5 resulted in no detection of signal (Figure 7-2 P-R).

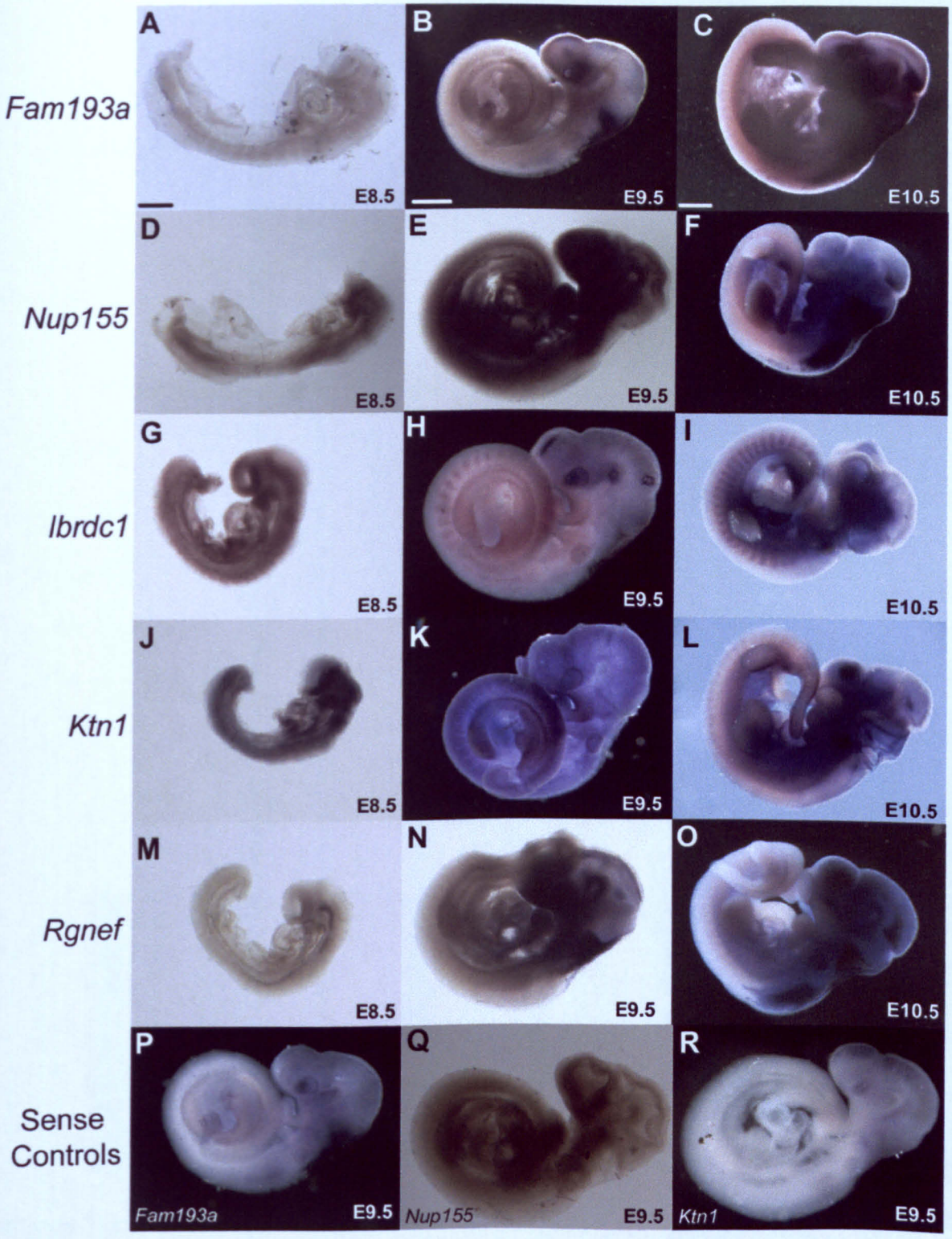

Figure 7-2: Expression patterns of putative interaction partners of Tulp3.
(A-O) Whole mount *in situ* hybridization using anti-sense probe to detect the expression of *Fam193a* (A-C), *Nup155* (D-F), *Ibrdc1* (G-I), *Ktn1* (J-L) and *Rgnef* (M-O) on E8.5 (A,D,G,J and M), E9.5 (B,E,H and N) and E10.5 (C,F,I and O) CD1 embryos. (P-R) Whole mount *in situ* hybridization using sense probe for *Fam193a* (P), *Nup155* (Q) and *Ktn1* (R) on E9.5 CD1 embryos. Scale bars represent 300 μM (E8.5), 500 μM (E9.5) and 700 μM (E10.5).

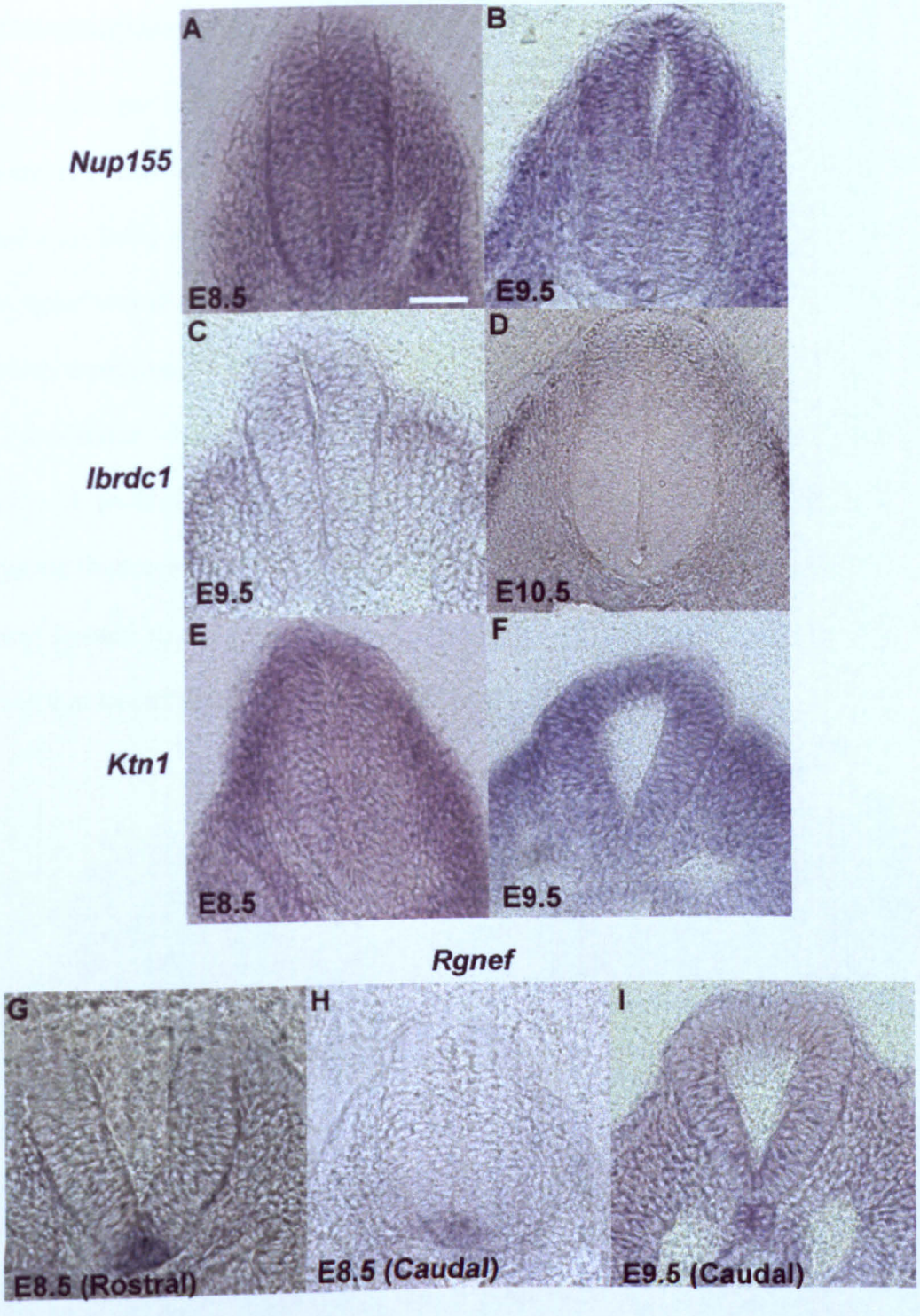

Figure 7-3: Distribution of putative interaction partners of Tulp3 in the neuroepithelium. (A - I) Transverse sections through E8.5 (A, G and H), E9.5 (B, C, F and I) and E10.5 (E) embryos stained with a probe to detect expression of *Nup155* (A and B), *Ibrdc1* (C and D), *Ktn1* (E and F) and *Rgnef* (G - I). All the sections are taken from the caudal ends of embryos (level of hind limb bud, when present) unless otherwise stated. The rostral section (G) is taken at the level of the hindbrain. Scale bar represent 5 μM in panels A-C, E-H; and 10 μM panel D.

7.2.3 Distribution of *Rgnef* is not affected in *hhkr*

All eight genes that came out of the Tulp3 yeast 2-hybrid screen are interesting and could potentially interact with Tulp3. The main aim of this study was to discover proteins that interacted with Tulp3 during the dorsoventral patterning of the neural tube and its closure. For this role *Rgnef* was considered to be the best candidate as it is expressed in the floor plate, a tissue which is required to establish the dorsoventral pattern of the neural tube.

To examine whether loss of *Tulp3* affected the distribution pattern of *Rgnef* during neurulation, I performed whole mount *in situ* hybridization on E9.0 *hhkr* mutant and heterozygous littermates using a probe to detect *Rgnef* (Figure 7-4). The result shows that the expression domain of *Rgnef* in *hhkr* mutants is similar to that of heterozygous littermates, suggesting that loss of *Tulp3* does not alter the expression domain of *Rgnef*.

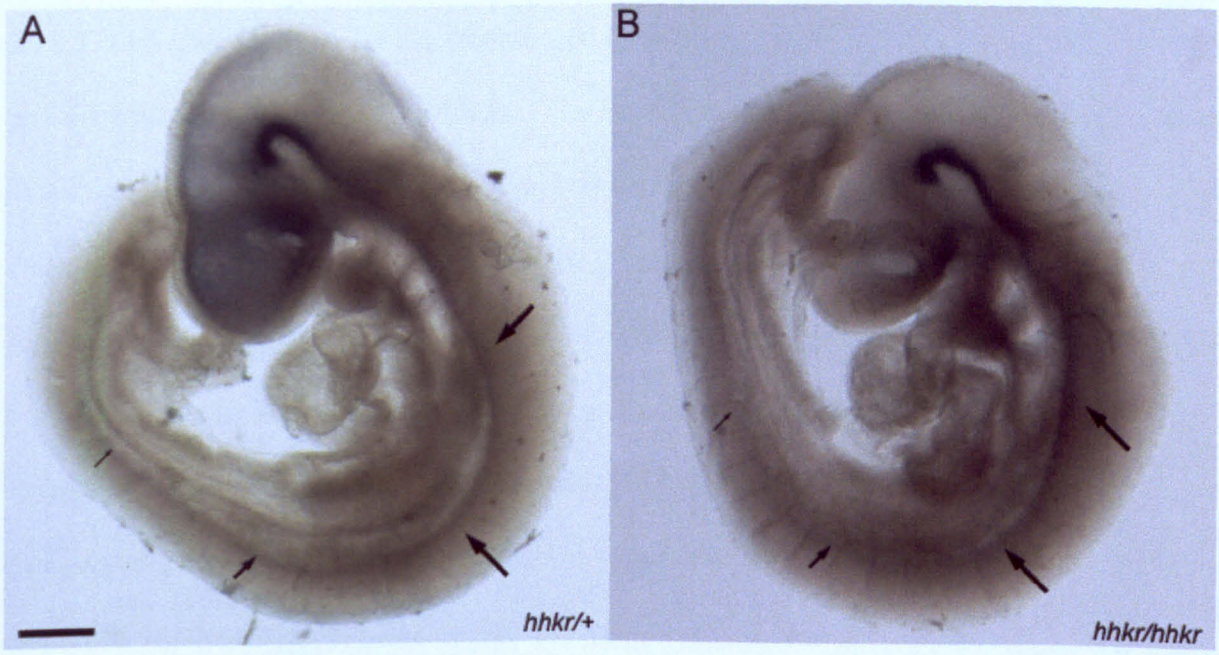

Figure 7-4: Expression domain of *Rgnef* does not change in *hhkr* mutant.
(A and B) Whole mount *in situ* hybridization using anti-sense probe to detect the expression of *Rgnef* on E9.0 *hhkr*/+ (A) and *hhkr/hhkr* (B) embryos. The distribution of *Rgnef* in *hhkr/hhkr* is similar to that in *hhkr*/+. Arrows point to the domain of expression at the floor plate and the thickness of the arrow corresponds to the intensity of the staining. Scale bar represent 500 μM.

7.2.4 Co-immunoprecipitation to verify interaction between Tulp3 and Rgnef

To verify the Y2H result that Tulp3 physically interacts with Rgnef, I co-expressed V5-tagged Tulp3 and HA-tagged Rgnef in HEK293T cells and performed a co-immunoprecipitation study.

7.2.4.1 Optimization of transfection

To optimize the transfection for HA-Rgnef (a gift from Dr Kranenburg, University Medical Center Utrecht, The Netherlands), I transfected HEK293T cells, grown to 90%-95% confluency in 25 cm^2 flasks with 0 μg, 5 μg, 7.5 μg and 10 μg of HA-Rgnef plasmid for 24 hours and 48 hours. Transfections were carried out as described in section 2.17.4 using Lipofectamine 2000 Transfection Reagent. I extracted total cell lysate as described in section 2.18.2 from transfected cells, electrophoresed through an SDS-PAGE gel, Western blotted and probed with a mouse-anti-HA antibody. The result showed that multiple bands were detected in all transfections when cells were transfected with HA-Rgnef. Only one of these bands was detected in cells that were mock transfected (Figure 7-5 A). The predicted size of full length Rgnef is ~190 kDa and the HA tag is ~9 kDa, so a band of ~200 kDa is expected. This size corresponds to the top band that is specific to the transfected cells (Figure 7-5 A, arrow HA-Rgnef). Other lower molecular weight bands are likely to be degraded products of HA-Rgnef. This result also showed that increasing the concentration of the plasmid did not result in increased or decreased production of full length HA-Rgnef as the intensity of the band corresponding to full length HA-Rgnef is the same for cell transfected with 5 μg, 7.5 μg or 10 μg of HA-Rgnef plasmid, for each time point. A longer transfection time results in increased level of full length HA-Rgnef, however a similar increase is also seen with other bands (Figure 7-5A, compare 24 hours to 48 hours). Transfection with 5 μg of HA-Rgnef plasmid for 24

hours was considered to be optimal as it results in production of full length HA-Rgnef while other bands appear weaker compared to other conditions. This condition was used for further transfection studies.

A His-tagged Tulp3 construct was regularly used in the lab for transfection. The optimized conditions for this construct was 5 μg of plasmid transfected for 24 hours (personal communication with Ms V. Patterson). I synthesized a Tulp3-V5 construct using the gateway system (Invitrogen). A entry vector (pDONR221) containing full length Tulp3 cDNA (constructed by Ms V. Patterson) was recombined with pcDNA/V5-DEST destination vector in the presence of LR clonase, which facilities the homologous recombination between AttL sites flanking the Tulp3 in the entry vector and AttR sites present within the destination vector to generate the expression construct. I used the same optimized conditions for His-tagged Tulp3 to transfect HEK293T cells with the Tulp3-V5 construct. I extracted the protein from transfected cells, electrophoresed, Western blotted and probed with a mouse anti-V5 antibody (Figure 7-5 B). The result showed that two bands were detected at ~55 kDa. These bands correspond closely to the expected size of tagged Tulp3. The top band is the full length Tulp3 and the bottom band arises from an alternative start site within the sequence of Tulp3 (personal communication with Ms V. Patterson). Other smaller bands are likely to be degraded forms of Tulp3-V5 protein.

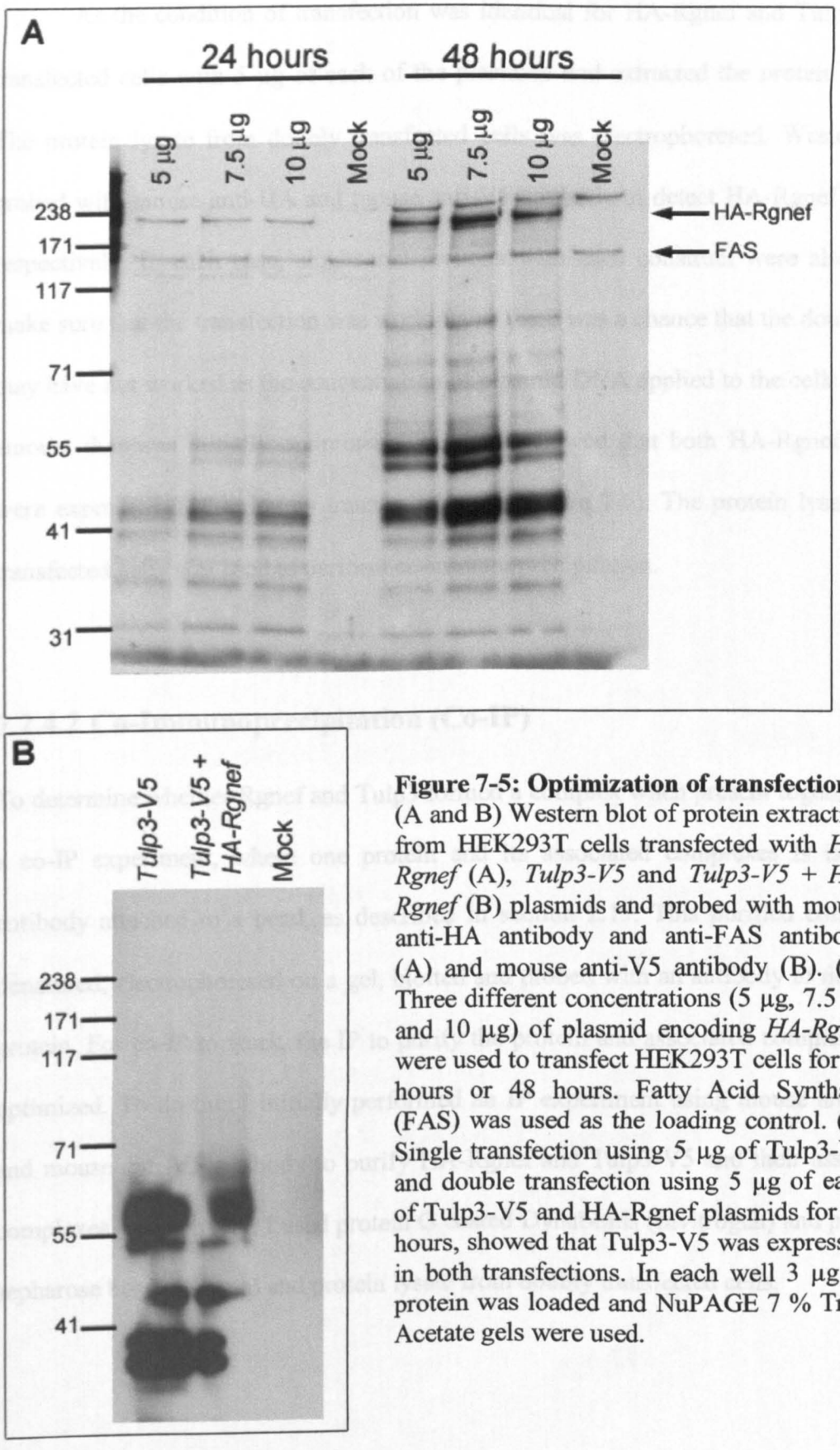

Figure 7-5: Optimization of transfection. (A and B) Western blot of protein extraction from HEK293T cells transfected with *HA-Rgnef* (A), *Tulp3-V5* and *Tulp3-V5* + *HA-Rgnef* (B) plasmids and probed with mouse anti-HA antibody and anti-FAS antibody (A) and mouse anti-V5 antibody (B). (A) Three different concentrations (5 µg, 7.5 µg and 10 µg) of plasmid encoding *HA-Rgnef* were used to transfect HEK293T cells for 24 hours or 48 hours. Fatty Acid Synthase (FAS) was used as the loading control. (B) Single transfection using 5 µg of Tulp3-V5 and double transfection using 5 µg of each of Tulp3-V5 and HA-Rgnef plasmids for 24 hours, showed that Tulp3-V5 was expressed in both transfections. In each well 3 µg of protein was loaded and NuPAGE 7 % Tris-Acetate gels were used.

As the condition of transfection was identical for HA-Rgnef and Tulp3-V5, I doubly transfected cells with 5 μg of each of the plasmids and extracted the protein after 24 hours. The protein lysate from doubly transfected cells was electrophoresed, Western blotted and probed with mouse anti-HA and mouse anti-V5 antibody to detect HA-Rgnef and Tulp3-V5, respectively. In each case, single transfections with each construct were also performed to make sure that the transfection was working, as there was a chance that the double transfection may have not worked as the concentration of plasmid DNA applied to the cells was double the amount that was initially optimized. The result showed that both HA-Rgnef and Tulp3-V5 were expressed in the doubly transfected cells (Figure 7-6). The protein lysate from doubly transfected cells was used to perform co-immunoprecipitation.

7.2.4.2 Co-Immunoprecipitation (Co-IP)

To determine whether Rgnef and Tulp3 formed a complex when present together, I performed a co-IP experiment, where one protein and its associated complexes is isolated with an antibody attached to a bead, as described in section 2.19. This purified complex was then denatured, electrophoresed on a gel, blotted and probed with an antibody to detect the second protein. For co-IP to work, the IP to purify the protein and associated complexes needs to be optimized. To do this I initially performed an IP experiment using mouse anti-HA antibody and mouse anti-V5 antibody to purify HA-Rgnef and Tulp3-V5 and their associated protein complexes, respectively. I used protein G coated Dynabeads (Invitrogen) and protein G coated sepharose beads (Sigma) and protein lysate from doubly transfected cells.

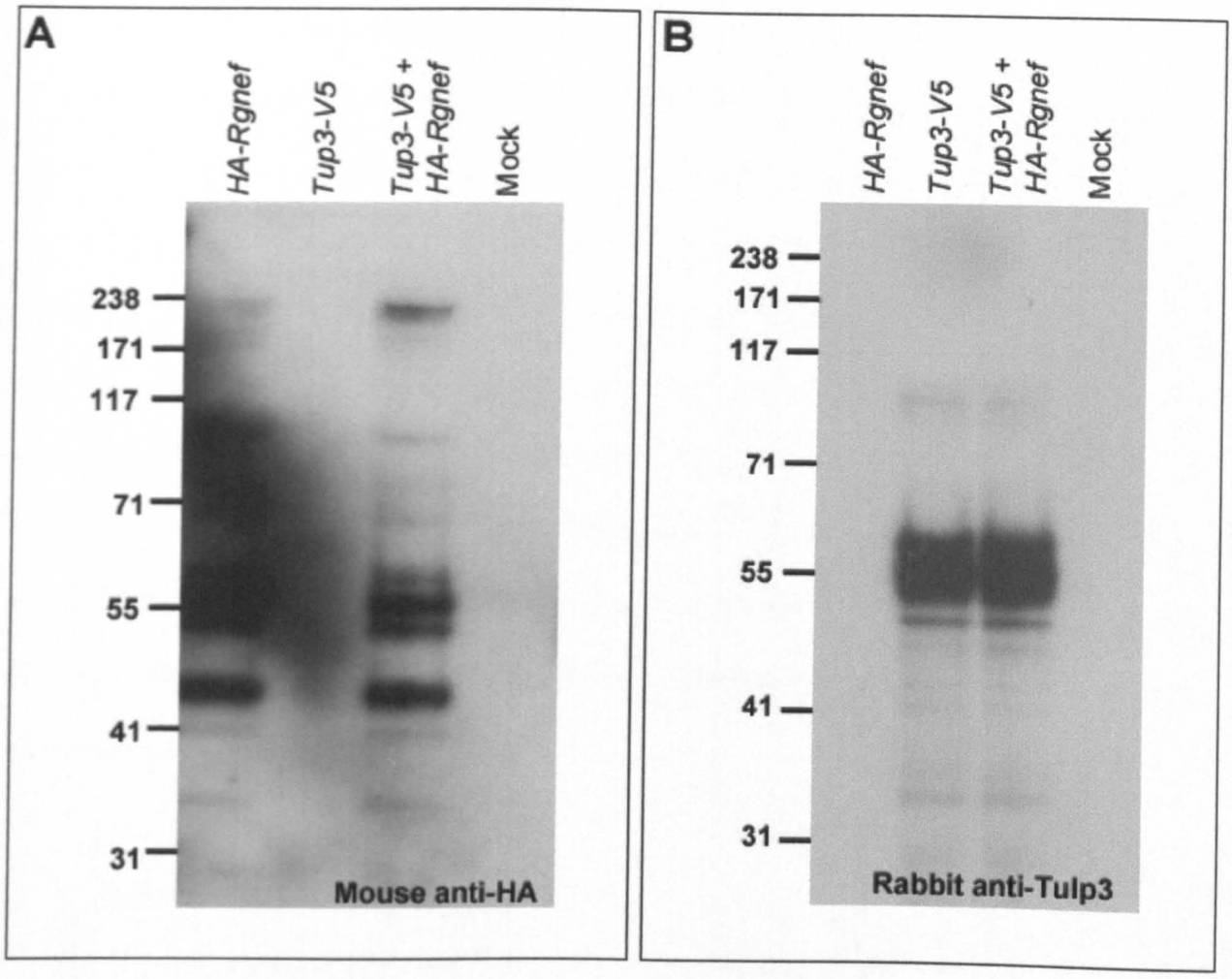

Figure 7-6: Full length HA-Rgnef and Tulp3-V5 are detected in doubly transfected cells. (A and B) Western blot to detect HA-Rgnef using a mouse anti-HA antibody (A) and Tulp3-V5 using a rabbit anti-Tulp3 antibody (B) on protein lysate extracted from cell transfected with construct encoding *HA-Rgnef* (lane 1), *Tulp3-V5*(lane 2), *Tulp3-V5 + HA-Rgnef* (lane 3) and mock transfection (lane 4). A band corresponding to full length HA-Rgnef (~200 kDa) is detected in lysate where cells were transfected with just *HA-Rgnef* and in lysate where cells were doubly transfected with *Tulp3-V5 + HA-Rgnef* (A, lane 1 and 3). A band corresponding to full length Tulp3-V5 (~55 kDa) is detected in lysate where cells were transfected with just - *Tulp3-V5* and in lysate where cells were doubly transfected with *Tulp3-V5 + HA-Rgnef* (B, lane 2 and 3).

For each IP, an aliquot of protein lysate at various steps in the protocol was also loaded in the gel while generating a western blot. These were included for two main reasons; firstly, to make sure that the protein of interest was present in the starting lysate and that it did not bind to the protein G beads in a non-specific way, and secondly, to ensure that most of the protein of interest was bound to the antibody conjugated to the beads and was not removed in the wash steps. A flow chart of steps involved in each IP is given in Figure 7-7 and the samples that were loaded in the gel are highlighted in red.

The blots were first probed with the antibody used during the IP to determine whether or not the IP enriched for the protein of interest. Next, to determine whether or not Tulp3-V5 and HA-Rgnef formed a complex and were co-purified, I probed the same blot with the antibody to recognize the second protein.

1. **Protein G Sepharose beads**

The IP with mouse anti-HA antibody was partly successful in purifying full length HA-Rgnef; however, a faint band of the same size was observed in the negative control where the IP was performed without the presence of the antibody (Figure 7-8 A). Furthermore, large amount of protein (including full length HA-Rgnef) was also present in the bead only eluate. Although HA-Rgnef appears to bind to protein G beads non-specifically, the fact that the intensity of the band in the IP lane with the antibody is stronger than that in the lane where no antibody was present, suggests that the IP with the antibody has enriched the full length HA-Rgnef. Probing the same blot with rabbit anti-Tulp3 antibody showed that the band corresponding to full length Tulp3-V5 was massively enriched in the IP with antibody compared to the negative control where no antibody was present (Figure 7-8 B).

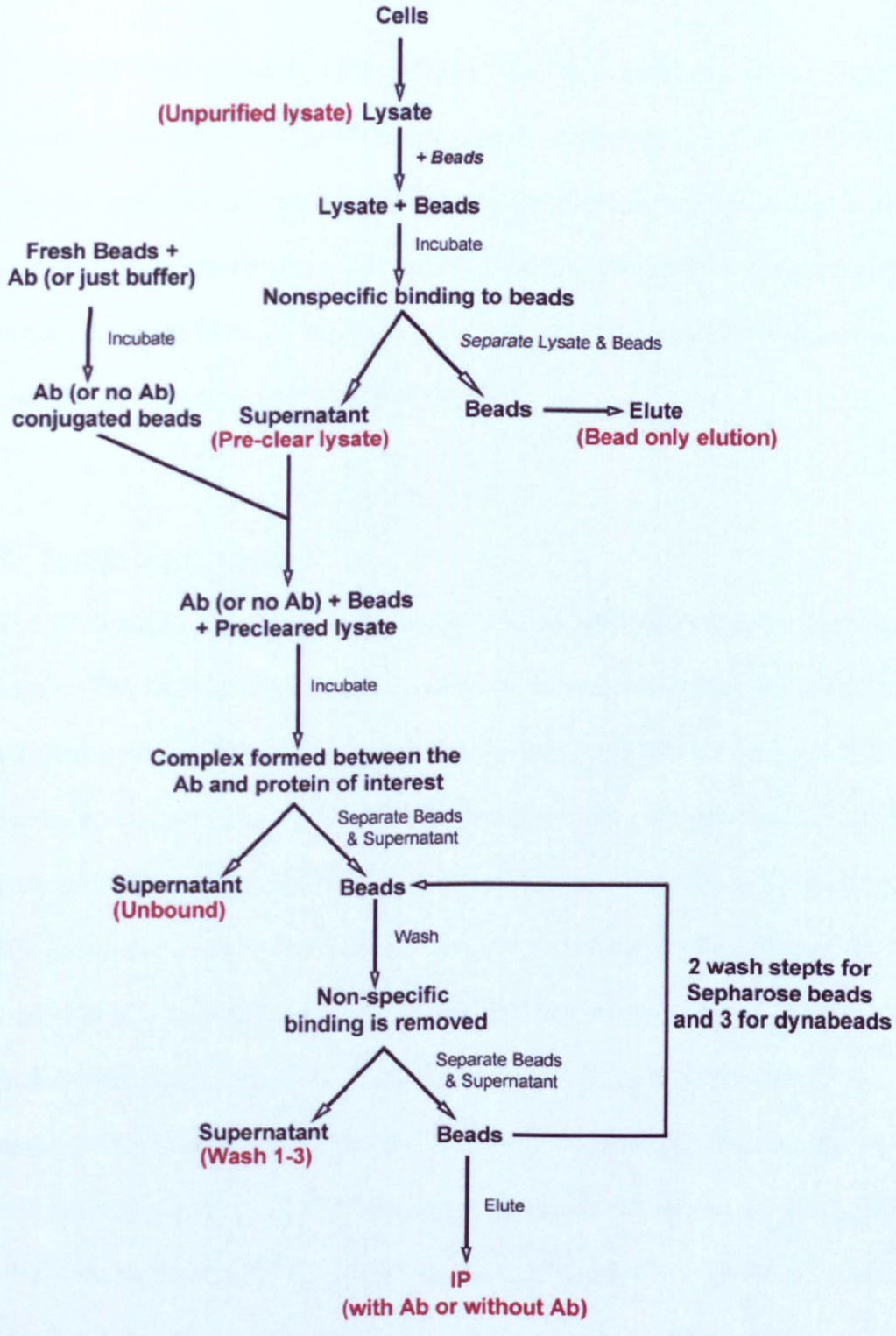

Figure 7-7: Flow chart of IP steps.
The protocol is as detailed in section 2.19. Control samples that were loaded on each IP gel are shown in red.

The IP with mouse anti-V5 antibody was non-specific as running both IP samples (with and without antibody) gave a strong signal corresponding to Tulp3-V5 (Figure 7-9 A). Probing the same blot with mouse anti-HA showed that full length HA-Rgnef was present in both IP with the antibody lane and in the IP without the antibody lane, however the band corresponding to full length HA-Rgnef is much stronger in the IP with the antibody lane compared to the negative control (Figure 7-9 B).

2. Protein G Dynabeads

The IP to purify HA-Rgnef with mouse anti-HA antibody bound to Dynabeads was not successful. The HA-Rgnef protein appears to be binding non-specifically to the beads as a large quantity of this protein was present in the bead only elution (Figure 7-10 A Lane 3). Furthermore, the amounts of HA-Rgnef present in the unbound fraction of the IP with antibody and without the antibody appears to be the same (Figure 7-10 A, compare lane 4 with land 7). Large quantities of this protein were also lost in the washes (Figure 7-10 A). A faint band of ~200 kDa was detected in the IP lane with the antibody; however, it was not possible to conclude whether there was a band of the same size in the IP without antibody lane due to a problem with the blot (Figure 7-10). To overcome this problem, samples from IP with and IP without antibody were run on a different gel and probed with mouse anti-HA antibody (Figure 7-10 B). This showed that a band of ~200 kDa was present in both IP with antibody and IP without antibody lanes, suggesting that purification of HA-Rgnef was unsuccessful.

Probing the same blot with rabbit anti-Tulp3 antibody showed that the band corresponding to full length Tulp3-V5 was present in both IP with antibody lane and in the negative control. The intensity of these bands was similar (Figure 7-10 C).

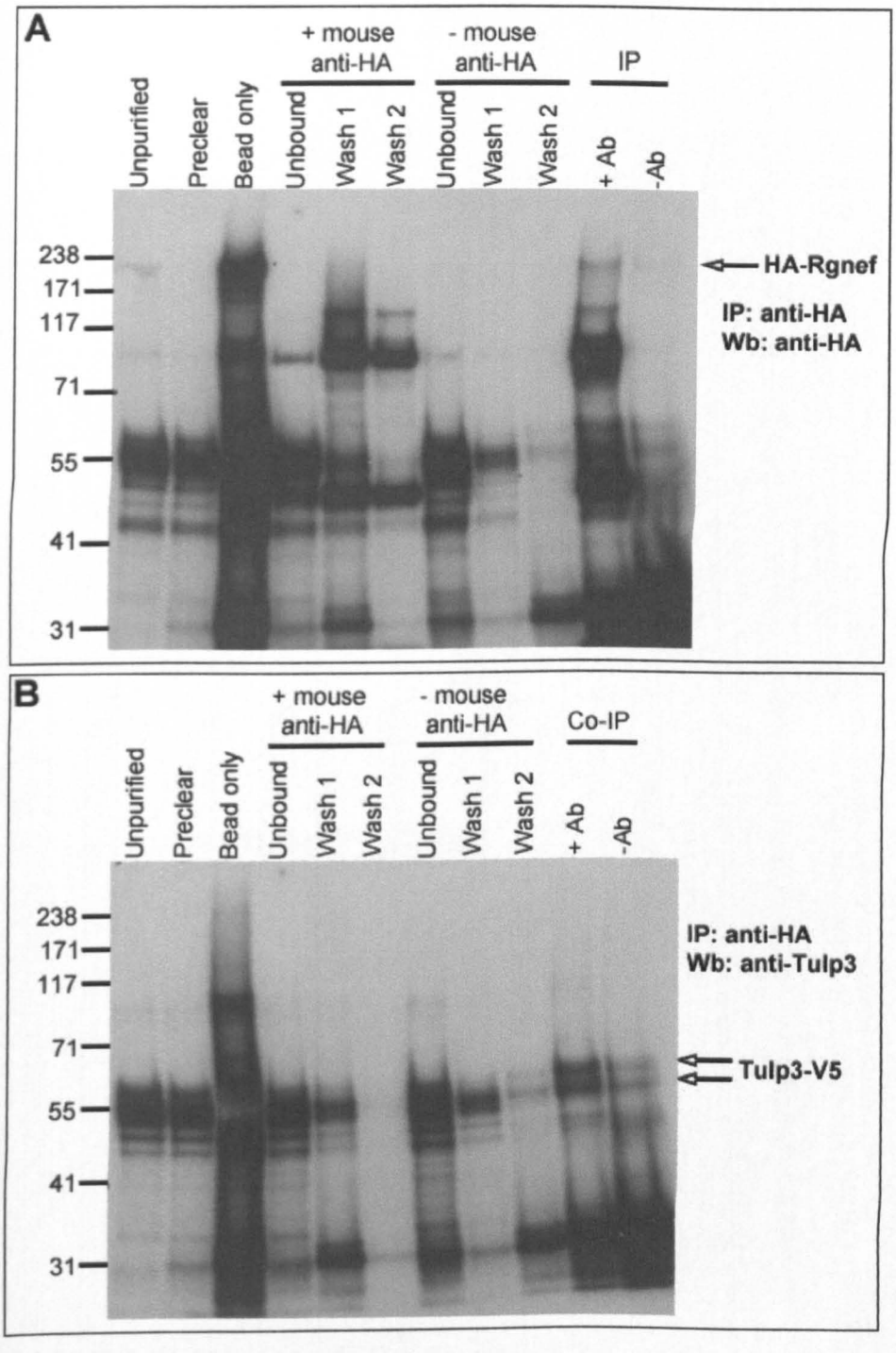

Figure 7-8: Co-IP to purify Tulp3-V5 with HA-Rgnef using sepharose beads and mouse anti-HA antibody.

(A and B) Western blots of IP with and without the mouse anti-HA antibody to purify HA-Rgnef and its associated complexes. (A) Probed with mouse anti-HA antibody to identify HA-Rgnef. (B) Probed with rabbit anti-Tulp3 antibody to determine whether Tulp3-V5 was present in a complex with HA-Rgnef. Details of samples loaded in each lane are given in Figure 7-7.

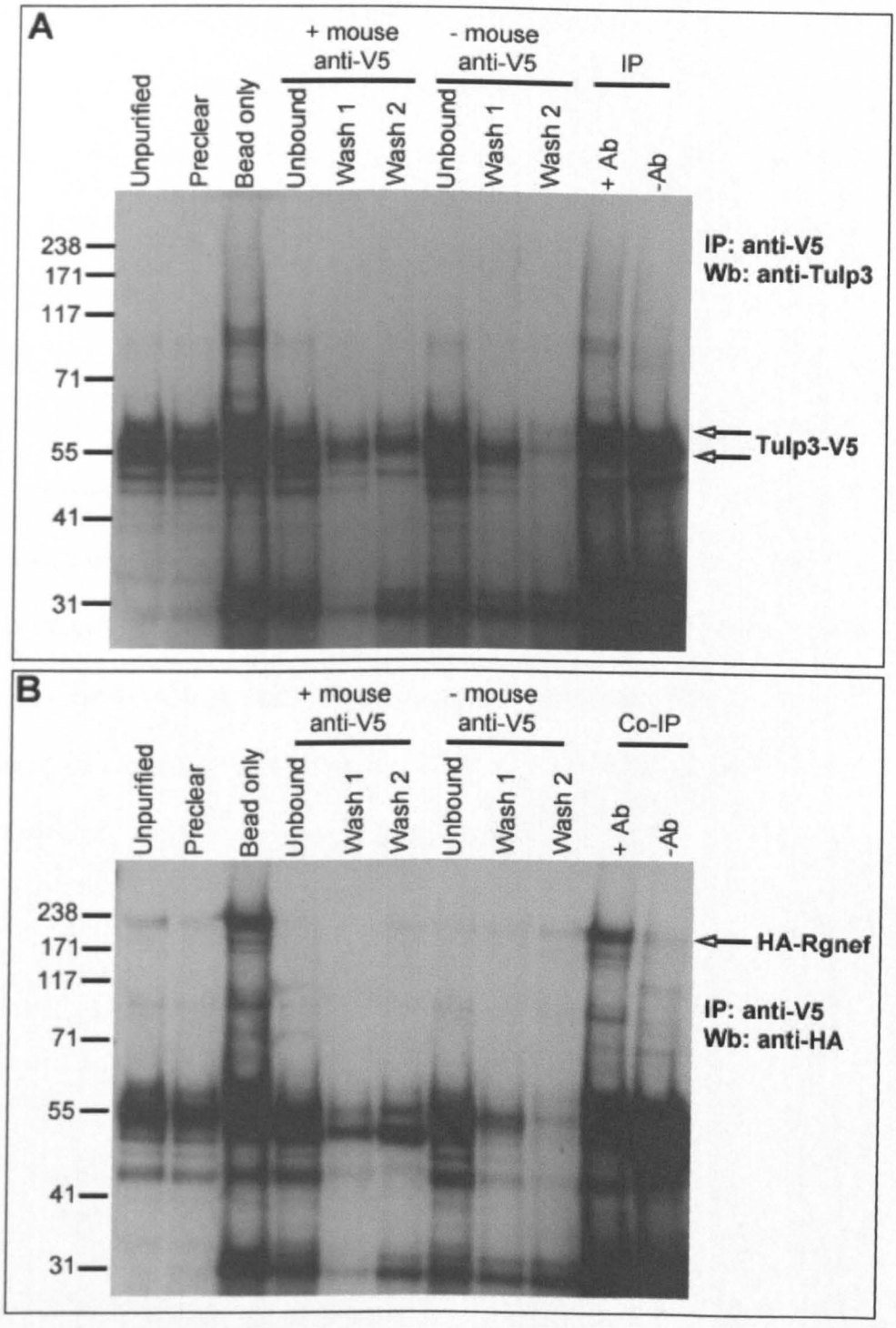

Figure 7-9: Co-IP to purify HA-Rgnef with Tulp3-V5 using sepharose beads and mouse anti-V5 antibody.

(A and B) Western blots of IP with and without mouse anti-V5 antibody to purify Tulp3-V5 and its associated complexes. (A) Probed with rabbit anti-Tulp3 antibody to identify Tulp3-V5. (B) Probed with mouse anti-HA antibody to determine whether HA-Rgnef was present in a complex with Tulp3-V5. Details of samples loaded in each lane are given in Figure 7-7.

The IP to purify Tulp3-V5 using mouse anti-V5 antibody and Dynabeads was successful. The band corresponding to full length Tulp3-V5 was present in the IP with antibody lane and absent from the IP without the antibody lane (Figure 7-11 A). For IP without the antibody, most of the Tulp3-V5 appears to be lost in the unbound fraction (Figure 7-11 A, lane 7), as you would expect.

Probing the same blot with mouse anti-HA antibody to check for co-purification of HA-Rgnef showed that a band of ~200 kDa appears enriched in the lane for IP with the antibody compared to the lane for IP without the antibody (Figure 7-11 B); however, due to the poor quality of that part of the blot it was not absolutely clear whether this band is present in the IP with no antibody lane. To overcome this problem the IP samples with antibody and the control IP sample without antibody were run on a second gel (Figure 7-11 C). This showed that the band of ~200 kDa is present in the IP with the antibody and is absent from the negative control.

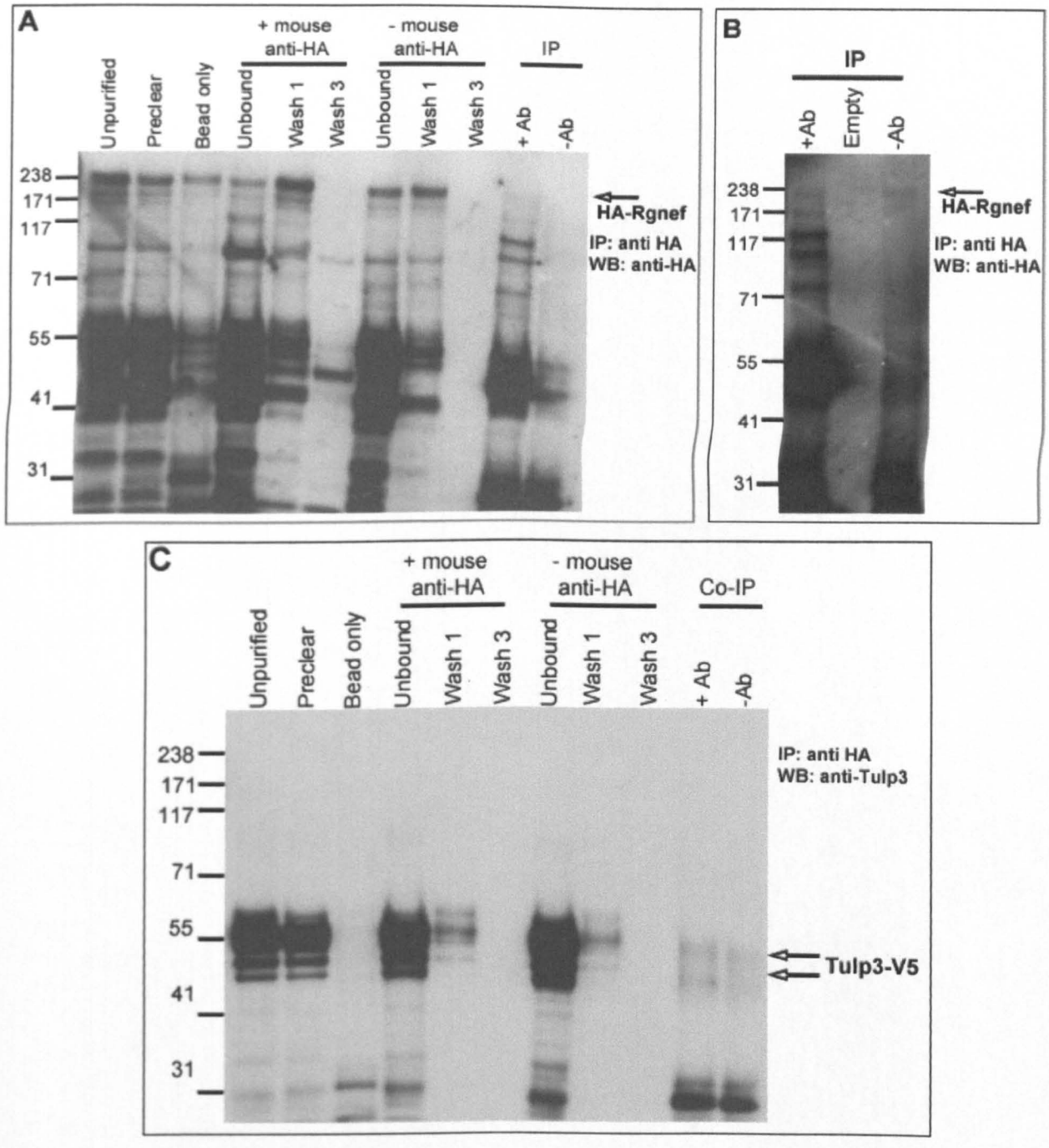

Figure 7-10: Co-IP to purify Tulp3-V5 with HA-Rgnef using dynabeads and mouse anti-HA antibody.

(A - C) Western blots of IP with and without the mouse anti-HA antibody to purify HA-Rgnef and its associated complexes. (B) Probed with mouse anti-HA antibody to identify HA-Rgnef. (C) Probed with rabbit anti-Tulp3 antibody to determine whether Tulp3-V5 was present in a complex with HA-Rgnef. Details of samples loaded in each lane are given in Figure 7-7.

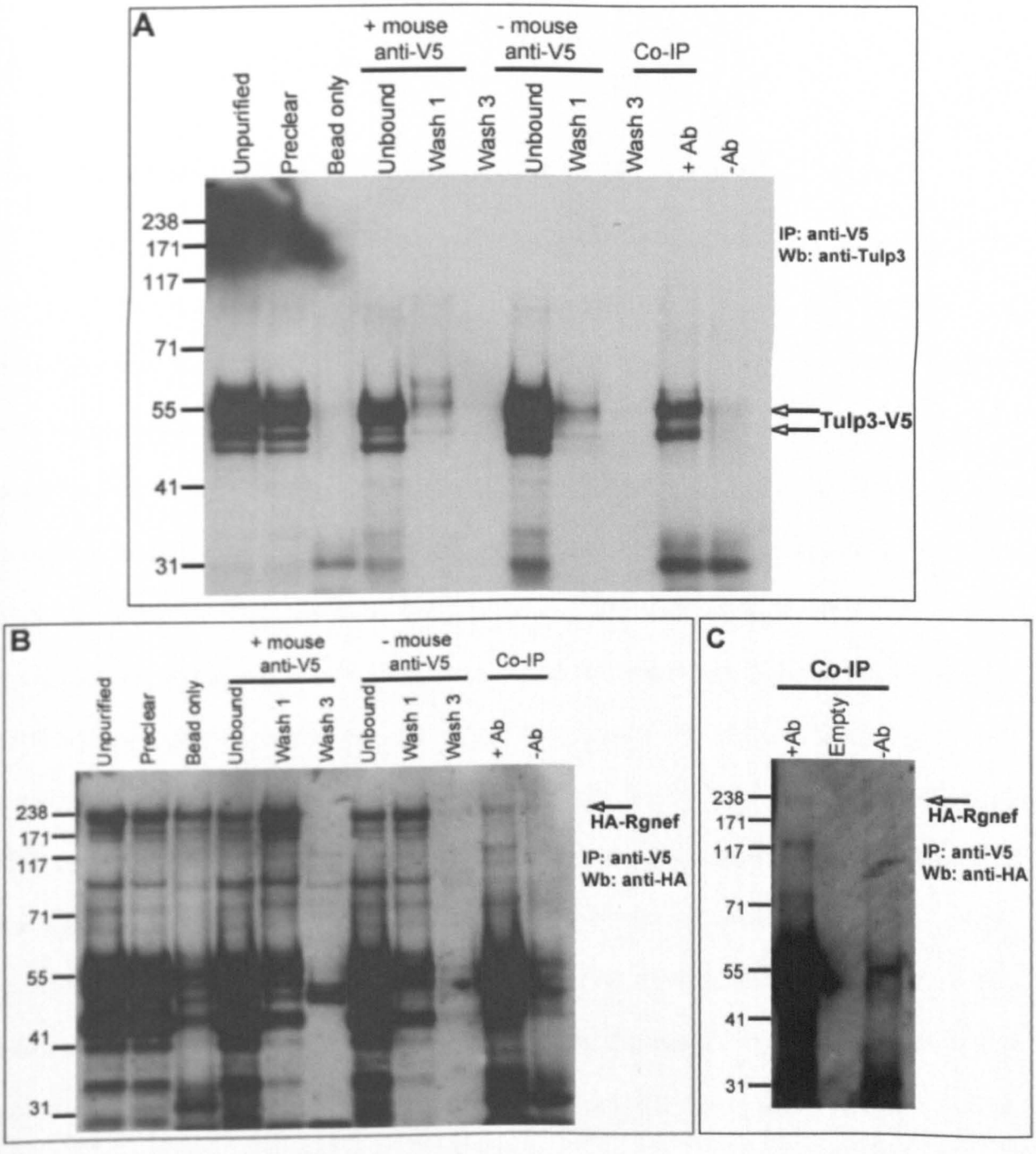

Figure 7-11: Co-IP to purify HA-Rgnef with Tulp3-V5 using dynabeads and mouse anti-V5 antibody.

(A - C) Western blots of IP with and without the mouse anti-V5 antibody to purify Tulp3-V5 and its associated complexes. (A) Probed with rabbit anti-Tulp3 antibody to identify Tulp3-V5. (B and C) Probed with mouse anti-HA antibody to determine whether HA-Rgnef was present in a complex with Tulp3-V5. Details of samples loaded in each lane are given in Figure 7-7.

7.3 Discussion

7.3.1 Expression profile of putative interaction partners of Tulp3

Tulp3 is ubiquitously expressed and yet analysis of *Tulp3* mutants suggests that only certain tissues are affected by the loss of *Tulp3* during development. This suggests that, although Tulp3 is present everywhere, it may have different roles in different tissues or that its role is compensated by other members of the Tulp family in certain tissues. Tissue-specific roles for Tulp3 may arise from interaction with different proteins that are present in specific tissues. Indeed, it is possible that interacting partners are absent from particular tissues, so that Tulp3 is not functionally active in these locations; this might perhaps explain why some tissues exhibit no phenotype when Tulp3 is mutated. A yeast 2-hybrid screen was carried out to identify the interacting partners of Tulp3 and this resulted in identification of nine genes corresponding to proteins that could potentially interact with Tulp3. One of these genes (RIKEN cDNA 4931406P16 gene) was not pursued further because it is predicted to encode for a protein without any recognizable domains and it was represented by only one clone; therefore was consider to be a low priority gene. Reverse transcriptase PCR showed that the other eight genes that came out of the yeast 2-hybrid screen were all expressed during neurulation (E8.5-E10.5), increasing the chance that they may be interacting with Tulp3 to regulate neural tube closure or patterning. To determine the expression domains of these genes and to investigate if any of these genes are expressed in tissue important for dorsoventral patterning of the neural tube and its closure (and hence interact with Tulp3 to regulate these processes) I performed whole mount *in situ* hybridization. The expression pattern of *Trim71* and *Alx1* during mouse development has been reported previously (Zhao et al., 1996; Lancman et al., 2005; Kanamoto et al., 2006), therefore the distribution of these genes was not

analyzed. Ccnb1 is a very well characterized protein and it is involved in regulating cell cycle. It is an essential component of all cell types suggesting that it is unlikely to be a protein that interacts with Tulp3 to establish the dorsoventral patterning of the neural tube and regulate its closure. This of course does not rule out the possibility that Ccnb1 and Tulp3 physically interact to regulate cell cycle; however, the main aim of this study was to identify proteins that interact with Tulp3 to regulate dorsoventral patterning and neural tube closure. For this reason expression pattern of *Ccnb1* was not analyzed.

The expression patterns of the other five genes (*Fam193a, Nup155, Ibrdc1* and *Rgnef*) have not been reported and their functions during mouse development have not been studied in detail, therefore their distribution was analyzed. Analysis of whole embryos shows that *Fam193a, Nup155* and *Ktn1* are ubiquitously expressed from E8.5 to E9.5. The lack of staining in control embryos probed with sense probes for these genes shows that all the staining we see in the embryos probed with anti-sense probe represents the actual expression of the gene. Probes used in this experiment were designed to detect all transcripts of each gene. There are two transcripts known for *Fam193a*, six for *Ktn1* and one for *Nup155* (Ensembl). It would be interesting to determine the expression pattern of each of the transcripts for *Fam193a* and *Ktn1* as they might reveal specific expression patterns which might indicate different roles for each of the transcripts. Interestingly, analysis of sections through the caudal ends of embryos showed that the expression of *Nup155* and *Ktn1* appears stronger in the dorsal region of the neural tube at E9.5 although at E8.5 there is no dorsoventral difference. Whether this variation in the level of expression between the dorsal half and the ventral half of the neural tube suggests a role for these proteins in dorsoventral patterning remains to be elucidated. This can be determined by analyzing dorsoventral patterning of the neural tube in embryos where the expression of *Nup155* and *Ktn1* is abolished. Mutation of *Nup155* is embryonic lethal and mutants die prior to E10.5 (Zhang et

al., 2008) therefore the role of *Nup155* in dorsoventral patterning of the neural tube can only be revealed by generating a mouse mutant line where the function is specifically disrupted in the developing neural tube. Surprisingly, the mutant of *Ktn1* is reported to be viable and normal (Plitz and Pfeffer, 2001) therefore any disruption in the dorsoventral patterning of the neural tube (if present) is likely to be very minor. Sections were not generated from embryos stained with *Fam193a* because the expression pattern of this gene was very weak and the staining was barely detectable, even in the whole embryos. The fact that *Fam193a, Nup155* and *Ktn1* are expressed ubiquitously, similar to *Tulp3*, suggests that they may interact together to regulate many different cellular functions and not just the dorsoventral patterning of the neural tube.

The expression pattern of *Ibrdc1* is interesting. At E8.5 it is ubiquitously expressed however by E9.5 it becomes highly enriched in the somites and stays on until E10.5. This expression pattern suggests that Tulp3 may interact with Ibrdc1 in the somites, perhaps explaining the vertebral defects observed in *hhkr* (Patterson et al., 2009).

The expression pattern of *Rgnef* during neurulation suggested that it is an excellent candidate gene for regulating Shh signalling with *Tulp3* during patterning of the neural tube. It is most highly expressed in the cells where the highest level of Shh is present i.e. the floor plate. Furthermore, it shows a difference in the level of expression in the rostral-caudal axis, where it is more strongly expressed in the rostral floor plate compared to the caudal floor plate. This is exciting because the function of Tulp3 is known to be different between the rostral neural tube and the caudal neural tube. In *hhkr*, the dorsoventral patterning defect and the neural tube closure defect are only observed in the caudal end of the embryo and not along the entire axis (Patterson et al., 2009). It is tempting to speculate that Rgnef may be acting on Tulp3 to inhibit the function of Tulp3 during neural tube development.

7.3.2 Detection of Rgnef and Tulp3 in transfected cells

The expression profile of *Rgnef* suggests that it is a good candidate binding partner of Tulp3 in its function in regulating dorsoventral patterning of the neural tube. To determine whether *Tulp3* and *Rgnef* form a complex when expressed together, I performed a co-immunoprecipitation experiment by transfecting HA-Rgnef and Tulp3-V5 constructs into HEK293T cells. Running the protein lysate extracted from cells transfected with HA-Rgnef construct on a protein gel and probing with an antibody against HA resulted in multiple bands. These multiple bands were not observed when lysate from mock transfected cells was used, suggesting that all extra bands that were detected in HA-Rgnef transfected cells were protein produced from the plasmid and are likely to be degraded or truncated product of the full length HA-Rgnef. This idea could be confirmed by probing the same blot with an antibody raised against full length Rgnef; however, we did not have access to this antibody.

The predicted size of Rgnef is 190 kDa and the HA tag is approximately 9 kDa; hence a band of ~200 kDa was expected for HA-Rgnef. The heaviest band that was present in the HA-Rgnef transfected cells was considered to be the band corresponding to the full length HA-Rgnef. This top band is slightly higher than the predicted 200 kDa, however it has been reported previously that Rgnef without any tag migrates more slowly on a protein gel than predicted so it appears ~200kDa instade of 190 kDa, and is thought to result from charges present in the coiled-coiled domain at the C-terminal region of Rgnef (Gebbink et al., 1997).

Running the protein lysate from cells transfected with Tulp3-V5 and probing it with rabbit anti-Tulp3 antibody resulted in detection of two bands of approximately 55 kDa. These are close to the predicted size of full length Tulp3. The smaller of these two bands is thought to arise from an alternative start site that is present towards the 5' end of the construct (personal communication with Ms V. Patterson). Smaller bands are also detected in the western blot upon probing for Tulp3. These bands are likely to be degraded protein products

as Lipofectamine is partly cytotoxic to cells therefore a proportion of cells may have been dead before the protein was extracted.

7.3.3 Validating the interaction between Tulp3 and Rgnef

Protein lysate from doubly transfected cells was used to perform co-immunoprecipitation studies using two different systems. Mouse anti-HA antibody and mouse anti-V5 antibody were bound to protein G sepharose beads or to protein G dynabeads and the lysate from doubly transfected cells was applied. The purified complex was run on a protein gel and probed with rabbit anti-Tulp3 antibody and mouse anti-HA antibody to detect Tulp3-V5 and HA-Rgnef, respectively. Mouse anti-V5 antibody was not used to detect Tulp3-V5 because mouse anti-HA antibody was used in IP hence an anti-mouse secondary antibody would detect the heavy chain of mouse immunoglobulin arising from the anti-HA antibody as well as from the anti-V5 antibody bound to Tulp3-V5 protein. This would be a problem because the size of both Tulp3-V5 and the heavy chain of immunoglobulin are ~55 kDa; therefore the signal from Tulp3-V5 would not be distinct. This was avoided by using anti-Tulp3 antibody as it was raised in rabbit, and an anti-rabbit secondary antibody could be used to detect Tulp3-V5 specifically and avoid any signals from mouse immunoglobulin.

Co-IP was performed with two separate systems; sepharose beads and dynabeads. The Co-IP experiment using sepharose beads was more successful when mouse anti-HA antibody was used to purify HA-Rgnef and its associated complexes. This showed that a detectable level of full length HA-Rgnef was purified in IP with the antibody and the level of this protein was very low in the control experiment where antibody was not present. Furthermore, probing the same blot with a rabbit anti-Tulp3 antibody showed that the band corresponding to the full length Tulp3-V5 was more intense in the lane from IP with antibody than without the

antibody. The fact that there was a detectable level of Tulp3-V5 present in the IP lane without the antibody suggests that this experiment needs to be further optimized, perhaps by increasing the number and stringency of washes. This is likely to reduce some signal in the IP without the antibody lane without affecting the signal in the IP with the antibody lane. Evidence for this comes from analyzing the strength of signal observed in two washes. In the sample where the antibody was present during the IP, the wash 2 lane is clear suggesting that all of the unbound Tulp-V5 was removed in wash 1 so any signal we see in the eluate was from Tulp3-V5 that was bound to the antibody conjugated to the bead. In the negative control, where the antibody was not used during IP, the majority of the protein is removed in wash 1; however, a detectable level of Tulp3-V5 is also present in wash 2. This indicates that, at least part of the signal observed in the negative IP lane is due to non specific binding of Tulp3-V5 that could be removed by further washes. It must be noted that the higher stringency washes may result in dissociation of the interaction between two proteins. To avoid this, the cells could be treated with protein crosslinking agents such as glutaraldehyde, prior to IP experiment in order to be able to use more stringent washes.

Using sepharose beads to purify Tulp3-V5 was unsuccessful as high levels of this protein were detected in both IP with antibody and in negative control lanes. However it must be noted that the intensity of the Tulp3-V5 band in both lanes is so high that any enrichment in the IP with the antibody would not be detected due to signal saturation. Again this needs to be further optimized by increasing the number of washes, as high levels of Tulp3-V5 are detected in both washes. Surprisingly, probing the same blot with mouse anti-HA antibody indicates that HA-Rgnef was enriched in the IP where antibody was used compared to the negative control; this would be consistent with the idea that Tulp3-V5 may be enriched in the IP with the antibody compared to the negative control. This could be clarified by running less protein in the IP lanes so the signal for Tulp3-V5 would not saturate. However, in doing this detection

of HA-Rgnef band might not be possible as the intensity of the band corresponding to full length HA-Rgnef is very low compared to that of Tulp3-V5; therefore reducing the amount of protein loaded to the gel may result in an undetectable level of HA-Rgnef.

The IP experiment using dynabeads failed to purify HA-Rgnef and its associated complexes. It appears that HA-Rgnef binds non-specifically to beads as a large amount is present in the bead only eluate. Furthermore, similar levels of this protein are present in the unbound fraction of both IP with antibody and in IP where no antibody was used, suggesting that the antibody was not purifying HA-Rgnef. In both the IP samples, with and without the antibody, a very low level of the band corresponding to full length HA-Rgnef is detected, suggesting that most of the HA-Rgnef has been removed in the wash steps. When the same blot was probed with rabbit anti-Tulp3, a faint band corresponding to Tulp3-V5 was detected in both IP with antibody and without antibody. This result suggests that dynabeads are not suitable for purifying HA-Rgnef as the protein appears to stick to the beads in a non-specific manner.

The IP experiment using dynabeads to purify Tulp3-V5 was successful and probing the same blot with mouse anti-HA resulted in detection of a faint band corresponding to the full length HA-Rgnef in the IP with antibody lane and this band was absent from the negative control. This suggests that Tulp3 and Rgnef are present in a complex. The reason why the band corresponding to HA-Rgnef is weak could be because a large proportion of this protein is lost in the unbound fraction and the washes.

Data presented in this report shows that sepharose bead system is more suitable for purifying HA-Rgnef than the dynabeads system. However, satisfactory levels of purification of Tulp3-V5 are only achieved when dynabeads were used. These results suggest that a different method of purification is required to achieve a convincing co-IP result. One way to overcome the problem of HA-Rgnef sticking to the dynabeads non-specifically might be to

use a truncated form of Rgnef as it might remove protein domains that are making HA-Rgnef stick to the dynabeads. Data from the yeast 2-hybrid result suggest that the DH domain of Rgnef is binding to Tulp3. Therefore, to validate this interaction a smaller construct encoding the DH domain of Rgnef could be used. Alternatively, there are several options available to purify a protein of interest. The simplest option is to use protein A conjugated beads instead of protein G as it might enable the antibody to bind more strongly to the beads and purify more protein. However, both mouse-IgG (anti HA antibody) and Rabbit-IgG (anti V5 antibody) are predicted to bind to both protein G and protein A with high efficiency. Other options would include pull down experiments using His-tagged proteins and purifying the protein and its complexes with nickel beads. Additionally there are many columns that are available to purify proteins of interest such as Sephadex Columns, Suprose Columns and Superdex Columns.

Despite the problems associated with protein purification in the two systems used in this project, there is some evidence to support the hypothesis that Tulp3 and Rgnef form a complex. In experiments with sepharose beads it is seen that the level of Tulp3-V5 and HA-Rgnef is enriched in the IP with mouse anti-HA antibody and mouse anti-V5 antibody, compared to the negative control. In experiments with dynabeads, IP with mouse anti-V5 antibody specifically purifies Tulp3-V5 and HA-Rgnef, suggesting that they form a complex.

7.3.4 The link between Rgnef and Shh signalling

Although *Rgnef* has not been directly implicated in the Shh signalling pathway, there are some lines of evidence to support its role in the pathway. It has been established that Smo is a G-Protein coupled receptor (GPCR) that signals through heterotrimeric G proteins and RhoA (Kasai et al., 2004; Ogden et al., 2008). Kasai *et al* show that increasing Shh ligand results in increased level activated RhoA and blockage of $G_{\alpha 12}$ heterotrimeric G proteins

results in a phenotype which suggest a decrease in Shh activity, suggesting that both of these proteins are involved in Shh signalling. Furthermore, there is evidence to suggest that the signal from activated heterotrimeric G protein is required to activate RhoGEFs before they are able to induce GDP/GTP exchange on RhoGTPases (Hart et al., 1998; Kozasa et al., 1998). Although there is no direct data to suggest that *Rgnef* is stimulated by heterotrimeric G, there is evidence to indicate that one or more cellular component(s) is required to unmask its ability to induce GDP/GTP exchange on RhoA. Evidence for this comes from a study where truncated *Rgnef* consisting of only the PH/DH domain is able to catalyse GDP/GTP exchange *in vitro*; in contrast the full length protein is not. The full length Rgnef is only able to catalyses GDP/GTP exchange on RhoA *in vivo* (van Horck et al., 2001).

In addition there is evidence suggesting that Tubby and Tulp3 both signal through G proteins (Santagata et al., 2001). It has been shown that Tubby and Tulp3 associate with the plasma membrane by binding to phosphatidylinositol 4,5-bisphosphate [PtdIns(4,5)P_2] via its C-terminal domain and it translocates to the nucleus after stimulation of $G\alpha_q$ or $G\alpha_{11}$ G-protein. Furthermore they show that Tubby physically interacts with activated and non-activated $G\alpha_q$.

It could be hypothesized that, in the absence of a signal from G-proteins, inactive Tulp3 and Rgnef form a complex masking each other's activity. Once the signal for heterotrimeric G-protein is presented Tulp3 and Rgnef dissociate, unmasking the active site of both proteins. Following this dissociation an unknown cellular factor activates Rgnef, which is able to catalyze GDP/GTP exchange in RhoA and activate the transcription of Shh target genes through an unknown mechanism. Dissociated Tulp3 translocates into the nucleus, where it may act to inhibit transcription of Shh target genes (Figure 7-12). Using this model it is also possible to explain the differences observed between the rostro-caudal spinal neural tube in *Tulp3* mutants, where the rostral neural tube patterning and its closure appears to be

independent of Tulp3, whereas the caudal neural tube closure and its patterning requires the function of Tulp3 (Ikeda et al., 2001; Norman et al., 2009; Patterson et al., 2009). I have shown that the level of *Rgnef* is higher in the rostral end of the embryo compared to the caudal end, in contrast the expression pattern of Tulp3 is reported to be ubiquitous and no substantial difference in the level of expression between the rostral and the caudal ends have been reported (Ikeda et al., 2001). It could be hypothesized that in the rostral end, a large proportion of Rgnef is not bound to Tulp3 because the level of Tulp3 is not as high as the level of Rgnef. This means that unbound Rgnef is able to transducer the Shh signal independently of Tulp3, supporting the result that Tulp3 mutants do not show a defect in Shh signalling in the rostral spinal cord. In the caudal spinal cord, the level of Rgnef is low while the level of Tulp3 has not changed. This may mean that most of Tulp3 is found to be dissociated and functions to inhibit the Shh target genes, and therefore Shh signalling depends on Tulp3. In intermediate neural tube, where the levels of Tulp3 and Rgnef may be equal, the dissociation between Rgnef and Tulp3 is required before the Shh signal is transduced; therefore Shh signalling partly depends on the function of Tulp3. This is supported by the observation that in *hhkr* the intermediate spinal neural tube is not as severely affected as the caudal spinal region, but a disruption in neural tube patterning is seen (personal communication with Dr J. N. Murdoch). To test this hypothesis, it is necessary to examine the dorsoventral patterning of the neural tube in an embryo that has lost the function of *Rgnef*. If this hypothesis is correct then we would see a reduced level of Shh signalling in the rostral spinal cord due to over activation of Tulp3 and failure to activate RhoA through Rgnef. Patterning in the caudal spinal cord, which is predicted to be largely independent of Rgnef, will be mostly normal.

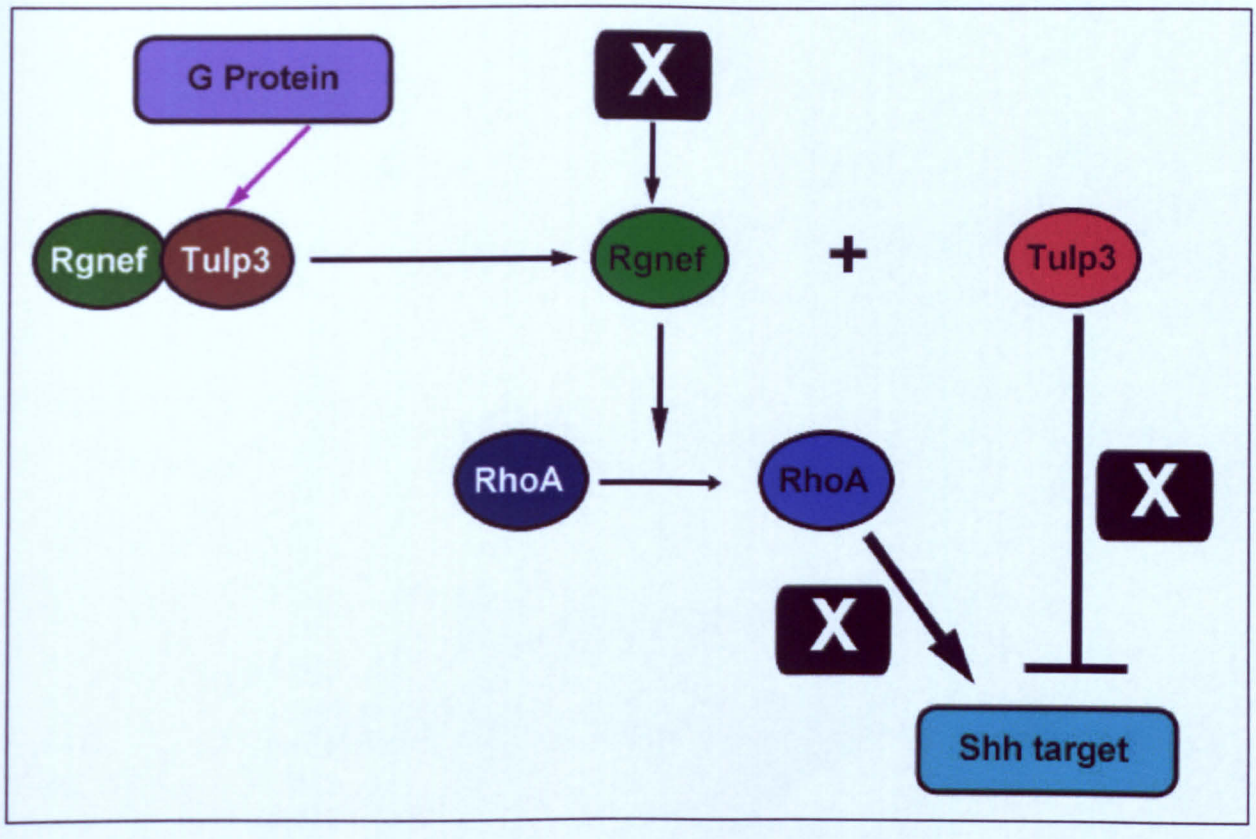

Figure 7-12: Proposed relationship between Tulp3 and Rgnef
Inactive Rgnef (dark green) and inactive Tulp3 (dark red) form a complex which dissociates after a signal from a G protein is presented. Dissociated Rgnef becomes activated (light green) by an unknown cellular component (black) and Tulp3 is activated (bright red) following dissociation from Rgnef. Activated Rgnef, activates RhoA (bright blue) from its inactive state (dark blue) and this results in transcriptional activation of Shh target genes. The activated Tulp3 inhibits the transcriptional activation of the Shh target genes.

CHAPTER 8

GENERAL DISCUSSION

8 General Discussion

The aim of this project was to investigate the genetic, cellular and molecular defects leading to neural tube defects in mice. I have analyzed the phenotypes of three different mouse mutants, all exhibiting neural tube defects. *chuzhoi* is a novel allele of *Ptk7*, *Circletail* is a mutant of *Scribble* (Murdoch et al., 2003) and *hitchhiker* is a strongly hypomorphic allele of *Tulp3* (Patterson et al., 2009).

8.1 Summary of results

In this thesis I have shown that *chuzhoi*, exhibiting craniorachischisis, carries a point mutation in *Ptk7* which affects splicing. *chuzhoi* mutants exhibit many phenotypes that are identical to the phenotypes observed in well established PCP mutants such as *Loop-tail, Circletail* and *Crash* and I have shown that *chuzhoi* genetically interacts with *Loop-tail* and *Crash*. Despite this, some of the phenotypes, such as limb defects, observed in *chuzhoi* are unique to *Ptk7* mutants. Furthermore the genetic interaction observed between *Ptk7* and the core members of the PCP pathway is of a weak nature. To obtain a hint towards understanding the molecular role of Ptk7 by identifying its interaction partners, a yeast 2-hybrid screen was carried out using the intracellular domain of Ptk7. This screen failed to identify any interacting partners.

It has been established that the primary defect leading to craniorachischisis in all mutants examined is the failure to narrow the embryonic midline. To address the possibility that orientation of cell division may play a role in narrowing of the embryonic midline, I measured the angle of cell division in the neuroepithelium of mouse embryos just prior to the

initiation of neural tube closure, at the site of closure 1. Results show that the orientation of cell division at this embryonic stage and at the site of closure 1 is random in mice.

To address the possibility that Tulp3 may function as a transcription factor, I performed a microarray screen to identify genes that are differentially expressed in *hhkr* compared to wildtype. This screen failed to identify any genes that were highly up- or down-regulated in *hhkr* mutants, when the function of Tulp3 was dramatically reduced, giving no evidence to support the hypothesis that Tulp3 acts as a transcription factor. To uncover the molecular role of Tulp3 by identifying its interacting partners, a yeast 2-hybrid screen was carried out. This identified nine putative interacting partners of Tulp3. Based on the expression pattern, *Rgnef* (one of the putative interaction partners) was chosen for validation by co-IP. My co-IP result suggests that Rgnef and Tulp3 may form a complex *in vitro*.

8.2 Contribution to the field

Results reported in this thesis are largely negative; however, some important conclusions can be drawn from these results.

Previously it was reported that Ptk7 is a regulator of the PCP pathway (Lu et al., 2004). In this thesis I have confirmed that Ptk7 has an ability to influence PCP signalling; however, my data suggests that it is unlikely to be a core component of the pathway. Additionally, detailed phenotypic studies show that some of the phenotypes observed in *chuzhoi* are different from those observed in core PCP mutants suggesting that Ptk7 may also have PCP-independent role(s).

Drosophila Scribble was originally reported to be an essential component required for the establishment of the apical-basal polarity and controlling the rate of proliferation (Bilder et al., 2000; Bilder and Perrimon, 2000). My data shows that the apical-basal polarity and the

rate of proliferation in the neuroepithelium of embryos undergoing neurulation is not affected when the function of Scribble is abolished, suggesting that mouse Scribble is not required for the establishment of apical-basal polarity and controlling rate of proliferation during neurulation.

Controlled orientation of *cell division* has been described as a mechanism for tissue elongation in many systems (Keller, 2006). Indeed, it has been shown that the PCP-dependent orientation of cell division is required for embryonic elongation during zebrafish gastrulation and renal tubule elongation during mammalian kidney development (Gong et al., 2004; Fischer et al., 2006). Since mutants of PCP signalling are characterized by a reduced rate of embryonic elongation leading to severe neural tube defects, we speculated that PCP-controlled orientation of cell division may play a role toward shaping the embryo prior to initiation of neural tube closure. Data presented in this thesis shows that the orientation of cell division in the neuroepithelium of embryos just prior to initiation of neural tube closure and at the site of closure 1 is random, suggesting that the orientation of cell division is not a mechanism for embryonic elongation in mouse.

In this thesis, two approaches were used to investigate the role of Tulp3; a microarray screen and a yeast 2-hybrid screen. Results from these studies suggest that Tulp3 is not likely to function by controlling the expression level of certain gene(s) but may be involved in many cellular functions by interacting with various different proteins. It remains to be seen how Tulp3 is dispensing its role as a negative regulator of the Shh signalling.

8.3 Future work

Understanding the role of Tulp3 during the neural tube closure and its patterning should be the major focus of any future work. For this it is important to identify the true interacting

partners of Tulp3 and understand how they are working together at a molecular level to regulate the neural tube closure and its patterning. In this thesis I have argued that Rgnef is a good candidate to interact with Tulp3 during neural tube development; however, this work needs to be taken further to understand how Tulp3 functions with Rgnef to negatively regulate Shh signalling. To do this, it is essential to perform experiments to understand the function of Rgnef and determine whether or not it has a potential to regulate Shh signalling.

Rgnef is required to activate RhoA. To determine whether or not this function of Rgnef is modulated by Tulp3, the ratio of activated RhoA and total RhoA can be examined in *hhkr*. This can be done by western blot using protein extracted from *hhkr* and wildtype littermates and probing the blot with an antibody to recognize the phosphorylated form of RhoA and a second antibody to recognize the total RhoA in the sample.

It has been previously shown that the N-terminal domain of p155RhoGEF can act as a dominant negative form to reduce the Shh signalling when electroporated into the developing neural tube of a rat embryo (Kasai et al., 2004). A similar experiment could be performed to investigate whether or not Rgnef can influence Shh signalling. During this experiment the N-terminal domain of *Rgnef* (*p190RhoGEF*), which may act in a similar fashion to the N-terminal domain of p155RhoGEF, will be electroporated into the developing neural tube of a mouse (or other model organism) embryo and the dorsoventral patterning of the neural tube could be analyzed to determine whether or not Shh signalling is affected.

To understand the role of *Rgnef* in Shh signalling, it is important to determine whether or not expression of *Rgnef* precedes the expression of *Shh*. This could be achieved by determining the precise stage at which *Rgnef* and *Shh* are first expressed in the floorplate and the notochord of the embryo. If it is found that expression of *Rgnef* precedes *Shh* expression then it is essential to analyze the expression of *Shh* when the function of Rgnef is abolished as it may indicate that Rgnef is required for the expression of *Shh*. Similarly if it is found that the

expression of *Shh* precedes the expression of *Rgnef* then the expression of *Rgnef* can be examined in *Shh* mutants to determine whether or not the expression of *Rgnef* is dependent on Shh signalling.

Finally, it is also important to determine whether or not Rgnef localizes to the primary cilia where the Shh signalling takes place in vertebrates. This can be achieved by performing immunohistochemistry on ciliated cells expressing *Rgnef* and using an antibody against Rgnef to determine its subcellular localization. It has been published that Rgnef binds to microtubules (van Horck et al., 2001), supporting the idea that it may localize to the cilia.

8.4 Concluding remarks

In this thesis I have investigated the roles of three genes associated with neural tube defects in mouse: *Ptk7* and *Scribble* (effectors of PCP), and *Tulp3* (a Shh negative regulator). Specifically, I have phenotypically assessed chemically-induced mutations in *Ptk7* and *Tulp3* (*chuzoi* and *hitchhiker* respectively); as well as the *Scribble* point mutant *circletail*. The identification and analysis of such mouse models will continue to be of crucial importance to aid our understanding of the underlying molecular mechanisms of neural tube development and the defects associated with its failed closure. Ultimately, the results of these studies can be applied in a pharmacological and medical setting, with the hope of treating the otherwise devastating conditions of failed neurulation.

CHAPTER 9

REFERENCES

9 References

Adams, R.J. (1996). Metaphase spindles rotate in the neuroepithelium of rat cerebral cortex. J Neurosci *16*, 7610-7618.

Ahmad, F.U., and Mahapatra, A.K. (2009). Neural tube defects at separate sites: further evidence in support of multi-site closure of the neural tube in humans. Surg Neurol *71*, 353-356.

Amin, M., Uhlig, H.H., Kamprad, M., Karbe, J., Osman, A.A., Grahmann, F., Hummelsheim, H., and Mothes, T. (2001). Neurological disease-associated autoantibodies against an unknown protein encoded by a RES4-22 homologous gene. Scand J Immunol *53*, 204-208.

Au, K.S., Ashley-Koch, A., and Northrup, H. (2010). Epidemiologic and genetic aspects of spina bifida and other neural tube defects. Dev Disabil Res Rev *16*, 6-15.

Aza-Blanc, P., Lin, H.Y., Ruiz i Altaba, A., and Kornberg, T.B. (2000). Expression of the vertebrate Gli proteins in Drosophila reveals a distribution of activator and repressor activities. Development *127*, 4293-4301.

Aza-Blanc, P., Ramirez-Weber, F.A., Laget, M.P., Schwartz, C., and Kornberg, T.B. (1997). Proteolysis that is inhibited by hedgehog targets Cubitus interruptus protein to the nucleus and converts it to a repressor. Cell *89*, 1043-1053.

Baena-López, L.A., Baonza, A., and García-Bellido, A. (2005). The Orientation of Cell Divisions Determines the Shape of Drosophila Organs. Current Biology *15*, 1640-1644.

Bai, C.B., Auerbach, W., Lee, J.S., Stephen, D., and Joyner, A.L. (2002). Gli2, but not Gli1, is required for initial Shh signaling and ectopic activation of the Shh pathway. Development *129*, 4753-4761.

Bai, C.B., and Joyner, A.L. (2001). Gli1 can rescue the in vivo function of Gli2. Development *128*, 5161-5172.

Bai, C.B., Stephen, D., and Joyner, A.L. (2004). All mouse ventral spinal cord patterning by hedgehog is Gli dependent and involves an activator function of Gli3. Dev Cell *6*, 103-115.

Balda, M.S., and Matter, K. (2000). The tight junction protein ZO-1 and an interacting transcription factor regulate ErbB-2 expression. EMBO J *19*, 2024-2033.

Bilder, D., Li, M., and Perrimon, N. (2000). Cooperative regulation of cell polarity and growth by Drosophila tumor suppressors. Science *289*, 113-116.

Bilder, D., and Perrimon, N. (2000). Localization of apical epithelial determinants by the basolateral PDZ protein Scribble. Nature *403*, 676-680.

Bilder, D., Schober, M., and Perrimon, N. (2003). Integrated activity of PDZ protein complexes regulates epithelial polarity. Nat Cell Biol *5*, 53-58.

Bitgood, M.J., Shen, L., and McMahon, A.P. (1996). Sertoli cell signaling by Desert hedgehog regulates the male germline. Curr Biol *6*, 298-304.

Boehlke, C., Bashkurov, M., Buescher, A., Krick, T., John, A.K., Nitschke, R., Walz, G., and Kuehn, E.W. (2010). Differential role of Rab proteins in ciliary trafficking: Rab23 regulates smoothened levels. J Cell Sci *123*, 1460-1467.

Bogani, D., Willoughby, C., Davies, J., Kaur, K., Mirza, G., Paudyal, A., Haines, H., McKeone, R., Cadman, M., Pieles, G., *et al.* (2005). Dissecting the genetic complexity of human 6p deletion syndromes by using a region-specific, phenotype-driven mouse screen. *Proc Natl Acad Sci U S A 102*, 12477-12482.

Boggon, T.J., Shan, W.S., Santagata, S., Myers, S.C., and Shapiro, L. (1999). Implication of tubby proteins as transcription factors by structure-based functional analysis. Science *286*, 2119-2125.

Botto, L.D., Moore, C.A., Khoury, M.J., and Erickson, J.D. (1999). Neural-tube defects. N Engl J Med *341*, 1509-1519.

Boutros, M., Paricio, N., Strutt, D.I., and Mlodzik, M. (1998). Dishevelled activates JNK and discriminates between JNK pathways in planar polarity and wingless signaling. Cell *94*, 109-118.

Brandeis, M., Rosewell, I., Carrington, M., Crompton, T., Jacobs, M.A., Kirk, J., Gannon, J., and Hunt, T. (1998). Cyclin B2-null mice develop normally and are fertile whereas cyclin B1-null mice die in utero. Proc Natl Acad Sci U S A *95*, 4344-4349.

Briscoe, J., Pierani, A., Jessell, T.M., and Ericson, J. (2000). A homeodomain protein code specifies progenitor cell identity and neuronal fate in the ventral neural tube. Cell *101*, 435-445.

Brugieres, L., Pierron, G., Chompret, A., Paillerets, B.B., Di Rocco, F., Varlet, P., Pierre-Kahn, A., Caron, O., Grill, J., and Delattre, O. (2010). Incomplete penetrance of the predisposition to medulloblastoma associated with germ-line SUFU mutations. J Med Genet *47*, 142-144.

Brumby, A., Secombe, J., Horsfield, J., Coombe, M., Amin, N., Coates, D., Saint, R., and Richardson, H. (2004). A genetic screen for dominant modifiers of a cyclin E hypomorphic mutation identifies novel regulators of S-phase entry in Drosophila. Genetics *168*, 227-251.

Bulgakov, O.V., Eggenschwiler, J.T., Hong, D.H., Anderson, K.V., and Li, T. (2004). FKBP8 is a negative regulator of mouse sonic hedgehog signaling in neural tissues. Development *131*, 2149-2159.

Bustin, S.A. (2000). Absolute quantification of mRNA using real-time reverse transcription polymerase chain reaction assays. J Mol Endocrinol *25*, 169-193.

Cameron, D.A., Pennimpede, T., and Petkovich, M. (2009). Tulp3 is a critical repressor of mouse hedgehog signaling. Dev Dyn *238*, 1140-1149.

Canete-Soler, R., Wu, J., Zhai, J., Shamim, M., and Schlaepfer, W.W. (2001). p190RhoGEF Binds to a destabilizing element in the 3' untranslated region of light neurofilament subunit mRNA and alters the stability of the transcript. J Biol Chem *276*, 32046-32050.

Casal, J., Lawrence, P.A., and Struhl, G. (2006). Two separate molecular systems, Dachsous/Fat and Starry night/Frizzled, act independently to confer planar cell polarity. Development *133*, 4561-4572.

Caspary, T., Larkins, C.E., and Anderson, K.V. (2007). The graded response to Sonic Hedgehog depends on cilia architecture. Dev Cell *12*, 767-778.

Chen, M.H., Gao, N., Kawakami, T., and Chuang, P.T. (2005). Mice deficient in the fused homolog do not exhibit phenotypes indicative of perturbed hedgehog signaling during embryonic development. Mol Cell Biol *25*, 7042-7053.

Chiang, C., Litingtung, Y., Lee, E., Young, K.E., Corden, J.L., Westphal, H., and Beachy, P.A. (1996). Cyclopia and defective axial patterning in mice lacking Sonic hedgehog gene function. Nature *383*, 407-413.

Chou, Y.H., and Hayman, M.J. (1991). Characterization of a member *of the immunoglobulin* gene superfamily that possibly represents an additional class of growth factor receptor. Proc Natl Acad Sci U S A *88*, 4897-4901.

Ciruna, B., Jenny, A., Lee, D., Mlodzik, M., and Schier, A.F. (2006). Planar cell polarity signalling couples cell division and morphogenesis during neurulation. Nature *439*, 220-224.

Concha, M.L., and Adams, R.J. (1998). Oriented cell divisions and cellular morphogenesis in the zebrafish gastrula and neurula: a time-lapse analysis. Development *125*, 983-994.

Conlon, F.L., Lyons, K.M., Takaesu, N., Barth, K.S., Kispert, A., Herrmann, B., and Robertson, E.J. (1994). A primary requirement for nodal in the formation and maintenance of the primitive streak in the mouse. Development *120*, 1919-1928.

Copp, A.J., Brook, F.A., Estibeiro, J.P., Shum, A.S., and Cockroft, D.L. (1990). The embryonic development of mammalian neural tube defects. Prog Neurobiol *35*, 363-403.

Copp, A.J., Checiu, I., and Henson, J.N. (1994). Developmental basis of severe neural tube defects in the loop-tail (Lp) mutant mouse: use of microsatellite DNA markers to identify embryonic genotype. Dev Biol *165*, 20-29.

Copp, A.J., Greene, N.D., and Murdoch, J.N. (2003). The genetic basis of mammalian neurulation. Nat Rev Genet *4*, 784-793.

Courbard, J.R., Djiane, A., Wu, J., and Mlodzik, M. (2009). The apical/basal-polarity determinant Scribble cooperates with the PCP core factor Stbm/Vang and functions as one of its effectors. Dev Biol *333*, 67-77.

Curtin, J.A., Quint, E., Tsipouri, V., Arkell, R.M., Cattanach, B., Copp, A.J., Henderson, D.J., Spurr, N., Stanier, P., Fisher, E.M., *et al.* (2003). Mutation of Celsr1 disrupts planar polarity of inner ear hair cells and causes severe neural tube defects in the mouse. Curr Biol *13*, 1129-1133.

da Silva, S.M., and Vincent, J.P. (2007). Oriented cell divisions in the extending germband of Drosophila. Development *134*, 3049-3054.

Dabdoub, A., Donohue, M.J., Brennan, A., Wolf, V., Montcouquiol, M., Sassoon, D.A., Hseih, J.C., Rubin, J.S., Salinas, P.C., and Kelley, M.W. (2003). Wnt signaling mediates reorientation of outer hair cell stereociliary bundles in the mammalian cochlea. Development *130*, 2375-2384.

Dai, P., Akimaru, H., Tanaka, Y., Maekawa, T., Nakafuku, M., and Ishii, S. (1999). Sonic Hedgehog-induced activation of the Gli1 promoter is mediated by GLI3. J Biol Chem *274*, 8143-8152.

Darken, R.S., Scola, A.M., Rakeman, A.S., Das, G., Mlodzik, M., and Wilson, P.A. (2002). The planar polarity gene strabismus regulates convergent extension movements in Xenopus. EMBO J *21*, 976-985.

Deane, C.M., Salwinski, L., Xenarios, I., and Eisenberg, D. (2002). Protein interactions: two methods for assessment of the reliability of high throughput observations. Mol Cell Proteomics *1*, 349-356.

DeSesso, J.M., Scialli, A.R., and Holson, J.F. (1999). Apparent lability of neural tube closure in laboratory animals and humans. Am J Med Genet *87*, 143-162.

Devenport, D., and Fuchs, E. (2008). Planar polarization in embryonic epidermis orchestrates global asymmetric morphogenesis of hair follicles. Nat Cell Biol *10*, 1257-1268.

Dollar, G.L., Weber, U., Mlodzik, M., and Sokol, S.Y. (2005). Regulation of Lethal giant larvae by Dishevelled. Nature *437*, 1376-1380.

Dow, L.E., Brumby, A.M., Muratore, R., Coombe, M.L., Sedelies, K.A., Trapani, J.A., Russell, S.M., Richardson, H.E., and Humbert, P.O. (2003). hScrib is a functional homologue of the Drosophila tumour suppressor Scribble. Oncogene *22*, 9225-9230.

Dow, L.E., Kauffman, J.S., Caddy, J., Zarbalis, K., Peterson, A.S., Jane, S.M., Russell, S.M., and Humbert, P.O. (2007). The tumour-suppressor Scribble dictates cell polarity during directed epithelial migration: regulation of Rho GTPase recruitment to the leading edge. Oncogene *26*, 2272-2282.

Dubourg, C., Bendavid, C., Pasquier, L., Henry, C., Odent, S., and David, V. (2007). Holoprosencephaly. Orphanet J Rare Dis *2*, 8.

Echelard, Y., Epstein, D.J., St-Jacques, B., Shen, L., Mohler, J., McMahon, J.A., and McMahon, A.P. (1993). Sonic hedgehog, a member of a family of putative signaling molecules, is implicated in the regulation of CNS polarity. Cell *75*, 1417-1430.

Eggenschwiler, J.T., Espinoza, E., and Anderson, K.V. (2001). Rab23 is an essential negative regulator of the mouse Sonic hedgehog signalling pathway. Nature *412*, 194-198.

Ermakov, A., Stevens, J.L., Whitehill, E., Robson, J.E., Pieles, G., Brooker, D., Goggolidou, P., Powles-Glover, N., Hacker, T., Young, S.R., *et al.* (2009). Mouse mutagenesis identifies novel roles for left-right patterning genes in pulmonary, craniofacial, ocular, and limb development. Dev Dyn *238*, 581-594.

Etheridge, S.L., Ray, S., Li, S., Hamblet, N.S., Lijam, N., Tsang, M., Greer, J., Kardos, N., Wang, J., Sussman, D.J., *et al.* (2008). Murine dishevelled 3 functions in redundant pathways with dishevelled 1 and 2 in normal cardiac outflow tract, cochlea, and neural tube development. PLoS Genet *4*, e1000259.

Etienne, W., Meyer, M.H., Peppers, J., and Meyer, R.A., Jr. (2004). Comparison of mRNA gene expression by RT-PCR and DNA microarray. Biotechniques *36*, 618-620, 622, 624-616.

Fanto, M., Clayton, L., Meredith, J., Hardiman, K., Charroux, B., Kerridge, S., and McNeill, H. (2003). The tumor-suppressor and cell adhesion molecule Fat controls planar polarity via physical interactions with Atrophin, a transcriptional co-repressor. Development *130*, 763-774.

Fanto, M., and McNeill, H. (2004). Planar polarity from flies to vertebrates. J Cell Sci *117*, 527-533.

Feiguin, F., Hannus, M., Mlodzik, M., and Eaton, S. (2001). The ankyrin repeat protein Diego mediates Frizzled-dependent planar polarization. Dev Cell *1*, 93-101.

Fields, S., and Song, O. (1989). A novel genetic system to detect protein-protein interactions. Nature *340*, 245-246.

Fields, S., and Sternglanz, R. (1994). The two-hybrid system: an assay for protein-protein interactions. Trends Genet *10*, 286-292.

Fischer, E., Legue, E., Doyen, A., Nato, F., Nicolas, J.F., Torres, V., Yaniv, M., and Pontoglio, M. (2006). Defective planar cell polarity in polycystic kidney disease. Nat Genet *38*, 21-23.

Formstone, C.J., Moxon, C., Murdoch, J., Little, P., and Mason, I. (2010). Basal enrichment within neuroepithelia suggests novel function(s) for Celsr1 protein. Molecular and Cellular Neuroscience *44*, 210-222.

Freemont, P.S. (2000). RING for destruction? Curr Biol *10*, R84-87.

Gardiol, D., Zacchi, A., Petrera, F., Stanta, G., and Banks, L. (2006). Human discs large and scrib are localized at the same regions in colon mucosa and changes in their expression patterns are correlated with loss of tissue architecture during malignant progression. Int J Cancer *119*, 1285-1290.

Gawenis, L.R., Bradford, E.M., Prasad, V., Lorenz, J.N., Simpson, J.E., Clarke, L.L., Woo, A.L., Grisham, C., Sanford, L.P., Doetschman, T., *et al.* (2007). Colonic anion secretory defects and metabolic acidosis in mice lacking the NBC1 Na+/HCO3- cotransporter. J Biol Chem *282*, 9042-9052.

Gebbink, M.F., Kranenburg, O., Poland, M., van Horck, F.P., Houssa, B., and Moolenaar, W.H. (1997). Identification of a novel, putative Rho-specific GDP/GTP exchange factor and a RhoA-binding protein: control of neuronal morphology. J Cell Biol *137*, 1603-1613.

Geelen, J.A., and Langman, J. (1979). Ultrastructural observations on closure of the neural tube in the mouse. Anat Embryol (Berl) *156*, 73-88.

Goetz, S.C., and Anderson, K.V. (2010). The primary cilium: a signalling centre during vertebrate development. Nat Rev Genet *11*, 331-344.

Goldsworthy, M., Hugill, A., Freeman, H., Horner, E., Shimomura, K., Bogani, D., Pieles, G., Mijat, V., Arkell, R., Bhattacharya, S., *et al.* (2008). Role of the transcription factor sox4 in insulin secretion and impaired glucose tolerance. Diabetes *57*, 2234-2244.

Gong, Y., Mo, C., and Fraser, S.E. (2004). Planar cell polarity signalling controls cell division orientation during zebrafish gastrulation. Nature *430*, 689-693.

Goodrich, L.V., Milenkovic, L., Higgins, K.M., and Scott, M.P. (1997). Altered neural cell fates and medulloblastoma in mouse patched mutants. Science *277*, 1109-1113.

Goto, H., Tomono, Y., Ajiro, K., Kosako, H., Fujita, M., Sakurai, M., Okawa, K., Iwamatsu, A., Okigaki, T., Takahashi, T., *et al.* (1999). Identification of a novel phosphorylation site on histone H3 coupled with mitotic chromosome condensation. J Biol Chem *274*, 25543-25549.

Goto, T., and Keller, R. (2002). The planar cell polarity gene strabismus regulates convergence and extension and neural fold closure in Xenopus. Dev Biol *247*, 165-181.

Graham, F.L., Smiley, J., Russell, W.C., and Nairn, R. (1977). Characteristics of a human cell line transformed by DNA from human adenovirus type 5. J Gen Virol *36*, 59-74.

Gray, R.S., Abitua, P.B., Wlodarczyk, B.J., Szabo-Rogers, H.L., Blanchard, O., Lee, I., Weiss, G.S., Liu, K.J., Marcotte, E.M., Wallingford, J.B., *et al.* (2009). The planar cell polarity effector Fuz is essential for targeted membrane trafficking, ciliogenesis and mouse embryonic development. Nat Cell Biol *11*, 1225-1232.

Greco, T.L., Takada, S., Newhouse, M.M., McMahon, J.A., McMahon, A.P., and Camper, S.A. (1996). Analysis of the vestigial tail mutation demonstrates that Wnt-3a gene dosage regulates mouse axial development. Genes Dev *10*, 313-324.

Greene, N.D., and Copp, A.J. (2009). Development of the vertebrate central nervous system: formation of the neural tube. Prenat Diagn *29*, 303-311.

Greene, N.D., Gerrelli, D., Van Straaten, H.W., and Copp, A.J. (1998). Abnormalities of floor plate, notochord and somite differentiation in the loop-tail (Lp) mouse: a model of severe neural tube defects. Mech Dev *73*, 59-72.

Greene, N.D., Stanier, P., and Copp, A.J. (2009). Genetics of human neural tube defects. Hum Mol Genet *18*, R113-129.

Gubb, D., and Garcia-Bellido, A. (1982). A genetic analysis of the determination of cuticular polarity during development in Drosophila melanogaster. J Embryol Exp Morphol *68*, 37-57.

Gubb, D., Green, C., Huen, D., Coulson, D., Johnson, G., Tree, D., Collier, S., and Roote, J. (1999). The balance between isoforms of the prickle LIM domain protein is critical for planar polarity in Drosophila imaginal discs. Genes Dev *13*, 2315-2327.

Gunther, T., Struwe, M., Aguzzi, A., and Schughart, K. (1994). Open brain, a new mouse mutant with severe neural tube defects, shows altered gene expression patterns in the developing spinal cord. Development *120*, 3119-3130.

Habas, R., Dawid, I.B., and He, X. *(2003). Coactivation of* Rac and Rho by Wnt/Frizzled signaling is required for vertebrate gastrulation. Genes Dev *17*, 295-309.

Habas, R., Kato, Y., and He, X. (2001). Wnt/Frizzled activation of Rho regulates vertebrate gastrulation and requires a novel Formin homology protein Daam1. Cell *107*, 843-854.

Hamblet, N.S., Lijam, N., Ruiz-Lozano, P., Wang, J., Yang, Y., Luo, Z., Mei, L., Chien, K.R., Sussman, D.J., and Wynshaw-Boris, A. (2002). Dishevelled 2 is essential for cardiac outflow tract development, somite segmentation and neural tube closure. Development *129*, 5827-5838.

Hammerschmidt, M., Pelegri, F., Mullins, M.C., Kane, D.A., Brand, M., van Eeden, F.J., Furutani-Seiki, M., Granato, M., Haffter, P., Heisenberg, C.P., *et al.* (1996). Mutations affecting morphogenesis during gastrulation and tail formation in the zebrafish, Danio rerio. Development *123*, 143-151.

Hans, F., and Dimitrov, S. (2001). Histone H3 phosphorylation and cell division. Oncogene *20*, 3021-3027.

Harland, R. (2000). Neural induction. Current Opinion in Genetics & Development *10*, 357-362.

Harris, M.J. (2009). Insights into prevention of human neural tube defects by folic acid arising from consideration of mouse mutants. Birth Defects Res A Clin Mol Teratol *85*, 331-339.

Harris, M.J., and Juriloff, D.M. (2007). Mouse mutants with neural tube closure defects and their role in understanding human neural tube defects. Birth Defects Res A Clin Mol Teratol *79*, 187-210.

Hart, M.J., Eva, A., Zangrilli, D., Aaronson, S.A., Evans, T., Cerione, R.A., and Zheng, Y. (1994). Cellular transformation and guanine nucleotide exchange activity are catalyzed by a common domain on the dbl oncogene product. J Biol Chem *269*, 62-65.

Hart, M.J., Jiang, X., Kozasa, T., Roscoe, W., Singer, W.D., Gilman, A.G., Sternweis, P.C., and Bollag, G. (1998). Direct stimulation of the guanine nucleotide exchange activity of p115 RhoGEF by Galpha13. Science *280*, 2112-2114.

Haycraft, C.J., Banizs, B., Aydin-Son, Y., Zhang, Q., Michaud, E.J., and Yoder, B.K. (2005). Gli2 and Gli3 localize to cilia and require the intraflagellar transport protein polaris for processing and function. PLoS Genet *1*, e53.

Heisenberg, C.-P., Tada, M., Rauch, G.-J., Saude, L., Concha, M.L., Geisler, R., Stemple, D.L., Smith, J.C., and Wilson, S.W. (2000). Silberblick/Wnt11 mediates convergent extension movements during zebrafish gastrulation. Nature *405*, 76-81.

Henderson, D.J., Conway, S.J., Greene, N.D., Gerrelli, D., Murdoch, J.N., Anderson, R.H., and Copp, A.J. (2001). Cardiovascular defects associated with abnormalities in midline development in the Loop-tail mouse mutant. Circ Res *89*, 6-12.

Henderson, D.J., Phillips, H.M., and Chaudhry, B. (2006). Vang-like 2 and noncanonical Wnt signaling in outflow tract development. Trends Cardiovasc Med *16*, 38-45.

Holmberg, J., Clarke, D.L., and Frisen, J. (2000). Regulation of repulsion versus adhesion by different splice forms of an Eph receptor. Nature *408*, 203-206.

Hopkinson, S.B., and Jones, J.C. (2000). The N terminus of the transmembrane protein BP180 interacts with the N-terminal domain of BP230, thereby mediating keratin cytoskeleton anchorage to the cell surface at the site of the hemidesmosome. Mol Biol Cell *11*, 277-286.

Huang, Y., Roelink, H., and McKnight, G.S. (2002). Protein kinase A deficiency causes axially localized neural tube defects in mice. J Biol Chem *277*, 19889-19896.

Huangfu, D., and Anderson, K.V. (2005). Cilia and Hedgehog responsiveness in the mouse. Proc Natl Acad Sci U S A *102*, 11325-11330.

Huangfu, D., Liu, A., Rakeman, A.S., Murcia, N.S., Niswander, L., and Anderson, K.V. (2003). Hedgehog signalling in the mouse requires intraflagellar transport proteins. Nature *426*, 83-87.

Hubbard, S.R., Mohammadi, M., and Schlessinger, J. (1998). Autoregulatory mechanisms in protein-tyrosine kinases. J Biol Chem *273*, 11987-11990.

Ikeda, A., Ikeda, S., Gridley, T., Nishina, P.M., and Naggert, J.K. (2001). Neural tube defects and neuroepithelial cell death in Tulp3 knockout mice. Hum Mol Genet *10*, 1325-1334.

Ingham, P.W. (1998). Transducing Hedgehog: the story so far. EMBO J *17*, 3505-3511.

Ivanov, A.I., Young, C., Beste, K.D., Capaldo, C.T., Humbert, P.O., Brennwald, P., Parkos, C.A., and Nusrat, A. (2010). Tumor suppressor scribble regulates assembly of tight junctions in the intestinal epithelium. Am J Pathol *176*, 134-145.

Jenny, A., Reynolds-Kenneally, J., Das, G., Burnett, M., and Mlodzik, M. (2005). Diego and Prickle regulate Frizzled planar cell polarity signalling by competing for Dishevelled binding. Nat Cell Biol *7*, 691-697.

Jia, J., Amanai, K., Wang, G., Tang, J., Wang, B., and Jiang, J. (2002). Shaggy/GSK3 antagonizes Hedgehog signalling by regulating Cubitus interruptus. Nature *416*, 548-552.

Jiang, J., and Struhl, G. (1998). Regulation of the Hedgehog and Wingless signalling pathways by the F-box/WD40-repeat protein Slimb. Nature *391*, 493-496.

Johnsson, N., and Varshavsky, A. (1994). Split ubiquitin as a sensor of protein interactions in vivo. Proc Natl Acad Sci U S A *91*, 10340-10344.

Jung, J.W., Ji, A.R., Lee, J., Kim, U.J., and Lee, S.T. (2002). Organization of the human PTK7 gene encoding a receptor protein tyrosine kinase-like molecule and alternative splicing of its mRNA. Biochim Biophys Acta *1579*, 153-163.

Jung, J.W., Shin, W.S., Song, J., and Lee, S.T. (2004). Cloning and characterization of the full-length mouse Ptk7 cDNA encoding a defective receptor protein tyrosine kinase. Gene *328*, 75-84.

Justice, M.J., Noveroske, J.K., Weber, J.S., Zheng, B., and Bradley, A. (1999). Mouse ENU mutagenesis. Hum Mol Genet *8*, 1955-1963.

Kajkowski, E.M., Price, L.A., Pausch, M.H., Young, K.H., and Ozenberger, B.A. (1997). Investigation of growth hormone releasing hormone receptor structure and activity using yeast expression technologies. J Recept Signal Transduct Res *17*, 293-303.

Kallay, L.M., McNickle, A., Brennwald, P.J., Hubbard, A.L., and Braiterman, L.T. (2006). Scribble associates with two polarity proteins, Lgl2 and Vangl2, via distinct molecular domains. J Cell Biochem *99*, 647-664.

Kanamoto, T., Terada, K., Yoshikawa, H., and Furukawa, T. (2006). Cloning and regulation of the vertebrate homologue of lin-41 that functions as a heterochronic gene in Caenorhabditis elegans. Dev Dyn *235*, 1142-1149.

Kasai, K., Takahashi, M., Osumi, N., Sinnarajah, S., Takeo, T., Ikeda, H., Kehrl, J.H., Itoh, G., and Arnheiter, H. (2004). The G12 family of heterotrimeric G proteins and Rho GTPase mediate Sonic hedgehog signalling. Genes Cells *9*, 49-58.

Keegan, L., Gill, G., and Ptashne, M. (1986). Separation of DNA binding from the transcription-activating function of a eukaryotic regulatory protein. Science *231*, 699-704.

Keller, R. (2006). Mechanisms of elongation in embryogenesis. Development *133*, 2291-2302.

Kempkens, O., Medina, E., Fernandez-Ballester, G., Ozuyaman, S., Le Bivic, A., Serrano, L., and Knust, E. (2006). Computer modelling in combination with in vitro studies reveals similar binding affinities of Drosophila Crumbs for the PDZ domains of Stardust and DmPar-6. Eur J Cell Biol *85*, 753-767.

Kennedy, C.L., and O'Bryan, M.K. (2006). N-ethyl-N-nitrosourea (ENU) mutagenesis and male fertility research. Hum Reprod Update *12*, 293-301.

Kibar, Z., Capra, V., and Gros, P. (2007a). Toward understanding the genetic basis of neural tube defects. Clin Genet *71*, 295-310.

Kibar, Z., Torban, E., McDearmid, J.R., Reynolds, A., Berghout, J., Mathieu, M., Kirillova, I., De Marco, P., Merello, E., Hayes, J.M., *et al.* (2007b). Mutations in VANGL1 associated with neural-tube defects. N Engl J Med *356*, 1432-1437.

Kibar, Z., Vogan, K.J., Groulx, N., Justice, M.J., Underhill, D.A., and Gros, P. (2001). Ltap, a mammalian homolog of Drosophila Strabismus/Van Gogh, is altered in the mouse neural tube mutant Loop-tail. Nat Genet *28*, 251-255.

Kieserman, E.K., and Wallingford, J.B. (2009). In vivo imaging reveals a role for Cdc42 in spindle positioning and planar orientation of cell divisions during vertebrate neural tube closure. J Cell Sci *122*, 2481-2490.

Kile, B.T., and Hilton, D.J. (2005). The art and design of genetic screens: mouse. Nat Rev Genet *6*, 557-567.

Kim, J., Kato, M., and Beachy, P.A. (2009). Gli2 trafficking links Hedgehog-dependent activation of Smoothened in the primary cilium to transcriptional activation in the nucleus. Proc Natl Acad Sci U S A *106*, 21666-21671.

Kim, Y., Kobayashi, A., Sekido, R., DiNapoli, L., Brennan, J., Chaboissier, M.C., Poulat, F., Behringer, R.R., Lovell-Badge, R., and Capel, B. (2006). Fgf9 and Wnt4 act as antagonistic signals to regulate mammalian sex determination. PLoS Biol *4*, e187.

Kinoshita, N., Iioka, H., Miyakoshi, A., and Ueno, N. (2003). PKC delta is essential for Dishevelled function in a noncanonical Wnt pathway that regulates Xenopus convergent extension movements. Genes Dev *17*, 1663-1676.

Kirby, M.L., Gale, T.F., and Stewart, D.E. (1983). Neural crest cells contribute to normal aorticopulmonary septation. Science *220*, 1059-1061.

Kirillova, I., Novikova, I., Auge, J., Audollent, S., Esnault, D., Encha-Razavi, F., Lazjuk, G., Attie-Bitach, T., and Vekemans, M. (2000). Expression of the sonic hedgehog gene in human embryos with neural tube defects. Teratology *61*, 347-354.

Klingensmith, J., Ang, S.L., Bachiller, D., and Rossant, J. (1999). Neural induction and patterning in the mouse in the absence of the node and its derivatives. Dev Biol *216*, 535-549.

Kobus, F.J., and Fleming, K.G. (2005). The GxxxG-containing transmembrane domain of the CCK4 oncogene does not encode preferential self-interactions. Biochemistry *44*, 1464-1470.

Kozasa, T., Jiang, X., Hart, M.J., Sternweis, P.M., Singer, W.D., Gilman, A.G., Bollag, G., and Sternweis, P.C. (1998). p115 RhoGEF, a GTPase activating protein for Galpha12 and Galpha13. Science *280*, 2109-2111.

Krasnow, R.E., Wong, L.L., and Adler, P.N. (1995). Dishevelled is a component of the frizzled signaling pathway in Drosophila. Development *121*, 4095-4102.

Lai, E.C. (2002). Notch cleavage: Nicastrin helps Presenilin make the final cut. Curr Biol *12*, R200-202.

Lampe, P.D., and Lau, A.F. (2004). The effects of connexin phosphorylation on gap junctional communication. Int J Biochem Cell Biol *36*, 1171-1186.

Lancman, J.J., Caruccio, N.C., Harfe, B.D., Pasquinelli, A.E., Schageman, J.J., Pertsemlidis, A., and Fallon, J.F. (2005). Analysis of the regulation of lin-41 during chick and mouse limb development. Dev Dyn *234*, 948-960.

Le Brigand, K., Russell, R., Moreilhon, C., Rouillard, J.M., Jost, B., Amiot, F., Magnone, V., Bole-Feysot, C., Rostagno, P., Virolle, V., *et al.* (2006). An open-access long oligonucleotide microarray resource for analysis of the human and mouse transcriptomes. Nucleic Acids Res *34*, e87.

Lee, J., Platt, K.A., Censullo, P., and Ruiz i Altaba, A. (1997). Gli1 is a target of Sonic hedgehog that induces ventral neural tube development. Development *124*, 2537-2552.

Lowry, O.H., Rosebrough, N.J., Farr, A.L., and Randall, R.J. (1951). Protein measurement with the Folin phenol reagent. J Biol Chem *193*, 265-275.

Lu, X., Borchers, A.G., Jolicoeur, C., Rayburn, H., Baker, J.C., and Tessier-Lavigne, M. (2004). PTK7/CCK-4 is a novel regulator of planar cell polarity in vertebrates. Nature *430*, 93-98.

Lum, L., Zhang, C., Oh, S., Mann, R.K., von Kessler, D.P., Taipale, J., Weis-Garcia, F., Gong, R., Wang, B., and Beachy, P.A. (2003). Hedgehog signal transduction via Smoothened association with a cytoplasmic complex scaffolded by the atypical kinesin, Costal-2. Mol Cell *12*, 1261-1274.

MacDonald, B.T., Tamai, K., and He, X. (2009). Wnt/beta-catenin signaling: components, mechanisms, and diseases. Dev Cell *17*, 9-26.

Maller Schulman, B.R., Liang, X., Stahlhut, C., DelConte, C., Stefani, G., and Slack, F.J. (2008). The let-7 microRNA target gene, Mlin41/Trim71 is required for mouse embryonic survival and neural tube closure. Cell Cycle *7*, 3935-3942.

Manner, J., Seidl, W., and Steding, G. (1993). Correlation between the embryonic head flexures and cardiac development. An experimental study in chick embryos. Anat Embryol (Berl) *188*, 269-285.

Marat, A.L., and McPherson, P.S. (2010). The connecdenn family, Rab35 guanine nucleotide exchange factors interfacing with the clathrin machinery. J Biol Chem *285*, 10627-10637.

Matise, M.P., Epstein, D.J., Park, H.L., Platt, K.A., and Joyner, A.L. (1998). Gli2 is required for induction of floor plate and adjacent cells, but not most ventral neurons in the mouse central nervous system. Development *125*, 2759-2770.

Maynard, T.M., Jain, M.D., Balmer, C.W., and LaMantia, A.S. (2002). High-resolution mapping of the Gli3 mutation extra-toes reveals a 51.5-kb deletion. Mamm Genome *13*, 58-61.

McLone, D.G., and Knepper, P.A. (1985). Role of complex carbohydrates and neurulation. Pediatr Neurosci *12*, 2-9.

Metais, J.Y., Navarro, C., Santoni, M.J., Audebert, S., and Borg, J.P. (2005). hScrib interacts with ZO-2 at the cell-cell junctions of epithelial cells. FEBS Lett *579*, 3725-3730.

Methot, N., and Basler, K. (1999). Hedgehog controls limb development by regulating the activities of distinct transcriptional activator and repressor forms of Cubitus interruptus. Cell *96*, 819-831.

Miller, M.A., and Steele, R.E. (2000). Lemon encodes an unusual receptor protein-tyrosine kinase expressed during gametogenesis in Hydra. Dev Biol *224*, 286-298.

Ming, J.E., Kaupas, M.E., Roessler, E., Brunner, H.G., Golabi, M., Tekin, M., Stratton, R.F., Sujansky, E., Bale, S.J., and Muenke, M. (2002). Mutations in PATCHED-1, the receptor for SONIC HEDGEHOG, are associated with holoprosencephaly. Hum Genet *110*, 297-301.

Mjaatvedt, C.H., Nakaoka, T., Moreno-Rodriguez, R., Norris, R.A., Kern, M.J., Eisenberg, C.A., Turner, D., and Markwald, R.R. (2001). The outflow tract of the heart is recruited from a novel heart-forming field. Dev Biol *238*, 97-109.

Mo, R., Freer, A.M., Zinyk, D.L., Crackower, M.A., Michaud, J., Heng, H.H., Chik, K.W., Shi, X.M., Tsui, L.C., Cheng, S.H., *et al.* (1997). Specific and redundant functions of Gli2 and Gli3 zinc finger genes in skeletal patterning and development. Development *124*, 113-123.

Mohammadi, M., Dikic, I., Sorokin, A., Burgess, W.H., Jaye, M., and Schlessinger, J. (1996). Identification of six novel autophosphorylation sites on fibroblast growth factor receptor 1 and elucidation of their importance in receptor activation and signal transduction. Mol Cell Biol *16*, 977-989.

Montcouquiol, M., Rachel, R.A., Lanford, P.J., Copeland, N.G., Jenkins, N.A., and Kelley, M.W. (2003). Identification of Vangl2 and Scrb1 as planar polarity genes in mammals. Nature *423*, 173-177.

Montcouquiol, M., Sans, N., Huss, D., Kach, J., Dickman, J.D., Forge, A., Rachel, R.A., Copeland, N.G., Jenkins, N.A., Bogani, D., *et al.* (2006). Asymmetric localization of Vangl2 and Fz3 indicate novel mechanisms for planar cell polarity in mammals. J Neurosci *26*, 5265-5275.

Morey, J.S., Ryan, J.C., and Van Dolah, F.M. (2006). Microarray validation: factors influencing correlation between oligonucleotide microarrays and real-time PCR. Biol Proced Online *8*, 175-193.

Morgan, D., Turnpenny, L., Goodship, J., Dai, W., Majumder, K., Matthews, L., Gardner, A., Schuster, G., Vien, L., Harrison, W., *et al.* (1998). Inversin, a novel gene in the vertebrate left-right axis pathway, is partially deleted in the inv mouse. Nat Genet *20*, 149-156.

Morita, K., Furuse, M., Fujimoto, K., and Tsukita, S. (1999). Claudin multigene family encoding four-transmembrane domain protein components of tight junction strands. Proc Natl Acad Sci U S A *96*, 511-516.

Morriss, G.M., and Solursh, M. (1978). Regional differences in mesenchymal cell morphology and glycosaminoglycans in early neural-fold stage rat embryos. J Embryol Exp Morphol *46*, 37-52.

Mossie, K., Jallal, B., Alves, F., Sures, I., Plowman, G.D., and Ullrich, A. (1995). Colon carcinoma kinase-4 defines a new subclass of the receptor tyrosine kinase family. Oncogene *11*, 2179-2184.

Murcia, N.S., Richards, W.G., Yoder, B.K., Mucenski, M.L., Dunlap, J.R., and Woychik, R.P. (2000). The Oak Ridge Polycystic Kidney (orpk) disease gene is required for left-right axis determination. Development *127*, 2347-2355.

Murdoch, J.N., and Copp, A.J. (2010). The relationship between sonic Hedgehog signaling, cilia, and neural tube defects. Birth Defects Res A Clin Mol Teratol *88*, 633-652.

Murdoch, J.N., Doudney, K., Paternotte, C., Copp, A.J., and Stanier, P. (2001a). Severe neural tube defects in the loop-tail mouse result from mutation of Lpp1, a novel gene involved in floor plate specification. Hum Mol Genet *10*, 2593-2601.

Murdoch, J.N., Henderson, D.J., Doudney, K., Gaston-Massuet, C., Phillips, H.M., Paternotte, C., Arkell, R., Stanier, P., and Copp, A.J. (2003). Disruption of scribble (Scrb1) causes severe neural tube defects in the circletail mouse. Hum Mol Genet *12*, 87-98.

Murdoch, J.N., Rachel, R.A., Shah, S., Beermann, F., Stanier, P., Mason, C.A., and Copp, A.J. (2001b). Circletail, a new mouse mutant with severe neural tube defects: chromosomal localization and interaction with the loop-tail mutation. Genomics *78*, 55-63.

Nagai, T., Aruga, J., Minowa, O., Sugimoto, T., Ohno, Y., Noda, T., and Mikoshiba, K. (2000). Zic2 regulates the kinetics of neurulation. Proc Natl Acad Sci U S A *97*, 1618-1623.

Nagasaka, K., Nakagawa, S., Yano, T., Takizawa, S., Matsumoto, Y., Tsuruga, T., Nakagawa, K., Minaguchi, T., Oda, K., Hiraike-Wada, O., *et al.* (2006). Human homolog of Drosophila tumor suppressor Scribble negatively regulates cell-cycle progression from G1 to S phase by localizing at the basolateral membrane in epithelial cells. Cancer Sci *97*, 1217-1225.

Nakagawa, S., and Huibregtse, J.M. (2000). Human scribble (Vartul) is targeted for ubiquitin-mediated degradation by the high-risk papillomavirus E6 proteins and the E6AP ubiquitin-protein ligase. Mol Cell Biol *20*, 8244-8253.

Narimatsu, M., Bose, R., Pye, M., Zhang, L., Miller, B., Ching, P., Sakuma, R., Luga, V., Roncari, L., Attisano, L., *et al.* (2009). Regulation of planar cell polarity by Smurf ubiquitin ligases. Cell *137*, 295-307.

Nieuwenhuis, E., Motoyama, J., Barnfield, P.C., Yoshikawa, Y., Zhang, X., Mo, R., Crackower, M.A., and Hui, C.C. (2006). Mice with a targeted mutation of patched2 are viable but develop alopecia and epidermal hyperplasia. Mol Cell Biol *26*, 6609-6622.

Nishina, P.M., North, M.A., Ikeda, A., Yan, Y., and Naggert, J.K. (1998). Molecular characterization of a novel tubby gene family member, TULP3, in mouse and humans. Genomics *54*, 215-220.

Nolan, P.M., Peters, J., Vizor, L., Strivens, M., Washbourne, R., Hough, T., Wells, C., Glenister, P., Thornton, C., Martin, J., *et al.* (2000). Implementation of a large-scale ENU mutagenesis program: towards increasing the mouse mutant resource. Mamm Genome *11*, 500-506.

Norman, R.X., Ko, H.W., Huang, V., Eun, C.M., Abler, L.L., Zhang, Z., Sun, X., and Eggenschwiler, J.T. (2009). Tubby-like protein 3 (TULP3) regulates patterning in the mouse embryo through inhibition of Hedgehog signaling. Hum Mol Genet *18*, 1740-1754.

Nusslein-Volhard, C., and Wieschaus, E. (1980). Mutations affecting segment number and polarity in Drosophila. Nature *287*, 795-801.

Ogden, S.K., Fei, D.L., Schilling, N.S., Ahmed, Y.F., Hwa, J., and Robbins, D.J. (2008). G protein Galphai functions immediately downstream of Smoothened in Hedgehog signalling. Nature *456*, 967-970.

Pabst, O., Herbrand, H., and Arnold, H.H. (1998). Nkx2-9 is a novel homeobox transcription factor which demarcates ventral domains in the developing mouse CNS. Mech Dev *73*, 85-93.

Padmanabhan, R. (2006). Etiology, pathogenesis and prevention of neural tube defects. Congenit Anom (Kyoto) *46*, 55-67.

Palmieri, F. (2004). The mitochondrial transporter family (SLC25): physiological and pathological implications. Pflugers Arch *447*, 689-709.

Park, H.L., Bai, C., Platt, K.A., Matise, M.P., Beeghly, A., Hui, C.C., Nakashima, M., and Joyner, A.L. (2000). Mouse Gli1 mutants are viable but have defects in SHH signaling in combination with a Gli2 mutation. Development *127*, 1593-1605.

Park, S.K., Lee, H.S., and Lee, S.T. (1996). Characterization of the human full-length PTK7 cDNA encoding a receptor protein tyrosine kinase-like molecule closely related to chick KLG. J Biochem *119*, 235-239.

Park, T.J., Haigo, S.L., and Wallingford, J.B. (2006). Ciliogenesis defects in embryos lacking inturned or fuzzy function are associated with failure of planar cell polarity and Hedgehog signaling. Nat Genet *38*, 303-311.

Patterson, V.L., Damrau, C., Paudyal, A., Reeve, B., Grimes, D.T., Stewart, M.E., Williams, D.J., Siggers, P., Greenfield, A., and Murdoch, J.N. (2009). Mouse hitchhiker mutants have spina bifida, dorso-ventral patterning defects and polydactyly: identification of Tulp3 as a novel negative regulator of the Sonic hedgehog pathway. Hum Mol Genet *18*, 1719-1739.

Persson, M., Stamataki, D., te Welscher, P., Andersson, E., Bose, J., Ruther, U., Ericson, J., and Briscoe, J. (2002). Dorsal-ventral patterning of the spinal cord requires Gli3 transcriptional repressor activity. Genes Dev *16*, 2865-2878.

Petalidis, L., Bhattacharyya, S., Morris, G.A., Collins, V.P., Freeman, T.C., and Lyons, P.A. (2003). Global amplification of mRNA by template-switching PCR: linearity and application to microarray analysis. Nucleic Acids Res *31*, e142.

Phillips, H.M., Murdoch, J.N., Chaudhry, B., Copp, A.J., and Henderson, D.J. (2005). Vangl2 acts via RhoA signaling to regulate polarized cell movements during development of the proximal outflow tract. Circ Res *96*, 292-299.

Phillips, H.M., Rhee, H.J., Murdoch, J.N., Hildreth, V., Peat, J.D., Anderson, R.H., Copp, A.J., Chaudhry, B., and Henderson, D.J. (2007). Disruption of planar cell polarity signaling results in congenital heart defects and cardiomyopathy attributable to early cardiomyocyte disorganization. Circ Res *101*, 137-145.

Plitz, T., and Pfeffer, K. (2001). Intact lysosome transport and phagosome function despite kinectin deficiency. Mol Cell Biol *21*, 6044-6055.

Preat, T. (1992). Characterization of Suppressor of fused, a complete suppressor of the fused segment polarity gene of Drosophila melanogaster. Genetics *132*, 725-736.

Price, M.A., and Kalderon, D. (1999). Proteolysis of cubitus interruptus in Drosophila requires phosphorylation by protein kinase A. Development *126*, 4331-4339.

Price, M.A., and Kalderon, D. (2002). Proteolysis of the Hedgehog signaling effector Cubitus interruptus requires phosphorylation by Glycogen Synthase Kinase 3 and Casein Kinase 1. Cell *108*, 823-835.

Pulido, D., Campuzano, S., Koda, T., Modolell, J., and Barbacid, M. (1992). Dtrk, a Drosophila gene related to the trk family of neurotrophin receptors, encodes a novel class of neural cell adhesion molecule. EMBO J *11*, 391-404.

Qian, D., Jones, C., Rzadzinska, A., Mark, S., Zhang, X., Steel, K.P., Dai, X., and Chen, P. (2007). Wnt5a functions in planar cell polarity regulation in mice. Dev Biol *306*, 121-133.

Qin, Y., Capaldo, C., Gumbiner, B.M., and Macara, I.G. (2005). The mammalian Scribble polarity protein regulates epithelial cell adhesion and migration through E-cadherin. J Cell Biol *171*, 1061-1071.

Quwailid, M.M., Hugill, A., Dear, N., Vizor, L., Wells, S., Horner, E., Fuller, S., Weedon, J., McMath, H., Woodman, P., *et al.* (2004). A gene-driven ENU-based approach to generating an allelic series in any gene. Mamm Genome *15*, 585-591.

Rachel, R.A., Wellington, S.J., Warburton, D., Mason, C.A., and Beermann, F. (2002). A new allele of Gli3 and a new mutation, circletail (Crc), resulting from a single transgenic experiment. Genesis *33*, 55-61.

Rajeevan, M.S., Vernon, S.D., Taysavang, N., and Unger, E.R. (2001). Validation of array-based gene expression profiles by real-time (kinetic) RT-PCR. J Mol Diagn *3*, 26-31.

Rida, P.C., and Chen, P. (2009). Line up and listen: Planar cell polarity regulation in the mammalian inner ear. Semin Cell Dev Biol *20*, 978-985.

Rivera-Perez, J.A., and Magnuson, T. (2005). Primitive streak formation in mice is preceded by localized activation of Brachyury and Wnt3. Dev Biol *288*, 363-371.

Robbins, D.J., Nybakken, K.E., Kobayashi, R., Sisson, J.C., Bishop, J.M., and Therond, P.P. (1997). Hedgehog elicits signal transduction by means of a large complex containing the kinesin-related protein costal2. Cell *90*, 225-234.

Roelink, H., Porter, J.A., Chiang, C., Tanabe, Y., Chang, D.T., Beachy, P.A., and Jessell, T.M. (1995). Floor plate and motor neuron induction by different concentrations of the amino-terminal cleavage product of sonic hedgehog autoproteolysis. Cell *81*, 445-455.

Roessler, E., Du, Y.Z., Mullor, J.L., Casas, E., Allen, W.P., Gillessen-Kaesbach, G., Roeder, E.R., Ming, J.E., Ruiz i Altaba, A., and Muenke, M. (2003). Loss-of-function mutations in the human GLI2 gene are associated with pituitary anomalies and holoprosencephaly-like features. Proc Natl Acad Sci U S A *100*, 13424-13429.

Rohatgi, R., Milenkovic, L., and Scott, M.P. (2007). Patched1 regulates hedgehog signaling at the primary cilium. Science *317*, 372-376.

Rossman, K.L., Der, C.J., and Sondek, J. (2005). GEF means go: turning on RHO GTPases with guanine nucleotide-exchange factors. Nat Rev Mol Cell Biol *6*, 167-180.

Russell, W.L., Kelly, E.M., Hunsicker, P.R., Bangham, J.W., Maddux, S.C., and Phipps, E.L. (1979). Specific-locus test shows ethylnitrosourea to be the most potent mutagen in the mouse. Proc Natl Acad Sci U S A *76*, 5818-5819.

Saburi, S., Hester, I., Fischer, E., Pontoglio, M., Eremina, V., Gessler, M., Quaggin, S.E., Harrison, R., Mount, R., and McNeill, H. (2008). Loss of Fat4 disrupts PCP signaling and oriented cell division and leads to cystic kidney disease. Nat Genet *40*, 1010-1015.

Sadler, T.W. (2005a). Embryology of neural tube development. Am J Med Genet C Semin Med Genet *135*, 2-8.

Sadler, T.W. (2005b). Embryology of neural tube development. Am J Med Genet C Semin Med Genet *135C*, 2-8.

Santagata, S., Boggon, T.J., Baird, C.L., Gomez, C.A., Zhao, J., Shan, W.S., Myszka, D.G., and Shapiro, L. (2001). G-protein signaling through tubby proteins. Science *292*, 2041-2050.

Sasaki, H., Nishizaki, Y., Hui, C., Nakafuku, M., and Kondoh, H. (1999). Regulation of Gli2 and Gli3 activities by an amino-terminal repression domain: implication of Gli2 and Gli3 as primary mediators of Shh signaling. Development *126*, 3915-3924.

Sausedo, R.A., Smith, J.L., and Schoenwolf, G.C. (1997). Role of nonrandomly oriented cell division in shaping and bending of the neural plate. J Comp Neurol *381*, 473-488.

Schena, M., Shalon, D., Davis, R.W., and Brown, P.O. (1995). Quantitative monitoring of gene expression patterns with a complementary DNA microarray. Science *270*, 467-470.

Schiller, M.R. (2006). Coupling receptor tyrosine kinases to Rho GTPases--GEFs what's the *link. Cell Signal 18, 1834-1843.*

Schmidt, A., and Hall, A. (2002). Guanine nucleotide exchange factors for Rho GTPases: turning on the switch. Genes Dev *16*, 1587-1609.

Schneider, M.R., and Wolf, E. (2009). The epidermal growth factor receptor ligands at a glance. Journal of Cellular Physiology *218*, 460-466.

Seifert, J.R., and Mlodzik, M. (2007). Frizzled/PCP signalling: a conserved mechanism regulating cell polarity and directed motility. Nat Rev Genet *8*, 126-138.

Seller, M.J. (1995). Further evidence for an intermittent pattern of neural tube closure in humans. J Med Genet *32*, 205-207.

Shin, W.S., Maeng, Y.S., Jung, J.W., Min, J.K., Kwon, Y.G., and Lee, S.T. (2008). Soluble PTK7 inhibits tube formation, migration, and invasion of endothelial cells and angiogenesis. Biochem Biophys Res Commun *371*, 793-798.

Shirane, M., Ogawa, M., Motoyama, J., and Nakayama, K.I. (2008). Regulation of apoptosis and neurite extension by FKBP38 is required for neural tube formation in the mouse. Genes Cells *13*, 635-651.

Shnitsar, I., and Borchers, A. (2008). PTK7 recruits dsh to regulate neural crest migration. Development *135*, 4015-4024.

Shum, A.S., and Copp, A.J. (1996). Regional differences in morphogenesis of the neuroepithelium suggest multiple mechanisms of spinal neurulation in the mouse. Anat Embryol (Berl) *194*, 65-73.

Simons, M., and Mlodzik, M. (2008). Planar cell polarity signaling: from fly development to human disease. Annu Rev Genet *42*, 517-540.

Simpson, F., Kerr, M.C., and Wicking, C. (2009). Trafficking, development and hedgehog. Mech Dev *126*, 279-288.

Smith, L.J., and Stein, K.F. (1962). Axial elongation in the mouse and its retardation in homozygous looptail mice. J Embryol Exp Morphol *10*, 73-87.

Southard-Smith, E.M., Kos, L., and Pavan, W.J. (1998). Sox10 mutation disrupts neural crest development in Dom Hirschsprung mouse model. Nat Genet *18*, 60-64.

St-Jacques, B., Hammerschmidt, M., and McMahon, A.P. (1999). Indian hedgehog signaling regulates proliferation and differentiation of chondrocytes and is essential for bone formation. Genes Dev *13*, 2072-2086.

Strutt, H., and Strutt, D. (2008). Differential stability of flamingo protein complexes underlies the establishment of planar polarity. Curr Biol *18*, 1555-1564.

Svard, J., Heby-Henricson, K., Persson-Lek, M., Rozell, B., Lauth, M., Bergstrom, A., Ericson, J., Toftgard, R., and Teglund, S. (2006). Genetic elimination of Suppressor of fused reveals an essential repressor function in the mammalian Hedgehog signaling pathway. Dev Cell *10*, 187-197.

Tahinci, E., Thorne, C.A., Franklin, J.L., Salic, A., Christian, K.M., Lee, L.A., Coffey, R.J., and Lee, E. (2007). Lrp6 is required for convergent extension during Xenopus gastrulation. Development *134*, 4095-4106.

Tam, P.P., and Behringer, R.R. (1997). Mouse gastrulation: the formation of a mammalian body plan. Mech Dev *68*, 3-25.

Tao, H., Suzuki, M., Kiyonari, H., Abe, T., Sasaoka, T., and Ueno, N. (2009). Mouse prickle1, the homolog of a PCP gene, is essential for epiblast apical-basal polarity. Proc Natl Acad Sci U S A *106*, 14426-14431.

Taylor, J., Abramova, N., Charlton, J., and Adler, P.N. (1998). Van Gogh: a new Drosophila tissue polarity gene. Genetics *150*, 199-210.

Thaminy, S., Auerbach, D., Arnoldo, A., and Stagljar, I. (2003). Identification of novel ErbB3-interacting factors using the split-ubiquitin membrane yeast two-hybrid system. Genome Res *13*, 1744-1753.

Torban, E., Patenaude, A.M., Leclerc, S., Rakowiecki, S., Gauthier, S., Andelfinger, G., Epstein, D.J., and Gros, P. (2008). Genetic interaction between members of the Vangl family causes neural tube defects in mice. Proc Natl Acad Sci U S A *105*, 3449-3454.

Torban, E., Wang, H.J., Groulx, N., and Gros, P. (2004). Independent mutations in mouse Vangl2 that cause neural tube defects in looptail mice impair interaction with members of the Dishevelled family. J Biol Chem *279*, 52703-52713.

Toyoshima, I., Yu, H., Steuer, E.R., and Sheetz, M.P. (1992). Kinectin, a major kinesin-binding protein on ER. J Cell Biol *118*, 1121-1131.

Tran, P.V., Haycraft, C.J., Besschetnova, T.Y., Turbe-Doan, A., Stottmann, R.W., Herron, B.J., Chesebro, A.L., Qiu, H., Scherz, P.J., Shah, J.V., *et al.* (2008). THM1 negatively modulates mouse sonic hedgehog signal transduction and affects retrograde intraflagellar transport in cilia. Nat Genet *40*, 403-410.

Usui, T., Shima, Y., Shimada, Y., Hirano, S., Burgess, R.W., Schwarz, T.L., Takeichi, M., and Uemura, T. (1999). Flamingo, a seven-pass transmembrane cadherin, regulates planar cell polarity under the control of Frizzled. Cell *98*, 585-595.

van Horck, F.P., Ahmadian, M.R., Haeusler, L.C., Moolenaar, W.H., and Kranenburg, O. (2001). Characterization of p190RhoGEF, a RhoA-specific guanine nucleotide exchange factor that interacts with microtubules. J Biol Chem *276*, 4948-4956.

Vandenberg, A.L., and Sassoon, D.A. (2009). Non-canonical Wnt signaling regulates cell polarity in female reproductive tract development via van gogh-like 2. Development *136*, 1559-1570.

Vashu, R., and Liew, N.S. (2010). Double neural tube defect: a case report and discussions on neural tube development. Childs Nerv Syst *26*, 697-701.

Villavicencio, E.H., Walterhouse, D.O., and Iannaccone, P.M. (2000). The sonic hedgehog-patched-gli pathway in human development and disease. Am J Hum Genet *67*, 1047-1054.

Vinson, C.R., Conover, S., and Adler, P.N. (1989). A Drosophila tissue polarity locus encodes a protein containing seven potential transmembrane domains. Nature *338*, 263-264.

Vivancos, V., Chen, P., Spassky, N., Qian, D., Dabdoub, A., Kelley, M., Studer, M., and Guthrie, S. (2009). Wnt activity guides facial branchiomotor neuron migration, and involves the PCP pathway and JNK and ROCK kinases. Neural Dev *4*, 7.

Wallingford, J.B., Fraser, S.E., and Harland, R.M. (2002). Convergent extension: the molecular control of polarized cell movement during embryonic development. Dev Cell *2*, 695-706.

Wallingford, J.B., and Harland, R.M. (2001). Xenopus Dishevelled signaling regulates both neural and mesodermal convergent extension: parallel forces elongating the body axis. Development *128*, 2581-2592.

Wallingford, J.B., and Harland, R.M. (2002). Neural tube closure requires Dishevelled-dependent convergent extension of the midline. Development *129*, 5815-5825.

Wallingford, J.B., Rowning, B.A., Vogeli, K.M., Rothbacher, U., Fraser, S.E., and Harland, R.M. (2000). Dishevelled controls cell polarity during Xenopus gastrulation. Nature *405*, 81-85.

Wang, C., Ruther, U., and Wang, B. (2007). The Shh-independent activator function of the full-length Gli3 protein and its role in vertebrate limb digit patterning. Dev Biol *305*, 460-469.

Wang, J., Hamblet, N.S., Mark, S., Dickinson, M.E., Brinkman, B.C., Segil, N., Fraser, S.E., Chen, P., Wallingford, J.B., and Wynshaw-Boris, A. (2006a). Dishevelled genes mediate a conserved mammalian PCP pathway to regulate convergent extension during neurulation. Development *133*, 1767-1778.

Wang, J., Mark, S., Zhang, X., Qian, D., Yoo, S.J., Radde-Gallwitz, K., Zhang, Y., Lin, X., Collazo, A., Wynshaw-Boris, A., *et al.* (2005). Regulation of polarized extension and planar cell polarity in the cochlea by the vertebrate PCP pathway. Nat Genet *37*, 980-985.

Wang, Y., Guo, N., and Nathans, J. (2006b). The role of Frizzled3 and Frizzled6 in neural tube closure and in the planar polarity of inner-ear sensory hair cells. J Neurosci *26*, 2147-2156.

Wang, Y., and Nathans, J. (2007). Tissue/planar cell polarity in vertebrates: new insights and new questions. Development *134*, 647-658.

Wansleeben, C., Feitsma, H., Montcouquiol, M., Kroon, C., Cuppen, E., and Meijlink, F. (2010). Planar cell polarity defects and defective Vangl2 trafficking in mutants for the COPII gene Sec24b. Development *137*, 1067-1073.

Weiss, A., and Schlessinger, J. (1998). Switching signals on or off by receptor dimerization. Cell *94*, 277-280.

Wen, S., Zhu, H., Lu, W., Mitchell, L.E., Shaw, G.M., Lammer, E.J., and Finnell, R.H. (2010). Planar cell polarity pathway genes and risk for spina bifida. Am J Med Genet A *152A*, 299-304.

Wilson, L., and Maden, M. (2005). The mechanisms of dorsoventral patterning in the vertebrate neural tube. Dev Biol *282*, 1-13.

Winberg, M.L., Tamagnone, L., Bai, J., Comoglio, P.M., Montell, D., and Goodman, C.S. (2001). The transmembrane protein Off-track associates with Plexins and functions downstream of Semaphorin signaling during axon guidance. Neuron *32*, 53-62.

Wong, R.L., Wlodarczyk, B.J., Min, K.S., Scott, M.L., Kartiko, S., Yu, W., Merriweather, M.Y., Vogel, P., Zambrowicz, B.P., and Finnell, R.H. (2008). Mouse Fkbp8 activity is required to inhibit cell death and establish dorso-ventral patterning in the posterior neural tube. Hum Mol Genet *17*, 587-601.

Xylourgidis, N., and Fornerod, M. (2009). Acting out of character: regulatory roles of nuclear pore complex proteins. Dev Cell *17*, 617-625.

Yamada, S., Pokutta, S., Drees, F., Weis, W.I., and Nelson, W.J. (2005). Deconstructing the Cadherin-Catenin-Actin Complex. Cell *123*, 889-901.

Yang, C.H., Axelrod, J.D., and Simon, M.A. (2002). Regulation of Frizzled by fat-like cadherins during planar polarity signaling in the Drosophila compound eye. Cell *108*, 675-688.

Yates, L.L., Schnatwinkel, C., Murdoch, J.N., Bogani, D., Formstone, C.J., Townsend, S., Greenfield, A., Niswander, L.A., and Dean, C.H. (2010). The PCP genes Celsr1 and Vangl2 are required for normal lung branching morphogenesis. Hum Mol Genet *19*, 2251-2267.

Ybot-Gonzalez, P., Cogram, P., Gerrelli, D., and Copp, A.J. (2002). Sonic hedgehog and the molecular regulation of mouse neural tube closure. Development *129*, 2507-2517.

Ybot-Gonzalez, P., and Copp, A.J. (1999). Bending of the neural plate during mouse spinal neurulation is independent of actin microfilaments. Dev Dyn *215*, 273-283.

Ybot-Gonzalez, P., Gaston-Massuet, C., Girdler, G., Klingensmith, J., Arkell, R., Greene, N.D., and Copp, A.J. (2007a). Neural plate morphogenesis during mouse neurulation is regulated by antagonism of Bmp signalling. Development *134*, 3203-3211.

Ybot-Gonzalez, P., Savery, D., Gerrelli, D., Signore, M., Mitchell, C.E., Faux, C.H., Greene, N.D., and Copp, A.J. (2007b). Convergent extension, planar-cell-polarity signalling and initiation of mouse neural tube closure. Development *134*, 789-799.

Yen, W.W., Williams, M., Periasamy, A., Conaway, M., Burdsal, C., Keller, R., Lu, X., and Sutherland, A. (2009). PTK7 is essential for polarized cell motility and convergent extension during mouse gastrulation. Development *136*, 2039-2048.

Young, K.H., and Ozenberger, B.A. (1995). Investigation of ligand binding to members of the cytokine receptor family within a microbial system. Ann N Y Acad Sci *766*, 279-281.

Zarbalis, K., May, S.R., Shen, Y., Ekker, M., Rubenstein, J.L., and Peterson, A.S. (2004). A focused and efficient genetic screening strategy in the mouse: identification of mutations that disrupt cortical development. PLoS Biol *2*, E219.

Zhai, J., Lin, H., Nie, Z., Wu, J., Canete-Soler, R., Schlaepfer, W.W., and Schlaepfer, D.D. (2003). Direct interaction of focal adhesion kinase with p190RhoGEF. J Biol Chem *278*, 24865-24873.

Zhang, W., Zhao, Y., Tong, C., Wang, G., Wang, B., Jia, J., and Jiang, J. (2005). Hedgehog-regulated Costal2-kinase complexes control phosphorylation and proteolytic processing of Cubitus interruptus. Dev Cell *8*, 267-278.

Zhang, X., Chen, S., Yoo, S., Chakrabarti, S., Zhang, T., Ke, T., Oberti, C., Yong, S.L., Fang, F., Li, L., *et al.* (2008). Mutation in nuclear pore component NUP155 leads to atrial fibrillation and early sudden cardiac death. Cell *135*, 1017-1027.

Zhang, X., Zhu, J., Yang, G.Y., Wang, Q.J., Qian, L., Chen, Y.M., Chen, F., Tao, Y., Hu, H.S., Wang, T., *et al.* (2007). Dishevelled promotes axon differentiation by regulating atypical protein kinase C. Nat Cell Biol *9*, 743-754.

Zhang, X.M., Ramalho-Santos, M., and McMahon, A.P. (2001). Smoothened mutants reveal redundant roles for Shh and Ihh signaling including regulation of L/R symmetry by the mouse node. Cell *106*, 781-792.

Zhao, Q., Behringer, R.R., and de Crombrugghe, B. (1996). Prenatal folic acid treatment suppresses acrania and meroanencephaly in mice mutant for the Cart1 homeobox gene. Nat Genet *13*, 275-283.

CHAPTER 10

APPENDIX

10 Appendix

Table 10-1: Details of primer and PCR conditions used to amplify and sequence Ptk7.

Name	Forward (5'→3')	Reverse (5'→3')	Product size (bp)	PCR condition
Ptk7(1)	AACCTCGCTGCTCGTCTG	CGGAACCACTGGTAGGTAGG	497	1
Ptk7(2)	AGTGTGTGGCTCGGGATAAC	GATGGGAGTCTCGTCCTCAA	500	1
Ptk7(3)	CAGCCAGAACTTCACCTTGAG	GCTTGCATGGCAGGTGTAG	550	1
Ptk7(4)	TGGTGATGAGGAACGAGTCA	GTTTTTCCAGCACCTGGACT	500**	2
Ptk7(5)	GGTACAGGAACCAGATGCTGA	GTGGCCCTGGTACACAGTTG	488**	2
Ptk7(6)	TACACTTTGCCCGAGTGACC	CAGGACCGCGATGATGTAG	497	2
Ptk7(7)	CAGGATGCACATCTTCCAGA	TTCCCCAGAGTGGTGATAGG	495	2
Ptk7(8)	GGAGGAGCCAGAGATGGAG	CCTTCTGTTTGGTGCTGAGG	500	1
Ptk7(9)	CGGAGAGAGGTGGAGATGTT	GGGGCATCTCTCCATGAGT	490	1
Ptk7(10)	CAGAGGCAGGTGAAGGTGTC	AGGGCCAAGGACAGGGTTA	494	1
Ptk7(17)*	TAGCCCCAGACCTCTCTCAG	TGGGGATATAGCTTTCCCTTC	595	2

* donates primer pair designed to detect point mutation at intron 8 in *chuzhoi*
** donates nine extra base pairs in *chuzhoi*

PCR Program 1:
95°C for 5 minutes [95°C for 15 seconds, 55°C for 30 seconds, 72°C for 15 seconds] x 30 cycles, 72°C for 5 minutes.

PCR Program 2:
95°C for 1 minutes [{95°C for 30 seconds, 60°C for 20 seconds (-0.5°C per cycle), 72°C for 20seconds} x13 cycles], [{95°C for 20 seconds, 60°C for 20 seconds, 72°C for 20 seconds} x 35 cycles] 72°C for 1 minute.

Table 10-2: Number of embryos analysed for each geneotype and somite stage to obtain the length to width ratio.

Number of somites	+/+	*chz/+*	*chz/chz*
3	3	10	2
4	6	8	6
5	9	7	5
6	4	6	5
7	2	9	6

Table 10-3: List of genes that were identified a microarray screen as being up-regulated in *hhkr* compare to wildtype in all three arrays.

Accession number	Gene Symbol	Gene name	Average fold change in *hhkr* compared to wildtype
BC010711	*N/D*	*N/D*	2.7
AK020444	*Yif1b*	*Yip1 interacting factor homolog B (S. cerevisiae)*	1.8
BC052948	*Ccnd2*	*Cyclin D2*	1.8
AK007756	*1810043H04Rik*	*RIKEN cDNA 1810043H04 gene*	1.6
NM_016871	*Tomm40*	*Translocase of outer mitochondrial membrane 40 homolog (yeast)*	1.8
NM_010364	*Gtf2h4*	*General transcription factor II H, polypeptide 4*	1.7
NM_031191	*Prl2c2*	*Prolactin family 2, subfamily c, member 2*	2.4
NM_015787	*Hist1h1e*	*Histone cluster 1, H1e*	1.9
NM_146425	*Olfr470*	*Olfactory receptor 470*	1.6
NM_172155	*Prl3d2*	*Prolactin family 3, subfamily d, member 1*	2.5

Table 10-4: List of genes that were identified a microarray screen as being down-regulated in *hhkr* compare to wildtype in two out of three arrays.

Accession number	Gene Symbol	Gene name	Average fold change in *hhkr* compared to wildtype
AK008813	*2210403K04Rik*	*RIKEN cDNA 2210403K04 gene*	1.4
AK020204	*8030450C14Rik*	*RIKEN cDNA 8030450C14 gene*	1.2
NM_029310	*Fabp12*	*Fatty acid binding protein 12*	1.4
NM_026481	*Tppp3*	*Tubulin polymerization-promoting protein family member 3*	1.4
NM_013723	*Podxl*	*Podocalyxin-like*	1.6
NM_010649	*Klra4*	*Killer cell lectin-like receptor, subfamily A, member 4*	2.0
NM_177243	*Slc26a9*	*Solute carrier family 26, member 9*	1.2
AF027504	*Magi1*	*Membrane associated guanylate kinase, WW and PDZ domain containing 1*	1.7
NM_008645	*Mug1*	*Murinoglobulin 1*	1.7
NM_031174	*Dscam*	*Down syndrome cell adhesion molecule*	1.7
NM_175169	*Cd47*	*CD47 antigen (Rh-related antigen, integrin-associated signal transducer)*	1.6
NM_025301	*Mrpl17*	*Mitochondrial ribosomal protein L17*	2.6
NM_146171	*Ncapd2*	*Non-SMC condensin I complex, subunit D2*	1.6
NR_001570	*Xist*	*Inactive X specific transcripts*	2.6
AK004276	*9430020K01Rik*	*RIKEN cDNA 9430020K01 gene*	1.5
NM_007648	*Cd3e*	*CD3 antigen, epsilon polypeptide*	1.6
NM_009273	*Srp14*	*Signal recognition particle 14*	1.6
NM_011269	*Rhag*	*Rhesus blood group-associated A glycoprotein*	2.5
NM_201518	*Flrt2*	*Fibronectin leucine rich transmembrane protein 2*	1.6
NM_009829	*Ccnd2*	*Cyclin D2*	1.5
NM_020509	*Retnla*	*Resistin like alpha*	1.7
NM_172296	*Dmrta2*	*Doublesex and mab-3 related transcription factor like family A2*	1.8

AK009626	*2310034P14Rik*	*RIKEN cDNA 2310034P14 gene*	1.3
AK016891	*Dmrtc1c1*	*DMRT-like family C1c1*	1.3
AK006913	*1700067G03Rik*	*RIKEN cDNA 1700067G03 gene*	1.4
AK019195	*2700001H16Rik*	*RIKEN cDNA 2700001H16 gene*	1.4
NM_181588	*Cmbl*	*Carboxymethylenebutenolidase-like (Pseudomonas)*	1.3
AK003121	*Colec11*	*Collectin sub-family member 11*	1.7
NM_054063	*Psg28*	*Pregnancy-specific glycoprotein 28*	1.4
AK018865	*1700057G04Rik*	*RIKEN cDNA 1700057G04 gene*	1.4
AK016333	*4930579P08Rik*	*RIKEN cDNA 4930579P08 gene*	1.1
NM_010921	*Nkx3-1*	*NK-3 transcription factor, locus 1 (Drosophila)*	1.7
NM_008701	*Nkx2-9*	*NK2 transcription factor related, locus 9 (Drosophila)*	1.7
BC024508	*Fkbp8*	*FK506 binding protein 8*	1.8
AF104414	*Lats1*	*Large tumor suppressor*	1.2
NM_026693	*Gabarapl2*	*Gamma-aminobutyric acid (GABA) A receptor-associated protein-like 2*	1.5
AK009491	*Kbtbd5*	*Kelch repeat and BTB (POZ) domain containing 5*	1.2
NM_010028	*Ddx3x*	*DEAD/H (Asp-Glu-Ala-Asp/His) box polypeptide 3, X-linked*	1.2
NM_146344	*Olfr1495*	*Olfactory receptor 1495*	1.8
AK045292	*Bdp1*	*B double prime 1, subunit of RNA polymerase III transcription initiation factor IIIB*	1.3
AK004064	*Dysfip1*	*Dysferlin interacting protein 1*	1.6
S73844	*Olfr2*	*Olfactory receptor 2*	2.2

Table 10-5: Details of primers used for quantative real time PCR

Name	Forward (5'→3')	Reverese (5'→3')	Product size (bp)
Yif1b	CAGGGCAAGGAGCTGGTAGA	CCGTGTCCACTGCAAAGTAATACT	82
Ccnd2	TGTGCGCTACCGACTTCAAG	GCTTCCAGTTGCAATCATCGA	59
Podx1	GCATACCCCTGCTGCTGTTC	TGCCCAATGGTTTGTGTGTAG	98
Dscam*	TCCACATCAAGGCTGTTTTACG	CATTGCCTCTCATGGTTTTCTG	72
Dscam**	ACAAGCTATCTGCTCAAGACTATG	GGGTGTACCCTTCACATTGC	134
Srp14	CGGGCAGCGTGTTCATC	CTTCCTCGGGATAGGTTTGGT	62
Flrt2*	CGCTCTAGCTTCTTCCCTTTCC	TCTGTAATCTGGCAGCCTTGTC	81
Flrt2**	GCTTCTTCCCTTTCCACCTC	CAGGCAGGCAAATCTTCTTT	152
Dmrta2	GGCGCAGAGGCCAAATT	GGCCGGCCTGAAGCA	61
Nkx2.9*	AGCCTCCTGAATTTACCTGAACAG	CTCGTCCGAGGACAGGTAGTG	123
Nkx2.9**	AACAGACGTGCGTTCCACAG	GAGTCTGCAGGGCTTGTCTC	100
Fkbp8	GGCCGCCAATTCCTATGAC	TCATGTCCACTTTGGTGTTGGA	62
Gabarapl2	CAGTCCCACAGTCCAGCCTAAC	GAATCCATCTTCATCTTTTTCCTTCT	65
Hprt	TTCCTCATGGACTGATTATGGAC	CAGCAGGTCAGCAAAGAACTTAT	128
Gapdh	GAGACAGCCGCATCTTCTTGT	TGACCAGGCGCCCAA	98

* donates first primer set; ** donates second primer set

Table 10-6: Average Ct value for each biological sample

Assays	+/+							*hhkr/hhkr*						
	1	2	3	4	5	6	7	8	9	10	11	12	13	14
Yif1b	23.82	23.97	23.74	23.88	24.92	24.94	24.91	25.11	24.01	23.97	23.92	24.90	23.85	24.50
Ccnd2	21.92	21.82	21.79	21.24	21.04	21.35	21.50	22.66	21.32	21.65	21.28	20.83	19.39	20.25
Podx1	22.82	22.87	22.75	22.28	23.61	23.98	24.72	24.15	22.37	22.92	21.95	23.66	22.70	23.70
Srp14	22.84	22.81	22.45	22.95	22.02	23.69	24.09	24.17	22.47	22.76	22.96	22.13	22.53	23.25
Flrt2	28.93	29.43	29.88	29.24	29.56	30.35	31.69	30.46	29.63	29.10	28.70	29.77	27.65	30.49
Dmrta2	28.48	28.43	27.92	27.96	27.78	28.79	27.64	29.95	29.09	27.90	28.44	27.74	28.78	28.21
Nkx2.9	27.61	27.91	27.85	26.46	27.45	28.96	28.38	25376	25.46	26.26	24.27	25.83	24.23	25.67
Fkbp8	21.03	21.26	21.77	21.14	21.01	20.67	21.36	22.24	21.36	22.02	21.42	21.28	19.85	21.09
Gabarapl2	24.90	24.79	24.27	24.17	22.87	23.22	23.12	25.80	24.52	24.29	24.45	22.93	22.75	22.67
Gapdh	17.48	17.93	18.76	18.36	18.09	18.89	18.43	17.90	16.50	17.62	17.23	17.19	16.25	16.50